Meteorological constraints on marine atmospheric halocarbons and their transport to the free troposphere

Dissertation

zur Erlangung des Doktorgrades
der Mathematisch-Naturwissenschaftlichen Fakultät
der Christian-Albrechts-Universität zu Kiel

Vorgelegt von

Steffen Fuhlbrügge

Kiel, September 2015

GEOMAR
Helmholtz-Zentrum für Ozeanforschung Kiel

Erstgutachter:	Frau Prof. Dr. Kirstin Krüger
Zweitgutachter:	Frau Prof. Dr. Christa Marandino
Tag der mündlichen Prüfung:	06.11.2015
Zum Druck genehmigt:	06.11.2015

_____

Gez. Prof. Dr. Wolfgang J. Duschl, Dekan

„Es irrt der Mensch, so lang er strebt.“

Johann Wolfgang von Goethe, Faust I, Vers 317 / Der Herr

Zusammenfassung

Mit Inkrafttreten des Montreal-Protokolls in 1989 wurde der globale Ausstoß anthropogener Halogenkohlenwasserstoffe reduziert, was zu einem stärkeren Beitrag natürlich produzierter Halogenkohlenwasserstoffe zum atmosphärischen Halogenhaushalt in der Zukunft führen wird. Solche natürlichen Halogenverbindungen mit einer mittleren atmosphärischen Lebenszeit von bis zu einem halben Jahr, sogenannte sehr kurzlebige Substanzen (Very Short-Lived Substances, VSLS) beeinflussen die Oxidationsfähigkeit der Troposphäre und Stratosphäre (von Glasow and Crutzen, 2007). Den größten Beitrag zum atmosphärischen Bromgehalt leisten Bromoform und Dibrommethan durch Produktion von Mikro- und Makroalgen (e.g. Quack and Wallace, 2003;Law and Sturges, 2007). Iodmethan (veraltet Methyliodid), welches sowohl von Mikro und Makro-Algen als auch durch photochemische Reaktionen im Oberflächenwasser entsteht, leistet hingegen einen signifikanten Beitrag zum atmosphärischen Iodhaushalt (e.g. Butler et al., 2007;Hughes et al., 2011). Erhöhte Emissionen dieser VSLS werden vorwiegend in tropischen Ozeanen, ozeanischen Auftriebsgebieten und küstennah beobachtet. Daher spielen diese Regionen eine entscheidende Rolle für den atmosphärischen Halogenhaushalt. In Verbindung mit intensiver tropischer Konvektion können VSLS bis in die obere Troposphäre, bzw. untere Stratosphäre gelangen (Montzka and Reimann, 2011).

Diese Doktorarbeit untersucht den Einfluss meteorologischer Bedingungen und ozeanischer Emissionen auf atmosphärische VSLS Konzentrationen über Ozeanen und deren Transport in die freie Troposphäre. Die Arbeit umfasst drei Schiffskampagnen in verschiedenen ozeanischen und atmosphärischen Regimen: die DRIVE (Diurnal and Regional Variability of halogen Emissions) Kampagne mit FS POSEIDON im tropischen und subtropischen Nordostatlantik im Mai und Juni 2010, die SHIVA (Stratospheric ozone: Halogen Impacts in a Varying Atmosphere) Kampagne mit FS SONNE im tropischen Südchinesischem Meer und der Sulusee im November 2011, sowie der M91 SOPRAN (Surface Ocean Processes in the Antropocene) Kampagne mit FS METEOR im tropischen Südostpazifik im Dezember 2012. Meteorologische Parameter (Temperatur, Wind, Feuchte) wurden von den Schiffssensoren und den Radiosondierungen an Bord während jeder Kampagne gemessen, um atmosphärische Gegebenheiten nahe der Oberfläche, in der marinen atmosphärischen Grenzschicht (Marine Atmospheric Boundary Layer, MABL) und in der freien Troposphäre zu untersuchen. VSLS Proben wurden regelmäßig im Oberflächenwasser und in der marinen Atmosphäre während der Fahrten genommen. Die ersten beiden Manuskripte präsentieren Beobachtungen der DRIVE Kampagne. Manuskript 1 untersucht meteorologische Einflüsse insbesondere der MABL auf atmosphärisches Bromoform, Dibrommethan und Iodmethan, sowie deren tägliche Schwankungen

(Fuhlbrügge et al., 2013), während das zweite Manuskript Einflussfaktoren auf ozeanische Emissionen dieser VSLS über dem mauretanischen Auftrieb auf täglicher und regionaler Basis untersucht (Hepach et al., 2014). Manuskript 3 und 4 werten Beobachtungen während der SHIVA Kampagne im Südchinesischem Meer und in der Sulusee aus. Das dritte Manuskript untersucht den Beitrag von VSLS Emissionen zu beobachteten Mischungsverhältnissen in der MABL und der freien Troposphäre mit Hilfe einer Beitrags-Verlust Abschätzung und FLEXPART Trajektorienberechnungen. Die aufgrund ozeanischer Emissionen berechneten Mischungsverhältnisse von Bromoform, Dibrommethan und Iodmethan in der MABL und der freien Troposphäre werden mit Flugzeugmessungen in der Region während der SHIVA Kampagne verglichen (Fuhlbrügge et al., 2015b). Manuskript 4 präsentiert VSLS Variationen im Oberflächenwasser, deren ozeanischer Emissionen und atmosphärische Mischungsverhältnisse entlang der Fahrtroute (Sentian et al., 2015). Die M91 SOPRAN Fahrt im tropischen Südostpazifik ist Teil der Manuskripte 5 und 6. Zur Bestätigung der Hauptergebnisse der DRIVE Kampagne im mauretanischen Auftrieb, untersucht Manuskript 5 ähnliche meteorologische Einflüsse auf ozeanische Emissionen und atmosphärische VSLS im peruanischen Auftrieb. Zusätzlich wird die neu entwickelte Beitrags-Verlust Abschätzung aus Manuskript 4 auf die Beobachtungen während M91 angewandt (Fuhlbrügge et al., 2015a). Das 6. Manuskript konzentriert sich auf den Beitrag iodierter Verbindungen aus ozeanischen Emissionen auf atmosphärische Konzentrationen, sowie deren Transport in die Troposphäre (Hepach et al., 2015, to be submitted).

Zusammenfassend wurden folgende neue Ergebnisse erzielt: Die Auftriebsgebiete entlang der mauretanischen und peruanischen Küsten wurden als Quellregionen für atmosphärisches Bromoform, Dibrommethan und Iodmethan ermittelt. Erhöhte atmosphärische Mischungsverhältnisse dieser Verbindungen wurden küstennah, insbesondere aber über dem ozeanischen Auftrieb in beiden Regionen beobachtet. Meteorologische Faktoren, wie die MABL Eigenschaften zeigten einen signifikanten Einfluss auf die ozeannahen atmosphärischen Mischungsverhältnisse der VSLS und deren ozeanischen Emissionen. Abhängig von der Höhe und Stabilität der MABL sowie der Passatinversion führten die VSLS Emissionen zu einer Anreicherung der Konzentrationen in der untersten Atmosphäre. Die resultierenden geringen Konzentrationsgradienten dämpften die ozeanischen Emissionen und führten zu geringen Schwankungen der VSLS Konzentrationen. Die mit den VSLS angereicherten Luftmassen blieben unterhalb der Inversionsschicht(en) und wurden vorwiegend horizontal und bodennah transportiert. In Regionen konvektiver Aktivität können die Luftmassen dann in die obere Troposphäre und Tropopause transportiert werden. Als Gegenbeispiel zeigten sich im Südchinesischem Meer und in der Sulusee trotz hoher ozeanischer Konzentrationen und Emissionen relativ geringe VSLS Konzentrationen bodennah und in der MABL. Hier sorgte eine konvektive, instabile MABL und

tropische Konvektion für einen schnellen Transport von Bodenluft in die freie Troposphäre und einer schnellen Verteilung ozeanischer Emissionen innerhalb dieser. Dieser schnelle vertikale Transport wurde als Grund für die beobachteten geringen MABL VSLS Mischungsverhältnisse identifiziert. Bromoform in der freien Troposphäre über dem Südchinesischem Meer und der Sulusee stammte nahezu vollständig aus dem örtlichen Südchinesischem Meer, während Dibrommethan und Iodmethan hingegen größtenteils von den Küsten Borneos und den Philippinen sowie des Westpazifiks advehiert wurden.

Abstract

Emissions of anthropogenic halocarbons have decreased since the commencement of the Montreal Protocol in 1989, which leads to a stronger contribution of naturally produced halocarbons to the atmospheric halogen budget in the future. Natural halocarbons with a mean atmospheric lifetime of up to 0.5 years, the so-called very short-lived substances (VSLS), are known to alter tropospheric and stratospheric oxidation capacity (von Glasow and Crutzen, 2007). Large contributors of atmospheric bromine are bromoform and dibromomethane, both emitted by micro and macro algae (e.g. Quack and Wallace, 2003;Law and Sturges, 2007). A significant contributor to atmospheric iodine is methyl iodide, which is in addition to micro and macro algae also produced by photochemical reactions in the surface water (e.g. Butler et al., 2007;Hughes et al., 2011). Elevated oceanic emissions are observed in tropical oceans along coasts and above oceanic upwelling. Thus, these regions play a crucial role for the atmospheric halogen budget. In combination with deep tropical convection, the VSLS emissions can be transported into the upper troposphere and lower stratosphere (Montzka and Reimann, 2011).

This thesis investigates the influence of meteorological conditions and oceanic emissions on atmospheric VSLS abundances above the oceans and their transport into the free troposphere during three ship campaigns in different oceanic and atmospheric regimes: the DRIVE (Diurnal and Regional Variability of halogen Emissions) campaign with R/V POSEIDON in the tropical and subtropical Northeast Atlantic during May and June 2010, the SHIVA (Stratospheric ozone: Halogen Impacts in a Varying Atmosphere) campaign with R/V SONNE in the tropical South China and Sulu Seas in November 2011, and the M91 SOPRAN (Surface Ocean Processes in the Antropocene) campaign with R/V METEOR in the tropical Southeast Pacific in December 2012. Meteorological data (e.g. temperature, wind, humidity) were measured from ships sensors and by radiosonde launches from the ships during each campaign to investigate atmospheric conditions near the surface, in the marine atmospheric boundary layer (MABL) and in the free troposphere. VSLS were regularly sampled in the surface water and in the marine atmosphere during the cruises. The first two manuscripts present results from observations during DRIVE. Manuscript 1 investigates meteorological impacts on atmospheric bromoform, dibromomethane and methyl iodide and their diurnal variability (Fuhlbrügge et al., 2013), while the second manuscript investigates drivers of oceanic emissions of these VSLS above the Mauritanian upwelling on a diel and regional basis (Hepach et al., 2014). Manuscripts 3 and 4 evaluate observations during SHIVA in the South China and Sulu Seas. The third manuscript investigates the contribution of VSLS emissions to observed MABL and free tropospheric

abundances by developing a source-loss estimate using FLEXPART trajectories. Computed MABL and free troposphere mixing ratios of bromoform, dibromomethane and methyl iodide from the oceanic emissions in the region are compared to SHIVA aircraft observations (Fuhlbrügge et al., 2015b). Manuscript 4 presents variations of VSLS in the surface water, oceanic emissions and atmospheric abundances along the cruise track (Sentian et al., 2015). The M91 SOPRAN cruise in the Southeast Pacific is part of manuscripts 5 and 6. To evaluate the major findings achieved during the DRIVE campaign at the Mauritanian upwelling, manuscript 5 investigates similar meteorological constraints on oceanic emissions and atmospheric VSLS in the Peruvian upwelling. In addition the new source-loss estimate developed in manuscript 4 is applied to the observations during the M91 cruise (Fuhlbrügge et al., 2015a). The 6th manuscript concentrates on the contribution of iodinated compounds from oceanic emissions to atmospheric abundances and their transport to the troposphere (Hepach et al., 2015, to be submitted).

Overall the following results were achieved. The upwelling regions along the Mauritanian and Peruvian coasts were identified to be medium source regions for atmospheric bromoform, dibromomethane and methyl iodide. Elevated atmospheric mixing ratios of these compounds were found towards the coasts especially above the oceanic upwelling in both regions. Meteorological factors, in particular the MABL characteristics, were identified to impact the atmospheric VSLS mixing ratios and the oceanic emissions significantly. Depending on the height and stability of the MABL as well as the trade inversion, VSLS from oceanic emissions led to an accumulation within the lowermost atmosphere. The resulting low concentration gradients dampened the oceanic emissions and led to minor variations of the marine atmospheric abundances. The VSLS enriched air masses stayed below the inversion layer(s) and were mainly transported horizontally. Within convective activity they could be lifted to the upper troposphere and tropopause. On the opposite, VSLS abundances at the surface and in the MABL were relatively low at coastal regions of the South China and Sulu Seas, despite the high elevated oceanic concentrations and emissions in this area. Here, a convective instable MABL and deep tropical convection led to a rapid exchange of surface air to the free troposphere and a fast distribution of oceanic emissions within the free troposphere. The rapid vertical transport was identified to explain the observed low MABL VSLS mixing ratios. Free tropospheric abundances of bromoform above the South China and Sulu Seas were shown to originate almost entirely from the local South China Sea, while dibromomethane and methyl iodide in contrast were found to be largely advected from the coast of Borneo and the Philippines and from the open West Pacific.

Manuscript overview

This thesis is based on the following manuscripts:

1. Manuscript: Fuhlbrügge S., Krüger K., Quack B., Atlas E., Hepach H. and Ziska F.: "*Impact of the marine atmospheric boundary layer conditions on VSLS abundances in the eastern tropical and subtropical North Atlantic Ocean*", Atmospheric Chemistry and Physics, 13, 6345-6357, 10.5194/acp-13-6345-2013, **published 2013**.

   1.1. Contribution: The results of the manuscript are partly based on the Diploma thesis "Analysis of atmospheric VSLS measurements during the DRIVE campaign in the tropical East Atlantic" by S. Fuhlbrügge. For the ACP publication, data and figures in the manuscript have been intensively revised and complimented with new results by S. Fuhlbrügge. The manuscript was written by S. Fuhlbrügge. K. Krüger and B. Quack provided input for the preparation and revision of the manuscript. H. Hepach computed the VSLS sea-air fluxes and wrote section 3.4. F. Ziska took atmospheric samples and launched the radiosondes during the DRIVE cruise. E. Atlas analysed the atmospheric VSLS samples.

2. Manuscript: Hepach H., Quack B., Ziska F., Fuhlbrügge S., Atlas E., Krüger K., Peeken I., and Wallace D. W. R.: "*Drivers of diel and regional variations of halocarbon emissions from the tropical North East Atlantic*", Atmospheric Chemistry and Physics, 14, 1255-1275, doi:10.5194/acp-14-1255-2014, **published 2014**.

   2.1. Contribution: H. Hepach measured the halocarbons in the sea surface water, evaluated the data, carried out the calculations, and wrote the manuscript. B. Quack contributed to the manuscript preparation and the review process. F. Ziska took air samples and launched radiosondes during the DRIVE cruise. S. Fuhlbrügge analysed and evaluated the meteorological data. E. Atlas measured the atmospheric VSLS samples. I. Peeken measured and calculated the phytoplankton pigments. F. Ziska, S. Fuhlbrügge, E. Atlas, I. Peeken, K. Krüger and D. W. R. Wallace helped revising the manuscript.

3. Manuscript: Fuhlbrügge S., Quack, B., Tegtmeier, S., Atlas, E., Hepach, H., Shi, Q., Raimund, S., and Krüger, K.: "*The contribution of oceanic very short lived halocarbons to marine and free troposphere air over the tropical West Pacific*", Atmospheric Chemistry and Physics Discuss., 15, 17887-17943, doi:10.5194/acpd-15-17887-2015, **published for discussion 2015**.

   3.1. Contribution: S. Fuhlbrügge and K. Krüger took atmospheric samples and launched radiosondes during the SHIVA cruise. S. Fuhlbrügge analysed the data, developed the methodologies and wrote the manuscript. K. Krüger and B. Quack assisted with the campaign preparation and post-processing, and provided input during the preparation of the manuscript. S. Tegtmeier calculated the FLEXPART runs and provided helpful comments during the preparation of the manuscript. E. Atlas analysed the atmospheric VSLS samples. H. Hepach, Q. Shi and S. Raimund measured halocarbons in the sea surface water.

4. Manuscript: Sentian J., Xiang, C. T., Jing, H. C., Quack, B., Fuhlbrügge, S., Krüger, K., and Atlas, E.: "*Observation of the Variations of Very Short-Lived Halocarbon Emissions in Tropical Coastal Marine Boundary Layer*", Advanced Science Letters, 21, 144-149, doi:10.1166/asl.2015.5856, **published 2015**.

   4.1. Contribution: S. Fuhlbrügge and K. Krüger took the atmospheric VSLS samples during the SHIVA cruise. E. Atlas analysed the atmospheric VSLS samples. J. Sentian wrote the manuscript. B. Quack took the water samples and computed the VSLS sea-air fluxes.

5. Manuscript: Fuhlbrügge, S., Quack B., Atlas E., Fiehn A., Hepach H., Krüger K.: "*Meteorological constraints on oceanic halocarbons above the Peruvian Upwelling*", Atmospheric Chemistry and Physics Discuss., 15, 20597-20628, doi:10.5194/acpd-15-20597-2015, **published for discussion 2015**.

   5.1. Contribution: S. Fuhlbrügge took the atmospheric VSLS samples and launched radiosondes during the M91 cruise, analysed the data, and wrote the manuscript. K. Krüger and B. Quack assisted with the campaign preparation and post-processing, and provided input during the preparation of the manuscript. E. Atlas analysed the atmospheric VSLS samples. A. Fiehn calculated the FLEXPART runs. H. Hepach measured halocarbons in the sea surface water.

6. Manuscript: Hepach H., Quack B., Tegtmeier S., Engel A., Bracher A., Fuhlbrügge S. , Galgani L., Raimund S., Atlas E., Lampel J. und Krüger K.: "*Biogenic halocarbons from the Peruvian upwelling as tropospheric halogen source*", **to be submitted**.

   6.1. Contribution: H. Hepach measured the halocarbons in surface water, calculated iodocarbon fluxes and wrote the manuscript. B. Quack helped writing the manuscript, interpreted the data and provided input during the correction of the manuscript. S. Tegtmeier calculated the contributions of organoiodine to IO and provided input during the correction of the manuscript. A. Engel and L. Galgani measured DOM in the SML and the subsurface and helped interpreting the data. A. Bracher provided the phytoplankton measurements and helped correcting the manuscript. S. Fuhlbrügge took the air samples and provided input during manuscript preparation. S. Raimund measured the halocarbon in the depth profiles. E. Atlas measured the atmospheric samples. J. Lampel was responsible for IO data onboard RV Meteor. K. Krüger helped correcting the manuscript.

Content

1. Introduction

Atmospheric halogenated trace gases from natural sources play a significant role in the oxidation capacity of the troposphere and stratosphere (e.g. von Glasow and Crutzen, 2007;Simpson et al., 2015). They also contribute to the atmospheric halogen loading and to the ozone budget. For example natural halocarbons from the ocean contribute up to 25 % to the halogen burden in the stratosphere (Dorf et al., 2006) and significantly deplete ozone there (Salawitch et al., 2005;Sinnhuber and Folkins, 2006;Yang et al., 2014). To estimate the global contribution of natural halocarbons, marine and atmospheric observations were investigated during various measurement campaigns around the globe (e.g. Quack and Suess, 1999;Carpenter et al., 2007;Brinckmann et al., 2012). Surface observations of these natural halocarbons were taken in the atmospheric boundary layer and their abundance thus may be influenced by meteorological conditions there such as the extent and condition of the boundary layer. The investigation of these natural halocarbons and their transport pathways in the lower atmosphere will help to identify source regions and hot spots in the ocean and help to evaluate the contribution of source regions to atmospheric abundances. This thesis concentrates on three halocarbons with natural sources in the oceans: Methyl iodide, an important carrier of iodine to the atmosphere (Saiz-Lopez et al., 2012), as well as bromoform and dibromomethane, which are the largest natural contributors to atmospheric bromine (Penkett et al., 1985;Quack and Wallace, 2003;Hossaini et al., 2012).

1.1 Halocarbons

The collective term ‘halocarbon’ refers to a broad spectrum of hydrocarbons in which at least one carbon atom is linked covalently to one or more halogen atoms, e.g. fluorine, chlorine, bromine or iodine. Anthropogenic halocarbons containing chlorine and fluorine, the so called chlorofluorocarbons (CFCs) and those containing bromine, the so called halons, were widely used as propellants, fire extinguishants, refrigerants and solvents since the 1930s. The emissions and the inert characteristic of these anthropogenic halocarbons led to an accumulation of these compounds in the atmosphere, which was first reported by Lovelock (1971) and by Lovelock and Maggs (1973). Solar radiation in the stratosphere can release halogen radicals from these halocarbons. The radicals are then involved in catalytic ozone cycles, leading to ozone loss in the stratosphere. Although this reaction was already suggested by Molina and Rowland (1974), it was not generally accepted in the scientific community until the discovery of the Antarctic ozone hole by Chubachi (1984) and Farman

et al. (1985). With the commencement of the Montreal Protocol in January 1989 the signatory states committed to fully abolish anthropogenic halocarbon emissions. Indeed, a decrease of the atmospheric halocarbon abundances and a slow recovery of the stratospheric ozone layer were observed in the last years (Pawson and Steinbrecht, 2015). The very long atmospheric lifetimes of certain halocarbons, e.g. CFC-11 with 52 years and CFC-12 with 102 years, lead to a delayed reduction of these compounds in the atmosphere (Pawson and Steinbrecht, 2015). With the decline of anthropogenic halocarbon emissions, naturally produced halocarbons and their contribution to the atmospheric halogen load moved further into the scientific focus (Ko and Poulet, 2003). In particular global climate changes e.g. sea surface temperature and wind speed changes, are expected to affect oceanic emissions of these halocarbons (Ziska et al., 2013). If the lifetime of a natural halocarbon exceeds transport timescales in the troposphere, it can be transported into the stratosphere, e.g. due to deep convection in the tropics (Montzka and Reimann, 2011). To estimate current and future halocarbon emissions from natural sources and their transport pathways in the atmosphere it is fundamental to investigate and identify present halocarbon source regions and their particular contribution to the atmospheric halogen loading. Therefore this thesis presents new unpublished halocarbon observations to improve global halocarbon climatologies, develops a method to estimate the contribution of natural halocarbons emissions to the observed boundary layer and free troposphere abundances, and investigates the meteorological constraints especially of boundary layer conditions on marine atmospheric halocarbon abundances.

1.2 Very Short-Lived Substances (VSLS)

Halogenated trace gases with local tropospheric lifetimes of less than 6 months and mainly natural sources have been summarized as Very Short-Lived Substances (VSLS) and can significantly contribute to the atmospheric halogen load (Ko and Poulet, 2003;Dorf et al., 2006;Law and Sturges, 2007;Montzka and Reimann, 2011).

1.2.1 Marine sources

VSLS sources mainly originate from the ocean. Marine abundances of bromoform and dibromomethane are known to originate from biotic sources. The production of both compounds in the open ocean is attributed predominantly to phytoplankton (Fogelqvist, 1985;Class and Ballschmiter, 1988;Moore and Tokarczyk, 1993;Quack and Wallace, 2003). In coastal regions, macro

algae such as brown, green and red algae are known to be dominant producers of oceanic bromoform and dibromomethane (Gschwend et al., 1985;Nightingale et al., 1995;Quack et al., 2004;Law and Sturges, 2007). Methyl iodide can be produced by algae and phytoplankton (Hughes et al., 2011;Manley and Dastoor, 1988;Manley and de la Cuesta, 1997), as well as abiotic due to photochemical processes in surface sea water (Butler et al., 2007;Chuck et al., 2005;Happell and Wallace, 1996;Moore and Zafiriou, 1994).

1.2.2 Sea-air gas exchange

Brominated and iodinated VSLS are predominantly emitted from the ocean. Known global emissions range from 116 – 820 Gg Br yr^{-1} for bromoform, 57 – 280 Gg Br yr^{-1} for dibromomethane and 157 – 550 Gg I yr^{-1} for methyl iodide (Table 1-1). While the majority of studies reveal a significantly higher contribution of coastal emissions to global emissions for bromoform with up to 81 %, dibromomethane and methyl iodide are mainly emitted from the open ocean with up to 78 % and 89 % respectively (Ziska et al., 2013). Although these estimates reveal large uncertainties due to the high spatial and temporal variability of the oceanic emissions, different emission estimates (top-down versus bottom-up approaches) and limited input data, elevated emissions are generally found in tropical regions (Yokouchi et al., 2005;Montzka and Reimann, 2011). While top-down estimates reproduce oceanic emissions via a synchronization of atmospheric VSLS-data with simulations of chemistry climate models, bottom-up estimates take surface measurements to compute air-sea fluxes directly. Ziska et al. (2013) were the first who established and used a database of worldwide halogenated VSLS observations (HalOcAt, https://halocat.geomar.de/de) for their bottom-up estimates. Since they used the highest number of available observations, their computed oceanic fluxes appear most reliable. However, the data base is very sparse which reveals the need for further observations to investigate the variability of the oceanic emissions und to improve these estimates.
VSLS observations of the first and second manuscript (DRIVE) are already included in the HalOcAt database, which was used for the Ziska climatology (Ziska et al., 2013). Measurements of the remaining manuscripts (3 - 6) are planned to be integrated into the HalOcAt database for future global VSLS climatologies.

Table 1-1: Oceanic emissions of bromoform and dibromomethane in Gg Br yr^{-1}, and methyl iodide in Gg I yr^{-1}. Coast includes shelf estimates. Studies using a bottom-up approach are marked by ↑, top-down by ↓ and model studies by ○. Ziska et al. (2013) uses 2 different methods, robust fit (RF) and ordinary least squares (OLS).

	Bromoform			**Dibromomethane**			**Methyl iodide**		
Reference	Global	Open Ocean	Coast	Global	Open Ocean	Coast	Global	Open Ocean	Coast
Bell et al. (2002) ○							305		
Quack and W. (2003) ↑	800	241	559						
Yokouchi et al. (2005) ↑	820								
Warwick et al. (2006) ↓	560	280	280	100					
Butler et al. (2007) ↑	800	150	650	280	50	230	550	270	280
Kerkweg et al. (2008) ↓	596			113					
Carpenter et al. (2009) ↑			200						
O'Brien et al. (2009) ↑	820								
Palmer et al. (2009) ↑	116								
Liang et al. (2010) ↓	430	260	170	57	34	23			
Pyle et al. (2011) ↓	382			100					
Ordonez et al. (2012) ↓	533			67			213		
Ziska et al. (2013) OLS ↑	199	50	149	78	61	17	184	163	21
Ziska et al. (2013) RF ↑	120	30	90	62	48	14	157	137	20

1.2.3 Sea-air flux parameterization

Direct flux measurement techniques of bromoform, dibromomethane and methyl iodide are still in development and testing. To investigate the sea-air gas exchange of these compounds, their fluxes are parameterized. Generally, a flux *F* between two fluids can be described after Eq. 1, with *k* as a transfer coefficient and *Δc* as the concentration gradient between the two fluids:

$$F = k \cdot \Delta c \qquad \text{(Eq. 1)}$$

Liss and Slater (1974) were the first to present a simple two-layer model of a flat gas-liquid interface (Figure 1-1). Assuming the gas film to obey the solubility of a gas in a liquid after Henry's Law and the main resistance occurring at the transfer through the specific gas/liquid film, Eq. 1 can be transformed into Eq. 2, with k_l as the transfer coefficient for the liquid, *H* as the Henry's Law coefficient that varies

with temperature and salinity, c_g as the concentration in the gas and c_l as the concentration in the liquid. In case of a low solubility of a gas in the liquid, Eq. 2 can be used to calculate the net flux (Nightingale, 2009). However, diffusion in the molecular layers can only be estimated which means the transfer coefficient k_l has to be parameterized.

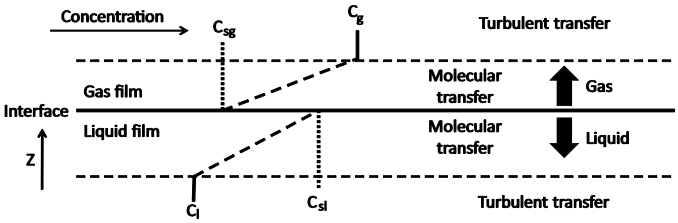

Figure 1-1: Two-layer model of sea-air gas exchange through an interface. Adopted from Liss and Slater (1974).

$$F = k_l \cdot (\frac{c_g}{H} - c_l) \qquad \text{(Eq. 2)}$$

Since various factors are known to influence the sea-air flux, e.g. wind speed, turbulence, heat flux, and mixing depths the range of known transfer coefficients reveals the complexity of considering all these factors (Wanninkhof et al., 2009;Garbe et al., 2014). To describe the viscosity of a gas in water, the Schmidt number *Sc* (Table 1-2) is used, which is defined as the ratio of momentum diffusivity (ϑ) to the diffusivity for mass transfer. The estimation of the transfer coefficients k_l for bromoform, dibromomethane and methyl iodide is based on a power law dependence of the parameterization by Nightingale (2009), which lies well in range of known transfer coefficients and is expressed for a Schmidt number of 600 for CO_2 at 20 °C in fresh water (Eq. 3) with u_{10} as a 10 minute wind speed mean at 10 m height.

$$k_{600} = 0.222 \cdot u_{10}^2 + 0.333 \cdot u_{10} \qquad \text{(Eq. 3)}$$

The specific diffusion coefficients can then be computed after Eq. 4 (Quack and Wallace, 2003), which leads to the final equation for the net sea-air flux (Eq. 5).

Table 1-2: Schmidt numbers (Sc_{VSLS}) and Henry's Law coefficient (H_{VSLS}) for bromoform, dibromomethane and methyl iodide with *T* as liquid temperature (Hayduk and Laudie, 1974;Wilke and Chang, 1955;Sander, 1999;Moore et al., 1995a;Moore et al., 1995b;Quack and Wallace, 2003).

VSLS	Sc_{VSLS}	H_{VSLS}
Bromoform	$\frac{\vartheta}{1.93 \cdot 10^{-9} \cdot T^2 + 1.686 \cdot 10^{-7} \cdot T + 4.0342 \cdot 10^{-6}}$	$e^{\left(\frac{-4973}{T+273.15}+13.16\right)}$
Dibromomethane	$\frac{\vartheta}{2.23 \cdot 10^{-9} \cdot T^2 + 1.9699 \cdot 10^{-7} \cdot T + 4.71321 \cdot 10^{-6}}$	$e^{\left(\frac{-4418}{T+273.15}+11.7\right)}$
Methyl iodide	$\frac{\vartheta}{2.10 \cdot 10^{-9} \cdot T^2 + 1.76 \cdot 10^{-7} \cdot T + 4.2 \cdot 10^{-6}}$	$e^{\left(\frac{-4338}{T+273.15}+13.22\right)}$

$$k_{VSLS} = k_{600} \cdot \left(\frac{600}{Sc_{VSLS}}\right)^{0.5} \quad \text{(Eq. 4)}$$

$$F = k_{VSLS} \cdot \left(c_l - \frac{c_g}{H_{VSLS}}\right) \quad \text{(Eq. 5)}$$

The fluxes of bromoform, dibromomethane and methyl iodide are used in order to estimate the contribution of oceanic emissions to atmospheric abundances.

1.2.4 Tropospheric abundances

The increasing number of atmospheric surface halogenated VSLS data points around the globe during the last decades helped to improve global VSLS climatologies (e.g. Warwick et al., 2006;Ziska et al., 2013) (Figure 1-2). Elevated mixing ratios of most brominated VSLS are found predominantly in coastal regions and in the tropics due to elevated oceanic emissions in these areas (Section 1.2.2). In tropical regions, the VSLS and their product gases can be transported by (deep) convection into higher altitudes when their atmospheric lifetimes are longer than transport processes in the atmosphere (Quack et al., 2004;Salawitch, 2006;Aschmann et al., 2009;Aschmann et al., 2011;Ashfold et al., 2012). The atmospheric lifetimes of bromoform, dibromomethane and methyl iodide are governed by several chemical reactions, once they are emitted into the atmosphere. Both bromoform and dibromomethane are degraded by photolysis and hydroxyl radicals (OH) (Figure 1-3). A source for OH radicals in the troposphere is ozone (O_3). Although about 90 % of global ozone is found in the stratosphere, tropospheric ozone acts as a toxic pollutant and greenhouse gas (Crutzen, 1971;Reeves et al., 2002;Weinhold, 2008;Stevenson et al., 2013).

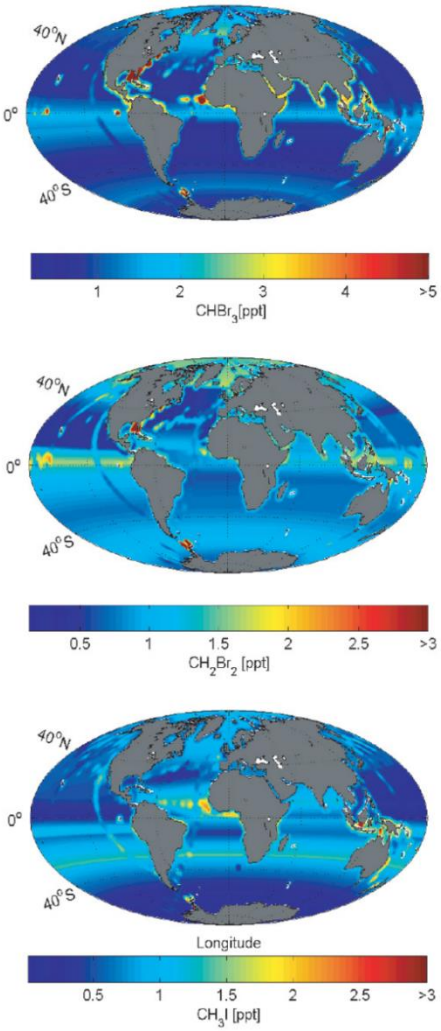

Figure 1-2: Global maps of atmospheric surface mixing ratios [ppt] of bromoform ($CHBr_3$), dibromomethane (CH_2Br_2) and methyl iodide (CH_3I) computed by Ziska et al. (2013)

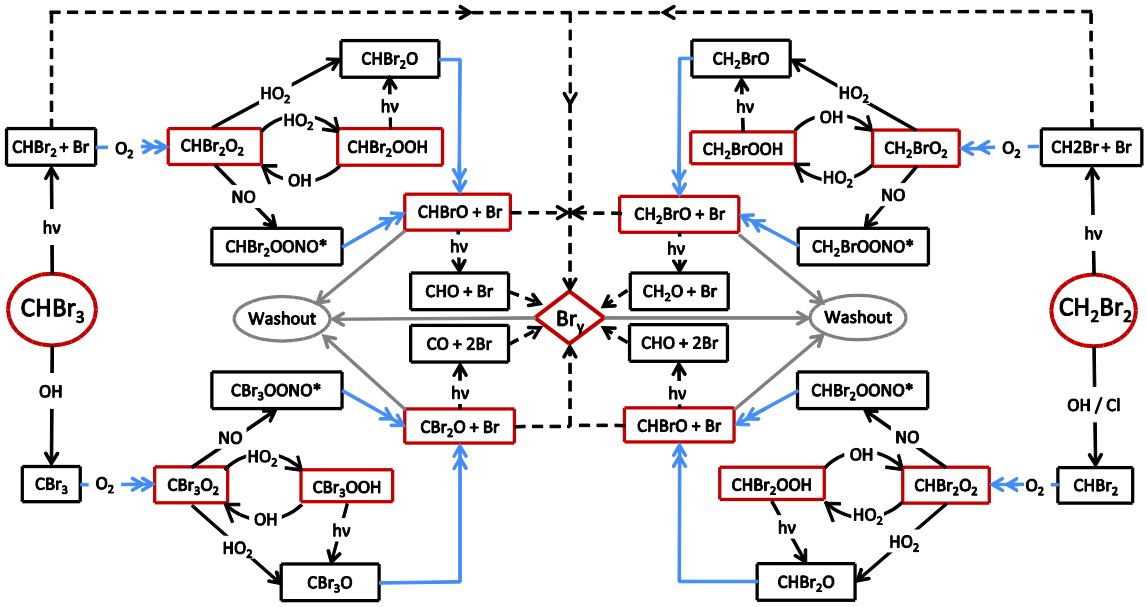

Figure 1-3: Tropospheric degradation scheme of bromoform ($CHBr_3$) and dibromomethane (CH_2Br_2) after Hossaini et al. (2010). Organic species are shown in red boxes, fast reactions are given by blue lines and the production of Br_y is given by dashed lines.

While bromoform is predominantly degraded by photolysis, dibromomethane is mainly degraded by reactions with OH. Estimates on the atmospheric lifetimes of bromoform and dibromomethane in the tropics have strongly varied during the past (McGivern et al., 2002;Ko and Poulet, 2003;McGivern et al., 2004;Law and Sturges, 2007). Most recent studies reveal a mean lifetime for bromoform of 15 days in the MABL and 17 days in the entire troposphere, respectively 94 days and 150 days for dibromomethane (Carpenter and Reimann, 2015). The major primary oxidation products of bromoform are carbonyl bromide (CBr_2O) and formyl bromide (CHBrO). The latter is also the major degradation product of dibromomethane. These compounds furthermore release HBr, HOBr and BrO, summarized as Br_y due to photolysis as reactive bromine, which has been shown to be 60 times more effective in ozone destruction than chlorine (Montzka and Reimann, 2011). Von Glasow (2004) and Yang et al. (2005) simulated a decrease of the tropospheric ozone by 5 to 30 % when considering bromine in the troposphere. Chemical degradation of methyl iodide in the MABL and free troposphere is even faster with a mean lifetime of 3, respectively 4 days (Carpenter and Reimann, 2015). It is rapidly photolyzed into inorganic iodine (I_y). Once Br_y and I_y are released into the atmosphere they enter catalytic reaction cycles with ozone (O_3). Catalytic key reactions in the troposphere involving halogen oxidation and halogen oxide self-reactions are (Read et al., 2008):

		$O_3 + X \rightarrow XO + O_2$	(R2.1)
$O_3 + X \rightarrow XO + O_2$	(R1.1)	$O_3 + Y \rightarrow YO + O_2$	(R2.2)
$O + XO \rightarrow X + O_2$	(R1.2)	$XO + YO \rightarrow X + Y + O_2$	(R2.3)
net: $O + O_3 \rightarrow 2O_2$	(R1.3)	net: $2O_3 \rightarrow 3O_2$	(R2.4)

Here, X and Y are representative for halogen radicals, either bromine (Br), or iodine (I) (or chlorine, Cl). They react within seconds with ozone and produce halogen oxides (XO, YO). The halogen radicals can also suppress ozone formation by perturbing HO_2/OH ratios (von Glasow et al., 2004):

$$XO + HO_2 \rightarrow HOX + O_2 \quad \text{(R3.1)}$$

$$HOX + h\nu \rightarrow OH + X \quad \text{(R3.2)}$$

Saiz-Lopez et al. (2014) estimated the integrated contribution of catalytic iodine reactions to the total rate of tropospheric ozone loss to be up to 5 times larger than the combined bromine and chlorine cycles.

1.3 The Marine Atmospheric Boundary Layer (MABL)

For surface trace gas observations it is fundamental to investigate the stability and structure of the lowermost atmosphere, which usually extends from the surface up to about 3 km height. Atmospheric constituents such as gases and aerosols emitted into the MABL are gradually dispersed before they are completely mixed within approximately one hour in the MABL due to turbulence and convection (Stull, 1988;Holton and Hakim, 2012). However, under stable conditions in the MABL complete mixing is often not fully reached (Seibert et al., 2000). MABL conditions can be observed by direct measurements (e.g. radiosondes, tethered balloons, weather masts, and aircrafts) and by remote sensing techniques (e.g. Doppler weather radars, LiDAR and SODAR). Two different kinds of MABLs exist (Figure 1-4), the convective boundary layer (CBL) and the stable boundary layer (SBL). The CBL consists of a surface layer (SL), which extents up to 100 m height and is strongly influenced by the Earth's surface, e.g. heating or cooling of the surface, evaporation and friction. Above lies the so-called mixed layer (ML) in which compounds are vertically well mixed. In the SL and ML, mixing occurs due to turbulence. The transition from the ML to the free troposphere is called entrainment layer (EL), where turbulence and vertical transport decline towards the top. In this thesis, the MABL height in the case of a convective boundary layer is chosen as the centre of the EL. The SBL can also be split into two layers, a lower layer of continuous turbulence (CTL) and a layer of sporadic

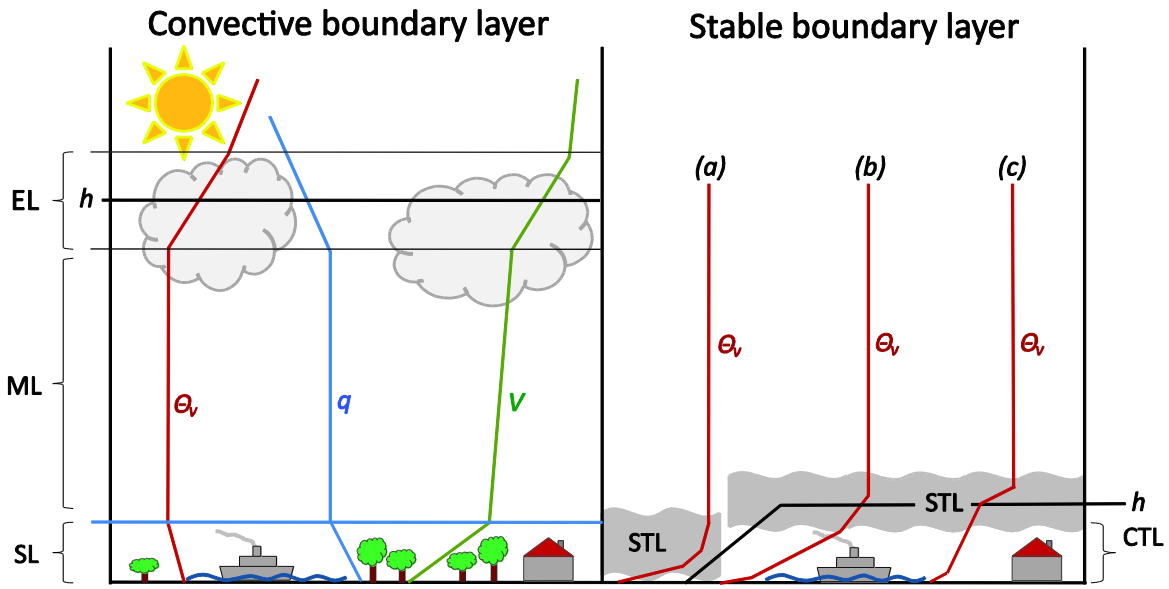

Figure 1-4: Exemplary profiles of convective (left) and stable (right) boundary layers (Stull, 1988;Seibert et al., 1997, 2000), virtual potential temperature (Θ_v, red), humidity (q, blue) and wind speed (V, green). The height of the boundary layer is given by *h*, the Surface Layer by SL, the Mixed Layer by ML, the Entrainment Layer by EL, the Continuously Turbulence Layer by CTL, and the Sporadic Turbulence Layer by STL. The height of the SBL varies with the height of the STL: (a) STL reaches the surface, (b) and (c) a CTL leads to an increase of the SBL height.

turbulence (STL) above. In case of low wind speeds and a strong stability of the lower atmosphere the STL can even extend to the ground and lead to very low boundary layer heights and thus a very small volume of air in which compounds are mixed (Figure 1-4, right side). With increase of the wind speed in the CTL, turbulence leads to an increase of the MABL height (b, c) (Seibert et al., 2000). In this thesis, CBL and SBL are investigated above different oceanic regimes by radiosonde launches. Major foci are mixing of trace gases within the MABL and the transport of surface air masses out of the MABL into the free troposphere under convective and stable MABL conditions. These require the determination of the MABL height and condition as well as the computation of trajectories to estimate the timescales of surface air remaining in the MABL, respectively leaving the MABL.

1.3.1 MABL height determination from radiosoundings

The height of the MABL determines the available volume in which compounds are rapidly mixed and is therefore an essential parameter e.g. for air pollution studies. Unfortunately, it is a rather unspecific meteorological quantity, with different definitions and estimations (Stull, 1988;Garratt, 1990;Seibert et al., 2000). In this thesis, the MABL is investigated by radiosonde observations. Definitions and characteristics of the MABL as well as methods to determine its height are adopted from Seibert et al. (2000). The MABL height can be determined from radiosonde derived atmospheric profiles of temperature, humidity and wind. With this data it can be derived objectively and subjectively. Objective methods include e.g. the Holzworth method (Holzworth, 1964, 1967, 1972), which basically starts at the surface with the measured temperature and follows the dry adiabate up to the point of intersection with the temperature of the most recent radiosounding. However, this method strongly depends on the surface temperature and thus results in high uncertainties of the estimated MABL height (Aron, 1983, 1985). Another objective method is the computation of the bulk Richardson number Ri_b (Troen and Mahrt, 1986;Vogelezang and Holtslag, 1996). It is a dimensionless number that relates the vertical stability to the vertical shear, respectively the thermally produced turbulence to shear induced turbulence, which makes it only suitable for unstable convective conditions (Seibert et al., 2000). Ri_b is computed at the height z from radiosonde measurements after Eq. 6 with g as the acceleration of gravity, $\Theta_v(z)$ as the virtual potential temperature at level z, Θ_{v1} as the virtual potential temperature at ground level, $U(z)$ as the zonal wind at level z and $V(z)$ as the meridional wind at level z. If Ri_b reaches a critical value of 0.25, $z(Rib \geq 0.25)$ defines the height of the MABL (Sørensen et al., 1996).

$$Ri_b(z) = \frac{gz}{\Theta_{v_1}} \frac{\Theta_v(z) - \Theta_{v_1}}{U(z)^2 + V(z)^2} \qquad \text{(Eq. 6)}$$

The potential temperature Θ describes the temperature of an air parcel that is lifted adiabatically to a surface pressure level p (von Bezold, 1888). In case of condensation and evaporation Θ is replaced by the virtual potential temperature Θ_v.

Besides this objective method the MABL height can be determined subjectively from the radiosoundings as well. Here, the temperature, humidity and wind profiles of the lower troposphere are used to identify stable layers under convective conditions. These stable layers, e.g. a temperature inversion, often coincide with significant reductions of humidity and wind shear (Seibert et al., 2000). Since the identification of stable layers in temperature profiles is not always straight forward, Θ_v can be used instead of the air temperature (Stull, 1988). Here, in case of a CBL, a decrease of Θ_v reveals

unstable atmospheric conditions, a constant Θ_v neutral atmospheric conditions and an increase of Θ_v the beginning of a stable layer (Figure 1-4). Stull (1988) suggested to take the base of the stable layer increased by half of the stable layer depth as the MABL height. Under SBL conditions, the stable layer can even reach the surface. In this case the MABL height depends on sporadic turbulence and can therefore be distinguished from vertical wind shear which influences the vertical gradient of Θ_v (Figure 1-4, SBL case: a, b, c).

1.3.2 Transport modelling

The transport timescale of MABL air into the free troposphere in this thesis were determined from the residence time of surface trajectories below the determined MABL height. These trajectories were computed with the Lagrangian Particle Dispersion Model FLEXPART, developed at the Norwegian Institute for Air Research in the Department of Atmospheric and Climate Research (Stohl et al., 2005). The model includes various parameterizations, e.g. for boundary layer and free troposphere turbulence and moist convection (Stohl and Thomson, 1999;Forster et al., 2007). 6-hourly meteorological input fields from the assimilation reanalysis product ERA-Interim (Dee et al., 2011) were used, including air temperature, boundary layer height, horizontal and vertical wind, humidity and convective, respectively large scale precipitation with a spatial resolution of 1° x 1° at 60 vertical levels up to 0.1 hPa. Except for the DRIVE ship campaign, radiosonde observations were instantly uploaded and assimilated into the Global Telecommunication System (GTS) to improve the accuracy of the ERA-Interim meteorological input fields for our investigations. For the investigation of the air mass transport, 10,000 trajectories were launched along the cruise tracks during SHIVA and M91. The release events were synchronized with the sampling of atmospheric and surface ocean data on the ships and performed within a time frame of ± 30 minutes and an area of 400 m^2 around the measurement locations. The time, these trajectories needed to exceed the determined MABL height was then related to the contribution of oceanic emissions to the MABL air content of the three investigated VSLS. In this mass balance calculation, the oceanic delivery acted against the loss of trajectories out of the MABL and the chemical degradation of the compounds in the MABL. The resulting imbalance was compensated by the advective delivery, respectively background concentration of the compounds in the MABL.

To estimate the contribution of MABL air and the VSLS therein to free tropospheric abundances, the volume of MABL air (400 m^2 x specific MABL height) was equally distributed to the trajectories of each release event. Each air parcel was then transported along the trajectory and related to the free tropospheric air masses above the measurement location of 400 m^2 assuming no horizontal

distribution. In combination with the source-loss estimate from the oceanic emissions, a direct contribution of the ocean to the free tropospheric VSLS abundances was derived. The methods are explained in detail in manuscript 3 and 5.

1.4 VSLS study regions

Tropical regions generally show the highest oceanic emissions of VSLS (Section 1.2.2). Krüger and Quack (2013) identified the tropical West Pacific as a strong oceanic source for atmospheric bromine. In addition, convective transport can lead to significant contribution of VSLS to the halogen budget in the free troposphere and stratosphere (Section 1.2.4). This thesis concentrates on three different tropical oceanic regimes of VSLS and their contributions to atmospheric abundances: open ocean, coasts and upwelling regions. Coastal upwelling regions of tropical oceans are investigated by the DRIVE campaign in the Northeast Atlantic and by the M91 campaign in the Southeast Pacific (Section 1.4.1). The open ocean and coastal regions are covered by the SHIVA campaign in the South China and Sulu Seas (Section 1.4.2).

1.4.1 Oceanic upwelling in the Northeast Atlantic and the Southeast Pacific

Coastal oceanic upwelling is caused by the combination of steady winds blowing along coasts and the Earth's Coriolis force. At the eastern boundaries of tropical oceans, southward surface winds on the northern hemisphere can create surface stress that leads to a net movement of surface water to the right due to Ekman transport, respectively to the left for northward winds on the southern hemisphere (Colling, 2001). The surface water is then replaced by cold and dense, nutrient rich deep upwelling water (Mann and Lazier, 2006). Coastal upwelling regions are linked to enhanced primary and VSLS production (Quack et al., 2007b;Carpenter et al., 2009;Raimund et al., 2011;Hepach et al., 2014) and may therefore significantly contribute to the atmospheric VSLS budget. Two different coastal upwelling regions are part of the investigations in this thesis, the Mauritanian upwelling in the Atlantic Ocean and the Peruvian upwelling in the Pacific Ocean. Upwelling along the Mauritanian coast occurs between 10° N – 25° N and is bound to seasonal variations of the trade winds (Mittelstaedt, 1986;Tomczak and Godfrey, 2003). The Peruvian upwelling extents between 4° N and 40° S along the west coast of South America. In this region, the northward winds sustain oceanic upwelling throughout the year (Zuta and Guillén, 1970;Tarazona and Arntz, 2001). Given that oceanic

upwelling areas are expected to be source regions for VSLS in the atmosphere, the transport of warmer surface air over cold upwelling water is expected to lead to stable atmospheric boundary layer conditions and thus a suppressed vertical mixing (Höflich, 1972). The influence of these marine regimes on the atmospheric VSLS is one key investigation of this thesis.

1.4.2 The South China and Sulu Seas in the tropical West Pacific

The South China Sea is part of the Pacific Ocean and can be described as marginal sea. Almost completely surrounded by land mass it covers an area of about 3.3 million km^2 and includes hundreds of islands, atolls, reefs and banks. Major rivers flowing into the South China Sea are e.g. Jiulong, Mekong, Min, Pahang, Pampanga, Pearl and Rajang (Morton and Blackmore, 2001). Due to its geographical position between the equator and the Tropic of Cancer at 22° N, and between 100° – 120° E (IHO, 1953) it is influenced by the moist Southwest Monsoon in summer, which leads to a clockwise ocean circulation pattern of the South China Sea, and by the dry Northeast Monsoon in winter, which creates an anticlockwise circulation pattern in the South China Sea. Adjacent to the South China Sea in the southeast and separated by Palawan is the Sulu Sea (Morton and Blackmore, 2001). The Sulu Sea covers about 0.4 million km^2 and includes several islands and reefs (IHO, 1953). Throughout the year it is dominated by western currents. Both, the South China and Sulu Seas are furthermore known to be habitat for several macro algae species (Morton, 1993;Liao et al., 2013) that lead to elevated oceanic concentrations of brominated VSLS (Nadzir et al., 2014) and significant halocarbon emissions in this region (Ziemianski et al., 2005;Leedham et al., 2013); these VSLS may be transported into higher altitudes of the atmosphere and contribute to oxidation of the atmosphere (Section 1.2.4). Therefore this thesis as well investigates the VSLS contribution from oceanic emissions of this hot spot region to the MABL and the free troposphere abundances. Vertical transport timescales in this expected strong convective region are investigated and ship and aircraft observations in the South China and Sulu Seas are compared and interpreted.

2. Thesis outline

The aim of this thesis is to investigate the influence of marine emissions and meteorological constraints on atmospheric VSLS (here: bromoform, dibromomethane and methyl iodide) abundances above the oceans. The results are based on ship observations in the Northeast Atlantic during DRIVE, in the South China and Sulu Seas during the combined ship and aircraft campaign SHIVA and in the Southeast Pacific during the M91 ship cruise. The investigations of this thesis started from the knowledge that brominated and iodinated VSLS are released from ocean surface waters, and enhanced atmospheric mixing ratios of e.g. bromoform are observed above coastal areas and upwelling regions, e.g. off the coast of Mauritania (Quack et al., 2007a). However, local oceanic emissions were not sufficient to explain the observed high atmospheric mixing ratios and implied either the need for an additional source of bromoform to the atmosphere, or an external additional factor. Available observations of the Mauritanian upwelling led to three new questions, which are addressed in the first manuscript "Impact of the marine atmospheric boundary layer conditions on VSLS abundances in the eastern tropical and subtropical North Atlantic Ocean" (Fuhlbrügge et al., 2013):

1. Is there an additional source for halocarbons in the Mauritanian upwelling?
2. How do meteorological parameters and lower atmospheric conditions influence VSLS mixing ratios above the Mauritanian upwelling?
3. Which factors drive the observed diurnal variability of atmospheric VSLS abundances in the tropical and subtropical Northeast Atlantic?

The influence of meteorological parameters on oceanic emissions is investigated in the second manuscript "Drivers of diel and regional variations of halocarbon emissions from the tropical North East Atlantic" (Hepach et al., 2014) with the question:

4. What influences diel and regional variations of VSLS emissions in the tropical Northeast Atlantic?

To further improve the understanding of oceanic contributions to atmospheric VSLS abundances, this thesis also investigates atmospheric VSLS abundances in an expected tropical hot spot region with strong atmospheric convective activity. Due to high convective activity, local VSLS sources were expected to significantly contribute to the upper troposphere and stratosphere. The observations during SHIVA are investigated with a new method, which can reveal the contribution of oceanic emissions to marine atmospheric abundances. The development of a simple mass-balance model,

applying data from high resolution oceanic and atmospheric halocarbon measurements and radiosonde launches together with the investigation of atmospheric transport with FLEXPART, lead to the revelation of "The contribution of oceanic very short lived halocarbons to marine and free troposphere air over the tropical West Pacific" in manuscript 3 (Fuhlbrügge et al., 2015b) and the "Observation of the Variations of Very Short-Lived Halocarbon Emissions in Tropical Coastal Marine Boundary Layer" in the manuscript 4 (Sentian et al., 2015) under the research questions

5. Are the South China and Sulu Seas significant source regions for atmospheric VSLS?
6. What is the role of meteorological constraints on atmospheric VSLS abundances in this convective region?
7. Can the oceanic VSLS emissions in these regions explain the MABL and free troposphere abundances observed on the ship and aircraft?
8. How well do different atmospheric VSLS measurements compare with each other?

The results of these studies raised new questions, whether the findings from the Mauritanian upwelling can be generalized for other oceanic upwelling regions, e.g. the Peruvian upwelling, where observations of oceanic VSLS emissions and atmospheric VSLS abundances were not present before the M91 cruise. The following questions were answered in manuscript 5: "Meteorological constraints on oceanic halocarbons above the Peruvian Upwelling" (Fuhlbrügge et al., 2015a) and manuscript 6: "Contributions of biogenic halogenated compounds from the Peruvian upwelling to the tropical troposphere" (Hepach et al., 2015, to be submitted):

9. To what extent do oceanic VSLS emissions from the Peruvian upwelling contribute to the observed marine VSLS abundances?
10. Are the VSLS observations from the Peruvian upwelling similar to the Mauritanian upwelling?
11. Is the adjacency of atmospheric and marine VSLS controlled by oceanic upwelling regimes?

3. Results

3.1 Manuscript 1

Impact of the marine atmospheric boundary layer conditions on VSLS abundances in the eastern tropical and subtropical North Atlantic Ocean

S. Fuhlbrügge[1], K. Krüger[1*], B. Quack[1], E. Atlas[2], H. Hepach[1], and F. Ziska[1]

[1] GEOMAR Helmholtz-Zentrum für Ozeanforschung Kiel, Kiel, Germany

[2] Rosenstiel School of Marine and Atmospheric Science (RSMAS), Miami, USA

[*] now at Department of Geosciences, University of Oslo (UiO), Oslo, Norway

Published in: Atmospheric Chemistry and Physics, Vol. 13, 6345-6357, doi: 10.5194/acp-13-6345-2013, 2013.

Atmos. Chem. Phys., 13, 6345–6357, 2013
www.atmos-chem-phys.net/13/6345/2013/
doi:10.5194/acp-13-6345-2013

Atmospheric Chemistry and Physics Open Access

Impact of the marine atmospheric boundary layer conditions on VSLS abundances in the eastern tropical and subtropical North Atlantic Ocean

S. Fuhlbrügge[1], K. Krüger[1], B. Quack[1], E. Atlas[2], H. Hepach[1], and F. Ziska[1]

[1]GEOMAR Helmholtz-Zentrum für Ozeanforschung Kiel, Kiel, Germany
[2]Rosenstiel School for Marine and Atmospheric Sciences, Miami, Florida, USA

Correspondence to: K. Krüger (kkrueger@geomar.de)

Received: 20 November 2012 – Published in Atmos. Chem. Phys. Discuss.: 5 December 2012
Revised: 13 May 2013 – Accepted: 30 May 2013 – Published: 4 July 2013

Abstract. During the DRIVE (Diurnal and Regional Variability of Halogen Emissions) ship campaign we investigated the variability of the halogenated very short-lived substances (VSLS) bromoform ($CHBr_3$), dibromomethane (CH_2Br_2) and methyl iodide (CH_3I) in the marine atmospheric boundary layer in the eastern tropical and subtropical North Atlantic Ocean during May/June 2010. The highest VSLS mixing ratios were found near the Mauritanian coast and close to Lisbon (Portugal). With backward trajectories we identified predominantly air masses from the open North Atlantic with some coastal influence in the Mauritanian upwelling area, due to the prevailing NW winds. The maximum VSLS mixing ratios above the Mauritanian upwelling were 8.92 ppt for bromoform, 3.14 ppt for dibromomethane and 3.29 ppt for methyl iodide, with an observed maximum range of the daily mean up to 50 % for bromoform, 26 % for dibromomethane and 56 % for methyl iodide. The influence of various meteorological parameters – such as wind, surface air pressure, surface air and surface water temperature, humidity and marine atmospheric boundary layer (MABL) height – on VSLS concentrations and fluxes was investigated. The strongest relationship was found between the MABL height and bromoform, dibromomethane and methyl iodide abundances. Lowest MABL heights above the Mauritanian upwelling area coincide with highest VSLS mixing ratios and vice versa above the open ocean. Significant high anti-correlations confirm this relationship for the whole cruise. We conclude that especially above oceanic upwelling systems, in addition to sea–air fluxes, MABL height variations can influence atmospheric VSLS mixing ratios, occasionally leading to elevated atmospheric abundances. This may add to the postulated missing VSLS sources in the Mauritanian upwelling region (Quack et al., 2007).

1 Introduction

Natural halogenated very short-lived substances (VSLS) contribute significantly to the halogen content of the troposphere and lower stratosphere (WMO, 2011). On-going environmental changes such as increases in seawater temperature and nutrient supply, as well as decreasing pH, are expected to influence VSLS production in the ocean. Thus, the oceanic emissions of VSLS might change in the future and, in connection with an altering efficiency of the atmospheric upward transport, might lead to significant future changes of the halogen budget of the troposphere/lower stratosphere (Kloster et al., 2007; Pyle et al., 2007; Dessens et al., 2009; Schmittner et al., 2008; Montzka and Reimann, 2011), as well as changes to the tropospheric oxidation capacity (Hossaini et al., 2012). Within the group of brominated VSLS, bromoform ($CHBr_3$) and dibromomethane (CH_2Br_2) are the largest natural sources for bromine in the troposphere and stratosphere. In combination with iodine compounds (i.e. methyl iodide, CH_3I), they can alter tropospheric oxidation processes, including ozone depletion (Read et al., 2008). The VSLS have comparably short tropospheric lifetimes (days to months); however, they can be rapidly transported by deep convection, especially in the tropics, to the upper troposphere and lower stratosphere and contribute to ozone depletion

there (Warwick et al., 2006; WMO, 2007, 2011; Tegtmeier et al., 2012, 2013). Previous studies have reported distinctive halocarbon emissions in tropical coastal and shelf water regions due to high biological productivity, i.e. by macro algae, seaweed and phytoplankton (Gschwend et al., 1985; Manley and Dastoor, 1988; Sturges et al., 1992; Moore and Tokarczyk, 1993; Carpenter and Liss, 2000; Quack et al., 2007). Elevated mixing ratios of the compounds have been found within the marine atmospheric boundary layer (MABL) around the Cape Verde Islands with a mean (range) for $CHBr_3$ of 8 (2.0–43.7) ppt, CH_2Br_2 of 2 (0.7–8.8) ppt and CH_3I of 3 (0.5–31.4) ppt (O'Brien et al., 2009) and in the area of the Mauritanian upwelling with a mean (range) of $CHBr_3$ around 6 (3–12) ppt (Carpenter et al., 2007; Quack et al., 2007) and CH_2Br_2 of 2.4 (1.75–3.44) ppt by Quack et al. (2007). These mean mixing ratios from the tropical Atlantic Ocean agree well with other tropical oceanic areas (e.g. Atlas et al., 1993; Butler et al., 2007). Quack et al. (2004) suggested regionally enhanced biogenic production in the water column of the Mauritanian upwelling and a high sea-to-air flux of VSLS to be responsible for elevated tropospheric VSLS mixing ratios in this region. However, Carpenter et al. (2007) and Quack et al. (2007) both pointed out that the marine boundary layer height, besides additional potential coastal sources, may affect the tropospheric VSLS mixing ratios as well. The theory of warm offshore air flowing over cool water and creating a stable internal boundary layer, as suggested by Garratt (1990), applies well in the area of the cold Mauritanian upwelling. Here, the sea surface roughness and near surface turbulence reduce each other over the water, while the flow leads to a collapse of turbulence and a very stable stratification of the lowermost atmosphere, as was observed by Vickers et al. (2001) at the coast of the United States and modelled by Skyllingstad et al. (2005).

In this study, we present first results from the DRIVE (Diurnal and Regional Variability of Halogen Emissions) ship campaign during May/June 2010, comprising high-resolution meteorological and VSLS measurements. We investigate the meteorological constraints on the VSLS abundances and whether the cold waters upwelled along the Mauritanian coast have a verifiable influence on the atmospheric boundary layer height and therefore on the mixing of air within the lowermost troposphere. The accompanying study by Hepach et al. (2013) investigates the VSLS sources in the ocean and the sea-to-air fluxes in detail.

This paper begins with a short overview of the meteorological conditions during the DRIVE cruise, followed by a data and method description (Sect. 2.1). In Sect. 3 we present results from the meteorological and VSLS measurements and the influence of meteorology and MABL height on the VSLS mixing ratios and emissions. Finally, a summary is given in Sect. 4.

2 Data and methods

2.1 Cruise overview

During May/June 2010 the DRIVE (P399/2-3) campaign examined the formation and emission of halocarbons and reactive inorganic halogen compounds in the eastern tropical and subtropical North Atlantic Ocean (Bange et al., 2011) as part of the SOPRAN (Surface Ocean Processes in the Anthropocene: www.sopran.pangaea.de) project. The main objectives are to investigate the diurnal and regional variability of marine short-lived substances, as well as oceanic influences on the atmosphere.

The ship expedition was carried out on board the German research vessel (R/V) *Poseidon*. The cruise itself was split into two legs: P399/2 (31 May–17 June 2010) from Las Palmas to Las Palmas and P399/3 (19–24 June 2010) from Las Palmas to Vigo, Spain. For diurnal observations, hourly VSLS measurements were performed at six 24 h stations during leg P399/2. Positions and times of the 24 h stations are given in Table 1. The location of the 24 h stations were chosen to cover the nutrient-rich coastal upwelling region near the Mauritanian coast as well as the nutrient-poor regions near the Cape Verde Islands. In addition, 21 atmospheric VSLS samples were taken during the return from the last station in the Mauritanian upwelling region to Las Palmas (Gran Canaria). During the transit leg P399/3, an additional 20 atmospheric air samples were taken. All VSLS measurements were also integrated into the HalOcAt database used for the Ziska et al. (2013) climatology.

2.2 Meteorology and MABL height

Meteorological data have been collected by the automatic on-board weather station of the German Weather Service (DWD): air and water temperatures, wind speed and direction, humidity and air pressure were recorded once per second and are averaged to 10 min means for our analysis. GRAW DFM-06 radiosondes (http://www.graw.de) were launched from the working deck of R/V *Poseidon* at about 3 m above sea level during the cruise to profile the atmospheric composition of air temperature (resolution: 0.1 °C; accuracy: < 0.2 °C), relative humidity (resolution: 1 %; accuracy: < 5 %), and wind (wind speed accuracy: $< 0.2\,m\,s^{-1}$; horizontal position accuracy: < 5 m) (http://www.gematronik.com/fileadmin/media/pdf/GRAW-Brochure_V01.30_en.pdf) from the sea level up to the middle stratosphere ($\sim$30 km altitude). At the 24 h stations, the launch frequency was increased from one radiosonde per day at 12:00 UTC to four per day at 00:00, 06:00, 12:00 and 18:00 UTC, amounting to 41 launches for the whole cruise.

The atmospheric boundary layer height is determined using the approaches summarized by Seibert et al. (2000). These methods include practical and theoretical

Table 1. 24 h stations: position and date.

24 h station	Position	Date/Time
1st	17.6° N, 24.0° W	3 June (23:00 UTC)–4 June 2010 (22:00 UTC)
2nd	18.0° N, 21.0° W	6 June (19:00 UTC)–7 June 2010 (17:00 UTC)
3th	18.0° N, 18.0° W	8 June (18:00 UTC)–9 June 2010 (17:00 UTC)
4th	18.5° N, 16.5° W	10 June (12:00 UTC)–11 June 2010 (11:00 UTC)
5th	19.0° N, 16.5° W	11 June (16:00 UTC)–12 June 2010 (15:00 UTC)
6th	20.0° N, 17.25° W	13 June (04:00 UTC)–14 June 2010 (03:00 UTC)

determinations from radiosoundings. The vertical extension of the boundary layer is in general limited aloft by a temperature inversion or a stable layer, or by a significant reduction in air moisture. Two general types of boundary layers exist, the convective boundary layer (CBL), whose stable layer is found between the lower 100 m of the atmosphere and about 3 km height, and the stable boundary layer (SBL), characterized by a surface inversion. In the case of a CBL, it is recommended to take the height of the base of the inversion, increased by half of the inversion layer depth (Stull, 1988). For a SBL we assume the absence of turbulence and vertical mixing (Garratt, 1990) and further declare that the boundary layer stays close to the surface. According to this, we subjectively determined the height of the boundary layer in our study from the temperature and humidity profiles, and additionally from the bulk Richardson number of the following equation (Troen and Mahrt, 1986; Vogelezang and Holtslag, 1996):

$$Ri_{\mathrm{B}} = \frac{gz(\theta_z - \theta_s)}{\theta_s(u^2 + v^2)}. \quad (1)$$

The quantities g and z are the gravitation acceleration and the geometric height. $\theta_z\theta_z$ and $\theta_{\mathrm{s}}\ \theta_{\mathrm{s}}$ are the virtual potential temperature at the height z and at the surface, and u and v are the zonal and meridional wind components. The virtual potential temperature can be regarded as a stability criterion for the atmosphere, considering the air moisture. It is constant with height for neutral conditions, increases for stable conditions and decreases if the air is statically unstable. To identify the boundary layer height theoretically, a fixed critical bulk Richardson number of $Ri_{\mathrm{c}} = 0.25$ is chosen as a threshold, following Sorensen (1998), where $Ri_{\mathrm{B}} \geq Ri_{\mathrm{c}}$. Due to missing wind data in the lowermost atmosphere during a number of radiosonde launches (failure of GPS sensor), we were not always able to determine Ri_{B} for the lower boundary layer. Therefore we use the subjectively determined boundary layer height for our investigations and calculate Ri_{B} to confirm our determined MABL height.

2.3 Air mass origin

For the analysis of the air mass origin, HYSPLIT trajectories (http://ready.arl.noaa.gov/HYSPLIT.php), based on NCEP/NCAR Reanalysis 1 (NNR), were calculated online. The NNR is a first-generation reanalysis from 1948 to the present and has a horizontal resolution of 208 km (T62) and 28 vertical levels (L28) with a model top at about 3 hPa. The data are globally distributed on a 2.5° latitude × 2.5° longitude Gaussian grid with a total of 144 × 73 grid points (Kalnay et al., 1996; Kistler et al., 2001).

2.4 VSLS measurements

A total of 187 air samples were taken on the monkey deck of R/V *Poseidon*, about 10 m above sea level. The air was pressurized up to 2 standard atmospheres in pre-cleaned stainless steel canisters, each with a volume of 2.6 L. The canisters were analysed within three months after the expedition at the Rosenstiel School for Marine and Atmospheric Sciences (RSMAS, Miami, Florida). The stability of the atmospheric samples has been demonstrated during more than 10 years of work with stainless steel canisters. The compounds reported here are typically stable for at least 6 months or more. The precision is estimated as an uncertainty of approximately 5 %, obtained from the standard variability during analysis and from examination of multiple samples within the same air mass. The analysis of the gases is performed with gas chromatography/mass spectrometry (GC/MS), while the calibration gases are standardized by gas chromatography with an atomic emission detector (AED) (Schauffler et al., 1999), and the entire standardization procedure was additionally adjusted to the NOAA scale in order to have better comparability to the NOAA measurements at surface stations. The preparation of standard gases is described in Montzka et al. (2003).

Our study concentrates on the atmospheric abundances of three VSLS: methyl iodide with a lifetime of ∼4 days (Solomon et al., 1994), bromoform of ∼26 days (Ko et al., 2003) and dibromomethane of ∼120 days (Ko et al., 2003).

Samples for dissolved halocarbons in sea water were taken from the continuously working pump from the ship's moon pool at a depth of 5 m on a nearly hourly basis at every 24 h station. A purge and trap system attached to a gas chromatograph with mass spectrometric detection in single-ion mode was used for analysis of the samples with a precision within 10 % determined from duplicates (Hepach et al., 2013).

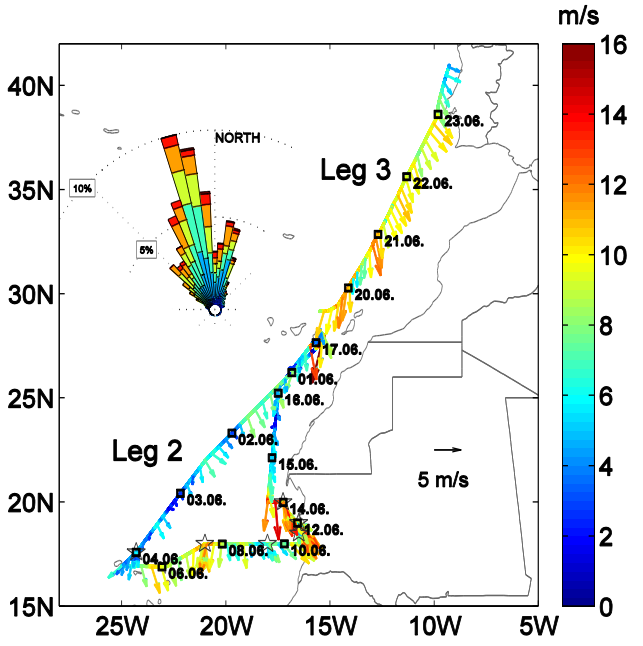

Fig. 1. DRIVE cruise track. In addition, the 3-hourly wind speed [m s^{-1}], direction (10 min averages) and windrose for the whole cruise are shown.

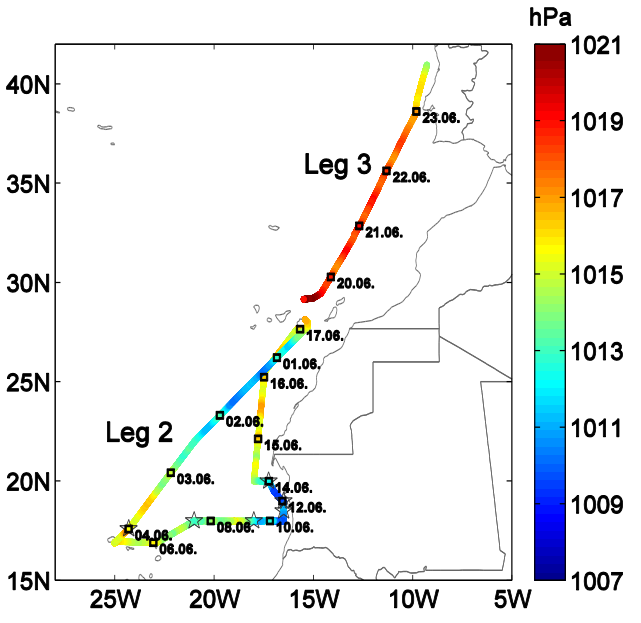

Fig. 2. 10 min average measurements of air pressure [hPa]. The stars indicate position and time of the diurnal stations.

2.5 Sea-to-air flux calculations

Sea-to-air fluxes (F) of methyl iodide, dibromomethane and bromoform were calculated with the air–sea gas transfer coefficient k_w and the air–sea concentration gradient Δc (Hepach et al., 2013):

$$F = k_w \cdot \Delta c \quad (2)$$

The parameterization of Nightingale et al. (2000), based on instantaneous wind speeds (10 min averages) and temperature-dependent Schmidt numbers according to Quack and Wallace (2003), was applied to determine k_w. Δc was calculated from the simultaneous water and air measurements at the 24 h stations.

3 Results

3.1 Meteorology

The cruise was mainly exposed to moderate weather conditions. Contrary to the climatological wind direction of northeasterly trade winds in the subtropics and westerlies north of 30° N during May/June, the mean absolute wind direction was NNW (Fig. 1) with a mean direction of 349° during leg 2 and 344° during leg 3. This caused a predominant influence of air masses with marine background conditions coming from the open North Atlantic Ocean. The mean wind speed during the whole cruise was moderate to fresh for both legs, with 7.4 m s^{-1} ± 2.9 m s^{-1} during leg 2 and 9.3 m s^{-1} ± 1.6 m s^{-1} during leg 3. The total air pressure difference of 13.4 hPa also reflects the moderate and steady weather conditions during the whole cruise with a minimum of 1007.6 hPa on 11 June 2010 close to the Mauritanian coast and a maximum air pressure of 1021 hPa at the beginning of leg 3 on 19 June 2010 close to the Canary Islands (Fig. 2). In addition, typical tropical diurnal variations up to 4 hPa (see also Krüger and Quack, 2012) due to atmospheric tides were observed in this study. The time series of 10 min average measured surface air temperature (T_{SAT}), sea surface temperatures (T_{SST}) and the difference ΔT (T_{SAT}–T_{SST}) are shown in Fig. 3. The temperature difference is related to the heat flux between atmosphere and ocean and indicates suppressing of convection, turbulence and therefore mixing within the boundary layer for a positive temperature difference (positive heat flux) and enhanced mixing for negative heat flux. As the ship cruise started to the south, the air and water temperatures increased until the maximum air temperature of 25.8 °C was recorded directly after the stop at Mindelo (Cape Verde Islands). On 11 June 2010, right after the 4th 24 h station, the ship reached the Mauritanian upwelling region at 18.75° N, 16.5° W. This is noticeable from the abrupt decrease in the water temperature and connected to an increase of the heat flux from the atmosphere to the ocean. After one day, the air temperature also drops, until T_{SAT} and T_{SST} stabilize between 18 °C and 20 °C (station 5). On 14 June 2010, after the ship has left the last 24 h station, the water temperature increases to about 23.5 °C. This increase coincides with a wind speed maximum of about 16 m s^{-1} from the north, indicating transport of water masses from outside the Mauritanian upwelling

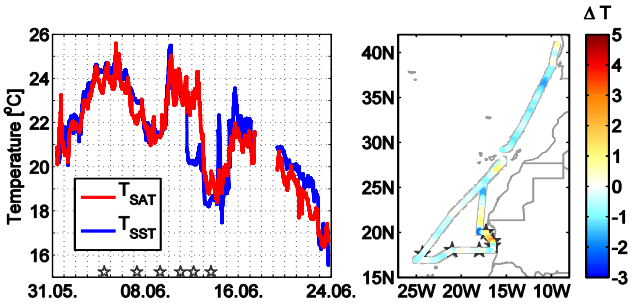

Fig. 3. Left: 10 min average measurements of T_{SAT} and T_{SST} [°C]. The stars indicate position and time of the diurnal stations. Right: the temperature gradient is given in [K].

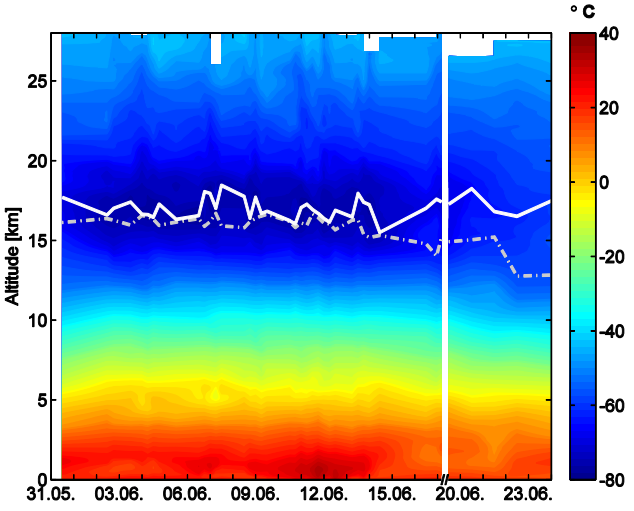

Fig. 4. Air temperature cross sections [°C] from radiosoundings for the whole cruise. Cold point tropopause and lapse rate tropopause are marked by the continuous and the dash-dotted lines, respectively. The measurement gap between leg 2 and 3 is shortened.

towards the ship, until the water temperature drops again to about 18 °C. On 15 June 2010 the ship left the Mauritanian upwelling region, indicated by increasing air and water temperatures until both decreased again while heading northward. A sudden decrease of the water temperature is also observed from 23 to 24 June 2010, as the ship enters the Iberian upwelling (Relvas and Barton, 2002).

3.1.1 Marine atmospheric boundary layer

In the following, we use the radiosonde measurements to analyse the state of the lower atmosphere. Profiles of air temperature along the cruise track are shown in Fig. 4. Lowest temperatures of −80 °C are observed between 2 and 15 June 2010 at 17 km height, indicating tropical air masses south of 25° N during leg 2. Two different tropopause definitions are used to identify the transition between tropical and extra-tropical air masses: the cold point

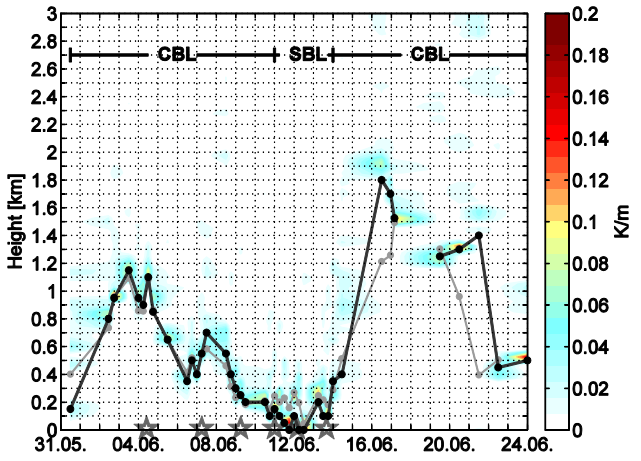

Fig. 5. Virtual potential temperature gradient (colour shading) with derived MABL heights (lines, in km). The black line shows the subjectively determined MABL height from temperature and humidity profiles, and the grey line is determined theoretically (Sect. 2.2). CBL and SBL identify convective and stable boundary layers. The 24 h stations are marked with stars.

tropopause (CPT; Highwood and Hoskins, 1998) and the lapse rate tropopause (LRT, WMO, 1957). During leg 2, the heights of the CPT and LRT are detected between 16 and 17 km altitude. A change of the atmospheric regime is reflected by the decrease of the LRT height to 15 km in contrast to the CPT height after 15 June 2010 at the end of leg 2, as the ship enters the extratropics. The air temperature profiles also reveal typical "trade inversions" (Neiburger et al., 1961) between 1 and 2 km height from the beginning of the cruise until 4 June and from 16 June 2010 until the end of the cruise. Beginning on 4 June 2010, the temperature inversions descend in height, until they migrate, due to cold upwelling deep water (Fig. 3) in the Mauritanian upwelling, to intense surface inversions. The neutral and stable stratification within the lower 3 km of the troposphere, and therefore the upper limit of the atmospheric boundary layer during the cruise, is shown by Fig. 5. The subjectively and theoretically derived MABL heights (see Sect. 2.2) show a good agreement with each other. Differences are found above the Mauritanian upwelling, due to missing near-surface winds for the calculation of the bulk Richardson number, but also at the end of leg 2 and the beginning of leg 3. This may be caused by our fixed Ri_c, which we took for convenience.

Except for the area at and south of the upwelling, observed from 11 to 14 June 2010, where we observed a SBL, the cruise was predominantly characterized by CBLs, without distinct short time or diurnal variations, considering the launch frequencies. Boundary layer heights from the surface up to 400 m at the upwelling area and about 400–2000 m above the open ocean agree with heights derived from trajectory models from previous studies along the Mauritanian coast (Carpenter et al., 2007; Quack et al., 2007). During

Table 2. Observed mixing ratios [in ppt] of bromoform ($CHBr_3$), dibromomethane (CH_2Br_2), their ratio and methyl iodide (CH_3I) for the whole cruise, open ocean (leg 2 except stations 3–6, and leg 3) and coastal stations (stations 3–6). Given are the mean, the range and the standard deviation values.

	$CHBr_3$ (ppt)		CH_2Br_2 (ppt)		$\frac{CH_2Br_2}{CHBr_3}$	CH_3I (ppt)	
	Mean (range)	stdv of mean	Mean (range)	stdv of mean	Mean	Mean (range)	stdv of mean
Whole cruise	3.75 (0.48–9.9)	2.29	1.85 (0.89–3.14)	0.63	0.69	1.25 (0.51–3.29)	0.56
Open ocean	1.74 (0.48–9.9)	1.34	1.28 (0.89–2.70)	0.31	0.98	0.93 (0.51–2.11)	0.24
Coastal stations	5.60 (4.07–8.92)	1.06	2.37 (1.87–3.14)	0.31	0.43	1.55 (0.90–3.29)	0.62

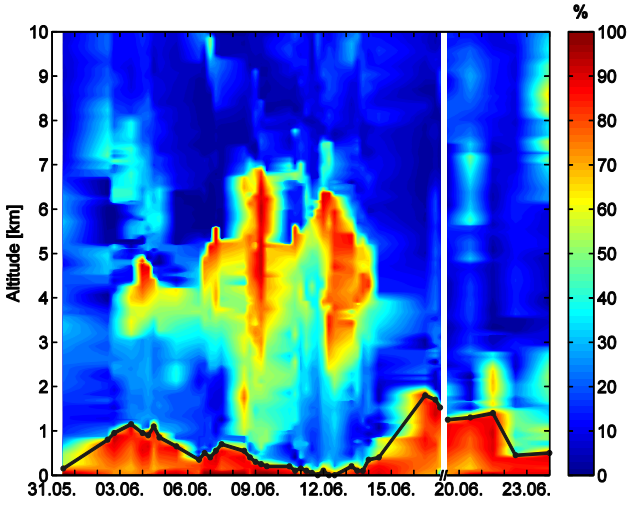

Fig. 6. Relative humidity cross sections [%] from radiosoundings for the whole cruise. The subjectively determined MABL height [km] is marked by the black line. The measurement gap between leg 2 and 3 is shortened.

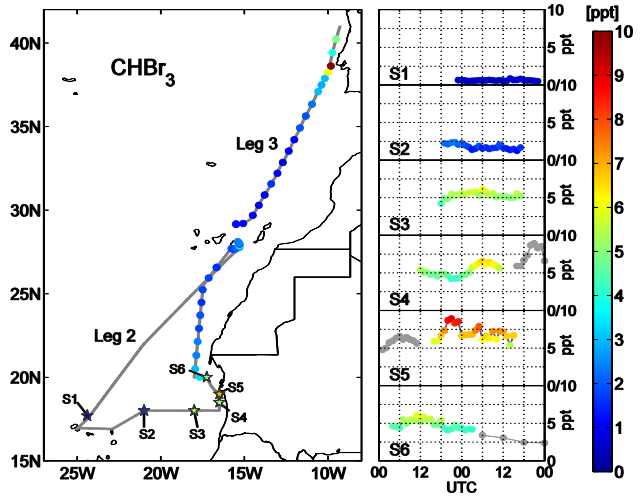

Fig. 7. Bromoform mixing ratios [ppt] measured during the DRIVE ship campaign from 31 May to 24 June 2010. Six 24 h stations (S1–S6) and measurements during transit are colour-coded according to the scale on the right side.

leg 3 the top of the boundary layer decreases from 1.4 km north of the Canary Islands to about 500 m near the coast of the Iberian Peninsula. The height of the MABL is also well reflected in the profiles of the relative humidity during the whole cruise as shown in Fig. 6. The increase of the surface/lowermost troposphere humidity between 15 and 22 June 2010 (Fig. 6) matches the observed elevation of the negative heat flux (Fig. 3). The height of the atmospheric boundary layer, determined from temperature observations, agrees very well with the surface maximum of relative humidity (Fig. 6). The vertical mixing within the MABL seems to be quite well reflected by the relative humidity observations. Especially the small extension of enhanced relative humidity above the surface of the Mauritanian upwelling from 11 to 12 June 2010 is consistent with the assumption of reduced vertical mixing (turbulence) in this area due to the positive heat flux, leading to a very stable and narrow MABL.

3.2 Atmospheric VSLS variability

The diurnal and regional variations of halogenated trace gas abundances in the MABL have been observed with hourly measurements at six 24 h stations near the Cape Verde Islands and in the Mauritanian upwelling. According to the regional distribution of the diurnal stations (Fig. 1), the first two stations (S1, S2) can be combined to an open ocean cluster. The following 4 diurnal stations are furthermore declared as coastal stations (S3–S6), since they show similar physical and biological characteristics (e.g. salinity and chlorophyll *a*) in the surface water (Hepach et al., 2013). Six-hourly measurements were also taken from 14 June 2010 after the 6th station to the coast of Gran Canaria and during leg 3 (19–23 June 2010). Also along the coast of Gran Canaria (17 June 2010) hourly samples were taken.

An increase of atmospheric mixing ratios from the Cape Verde Islands to the Mauritanian upwelling area is found for all three trace gases: bromoform (Fig. 7), dibromomethane (Fig. 8) and methyl iodide (Fig. 9). Within the open ocean cluster, the mixing ratios ranged 0.48–9.9 ppt

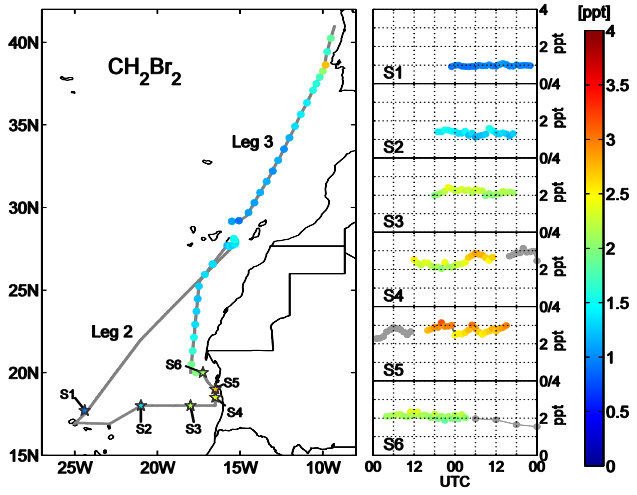

Fig. 8. Dibromomethane mixing ratios [ppt] measured during the DRIVE ship campaign from 31 May to 24 June 2010. Six 24 h stations (S1–S6) and measurements during transit are colour-coded according to the scale on the right side.

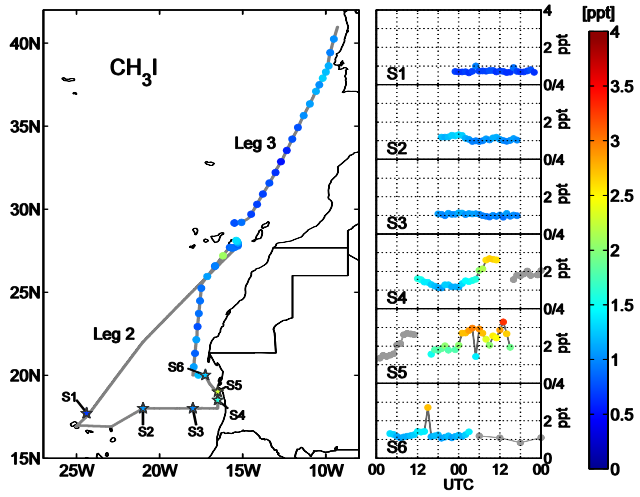

Fig. 9. Methyl iodide mixing ratios [ppt] measured during the DRIVE ship campaign from 31 May to 24 June 2010. Six 24 h stations (S1–S6) and measurements during transit are colour-coded according to the scale on the right side.

with a mean of 1.74 ppt for $CHBr_3$, 0.91–1.59 ppt with a mean of 1.28 ppt for CH_2Br_2, and 0.63–1.32 ppt with a mean of 0.93 ppt for CH_3I. The mixing ratio of CH_2Br_2 and $CHBr_3$ has often been observed to be around 0.1 in source areas, where the air has been influenced e.g. by fresh coastal emissions (Yokouchi, 2005 and references therein). The ratio increases towards the open ocean due to the different lifetimes of both compounds. A higher value implies an aged air mass and aged emission, while a lower value indicates fresher emissions and air masses. With an overall mean CH_2Br_2 / $CHBr_3$ ratio of 1.21 (Table 2) during stations 1 and 2, typical open ocean air masses were observed (Quack et al., 2004; Butler et al., 2007). At the third 24 h station, the bromocarbons increase to 4.22–6.12 ppt for $CHBr_3$ and 1.96–2.42 ppt for CH_2Br_2, while CH_3I mixing ratios remain at open ocean values. A mean CH_2Br_2 / $CHBr_3$ ratio of 0.41 now indicates fresher emissions. Slightly increased atmospheric mixing ratios of $CHBr_3$ with 4.21–6.58 ppt and of CH_2Br_2 with 2.04–2.87 ppt, and a CH_2Br_2 / $CHBr_3$ ratio of 0.46 are found at the 4th 24 h station. For the first time, the CH_3I mixing ratios show intense variations of 1.11–2.68 ppt at this coastal station. In addition, a diurnal pattern is striking for all three VSLS at this station (S4, Fig. 7). They show a slight decrease from 12:00 UTC to 00:00 UTC followed by an increase from 06:00 UTC to 09:00 UTC on the following day, which coincides with a decrease of the MABL height and the sunrise at about 06:30 UTC. The highest atmospheric mixing ratios for all three VSLS during leg 2 were observed during the 5th station at 19° N and 16.5° W. At this station also the most pronounced variations within one day are observed, with maximum mixing ratios of 8.92 ppt for $CHBr_3$, 3.14 ppt for CH_2Br_2 and 3.29 ppt for CH_3I. The extreme minimum of CH_3I at 05:00 UTC appears as an unreliable outlier due to the high variation of more than 1 ppt within two hours, which is nearly consistent with the whole diurnal variation of CH_3I at station 4. Although this station has the lowest CH_2Br_2 / $CHBr_3$ ratio of 0.40 during leg 2, this value is two to three times higher than previously reported ratios of 0.1–0.25 for coastal source regions in the North Atlantic Ocean and the northwest of Tasmania (Carpenter et al., 2003) and tropical islands and the open Pacific Ocean (Yokouchi et al., 2005), suggesting the presence of slightly aged air masses and emissions. While the ship moved away from the Mauritanian coast, southwest of the Banc d'Arguin National Park, the last coastal station (S6) shows an increase of the CH_2Br_2 / $CHBr_3$ ratio to 0.44 and a decrease of the trace gas mixing ratios to 4.85 ppt (range: 4.07–6.01 ppt) for bromoform, 2.11 ppt (1.87–2.34 ppt) for dibromomethane and 1.28 ppt (1.07–2.71 ppt) for methyl iodide. The extreme CH_3I maximum at 15:00 UTC appears again as an outlier. A further decrease of the atmospheric abundances is observed up to 22° N. Mixing ratios thereafter remain nearly constant to the Canary Islands, except for methyl iodide, which shows a maximum of 2 ppt southwest of Gran Canaria. Minor variations occur for all three VSLS at the Canarian coast, while the means of 2.29 ppt $CHBr_3$, 1.38 ppt CH_2Br_2 and 1.14 ppt CH_3I are in agreement with open ocean values and remain at this level until 35° N. An increase of the brominated halocarbons is observed as the cruise approaches the Portuguese coast. While dibromomethane only reaches 2.70 ppt, bromoform reaches the highest mixing ratio of 9.9 ppt during the whole DRIVE cruise close to Lisbon (Portugal), leading to a ratio of both compounds of 0.27. Raimund et al. (2011) related the increased abundances of halogenated trace gases in the Iberian upwelling system to strong intertidal coastal

Table 3. Correlation coefficients of bromoform ($CHBr_3$), dibromomethane (CH_2Br_2) and methyl iodide (CH_3I) mixing ratios with wind speed (w_{spd}), wind direction (w_{dir}), surface air pressure (p), surface air temperature (T_{SAT}), sea surface temperature (T_{SST}), temperature difference ($\Delta T = T_{SAT} - T_{SST}$), relative humidity ($U$), and MABL height. Whole cruise (leg 2 and 3) includes $n = 181$ samples for all parameters except MABL height (30 samples), open ocean (leg 2, except stations 3–6 and leg 3) includes $n = 85$ samples for all parameters except MABL height (15 samples) and coastal stations (stations 3–6) include $n = 96$ samples for all parameters except MABL height (15 samples). Bold coefficients have a p value of less than 5 %.

	$CHBr_3$			CH_2Br_2			CH_3I		
	Whole cruise	Open ocean	Coastal stations	Whole cruise	Open ocean	Coastal stations	Whole cruise	Open ocean	Coastal stations
w_{spd}	**0.23**	**0.23**	−0.17	**0.27**	**0.32**	−0.05	**0.24**	**0.37**	0.06
w_{dir}	**−0.49**	**−0.31**	0.04	**−0.52**	**−0.32**	−0.18	**−0.28**	−0.12	−0.01
p	**−0.76**	−0.01	**−0.53**	**−0.82**	−0.11	**−0.71**	**−0.64**	**−0.33**	**−0.52**
T_{SAT}	−0.04	**−0.68**	**0.42**	0.05	**−0.67**	**0.59**	**0.24**	**−0.26**	**0.48**
T_{SST}	**−0.45**	**−0.70**	−0.04	**−0.39**	**−0.69**	0.13	**−0.21**	**−0.24**	0.00
ΔT	**0.70**	0.17	**0.64**	**0.71**	0.18	**0.63**	**0.73**	−0.13	**0.68**
U	**0.52**	**0.47**	−0.16	**0.50**	**0.58**	**−0.32**	**0.21**	**0.50**	**−0.38**
MABL	**−0.81**	−0.32	**−0.60**	**−0.82**	−0.40	**−0.62**	**−0.64**	**−0.58**	**−0.70**

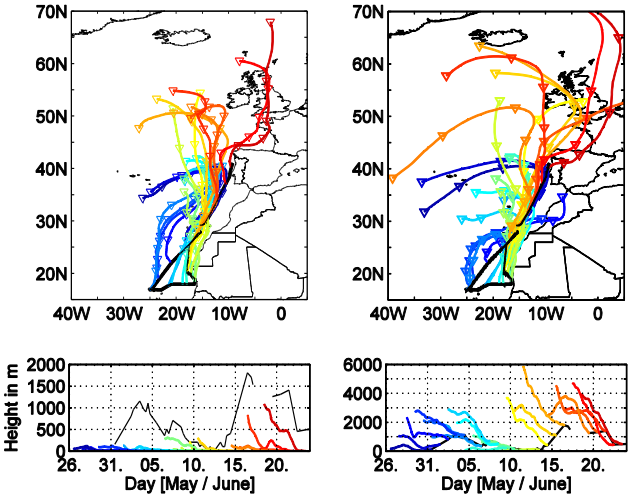

Fig. 10. HYSPLIT 5-day backward trajectories: initiated at the surface (left side) and at the top of the determined marine atmospheric boundary layer (right side) each day at 12:00 UTC. The colours of the trajectories indicate the time when the specific trajectory reached the ships position, e.g. blue at the beginning and red at the end of the cruise. The upper plots show the horizontal and the lower plots the vertical distribution of the trajectories. The black line indicates the height of the MABL. Trajectory and MABL heights are given in [m].

sources and advection of halocarbon-enriched coastal upwelling, but also anthropogenic sources as river outflow are likely (Quack and Wallace, 2003).

3.2.1 Air mass origin

Investigating the air mass history is a good way to reveal potential source regions (Fig. 10). Surface (STs) and boundary layer height trajectories (BLTs) indicate primarily northerly origin of air masses during the cruise. From 31 May to 3 June 2010 the air masses mainly arrive from the Azores. While the HYSPLIT model projects that the STs do not extend 100 m altitude, the BLTs arise from about 3 km height with little Moroccan influence. A high-pressure system, located between the Azores and the coast of Portugal, deflects the air masses up to 40° N–50° N, close to the coast of Portugal, and redirects, in combination with the trade winds, the air southwards to the ship. From 6 to 17 June 2010 the light blue, yellow and orange trajectories show a more varying origin, between 30° N and 60° N. Most of the STs descend from heights up to 300 m to the surface 1–2 days before hitting the ship. This air mass descent is typical for a high-pressure system. Reaching the ground, the surface inversions, as described in Sect. 3.1.1, prevent the air masses from ascending. The resulting stable, isolated and very low boundary layer leads to similar origins of offshore STs and BLTs. In the area of the Mauritanian upwelling, from 10 to 15 June 2010, the trajectories also pass the west coast of Mauritania and the western part of West Sahara within the last 24 h; however, the air approaches predominantly from the North Atlantic Ocean between 45° N and 60° N and west of Great Britain. These origins have also been observed in previous measurement campaigns (Quack et al., 2007; Carpenter et al., 2010). In comparison, the BLTs are spatially more widespread over the North Atlantic Ocean, indicating the higher wind speed in the free troposphere. At leg 3 the STs and BLTs have a mid- to polar latitude origin (30° N to 80° N); however, continental influences from northern Europe dominate for the BLTs east of the prime meridian.

3.3 Meteorological constraints on VSLS variability

To distinguish meteorological constraints on the VSLS abundances we correlate meteorological parameters with bromoform, dibromomethane and methyl iodide (Table 3). In the following we highlight the significant correlations. We find a weak but significant correlation between the trace gas abundances and the wind speed for the open ocean and for the whole cruise. In contrast, the wind direction reveals

an overall anti-correlation of −0.5 for the brominated halocarbons and −0.3 for methyl iodide. This means increased VSLS abundances generally coincide with a westerly wind component and reduced abundances coincide with an easterly wind component during the whole cruise. To evaluate land–sea breeze constraints on the trace gas abundances, we take a look to stations 4 and 5. Indeed, both stations show typical land-sea breeze caused diurnal variations in wind speed and direction. The atmospheric abundances reveal significant high correlations of $r = 0.82$ for bromoform, $r = 0.73$ for dibromomethane and 0.82 for methyl iodide with the wind direction at station 4 in contrast to the overall anti-correlation (not shown here). At the 4th station, trace gas abundances increase with an increasing easterly component of the wind, while the abundances decrease with an increasing westerly wind component, related to differences in air mass origin (coastal versus open ocean), as also shown by the trajectories in Fig. 10. At the 5th station, 3-hourly trajectory calculations reveal ground-level air masses with potential coastal and anthropogenic influence along the coast of Western Sahara, with air masses from the open ocean leading to an increase of the dibromomethane abundances ($r = -0.55$) in contrast to the variations of bromoform and methyl iodide, which seem more related to local sources (not shown here). Anti-correlations of −0.6 to −0.8 are also found between the air pressure and the trace gases, caused by predominantly higher pressures at higher latitudes, and over open ocean, with lower VSLS abundances and vice versa for the coastal stations 3–6. At these stations, the anti-correlation is further dominated by the atmospheric tides of the air pressure and amounts to −0.5 for bromoform and methyl iodide and even −0.7 for dibromomethane. Whether or not this relation between the 12-hourly oscillations of sea level pressure and the trace gas variations can be generalized should be investigated in more detail in a future study. The relative humidity correlates with the trace gases in the open ocean with $r = 0.5$ to 0.6 and at the coastal stations with $r = -0.2$ to −0.4 (Table 3). The vertical distribution of the relative humidity has been a good indicator for mixing in and thickness of the MABL (Sect. 3.1.1), which may point to an additional correlation between the surface relative humidity and the VSLS abundances reflected by the high correlation for the whole cruise. However, over the upwelling areas this relationship does not hold. The cold upwelling water creates a positive ΔT and a negative sensible heat flux that suppresses convection and leads to a low relative humidity, which is in contrast to the VSLS abundances. This would explain the reversed correlation above the upwelling. The VSLS abundances are significantly anti-correlated with SAT and SST variations in the open ocean and correlated with SAT in the coastal upwelling. The sensible heat flux, reflected by the temperature difference ΔT (T_{SAT}–T_{SST}), correlates with r values of at least 0.7 for all trace gases during the whole cruise and at least 0.6 at the coastal stations. The combination of higher air and lower water temperatures coincides with increased trace gas abundances and vice versa, although this is inappropriate for evaporation. This shows that from surface relative humidity one cannot simply infer VSLS abundances or even the MABL height. The temperature difference ΔT further affects the atmospheric stability near the surface. The cold upwelling water at the Mauritanian upwelling converges with warm air from the African coast (Sect. 3.2.1) and creates a negative sensible heat flux between air and water, which cools the near-surface air layer. As a result, surface inversions, or at least a stable stratification of the lower atmosphere, are formed, which suppresses the vertical movement of air. The resulting reduced volume of air that is available for mixing leads to a low MABL height. An anti-correlation of −0.74 between ΔT and the MABL height at the coastal stations confirms this (not shown here). A comparison of bromoform, dibromomethane and methyl iodide with the MABL height during the whole cruise is shown in Fig. 11. Higher VSLS concentrations obviously coincide with a lower MABL height and vice versa. During leg 2 the highest mixing ratios are observed while the MABL height stays between the surface and 500 m in the area of the Mauritanian upwelling (stations 3–6). On the other hand, low mixing ratios measured over the open ocean coincide with a high boundary layer top. The transit towards Vigo (Spain) also shows a decrease of the MABL height and an increase of the three VSLS mixing ratios close to the Iberian coast. In contrast to the other meteorological parameters we derive anti-correlations between the atmospheric trace gas abundances and the MABL height for all regions, reflecting the distinct connection between these variables. The linear correlations of bromoform, dibromomethane and methyl iodide with the MABL height for the whole cruise are represented in Fig. 12a–c. Bromoform, with $r = -0.81$, and dibromomethane, with $r = -0.82$, show the

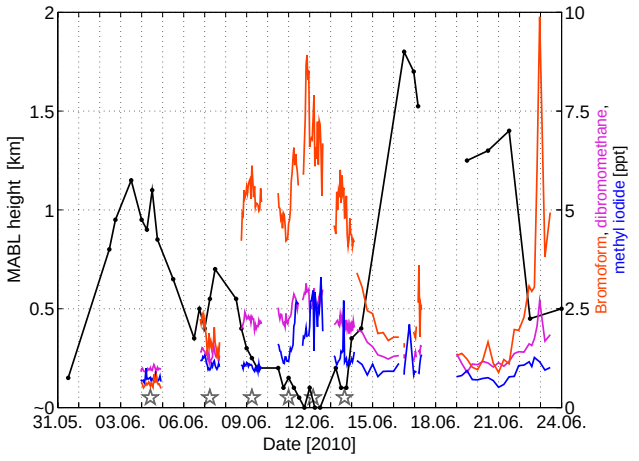

Fig. 11. Comparison of MABL height (left scale, in km) with bromoform, dibromomethane and methyl iodide mixing ratios (right scale, in ppt).

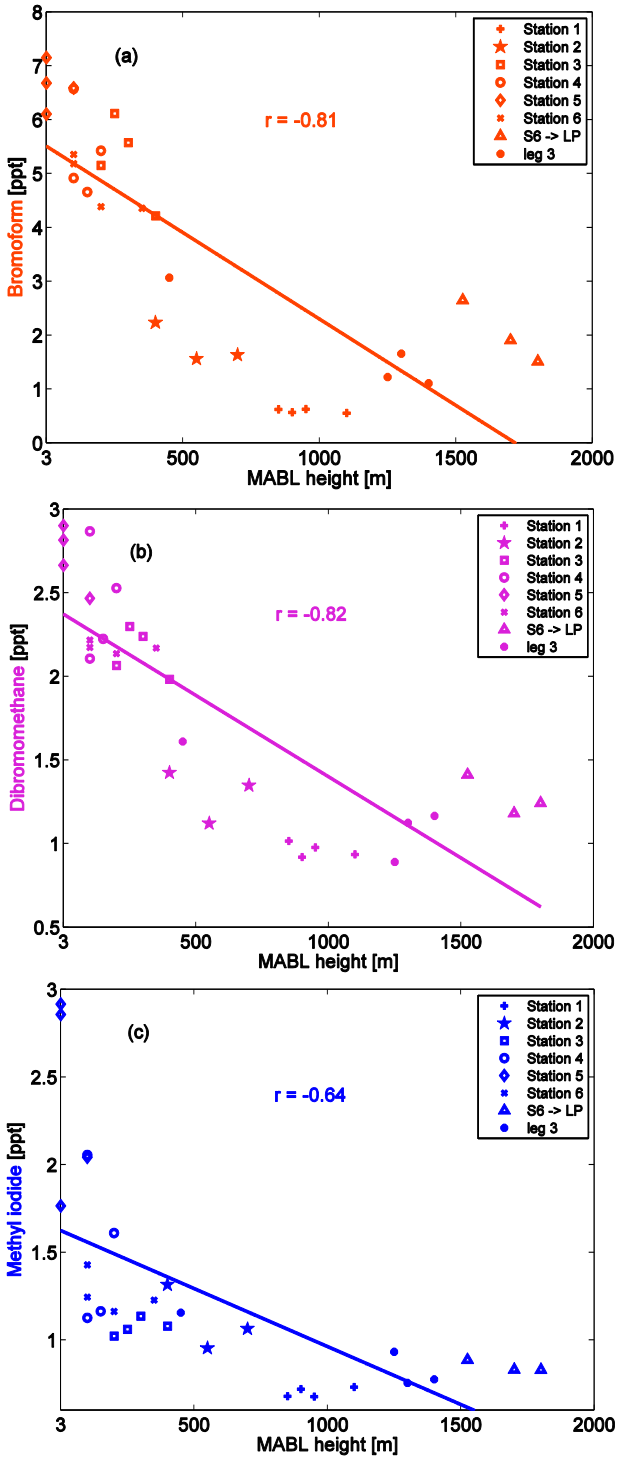

Fig. 12. Correlation between MABL height [m] and **(a)** bromoform, **(b)** dibromomethane and **(c)** methyl iodide abundances [ppt] for the whole cruise. The different markers reflect the different locations: leg 2 including stations 1–6, the transit between station 6 and Las Palmas, and leg 3. The according p values are less than 1 % for all three correlations, with each including 30 samples.

highest anti-correlations. Although the anti-correlation of methyl iodide, $r = -0.64$, is not as high as for the brominated halocarbons, it is significant at the 99 % level.

3.4 Correlations of meteorological parameters and atmospheric abundances with VSLS fluxes

The sea-to-air fluxes, which are calculated depending on wind speed and the concentration gradient Δc between sea water and air (Sect. 2.1), show significant correlations with wind speed and anti-correlations with MABL height (Table 4). The inverse relationship of atmospheric VSLS to MABL height as described in Sect. 3.3 should lead to lower sea-to-air fluxes, F, as lower MABL heights lead to higher atmospheric mixing ratios, decreasing the concentration gradient, Δc (Eq. 2). However, higher sea-to-air fluxes are observed in the lower MABL height areas for dibromomethane and bromoform, with an accordingly positive relationship of F to ΔT (Table 4). This is due to elevated sea water production of brominated VSLS in the cold waters, leading to a large increase in the concentration gradient, which masks the flux suppression by the higher atmospheric mixing ratios (Hepach et al., 2013). Also the elevated atmospheric mixing ratios of methyl iodide have no effect on the fluxes, because methyl iodide is strongly supersaturated in the sea surface water throughout the entire cruise. On the other hand, the observed sea-to-air fluxes reveal correlations with the atmospheric VSLS abundances (Table 5), showing that MABL height and sea-to-air fluxes in combination add to the VSLS variations in the atmosphere. The detailed analysis of the sea-to-air fluxes, their driving factors, such as the sea water concentrations, and their influences on the atmospheric VSLS abundances are discussed in detail in Hepach et al. (2013).

4 Summary

The diurnal and regional variability of atmospheric VSLS has been investigated during the DRIVE ship campaign in May/June 2010 in the eastern tropical and subtropical North Atlantic Ocean. Additionally, we analyse meteorological influences on the observed VSLS mixing ratios using simultaneous high-resolution data. VSLS measurements were conducted hourly at six 24 h stations and during passage from the coast of Mauritania to Vigo (Spain), resulting in a total of 187 atmospheric VSLS measurements during DRIVE. We concentrated our investigation on three trace gases: bromoform, dibromomethane and methyl iodide. Higher mean VSLS mixing ratios were found over the Mauritanian upwelling region (5.60 ppt, 2.37 ppt and 1.50 ppt for bromoform, dibromomethane and methyl iodide, respectively) than over the open ocean (1.74 ppt, 1.28 ppt and 0.93 ppt for bromoform, dibromomethane and methyl iodide, respectively). The upwelling region also shows diurnal variations of the VSLS with highest fluctuations between maximum and minimum

Table 4. Correlation coefficients of bromoform ($CHBr_3$), dibromomethane (CH_2Br_2) and methyl iodide (CH_3I) fluxes with wind speed (w_{spd}), wind direction (w_{dir}), surface air pressure (p), surface air temperature (T_{SAT}), sea surface temperature (T_{SST}), temperature difference ($\Delta T = T_{SAT} - T_{SST}$), relative humidity ($U$), and MABL height. Whole cruise (leg 2 and 3) includes $n = 109$ samples for all parameters except MABL height (21 samples), open ocean (leg 2 except stations 3–6 and leg 3) includes $n = 37$ samples for all parameters except MABL height (8 samples) and coastal stations (stations 3–6) include $n = 70$ samples for all parameters except MABL height (13 samples). Bold coefficients have a p value of less than 5 %.

	$CHBr_3$ flux			CH_2Br_2 flux			CH_3I flux		
	Whole cruise	Open ocean	Coastal stations	Whole cruise	Open ocean	Coastal stations	Whole cruise	Open ocean	Coastal stations
w_{spd}	**0.37**	0.19	**0.48**	**0.54**	**0.84**	**0.71**	**0.54**	**0.52**	**0.61**
w_{dir}	**−0.37**	0	0.06	**−0.51**	0.09	−0.13	0.07	−0.04	0.07
p	**−0.67**	−0.10	**−0.57**	**−0.81**	**−0.71**	**−0.73**	−0.08	−0.30	−0.14
T_{SAT}	−0.08	−0.13	0.15	−0.06	**−0.75**	**0.27**	**−0.20**	**−0.4**	−0.21
T_{SST}	**−0.54**	−0.29	**−0.31**	**−0.51**	**−0.84**	−0.17	**−0.24**	**−0.55**	**−0.36**
ΔT	**0.76**	**0.35**	**0.67**	**0.75**	−0.15	**0.63**	0.12	0.18	0.22
U	−0.04	−0.14	**−0.43**	−0.02	**0.65**	**−0.61**	−0.08	0.21	**−0.27**
MABL	−0.58	0.26	**−0.58**	**−0.68**	**−0.93**	**−0.68**	−0.27	−0.12	**−0.59**

Table 5. Correlation coefficients of bromoform ($CHBr_3$), dibromomethane (CH_2Br_2) and methyl iodide (CH_3I) fluxes with according mixing ratios. Whole cruise (leg 2 and 3) includes $n = 109$ samples, open ocean (leg 2 except stations 3–6 and leg 3) includes $n = 37$ samples and coastal stations (stations 3–6) include $n = 70$ samples. Bold coefficients have a p value of less than 5 %.

	$CHBr_3$ flux			CH_2Br_2 flux			CH_3I flux		
	Whole cruise	Open ocean	Coastal stations	Whole cruise	Open ocean	Coastal stations	Whole cruise	Open ocean	Coastal stations
$CHBr_3$ mixing ratio	**0.58**	−0.20	**0.33**	**0.68**	**0.60**	**0.39**	−0.08	0.22	−0.16
CH_2Br_2 mixing ratio	**0.61**	−0.05	**0.40**	**0.71**	**0.56**	**0.49**	−0.04	**0.33**	−0.08
CH_3I mixing ratio	**0.62**	−0.09	**0.50**	**0.66**	**0.62**	**0.51**	0.09	0.21	0.12

of 3.57 ppt for bromoform, 0.83 ppt for dibromomethane and 1.85 ppt for methyl iodide. A strong coastal gradient of the VSLS is also observed towards Lisbon (Portugal), where we detect the highest bromoform mixing ratio of the whole cruise of 9.8 ppt.

The air mass origin is investigated by 5-day backward trajectories starting at the surface and at the top of the determined marine atmospheric boundary layer. We identify a predominantly North Atlantic origin of the air due to the prevailing NW winds during the whole cruise, with minor coastal influence at the Mauritanian upwelling area.

To distinguish atmospheric constraints on the VSLS we compare several meteorological parameters with the trace gas abundances. Although we do not find an overall relationship with the wind, we detect a significant correlation between VSLS abundance and easterly wind direction changes ($r > 0.7$) at the 4th station, northwest of Nouakchott (Mauritania), which is linked to land–sea breeze influence. We find a strong anti-correlation between air–sea surface temperature difference and MABL height, derived from radiosoundings. The MABL heights are dependent on the location, as we determine heights from surface level to only 400 m in the upwelling region and between 400 and 1700 m over the open ocean. In the Mauritanian upwelling a stable boundary layer leads to stable atmospheric conditions near the surface, due to warm air flowing over cold upwelling water, suppressing the mixing of air. In the open ocean part of the cruise, the top of the MABL is limited by trade inversions. Overall a significant anti-correlation between the VSLS mixing ratios and the marine atmospheric boundary layer height is found. With correlation coefficients of $r = -0.81$ for bromoform, $r = -0.82$ for dibromomethane and $r = -0.64$ for methyl iodide, the MABL height appears to have a significant influence on the trace gas mixing ratios. This relationship may help explain observed events in the tropical eastern Atlantic with increased atmospheric VSLS mixing ratios in the Mauritanian upwelling. Whether this influence can also be found in different seasons or other oceanic regions should be addressed in future studies. Of particular interest would be to investigate other oceanic upwelling regions, which are expected to also have high VSLS sources as the Mauritanian upwelling/Cape Verde Islands region does.

Acknowledgements. We thank the authorities of Cape Verde, Mauritania, Portugal and Spain for the permissions to work in their territorial waters. We acknowledge the NOAA Air Resources Laboratory (ARL) for the provision of NCEP reanalysis data and the HYSPLIT transport and dispersion model used in this publication. We thank S. Tegtmeier for helpful comments and M. Toohey for proofreading. We acknowledge the support of the captain and crew of R/V *Poseidon* as well as Hermann Bange, chief scientist of P399 legs 2 and 3. We also thank the 3 anonymous reviewers and the editor Bill Sturges for the helpful comments. Financial support for this study was provided by the BMBF grant SOPRAN II FKZ 03F0611A. This work also contributes to European Union's

Seventh Framework Programme FP7/2007–2013 under grant agreement no. 226224 – SHIVA.

The service charges for this open access publication have been covered by a Research Centre of the Helmholtz Association.

Edited by: W. T. Sturges

References

Atlas, E., Pollock, W., Greenberg, J., Heidt, L., and Thompson, A.: Alkyl nitrates, nonmethane hydrocarbons, and halocarbon gases over the equatorial Pacific Ocean during SAGA-3, J. Geophys. Res.-Atmos., 98, 16933–16947, doi:10.1029/93JD01005, 1993.

Bange, H., Atlas, E., Bahlmann, E., Baker, A., Bracher, A., Cianca, A., Dengler, M., Fuhlbrügge, S., Großmann, K., Hepach, H., Lavrič, J., Löscher, C., Krüger, K., Orlikowska, A., Peeken, I., Quack, B., Schafstall, J., Steinhoff, T., Williams, J., and Wittke, F.: FS Poseidon cruise report P399 legs 2 and 3, 74, IFM-GEOMAR, Kiel, Germany, 2011.

Butler, J., King, D., Lobert, J., Montzka, S., Yvon-Lewis, S., Hall, B., Warwick, N., Mondeel, D., Aydin, M., and Elkins, J.: Oceanic distributions and emissions of short-lived halocarbons, Global Biogeochem. Cy., 21, doi:10.1029/2006GB002732, 2007.

Carpenter, L. and Liss, P.: On temperate sources of bromoform and other reactive organic bromine gases, J. Geophys. Res.-Atmos., 105, 20539–20547, doi:10.1029/2000JD900242, 2000.

Carpenter, L., Liss, P., and Penkett, S.: Marine organohalogens in the atmosphere over the Atlantic and Southern Oceans, J. Geophys. Res.-Atmos., 108, 4256, doi:10.1029/2002JD002769, 2003.

Carpenter, L., Wevill, D., Hopkins, J., Dunk, R., Jones, C., Hornsby, K., and McQuaid, J.: Bromoform in tropical Atlantic air from 25 degrees N to 25 degrees S, Geophys. Res. Lett., 34, L11810, doi:10.1029/2007GL029893, 2007.

Carpenter, L., Fleming, Z., Read, K., Lee, J., Moller, S., Hopkins, J., Purvis, R., Lewis, A., Muller, K., Heinold, B., Herrmann, H., Fomba, K., van Pinxteren, D., Muller, C., Tegen, I., Wiedensohler, A., Muller, T., Niedermeier, N., Achterberg, E., Patey, M., Kozlova, E., Heimann, M., Heard, D., Plane, J., Mahajan, A., Oetjen, H., Ingham, T., Stone, D., Whalley, L., Evans, M., Pilling, M., Leigh, R., Monks, P., Karunaharan, A., Vaughan, S., Arnold, S., Tschritter, J., Pohler, D., Friess, U., Holla, R., Mendes, L., Lopez, H., Faria, B., Manning, A., and Wallace, D.: Seasonal characteristics of tropical marine boundary layer air measured at the Cape Verde Atmospheric Observatory, J. Atmos. Chem., 67, 87–140, doi:10.1007/s10874-011-9206-1, 2010.

Dessens, O., Zeng, G., Warwick, N., and Pyle, J.: Short-lived bromine compounds in the lower stratosphere; impact of climate change on ozone, Atmospheric Science Letters, 10, 201–206, doi:10.1002/asl.236, 2009.

Garratt, J.: The internal boundary-layer – a review, Bound.-Lay. Meteorol., 50, 171–203, doi:10.1007/BF00120524, 1990.

Gschwend, P., Macfarlane, J., and Newman, K.: Volatile halogenated organic-compounds released to seawater from temperate marine macroalgae, Science, 227, 1033-1035, doi:10.1126/science.227.4690.1033, 1985.

Hepach, H., Quack B., Ziska F., Fuhlbrügge, S., Atlas, E. L., Peeken, I., Krüger, K., and Wallace, D. W. R.: Drivers of diel and regional variations of halocarbon emissions from the tropical North East Atlantic, in preparation, 2013.

Highwood, E. and Hoskins, B.: The tropical tropopause, Q. J. Roy. Meteorol. Soc., 124, 1579–1604, doi:10.1256/smsqj.54910, 1998.

Hossaini, R., Chipperfield, M., Dhomse, S., Ordonez, C., Saiz-Lopez, A., Abraham, N., Archibald, A., Braesicke, P., Telford, P., Warwick, N., Yang, X., and Pyle, J.: Modelling future changes to the stratospheric source gas injection of biogenic bromocarbons, Geophys. Res. Lett., 39, L20813, doi:10.1029/2012GL053401, 2012.

Kalnay, E., Kanamitsu, M., Kistler, R., Collins, W., Deaven, D., Gandin, L., Iredell, M., Saha, S., White, G., Woollen, J., Zhu, Y., Chelliah, M., Ebisuzaki, W., Higgins, W., Janowiak, J., Mo, K., Ropelewski, C., Wang, J., Leetmaa, A., Reynolds, R., Jenne, R., and Joseph, D.: The NCEP/NCAR 40-year reanalysis project, B. Am. Meteorol. Soc., 77, 437-471, doi:10.1175/1520-0477(1996)077<0437:TNYRP>2.0.CO;2, 1996.

Kistler, R., Kalnay, E., Collins, W., Saha, S., White, G., Woollen, J., Chelliah, M., Ebisuzaki, W., Kanamitsu, M., Kousky, V., van den Dool, H., Jenne, R., and Fiorino, M.: The NCEP-NCAR 50-year reanalysis: Monthly means CD-ROM and documentation, B. Am. Meteorol. Soc., 82, 247–267, doi:10.1175/1520-0477(2001)082<0247:TNNYRM>2.3.CO;2, 2001.

Kloster, S., Six, K., Feichter, J., Maier-Reimer, E., Roeckner, E., Wetzel, P., Stier, P., and Esch, M.: Response of dimethylsulfide (DMS) in the ocean and atmosphere to global warming, J. Geophys. Res.-Biogeosci., 112, G03005, doi:10.1029/2006JG000224, 2007.

Ko, M. K. W., Poulet, G., and Blake, D. R.: Very short-lived halogen and sulfur substances, Scientific assessment of ozone depletion: 2002, Global Ozone Research and Monitoring Project. Report No. 47, Chapter 2, World Meteorological Organization, Geneva, 2003.

Krüger, K. and Quack, B.: Introduction to special issue: the Trans-Brom Sonne expedition in the tropical West Pacific, Atmos. Chem. Phys. Discuss., 12, 1401–1418, doi:10.5194/acpd-12-1401-2012, 2012.

Manley, S. and Dastoor, M.: Methyl-iodide (CH3I) production by kelp and assoviated microbes, Marine Biol., 98, 477–482, doi:10.1007/BF00391538, 1988.

Montzka, S. A. and Reimann, S.: Ozone-depleting substances and related chemicals, Scientific Assessment of Ozone Depletion: 2010, Global Ozone Research and Monitoring Project – Report No. 52, Geneva, Switzerland, 2011.

Moore, R. and Tokarczyk, R.: Volatile biogenic halocarbons in the northwest Atlantic, Global Biogeochem. Cy., 7, 195–210, doi:10.1029/92GB02653, 1993.

Neiburger, M., Johnson, D., and Chien, C.: Studies of the structure of the atmosphere over the Eastern Pacific Ocean in summer: I. The inversion over the Eastern North Pacific Ocean, 1, Univ. of Calif., Publications in Meteorology, 94 pp., 1961.

Nightingale, P., Malin, G., Law, C., Watson, A., Liss, P., Liddicoat, M., Boutin, J., and Upstill-Goddard, R.: In situ evaluation of air-sea gas exchange parameterizations using novel conservative and volatile tracers, Global Biogeochem. Cy., 14, 373–387, doi:10.1029/1999GB900091, 2000.

O'Brien, L., Harris, N., Robinson, A., Gostlow, B., Warwick, N., Yang, X., and Pyle, J.: Bromocarbons in the tropical marine boundary layer at the Cape Verde Observatory – measurements and modelling, Atmos. Chem. Phys., 9, 9083–9099, doi:10.5194/acp-9-9083-2009, 2009.

Pyle, J., Warwick, N., Yang, X., Young, P., and Zeng, G.: Climate/chemistry feedbacks and biogenic emissions, Phil. Trans. Roy. Soc. a-Mathematical Phys. Eng. Sci., 365, 1727–1740, doi:10.1098/rsta.2007.2041, 2007.

Quack, B. and Wallace, D.: Air-sea flux of bromoform: Controls, rates, and implications, Global Biogeochem. Cy., 17, 1023, doi:10.1029/2002GB001890, 2003.

Quack, B., Atlas, E., Petrick, G., Stroud, V., Schauffler, S., and Wallace, D.: Oceanic bromoform sources for the tropical atmosphere, Geophys. Res. Lett., 31, L23S05, doi:10.1029/2004GL020597, 2004.

Quack, B., Atlas, E., Petrick, G., and Wallace, D.: Bromoform and dibromomethane above the Mauritanian upwelling: Atmospheric distributions and oceanic emissions, J. Geophys. Res.-Atmos., 112, D09312, doi:10.1029/2006JD007614, 2007.

Raimund, S., Quack, B., Bozec, Y., Vernet, M., Rossi, V., Garcon, V., Morel, Y., and Morin, P.: Sources of short-lived bromocarbons in the Iberian upwelling system, Biogeosciences, 8, 1551–1564, doi:10.5194/bg-8-1551-2011, 2011.

Read, K., Mahajan, A., Carpenter, L., Evans, M., Faria, B., Heard, D., Hopkins, J., Lee, J., Moller, S., Lewis, A., Mendes, L., McQuaid, J., Oetjen, H., Saiz-Lopez, A., Pilling, M., and Plane, J.: Extensive halogen-mediated ozone destruction over the tropical Atlantic Ocean, Nature, 453, 1232–1235, doi:10.1038/nature07035, 2008.

Relvas, P., and Barton, E.: Mesoscale patterns in the Cape Sao Vicente (Iberian Peninsula) upwelling region, J. Geophys. Res.-Ocean., 107, 3164, doi:10.1029/2000JC000456, 2002.

Schmittner, A., Oschlies, A., Matthews, H., and Galbraith, E.: Future changes in climate, ocean circulation, ecosystems, and biogeochemical cycling simulated for a business-as-usual $CO_{(2)}$ emission scenario until year 4000 AD, Global Biogeochem. Cy., 22, GB1013, doi:10.1029/2007GB002953, 2008.

Seibert, P., Beyrich, F., Gryning, S., Joffre, S., Rasmussen, A., and Tercier, P.: Review and intercomparison of operational methods for the determination of the mixing height, Atmos. Environ., 34, 1001–1027, doi:10.1016/S1352-2310(99)00349-0, 2000.

Skyllingstad, E., Samelson, R., Mahrt, L., and Barbour, P.: A numerical Modeling study of warm offshore flow over cool water, Mont. Weather Rev., 133, 345–361, doi:10.1175/MWR-2845.1, 2005.

Solomon, S., Garcia, R., and Ravishankara, A.: On the role of iodine in ozone depletion, J. Geophys. Res.-Atmos., 99, 20491–20499, doi:10.1029/94JD02028, 1994.

Sorensen, J.: Sensitivity of the DERMA long-range gaussian dispersion model to meteorological input and diffusion parameters, Atmos. Environ., 32, 4195–4206, doi:10.1016/S1352-2310(98)00178-2, 1998.

Stull, R.: An Introduction to Boundary Layer Meteorology, Kluwer Academic Publishers, Dordrecht, the Netherlands, 1988.

Sturges, W., Cota, G., and Buckley, P.: Bromoform emission from arctic ice algae, Nature, 358, 660–662, doi:10.1038/358660a0, 1992.

Tegtmeier, S., Krüger, K., Quack, B., Atlas, E. L., Pisso, I., Stohl, A., and Yang, X.: Emission and transport of bromocarbons: from the West Pacific ocean into the stratosphere, Atmos. Chem. Phys., 12, 10633–10648, doi:10.5194/acp-12-10633-2012, 2012.

Tegtmeier, S., Krüger, K., Quack, B., Atlas, E., Blake, D. R., Boenisch, H., Engel, A., Hepach, H., Hossaini, R., Navarro, M. A., Raimund, S., Sala, S., Shi, Q., and Ziska, F.: The contribution of oceanic methyl iodide to stratospheric iodine, Atmos. Chem. Phys. Discuss., 13, 11427–11471, doi:10.5194/acpd-13-11427-2013, 2013.

Troen, I., and Mahrt, L.: A simple-model of the atmospheric boundary-layer: Sensitivity to surface evaporation, Bound.-Lay. Meteorol., 37, 129–148, doi:10.1007/BF00122760, 1986.

Vickers, D., Mahrt, L., Sun, J., and Crawford, T.: Structure of offshore flow, Mon. Weather Rev., 129, 1251–1258, doi:10.1175/1520-0493(2001)129<1251:SOOF>2.0.CO;2, 2001.

Vogelezang, D., and Holtslag, A.: Evaluation and model impacts of alternative boundary-layer height formulations, Bound.-Lay. Meteorol., 81, 245-269, doi:10.1007/BF02430331, 1996.

Warwick, N., Pyle, J., Carver, G., Yang, X., Savage, N., O'Connor, F., and Cox, R.: Global modeling of biogenic bromocarbons, J. Geophys. Res.-Atmos., 111, D244305, doi:10.1029/2006JD007264, 2006.

WMO: Definition of the thermal tropopause, WMO Bulletin, 136–137, 1957.

WMO: Scientific Assessment of Ozone Depletion: 2006, Geneva, Switzerland, 572, 2007.

WMO: Scientific Assessment of Ozone Depletion: 2010, World Meteorological Organization, Geneva, 2011.

Yokouchi, Y., Hasebe, F., Fujiwara, M., Takashima, H., Shiotani, M., Nishi, N., Kanaya, Y., Hashimoto, S., Fraser, P., Toom-Sauntry, D., Mukai, H., and Nojiri, Y.: Correlations and emission ratios among bromoform, dibromochloromethane, and dibromomethane in the atmosphere, J. Geophys. Res.-Atmos., 110, D23309, doi:10.1029/2005JD006303, 2005.

Ziska, F., Quack, B., Abrahamsson, K., Archer, S. D., Atlas, E., Bell, T., Butler, J. H., Carpenter, L. J., Jones, C. E., Harris, N. R. P., Hepach, H., Heumann, K. G., Hughes, C., Kuss, J., Krüger, K., Liss, P., Moore, R. M., Orlikowska, A., Raimund, S., Reeves, C. E., Reifenhäuser, W., Robinson, A. D., Schall, C., Tanhua, T., Tegtmeier, S., Turner, S., Wang, L., Wallace, D., Williams, J., Yamamoto, H., Yvon-Lewis, S., and Yokouchi, Y.: Global sea-to-air flux climatology for bromoform, dibromomethane and methyl iodide, Atmos. Chem. Phys. Discuss., 13, 5601–5648, doi:10.5194/acpd-13-5601-2013, 2013.

3.2 Manuscript 2

Drivers of diel and regional variations of halocarbon emissions from the tropical North East Atlantic

H. Hepach[1], B. Quack[1], F. Ziska[1], S. Fuhlbrügge[1], E. Atlas[2], K. Krüger[1*], I. Peeken[3,4], and D. W. R. Wallace[1**]

[1] GEOMAR Helmholtz-Zentrum für Ozeanforschung Kiel, Kiel, Germany

[2] Rosenstiel School of Marine and Atmospheric Science (RSMAS), Miami, USA

[3] Alfred-Wegener-Institut (AW) – Helmholtz-Zentrum für Polar und Meeresforschung, Bremerhaven, Germany

[4] MARUM – Zentrum für Marine Umweltwissenschaften, University Bremen, Bremen, Germany

[*] now at Department of Geosciences, University of Oslo (UiO), Oslo, Norway

[**] now at Department of Oceanography, Dalhousie University, Halifax, Canada

Published in: Atmospheric Chemistry and Physics, Vol. 14, 1255-1275, doi:10.5194/acp-14-1255-2014, 2014.

Atmos. Chem. Phys., 14, 1255–1275, 2014
www.atmos-chem-phys.net/14/1255/2014/
doi:10.5194/acp-14-1255-2014

Atmospheric Chemistry and Physics Open Access

Drivers of diel and regional variations of halocarbon emissions from the tropical North East Atlantic

H. Hepach[1], B. Quack[1], F. Ziska[1], S. Fuhlbrügge[1], E. L. Atlas[2], K. Krüger[1,*], I. Peeken[3,4], and D. W. R. Wallace[1,]**

[1]GEOMAR Helmholtz-Zentrum für Ozeanforschung Kiel, Germany
[2]Rosenstiel School of Marine and Atmospheric Science (RSMAS), University of Miami, USA
[3]Alfred-Wegener-Institut für Polar und Meeresforschung (AWI), Bremerhaven, Germany
[4]MARUM – Center for Marine Environmental Sciences, University Bremen, Bremen, Germany
[*]now at: Department of Geosciences, University of Oslo (UiO), Oslo, Norway
[**]now at: Department of Oceanography, Dalhousie University, Halifax, Canada

Correspondence to: H. Hepach (hhepach@geomar.de)

Received: 15 July 2013 – Published in Atmos. Chem. Phys. Discuss.: 25 July 2013
Revised: 9 December 2013 – Accepted: 10 December 2013 – Published: 3 February 2014

Abstract. Methyl iodide (CH_3I), bromoform ($CHBr_3$) and dibromomethane (CH_2Br_2), which are produced naturally in the oceans, take part in ozone chemistry both in the troposphere and the stratosphere. The significance of oceanic upwelling regions for emissions of these trace gases in the global context is still uncertain although they have been identified as important source regions. To better quantify the role of upwelling areas in current and future climate, this paper analyzes major factors that influenced halocarbon emissions from the tropical North East Atlantic including the Mauritanian upwelling during the DRIVE expedition. Diel and regional variability of oceanic and atmospheric CH_3I, $CHBr_3$ and CH_2Br_2 was determined along with biological and physical parameters at six 24 h-stations. Low oceanic concentrations of CH_3I from 0.1–5.4 pmol L^{-1} were equally distributed throughout the investigation area. $CHBr_3$ and CH_2Br_2 from 1.0 to 42.4 pmol L^{-1} and to 9.4 pmol L^{-1}, respectively were measured with maximum concentrations close to the Mauritanian coast. Atmospheric CH_3I, $CHBr_3$, and CH_2Br_2 of up to 3.3, 8.9, and 3.1 ppt, respectively were detected above the upwelling, as well as up to 1.8, 12.8, and 2.2 ppt at the Cape Verdean coast. While diel variability in CH_3I emissions could be mainly ascribed to oceanic non-biological production, no main driver was identified for its emissions over the entire study region. In contrast, biological parameters showed the greatest influence on the regional distribution of sea-to-air fluxes of bromocarbons. The diel impact of wind speed on bromocarbon emissions increased with decreasing distance to the coast. The height of the marine atmospheric boundary layer (MABL) influenced halocarbon emissions via its influence on atmospheric mixing ratios. Oceanic and atmospheric halocarbons correlated well in the study region, and in combination with high oceanic CH_3I, $CHBr_3$ and CH_2Br_2 concentrations, local hot spots of atmospheric halocarbons could solely be explained by marine sources. This conclusion is in contrast to previous studies that hypothesized elevated atmospheric halocarbons above the eastern tropical Atlantic to be mainly originated from the West-African continent.

1 Introduction

Volatile halogenated hydrocarbons (halocarbons) occur naturally in the oceans from where they are emitted into the atmosphere. Bromine and iodine atoms released from these compounds by photolysis and oxidation can take part in catalytic ozone destroying cycles in both the troposphere and stratosphere (McGivern et al., 2000; Salawitch et al., 2005; Montzka and Reimann, 2011) with iodine also participating in aerosol formation (O'Dowd et al., 2002). Halocarbons comprise brominated and iodinated methanes such as bromoform ($CHBr_3$) and dibromomethane (CH_2Br_2), methyl iodide (CH_3I) and diiodomethane, as well as longer chained and mixed halogenated compounds such as iodoethane, chloroiodomethane, and dibromochloromethane.

While $CHBr_3$ and CH_2Br_2 represent the largest contributors to atmospheric organic bromine from the ocean to the atmosphere (Hossaini et al., 2012a), methyl iodide (CH_3I), originating mostly from marine sources, is the most abundant organoiodine in the atmosphere (Saiz-Lopez et al., 2012). Although these three halocarbons are among those that receive the most attention due to their large contributions to atmospheric organic halogens, many uncertainties remain regarding their formation pathways, influences on their emissions, and their fate in the ocean and the atmosphere.

Elevated halocarbon concentrations, particularly of $CHBr_3$ and CH_2Br_2, occur in coastal regions where macro algae are thought to be the most dominant sources (Carpenter and Liss, 2000; Laturnus, 2001). Elevated concentrations of halocarbons are often observed in upwelling regions with large phytoplankton activity, where cold, nutrient rich water is brought up to the sea surface (Tokarczyk and Moore, 1994; Quack et al., 2004). Abiotic production such as photochemical processes could be of high significance for the marine formation of iodinated organic trace gases (Martino et al., 2009), e.g. CH_3I. Hence, its distribution in the ocean may depend on physical parameters such as insolation (Moore and Groszko, 1999; Richter and Wallace, 2004; Yokouchi et al., 2008; Stemmler et al., 2013).

The subtropical and tropical regions represent the largest contributors to global emission budgets of CH_3I, $CHBr_3$ and CH_2Br_2 (Ziska et al., 2013). The compounds and their degradation products can be carried into the stratosphere in significant quantities (Solomon et al., 1994; Hossaini et al., 2010; Aschmann et al., 2011; Montzka and Reimann, 2011; Tegtmeier et al., 2013), since deep tropical convection can lift surface air very rapidly into the tropical tropopause layer (Tegtmeier et al., 2012). Studies by Pyle et al. (2007) and Hossaini et al. (2012b) projected considerable changes in future inorganic bromine in the tropical troposphere and to the stratosphere from biogenic halocarbon emissions due to strengthening of convection, increasing their importance in the tropics. Coastal upwelling systems might play a crucial role in a changing climate. The tropical Mauritanian upwelling is an example of a recently intensified coastal eastern boundary upwelling (McGregor et al., 2007). Primary production could increase with enhanced entrainment of nutrient rich deep water into the surface ocean leading to amplified production of halocarbons. Increasing wind speeds, caused by enhanced pressure gradients (Bakun, 1990), would also directly influence the sea-to-air fluxes of all trace gases via a faster transfer coefficient (e.g. Nightingale et al., 2000). Thus the identification of factors impacting halocarbon sea-to-air fluxes is crucial for assessing possible effects of climate change on future emissions from coastal upwelling systems.

This paper reports on oceanic and atmospheric halocarbon distributions and sea-to-air fluxes from the DRIVE (Diurnal and RegIonal Variability of halogen Emissions) campaign of RV *Poseidon* in the eastern tropical North Atlantic and the Mauritanian upwelling in June 2010. We present results from six 24 h-stations in different distances from the Mauritanian coast and from two simultaneous diel stations on the Cape Verde island Sao Vincente. We aim at describing and quantifying significant factors that control the concentrations and emission fluxes of CH_3I, $CHBr_3$, and CH_2Br_2 both on a diel and a regional scale, including biological production, wind speed, and atmospheric transport. Previous studies have hypothesized that elevated atmospheric mixing ratios of $CHBr_3$ and CH_2Br_2 above the Mauritanian upwelling area were mainly of continental origin, since sea-to-air fluxes of these compounds appeared not sufficient to explain the observations (Quack et al., 2007a; Carpenter et al., 2009). In contrast, the investigation by Fuhlbrügge et al. (2013) revealed high atmospheric mixing ratios of CH_3I, $CHBr_3$ and CH_2Br_2 close to the coast also in air masses transported from the open ocean, with a significant anticorrelation between the atmospheric mixing ratios and the height of MABL. We therefore examine how oceanic emissions contribute to the mixing ratios of atmospheric halocarbons taking the height of the marine atmospheric boundary layer (MABL) into account. Meteorological constraints on the atmospheric distributions during the cruise are investigated in the accompanying paper by Fuhlbrügge et al. (2013).

2 Methods

The cruise P399/2 (Poseidon 399 leg 2) named DRIVE (Diurnal and RegIonal Variability of halogen Emissions) of RV*Poseidon* took place from May 31 to June 17 in 2010 in the eastern tropical North Atlantic and the Mauritanian upwelling. The ship followed a course from Las Palmas (Canary Islands, 28.1° N and 15.4° W) back to Las Palmas with a short stop at Mindelo (Sao Vicente, Cape Verde, 16.9° N and 25.0° W). The cruise track included six stations located at 17.6° N and 24.3° W (S1), 18.0° N and 21.0° W (S2), 18.0° N and 18.0° W (S3), 18.5° N and 16.5° W (S4), 19.0° N and 16.6° W (S5), and 20.0° N and 17.3° W (S6) where the ship remained at its position for 24 h (Fig. 1). Samples for dissolved halocarbons in sea water, atmospheric halocarbons and phytoplankton pigments were taken at all 24h-stations in parallel, and additionally four radio sonde launches per 24h-station were accomplished to determine the MABL properties. More details on the campaign and the meteorological conditions can be found in Bange et al. (2011) and Fuhlbrügge et al. (2013).

Related to the ship expedition a land-based operation took place from 3 to 8 June 2010 at the Cape Verde Atmospheric Observatory (CVAO) on Sao Vincente close to Mindelo at 17.6° N and 24.3° W (Fig. 1) where samples of atmospheric halocarbons were taken during two days.

Atmospheric halocarbon mixing ratios and meteorological conditions were also determined during a second cruise leg P399/3 from Las Palmas, Spain to Vigo, Spain and are covered in Fuhlbrügge et al. (2013). In contrast, this manuscript

focuses only on results from leg P399/2. The words "whole cruise" will refer to leg 2 and "whole campaign" includes leg 2 and the land-based operation at Cape Verde.

2.1 Sampling and analysis of halocarbons in sea surface water and air

Dissolved halocarbons were sampled in 500 mL amber glass bottles from a continuously working pump from the ships moon pool at a depth of 4.4 m. This allowed for nearly hourly sampling of sea surface water at every diel station. In between 24h-stations, the samples were taken every 3 h. The water was analyzed for halocarbons using a purge and trap system attached to a gas chromatograph with mass spectrometric detection (GC-MS). 80 mL of water were purged at 70 °C for 60 min with a stream of helium at 30 mL min^{-1} in a glass chamber with a purge efficiency of more than 98 % for all three halocarbons. The volatilized trace gases were desiccated with a Nafion® dryer and were trapped on glass beads at −100 °C. After purging, the compounds were desorbed at 100° C onto a deactivated capillary in liquid nitrogen as second trap. After three minutes, the sample was injected into the GC-MS, where the trace gases were separated on a Rtx-VGC capillary column with a length of 60 m, a diameter of 0.25 mm and a film thickness of 1.40 µm, and were detected in single ion mode. Quantification was achieved with volumetrically prepared standards in methanol. Four calibration curves were performed using different dilutions, each injected in triplicate. One standard was injected once a day in triplicate to monitor the internal drift of the instrumental set up which was low during the whole cruise. Precision for these measurements lay within 16 % for CH_3I, and 6 % for $CHBr_3$ and CH_2Br_2, determined only from duplicates due to time constraints.

Air samples were taken hourly at the diel stations. They were pumped into stainless steel canisters on the compass deck at a height of 13.7 m with a metal bellows pump. Samples were analyzed within a month at the Rosenstiel School of Marine and Atmospheric Science in Miami with a precision of approximately 5 % using GC-MS (Schauffler et al., 1999). Previous campaigns show that stability of the measured compounds in the canisters is not an issue over this time period. Additionally, air samples were taken at CVAO on an hourly basis parallel to the first two diel stations of the ship. Samples were taken according to the method onboard the RV *Poseidon* in approximately 3 m height above ground and then analyzed along with the other canisters collected during the cruise. Oceanic and atmospheric measurements were intercalibrated against whole air working-standards obtained from the NOAA Global Monitoring Division (Boulder, USA).

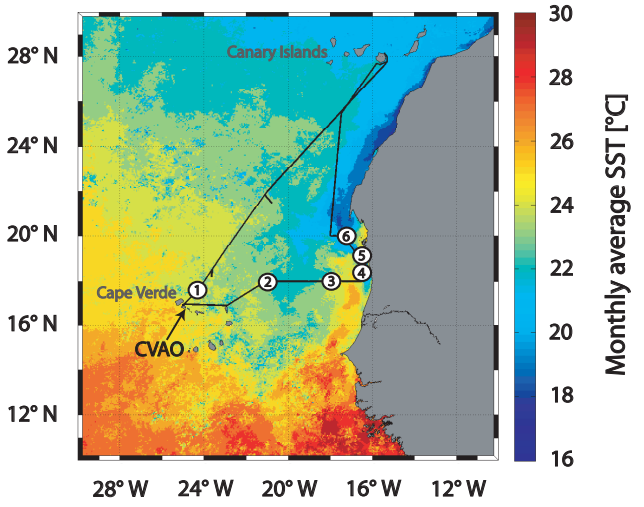

Fig. 1. Cruise track (black line) during DRIVE on SST derived from the monthly composite of June 2010 of MODIS-Aqua level 3 data. White circles with black numbers indicate 24 h-stations. Also marked is the location of the CVAO (Cape Verde Atmospheric Observatory).

2.2 Phytoplankton pigment analysis and flow cytometry

Samples for pigment analysis were taken approximately every 2 h at every diel station. 1 L of sea surface water from the continuously working pump in the ships moon pool was filtered through 25 mm Whatman GF/F filters and stored at −80 °C until analysis. Back in the lab, phytoplankton pigments were analyzed according to Tran et al. (2013) using a Waters high-performance liquid chromatography (HPLC) system at the Alfred Wegener Institute for Polar and Marine Research Bremerhaven (AWI). Apart from chlorophyll *a* (Chl *a*), the 27 marker pigments for which samples were analyzed include various chlorophyll type pigments such as chlorophyll *c1*, *c2* and *c3*, divinyl chlorophyll *b*, chlorophyll *b*, divinyl chlorophyll *a*, and phaeophytin *a*. The following carotenoids were detected: peridin, predinin derivative, 19-butanoyloxyfucoxanthin, fucoxanthin, neoxanthin, 19-hexanoyloxyfucoxanthin, violaxanthin, astaxanthin, prasinoxanthin, diadinoxanthin, alloxanthin, diatoxanthin, anthreaxanthin, zeaxanthin, lutein, α-carotene, and β-carotene. Marker pigments and their relative abundance are indicative for different phytoplankton groups.

For flow cytometry, 4 mL of water from the underway pump system were preserved with glutaraldehyde with a final concentration of 0.1 %, shock frozen in liquid nitrogen and stored at −80 °C. Flow cytometry samples were analyzed for nanoplankton, picoplankton, *Prochlorococcus*, and *Synechococcus* at the AWI according to Taylor et al. (2011). Potential cell loss associated with the sample fixation has not been taken into account.

Table 1. Means and ranges (minimum – maximum) of ambient parameters (SST, salinity, Chl *a*, wind speed, MABL height) during DRIVE for open ocean stations S1–S2 and coastal stations S3–S6.

		S1	S2	S3	S4	S5	S6
Parameter	Unit	17.6° N and 24.3° W	18.0° N and 21.0° W	18.0° N and 18.0° W	18.5° N and 16.5° W	19.0° N and 16.6° W	20.0° N and 17.3° W
SST	°C	24.5 (24.4–24.7)	23.2 (23.0–23.6)	21.7 (21.6–21.8)	23.3 (23.1–23.4)	20.4 (20.2–21.0)	18.6 (18.4–18.7)
Salinity		36.7 (36.7–36.7)	36.4 (36.4–36.5)	35.9 (35.9–35.9)	35.9 (35.9–35.9)	35.8 (35.8–35.8)	35.9 (35.8–35.9)
Chl *a*	$\mu g\,L^{-1}$	0.05 (0 -0.08)	0.30 (0.10–0.43)	1.00 (0.58–1.79)	1.63 (0.81–3.01)	4.50 (1.69–8.12)	4.80 (7.40–6.70)
Wind speed	$m\,s^{-1}$	4.6 (2.0–7.1)	11.0 (7.8–14.8)	6.0 (3.9–9.0)	9.7 (6.7–12.9)	8.9 (4.3–13.7)	11.0 (6.8–14.2)
MABL height	m	950 (850–1100)	540 (400–700)	290 (200–400)	120 (50–200)	25 (surface–100)	190 (100–350)

2.3 Calculation of sea-to-air fluxes and saturation anomaly

Sea-to-air fluxes (F) of CH_3I, $CHBr_3$ and CH_2Br_2 were calculated using the air-sea gas exchange parameterization of Nightingale et al. (2000). Schmidt number (Sc) corrections for the compound specific transfer coefficients k_w derived with the transfer coefficient k_{CO_2} of CO_2 as reported by Quack and Wallace (2003) were applied.

$$\frac{k_w}{k_{CO_2}} = \frac{Sc^{-\frac{1}{2}}}{660} \quad (1)$$

The air-sea concentration gradient was derived from all simultaneous water (c_w) and air (c_{atm}) measurements calculated with the Henry's law constants H of Moore and coworkers (Moore et al., 1995a, b) to obtain the theoretical equilibrium concentration c_{atm}/H.

$$F = k_w \cdot \left(c_w - \frac{c_{atm}}{H}\right) \quad (2)$$

The saturation anomaly S was calculated from the concentration gradient as the percentage of the equilibrium concentration.

$$S = \left(\left(c_w - \frac{c_{atm}}{H}\right) \cdot 100\right) \cdot \left(\frac{c_{atm}}{H}\right)^{-1} \quad (3)$$

Water temperature and salinity were continuously recorded using the ships' thermosalinograph. Air pressure and wind speed were determined by sensors on the compass deck and in 25.5 m height, respectively. Ten minute averages of these four parameters were included in the calculations, and wind speed was corrected to 10 m values.

3 Hydrography and environmental parameters during DRIVE

High SST values between 23.0 and 24.7 °C and high salinities from 36.4 to 36.7 observed at S1 and S2 close to Cape Verde (Figs. 1–2a, Table 1) were consistent with tropical surface water characteristics (Tsuchiya et al., 1992). Low Chl *a* concentrations between 0.00 and 0.43 $\mu g\,L^{-1}$ were a sign of low primary production there. Stations S1 and S2 are hence defined as open ocean. Wind speed had the lowest mean of the whole cruise at S1 with 4.6 $m\,s^{-1}$ and was highest at S2 with a mean of 11.0 $m\,s^{-1}$. The MABL height in this region determined by Fuhlbrügge et al. (2013) ranged between 400 and 1100 m (Table 1). With decreasing distance to the Mauritanian coast, a decrease in SST and salinity and an increase in Chl *a* concentrations were observed. This is a sign of the North West African upwelling system on the African shelf as part of the wind-driven Canary Current extending from 30° N to 10° N (Fedoseev, 1970). South Atlantic Central Water (SACW), characterized as a straight T-S curve between 5 °C and 34.3 and 20 °C and 36.0 (Tomczak and Godfrey, 2005), is transported to the Mauritanian coast by a poleward directed undercurrent. Between 12° N and 20° N upwelling of the cold nutrient rich SACW takes place from late fall to late spring (Minas et al., 1982; Tomczak, 1982; Hagen, 2001) after which the upwelling starts to cease due to changing atmospheric conditions induced by the shift of the Intertropical Convergence Zone (Mittelstaedt, 1982). Although the upwelling already began to cease during our cruise, stations S3–S6 are defined as upwelling and coastal stations (further on called coastal stations) due to the lower SSTs observed there. The lowest SST with 18.4 °C as well as the highest daily mean Chl *a* concentration of 4.80 $\mu g\,L^{-1}$ were found at the northernmost station (S6), while the overall maximum Chl *a* concentration of 8.12 $\mu g\,L^{-1}$ was observed at S5. MABL heights generally ranged between surface and 400 m

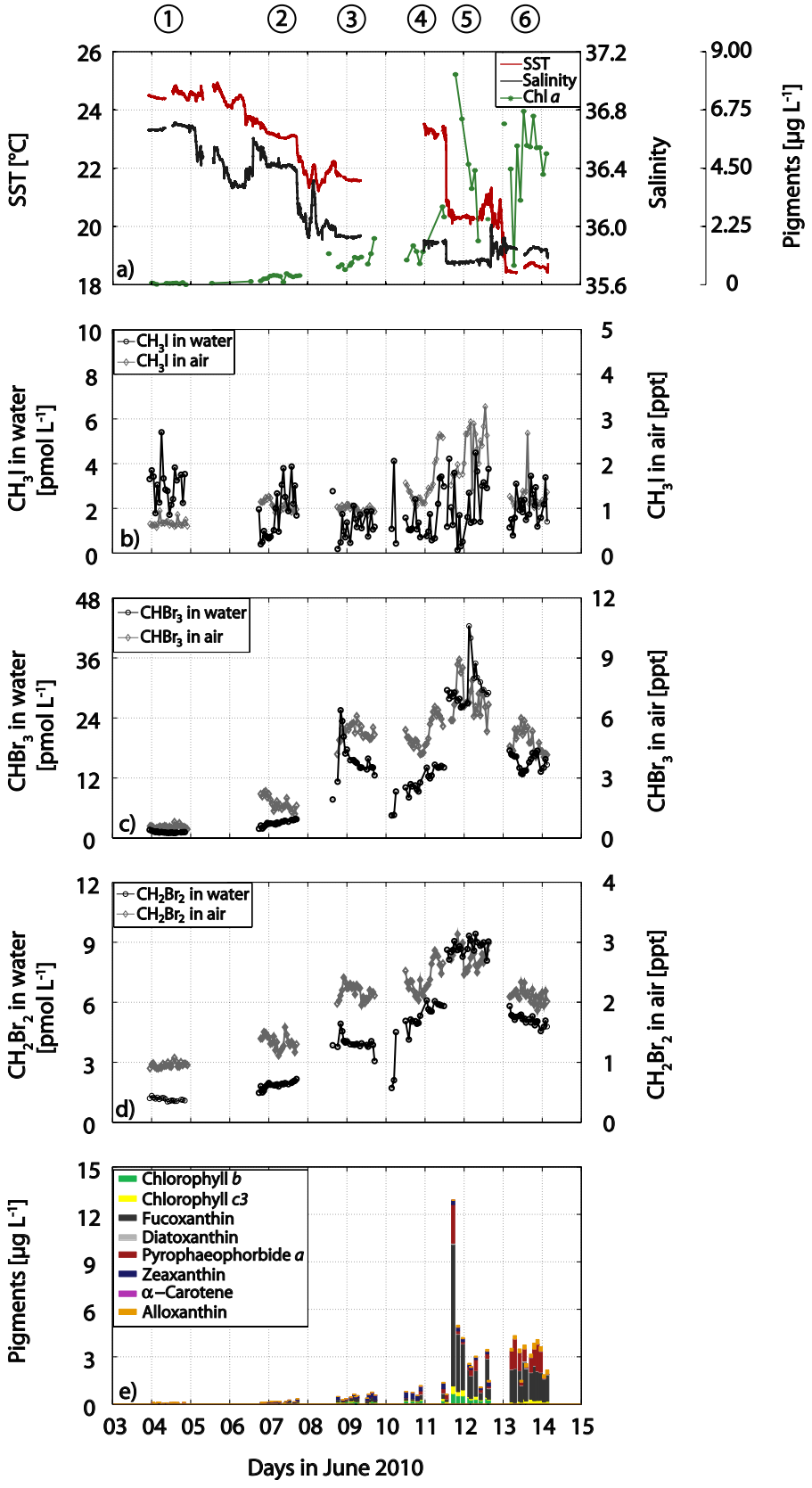

Fig. 2. SST, salinity and Chl *a* **(a)** along with halocarbon concentrations in water and atmospheric mixing ratios of CH_3I **(b)**, $CHBr_3$ **(c)** and CH_2Br_2 **(d)** and pigments significant for the regional distribution of $CHBr_3$ and CH_2Br_2 **(e)** during the DRIVE campaign.

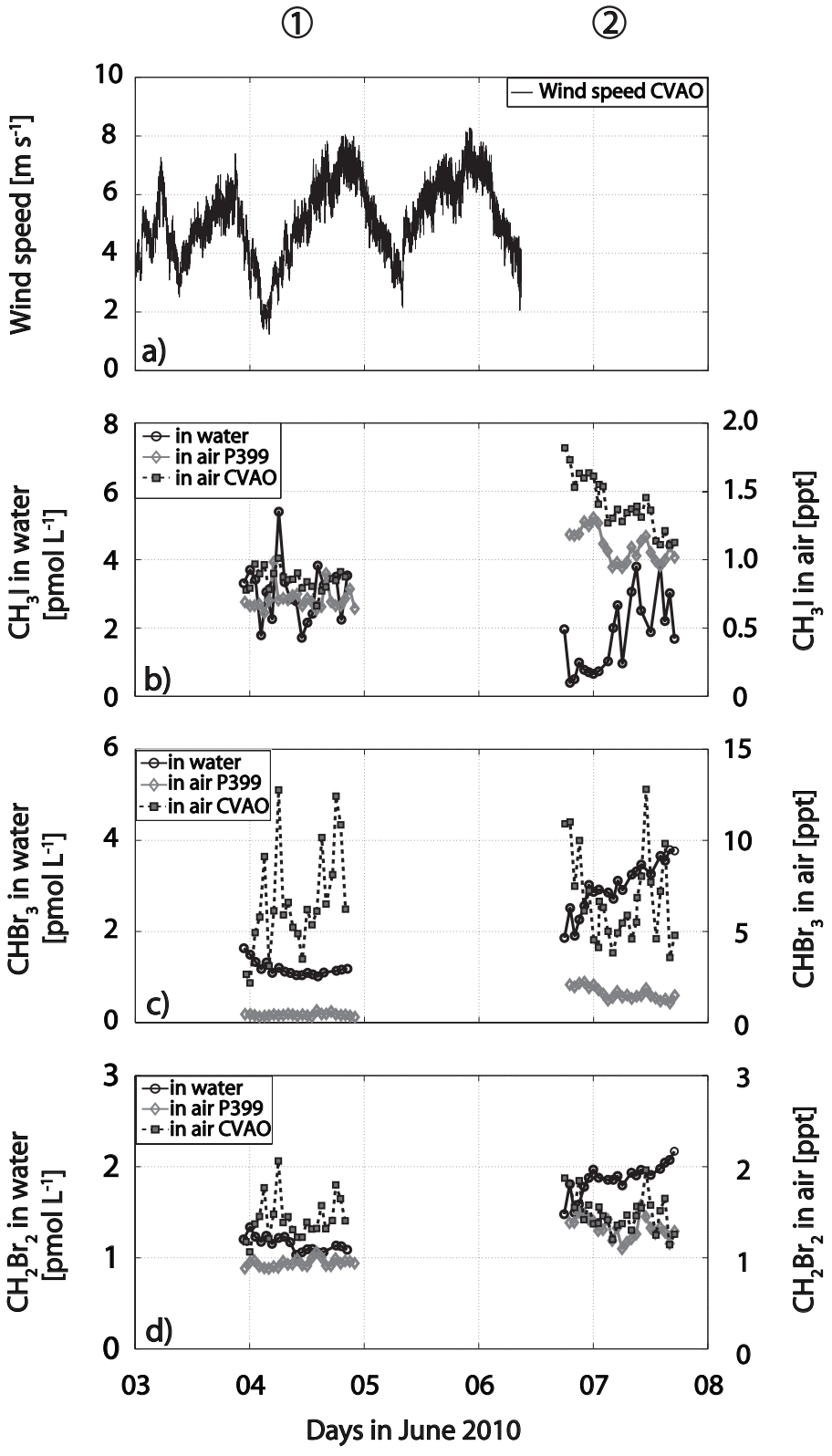

Fig. 3. Open ocean surface water and atmospheric halocarbons during stations S1 and S2 and atmospheric halocarbons measured parallel at CVAO as well as wind speed (wind speed in **a**, CH_3I in **b**, $CHBr_3$ in **c**, and CH_2Br_2 in **d**). Wind speed data for 7 and 8 June in 2010 was not available.

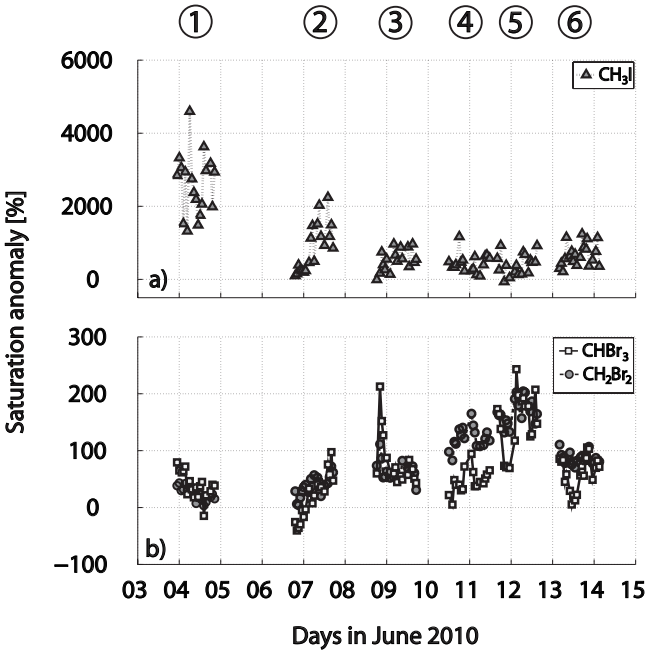

Fig. 4. Saturation anomalies of CH_3I **(a)** and $CHBr_3$ and CH_2Br_2 **(b)** throughout the RV *Poseidon* cruise.

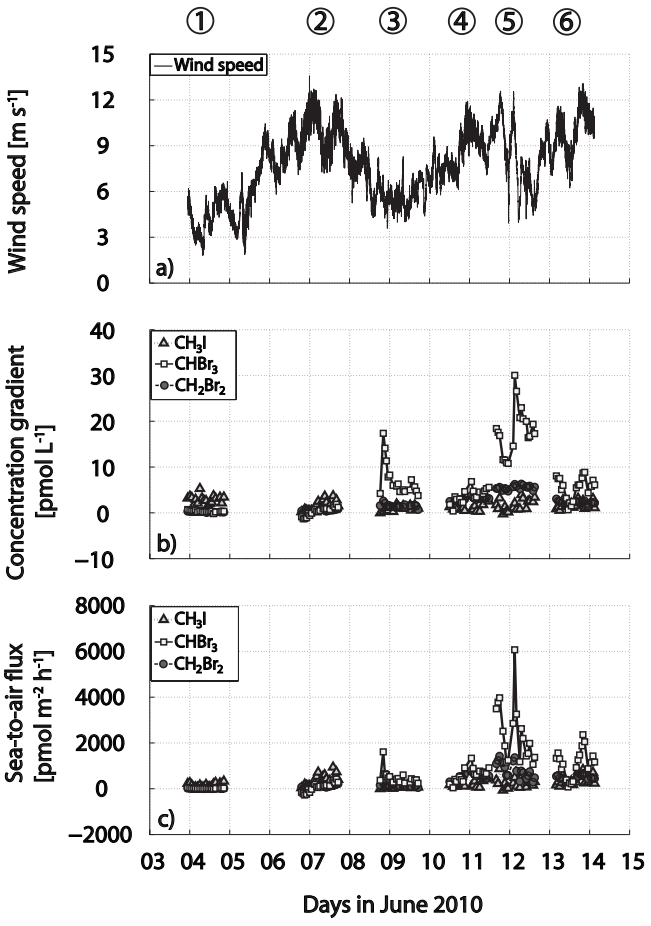

Fig. 5. Wind speed **(a)**, concentration gradients **(b)** and sea-to-air fluxes **(c)** of CH_3I, $CHBr_3$ and CH_2Br_2 during DRIVE.

at S3–S6, while wind speeds varied between 3.9 (S3) and 14.2 m s^{-1} (S6). At S5, the lowest MABL heights (close to the surface) together with the highest relative standard deviation (further on referred to as variability) in wind speed with a mean of 8.9 m s^{-1} and a variability of 27 % was observed at one station in the course of 24 h (Table 1). Due to the classification of the stations into two regions, average values of both open ocean stations together are based on fewer measurements than average values of the four coastal stations.

4 Results

4.1 Methyl iodide (CH_3I)

4.1.1 Regional distribution

At the open ocean stations S1 and S2 higher mean oceanic CH_3I of 2.4 pmol L^{-1} was found than at coastal stations S3–S6 with a mean of 1.8 pmol L^{-1} (Fig. 2b, Table 2). The maximum mean oceanic CH_3I of 3.0 (1.7–5.4) pmol L^{-1} was observed at S1, while S3 showed the lowest mean of 1.2 (0.2–2.1) pmol L^{-1} during 24 h. In total, the regional variability of CH_3I, which is the relative standard deviation between the means of the individual stations, was the lowest of all three halocarbons with 56 %. Correlations to neither phytoplankton pigments nor to picoplankton abundances were found for CH_3I in sea surface water (Table 3).

Atmospheric CH_3I with an overall mean of 1.3 (0.6–3.3) ppt revealed a different distribution in comparison to oceanic CH_3I (Fig. 2a). It was generally lower above the open ocean with 0.9 (0.6–1.3) ppt on average and increased towards the coast with a mean (range) of 1.6 (0.9–3.3) ppt (see also Fuhlbrügge et al., 2013). In total, atmospheric CH_3I had a lower regional variability of 44 % than oceanic CH_3I.

4.1.2 Diel variations

Of all three halocarbons, oceanic CH_3I showed the largest diel variability which was also larger than its regional variability. The lowest and the highest mean variability during 24 h were found at the open ocean stations S1 with 29 % and at S2 with 62 %. At the coastal stations oceanic CH_3I varied between 37 % (S6) and 60 % (S4). While at four stations maxima of CH_3I in the surface water were found in the morning hours, elevations in the afternoon were observed at open ocean station S2 and coastal station S6. Hence, no overall diurnal cycle could be detected.

Low relative diel variability between 9 % (S2) and 11 % (S1) was observed in atmospheric CH_3I above the open ocean. The variability at CVAO at the same time ranged

Table 2. Results of halocarbon measurements (water and air) and calculations (saturation anomalies and sea-to-air fluxes) for all six diel stations and parallel air sampling at CVAO.

			S1	S2	S3	S4	S5	S6
			17.6° N and 24.3° W	18.0° N and 21.0° W	18.0° N and 18.0° W	18.5° N and 16.5° W	19.0° N and 16.6° W	20.0° N and 17.3° W
Compound	Parameter	Unit						
CH_3I	Water	pmol L^{-1}	3.0 (1.7–5.4)	1.8 (0.4–3.9)	1.2 (0.2–2.1)	1.6 (0.6–3.4)	2.2 (0.1–4.5)	2.0 (0.8–3.5)
	Air	ppt	0.7 (0.6–1.0)	1.1 (1.0–1.3)	1.0 (0.9–1.1)	1.6 (1.1–2.7)	2.3 (1.4–3.3)	1.3 (1.1–2.7)
	CVAO air	ppt	0.9 (0.7–1.0)	1.4 (1.1–1.8)	–	–	–	–
	Saturation anomaly	%	2606.3 (1321.1–4597.1)	870.2 (99.4–2243.7)	532.2 (−8.5–967.1)	445.6 (90.8–1167.4)	410.8 (−65.8–928.7)	672.1 (210.1–1242.3)
	Sea-to-air flux	pmol m^{-2} h^{-1}	158.3 (59.3–330.4)	372.6 (39.6–941.6)	79.0 (−1.7–212.2)	227.7 (61.4–500.5)	259.6 (−64.6–871.6)	382.5 (106.1–837.9)
$CHBr_3$	Water	pmol L^{-1}	1.2 (1.0–1.6)	3.0 (1.9–3.8)	16.2 (11.3–25.5)	11.9 (8.1–14.7)	30.6 (26.1–42.4)	15.3 (12.8–17.5)
	Air	ppt	0.6 (0.5–0.8)	1.8 (1.2–2.4)	5.3 (4.2–6.1)	5.3 (4.2–6.6)	7.0 (5.4–8.9)	4.9 (4.1–6.0)
	CVAO air	ppt	6.7 (2.3–12.8)	6.8 (3.7–12.8)	–	–	–	–
	Saturation anomaly	%	39.6 (−14.7–79.3)	17.7 (−40.3–97.3)	80.6 (43.0–212.7)	46.1 (5.2–94.4)	148.0 (69.4–243.1)	59.4 (5.4–105.5)
	Sea-to-air flux	pmol m^{-2} h^{-1}	15.5 (−8.5–45.0)	65.6 (−273.4–426.7)	489.1 (241.4–1610.9)	611.7 (41.7–1333.8)	2423.0 (1063.3–6068.9)	1098.2 (77.8–2360.2)
CH_2Br_2	Water	pmol L^{-1}	1.2 (1.0–1.3)	1.9 (1.5–2.2)	4.0 (3.1–4.9)	5.4 (4.1–6.1)	8.8 (8.1–9.4)	5.1 (4.6–5.8)
	Air	ppt	1.0 (0.9–1.1)	1.4 (1.1–1.6)	2.2 (2.0–2.4)	2.4 (2.0–2.9)	2.8 (2.5–3.1)	2.1 (1.9–2.3)
	CVAO air	ppt	1.4 (1.1–2.1)	1.5 (1.2–2.0)	–	–	–	–
	Saturation anomaly	%	24.7 (3.4–43.2)	37.7 (4.1–72.2)	64.7 (30.9–111.5)	122.0 (82.7–165.0)	169.0 (131.8–204.3)	86.1 (70.1–110.6)
	Sea-to-air flux	pmol m^{-2} h^{-1}	10.6 (1.8–27.9)	118.5 (14.5–214.3)	115.7 (50.0–260.3)	511.8 (207.9–801.0)	815.4 (285.6–1429.4)	470.4 (295.5–671.6)

between 9 % (4 June, parallel to S1) and 14 % (June 6 and 7, parallel to S2) (Fig. 3a, Table 2) with mean mixing ratios of 1.2 ppt (0.7 ppt, 4 June–1.8 ppt, 6 June). At the coastal stations S3–S6, diel variability of 7 (S3) – 33 % (S4) was observed. The highest mean atmospheric variability at S4 coincides with the largest oceanic variability. Similarly to oceanic CH_3I, there is no overall diurnal cycle in atmospheric mixing ratios. Maxima and minima occurred in both day and night hours.

4.1.3 Saturation anomaly, sea-air concentration gradient and sea-to-air fluxes

Saturation anomalies (Fig. 4), concentration gradient (Fig. 5b) as well as sea-to-air fluxes (Fig. 5c) were calculated according to Eqs. (1)–(3) (Table 2). To constrain the atmospheric influence on the concentration gradient, thus on the sea-to-air fluxes, the fraction of the equilibrium concentration c_{atm}/H of the oceanic concentration c_w was calculated (Fig. 6a). This is the relative reduction of the sea-to-air flux by the atmospheric mixing ratios compared to an empty atmosphere, which will be referred to as "flux reducing effect" further on.

For CH_3I the highest saturation anomalies with means of 931 (−66–4597) % (Fig. 4a, Table 2) and the lowest concentration gradients of 1.7 (−0.3–5.3) pmol L^{-1} (Fig. 5b) of the three halocarbons were calculated for CH_3I for the whole cruise. Both were consistent with the oceanic distribution: they were highest in the open ocean with maxima at S1 where however no high emissions of this compound were calculated because of the prevailing low wind speeds during that time (Fig. 5c). The open ocean was generally highly supersaturated with mean anomalies of 1715 % on average, decreasing towards the coastal stations to a mean of 522 %. The reducing effect of atmospheric CH_3I on the sea-to-air flux was low, usually less than 50 %. One exception was S5 where low oceanic CH_3I coincided with high atmospheric mixing ratios, and the flux reducing effect reached 300 % leading to a flux into the water. Mainly positive sea-to-air fluxes of CH_3I could be observed with a mean of 254 pmol m^{-2} h^{-1} for the whole cruise (−65 at coastal station S5 to 942 pmol m^{-2} h^{-1} at open ocean station S2) (Fig. 5c, Table 2). Open ocean and mean coastal fluxes of 268 and 246 pmol m^{-2} h^{-1}, respectively were in a similar range though with potentially higher fluxes in the open ocean due to its large supersaturation there.

Table 3. Correlation coefficients R^2 of halocarbons to nano- and picoplankton abundances as well as to phytoplankton pigment data (MLR – Multiple Linear Regression). The correlations to Prochlorococchus are all significant on the p <0.05 level. Negative correlations are printed in italic.

		n	CH_3I	$CHBr_3$	CH_2Br_2
Nano- and picoplankton	Prochlorococcus	72	0.10	*0.39*	*0.26*
	Others	72	< 0.08	< 0.09	< 0.10
Phyotplankton pigments	Chl *a*	61	0.00	0.38	0.49
	MLR	61	None	0.79	0.77

4.1.4 Impact of oceanic CH_3I and wind speed on fluxes

The sea-to-air flux of CH_3I showed significant but low regional correlations with sea surface concentrations ($R^2 = 0.37$) and wind speed ($R^2 = 0.24$) for the whole cruise (Fig. 7a, d, Table 4). Considering each station individually, high significant correlations of oceanic CH_3I and sea-to-air flux were found at open ocean station S2 and at all coastal stations with R^2 ranging between 0.57 and 0.91. Significant correlations of wind speed to the CH_3I sea-to-air flux only existed at coastal station S3 and open ocean station S1 ($R^2 = 0.24$ and 0.76).

4.2 Bromoform ($CHBr_3$) and dibromomethane (CH_2Br_2)

4.2.1 Regional distribution

$CHBr_3$ and CH_2Br_2 were both lower in the open ocean with means of 2.3 (1.0–3.8) pmol L^{-1} for $CHBr_3$ and 1.6 (1.0–2.2) pmol L^{-1} for CH_2Br_2 with minimum concentrations occurring at S1 (Fig. 2c, d, Table 2). Both compounds had higher coastal concentrations of 18.3 (8.1–42.4) pmol L^{-1} for $CHBr_3$ and 5.8 (3.1–9.4) pmol L^{-1} for CH_2Br_2 with maxima at S5 and a much more pronounced increase in oceanic $CHBr_3$ than in CH_2Br_2. $CHBr_3$ and CH_2Br_2 in sea surface water demonstrated much higher relative regional variability of 78 % ($CHBr_3$) and 59 % (CH_2Br_2) than oceanic CH_3I.

Atmospheric $CHBr_3$ and CH_2Br_2 increased towards the coast similarly to their oceanic counterparts (Fig. 2c, d, Table 2). The highest mean regional variability was found for $CHBr_3$ (56 %), while atmospheric CH_2Br_2 showed the lowest (33 %) of the three halocarbons.

4.2.2 Diel variations

Diel variations of both $CHBr_3$ and CH_2Br_2 in sea surface water were generally lower than their regional variations. The variability of $CHBr_3$ ranged between 14 % (S1) and 19 % (S2) in the open ocean, while the variability of CH_2Br_2 was even lower with 7 % (S1) and 9 % (S2). At most of the coastal stations $CHBr_3$ and CH_2Br_2 revealed similar distributions throughout 24 h with maxima in the evening and night hours with the exception of S5 where maxima

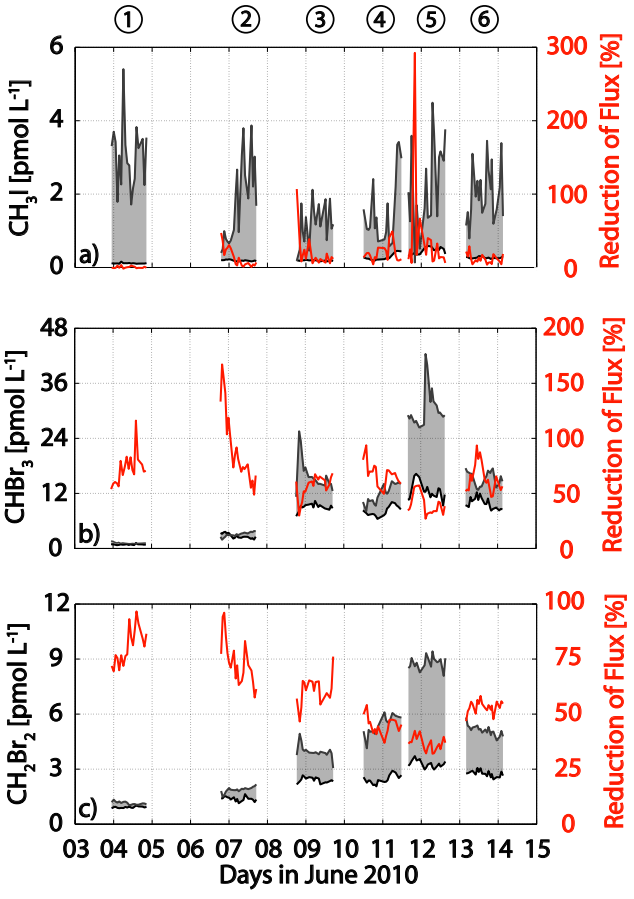

Fig. 6. Influence of atmospheric mixing ratios on the amount of oceanic halocarbons emitted for CH_3I **(a)**, $CHBr_3$ **(b)**, and CH_2Br_2 **(c)**. Oceanic concentrations are plotted in grey (left axis), the equilibrium concentration is delineated in black, and the concentration gradient is shaded in grey. The percentaged reduction of the concentration gradient by the equilibrium concentration (flux reducing effect) derived from the atmospheric measurements (equilibrium concentration in percent in relation to the water concentrations) is shown in red (right axis). Values above 100 % refer to fluxes from the atmosphere into the ocean.

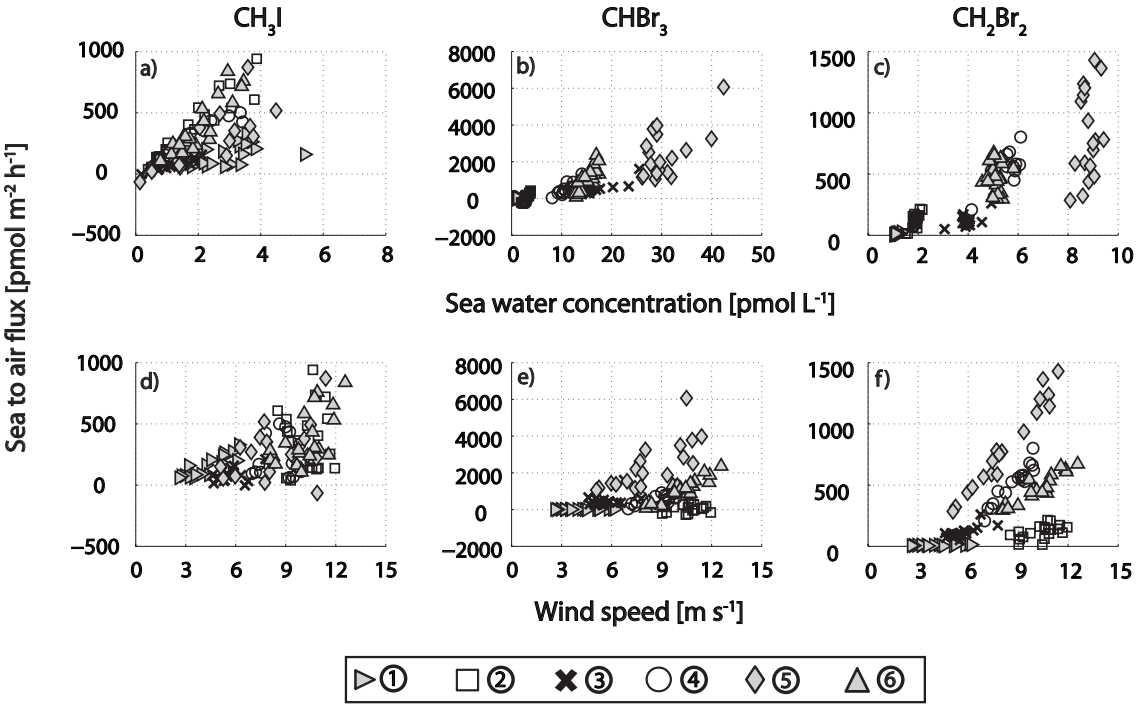

Fig. 7. Sea-to-air fluxes versus sea water concentrations of CH_3I **(a)**, $CHBr_3$ **(b)** and CH_2Br_2 **(c)** and wind speed **(d–f)** during DRIVE.

of 42.4 pmol L^{-1} ($CHBr_3$) and 9.4 pmol L^{-1} (CH_2Br_2) were found in the morning hours. The highest diel variation of 23 % was found at coastal station S3 for oceanic $CHBr_3$, while CH_2Br_2 was generally less variable ranging from 4 (S5) to 10 % (S4).

Atmospheric mixing ratios of bromocarbons were low at the open ocean stations S1–S2 with means between 0.6 and 1.78 ppt and relative standard deviations of 13–19 % for $CHBr_3$ and atmospheric CH_2Br_2 ranging on average between 1.0 and 1.4 ppt with a relative standard deviation of 5–9 %. At CVAO mean mixing ratios of 6.7–6.8 ppt $CHBr_3$ and of 1.4–1.5 ppt CH_2Br_2 were higher than at S1–S2, as was their diel variability ranging from 35–43 % for $CHBr_3$ and 14–16 % for CH_2Br_2 (Fig. 3b, c, Table 2). The highest atmospheric $CHBr_3$ during the whole campaign of 12.8 ppt was measured at CVAO on 7 June. The diel variability of atmospheric $CHBr_3$ at the coastal stations S3–S6 was generally lower than what was observed above the open ocean with 7 (S3)–14 % (S4) and means of 4.8 (S6)–7.0 ppt (S5). The diel variability of atmospheric CH_2Br_2 at the coast was similar to the open ocean with 5 (S6)–10 % (S4) and means of 2.1 (S6)–2.8 ppt (S5). Atmospheric $CHBr_3$ and CH_2Br_2 showed no overall diurnal cycles above neither open ocean nor coastal stations with maxima during both day and night hours.

4.2.3 Correlations of $CHBr_3$ and CH_2Br_2 with phytoplankton pigments

Surface water concentrations of $CHBr_3$ and CH_2Br_2 correlated significantly with Chl *a* at the 95 % level with correlation coefficients R^2 of 0.38 and 0.49 (Table 3, Figure 2a). Multiple linear regressions (MLR) of brominated halocarbons to all phytoplankton marker pigments were carried out for the whole cruise. All pigment data related to $CHBr_3$ or CH_2Br_2 with $p < 0.05$ was regarded as significant. The six pigments chlorophyll *b*, chlorophyll *c3*, fucoxanthin, diatoxanthin, pyrophaeophorbide *a* and zeaxanthin were found to describe the regional distribution of $CHBr_3$ best (Fig. 2e, Table 3). Chlorophyll *b*, fucoxanthin, α-carotene (negatively correlated) and alloxanthin were important for CH_2Br_2 in the order of explanatory power. Additionally, significant but low correlations of $CHBr_3$ and CH_2Br_2 were found to *Prochlorococcus* with $R^2 = 0.39$ and $R^2 = 0.26$ (negatively correlated).

4.2.4 Saturation anomaly, sea-air concentration gradients and sea-to-air fluxes

The ocean was generally supersaturated with $CHBr_3$ and CH_2Br_2 (Fig. 4, Table 2). The overall saturation anomaly of 65 (−40 – 243) % for $CHBr_3$ was slightly lower than the mean of CH_2Br_2 with 84 (3–204) % (Fig. 4b). Both displayed similar trends opposite to CH_3I: lower anomalies of around 30 % in the open ocean stations, increasing towards the coastal stations S3 – S6 with means of

83 % for $CHBr_3$ and 110 % for CH_2Br_2. Maximum saturation anomalies coincided with maximum oceanic and atmospheric bromocarbons at S5 with daily means of 148 % for $CHBr_3$ and 169 % for CH_2Br_2. The concentration gradient $c_w - c_{atm}/H$ of $CHBr_3$ was the highest of all three halocarbons with a total mean of 5.8 (−1.3–30.0) pmol L^{-1}, followed by CH_2Br_2 with a mean of 2.2 (0–6.3) pmol L^{-1} and minima in the open ocean region (Fig. 5b). The reducing effect of atmospheric $CHBr_3$ and CH_2Br_2 on the sea-to-air flux was > 75 % in the open ocean where both compounds were close to equilibrium and decreases simultaneously with the strongly increasing concentration gradient towards the coast (Fig. 6b, c). For $CHBr_3$ and CH_2Br_2 the flux reducing effect was around 50 % at the four coastal stations (S3–S6). Sea-to-air fluxes of $CHBr_3$ and CH_2Br_2 for the whole cruise were on average higher than CH_3I fluxes with 787 (−273–6069) pmol m^{-2} h^{-1} and 341 (2–1429) pmol m^{-2} h^{-1}, respectively (Fig. 5c, Table 2). Fluxes of both compounds were low in the open ocean region with means of 41 pmol m^{-2} h^{-1} for $CHBr_3$ and of 66 pmol m^{-2} h^{-1} for CH_2Br_2. Higher sea-to-air fluxes of $CHBr_3$ and CH_2Br_2 with means of 1171 and 483 pmol m^{-2} h^{-1} were observed at the coastal stations S3–S6. The maximum fluxes of both compounds were found at coastal station 5.

4.2.5 Impact of oceanic $CHBr_3$ and CH_2Br_2 and wind speed on fluxes

Sea surface water concentrations of $CHBr_3$ and CH_2Br_2 correlated regionally to sea-to-air fluxes with R^2 = 0.68 ($CHBr_3$) and 0.71 (CH_2Br_2) for the whole cruise (Fig. 7, Table 4). Significant correlations of $CHBr_3$ fluxes with sea surface water concentrations were found at all 24h-stations (R^2 from 0.34 to 0.78). The highest correlations of sea surface CH_2Br_2 to its sea-to-air fluxes were found at open ocean station S2 (0.64) and coastal stations S3 and S4 (0.42, 0.53). No significant correlations could be observed at coastal stations S5 and S6. In contrast, wind speed showed low but regionally significant correlations to the overall sea-to-air fluxes with $R^2 = 0.14$ ($CHBr_3$) and $R^2 = 0.29$ (CH_2Br_2). Considering the stations individually, $CHBr_3$ and CH_2Br_2 revealed high correlations of wind speed with sea-to-air flux at coastal stations S4–S6 with R^2 from 0.56 to 0.95.

Table 4. Correlation coefficients for water concentrations of halocarbons and wind speed with sea-to-air fluxes of halocarbons for the whole cruise and for the individual stations. Coefficients printed in bold represent significant correlations with $p < 0.05$.

Station	R^2 of	with F of			n
		CH_3I	$CHBr_3$	CH_2Br_2	
Whole cruise	Water conc.	**0.37**	**0.68**	**0.71**	109
	Wind speed	**0.24**	**0.14**	**0.29**	
S1	Water conc.	**0.24**	**0.66**	**0.35**	18
	Wind speed	**0.73**	**0.28**	0.21	
S2	Water conc.	**0.89**	**0.78**	**0.64**	19
	Wind speed	0.00	0.00	0.15	
S3	Water conc.	**0.67**	**0.66**	**0.42**	17
	Wind speed	**0.24**	0.21	**0.56**	
S4	Water conc.	**0.91**	**0.60**	**0.53**	17
	Wind speed	0.02	**0.67**	**0.93**	
S5	Water conc.	**0.57**	**0.34**	0.09	18
	Wind speed	0.02	**0.55**	**0.95**	
S6	Water conc.	**0.79**	**0.70**	0.00	20
	Wind speed	0.06	**0.82**	**0.78**	

5 Discussion

5.1 Sea-to-air fluxes of CH_3I

5.1.1 Oceanic and atmospheric CH_3I as drivers of the regional and diel variability of the concentration gradient

The ocean was highly supersaturated with CH_3I throughout most of the cruise which is underlined by the low impact of atmospheric CH_3I on its concentration gradient (Fig. 6a). Regional and diel variability in the concentration gradient was primarily a result of varying oceanic CH_3I. The oceanic concentrations during DRIVE (0.1 to 5.4 pmol L^{-1}, Table 2) compare well to the measurements by Schall et al. (1997) of 0–3 pmol L^{-1} in the Atlantic, north of 42° N during boreal wintertime. In contrast, Richter and Wallace (2004) measured 3–5 times higher oceanic CH_3I with 7.1–16.4 pmol L^{-1} in boreal fall south of 15° N, and Jones et al. (2010) reported even 6 times higher concentrations (total range from min to max: 1.0–36.5 pmol L^{-1}, data from Jones et al., 2010; Ziska et al., 2013) in the same region and season. Similarly to DRIVE, Jones et al. (2010) found no significant difference between open ocean and coastal regions which was ascribed to photochemical sources supported by the incubation experiments of Richter and Wallace (2004) from the equatorial Atlantic. Richter (2004) found a relationship of oceanic CH_3I with wind speed within this data which was not found during DRIVE: lower wind speeds led to elevated oceanic CH_3I. The much more elevated oceanic CH_3I of Jones et al. (2010) was measured in our study region and season. A possible explanation for their largely elevated CH_3I concentrations compared to our and other open ocean values (Ziska et al., 2013) might be enhanced photochemistry, but more detailed information is not given in the study of Jones et al. (2010). Smythe-Wright et al. (2006) measured CH_3I as high as 45 pmol L^{-1} in the Atlantic region south of 40° N in late summer which was accompanied by high *Prochlorococcus* abundance. In contrast, no outstanding relationship of CH_3I with picoplankton including *Prochlorococcus* or the marker pigment divinyl chlorophyll *a* indicative of these species was found during DRIVE. Additionally, no correlation with diatom pigments as suggested by Lai et al. (2011) for the production of open ocean CH_3I was

observed, supporting photochemistry as important production pathway for its formation as suggested by Moore and Zafiriou (1994). The likely non-biological formation of CH_3I also leads to high saturation anomalies in open ocean surface waters. The lower saturation anomalies in the coastal zone might likely be a result of upwelled water diluting the more concentrated surface water (Happell and Wallace, 1996) combined with the elevated atmospheric CH_3I above the upwelling. The large supersaturation of CH_3I in surface water of the open ocean region indicates their potential for largely elevated sea-to-air fluxes in contrast to the coastal area. However, CH_3I production may not be completely independent of biological parameters. Lacking correlations of CH_3I concentrations with pigment and flow cytometry data does not necessarily allow for excluding a biological source completely. The concentrations are a result of production and loss processes, which may partly be temporally and spatially decoupled. Another possible source for CH_3I involves bacteria (Manley and Dastoor, 1998; Amachi et al., 2001; Fuse et al., 2003) which has not been taken into account during DRIVE. Additionally, Bell et al. (2002) suggested that organic precursors from phytoplankton production could be involved in the photochemical formation of CH_3I in the surface ocean.

Atmospheric CH_3I (0.6 to 3.3 ppt) measured during DRIVE falls well within the range of tropical Atlantic values reported by Williams et al. (2007) of 1.4 (0.6–3.0) ppt. Air mass back trajectory analysis and similar ranges of atmospheric CH_3I at open ocean station S1 and parallel at CVAO on Cape Verde indicate open ocean air masses at both locations on 4 June (Fuhlbrügge et al., 2013). Wind speed at Cape Verde was highly variable on June 6 (Fig. 3d) leading to high variations in local sea-to-air fluxes likely causing the observed higher mean variability in atmospheric CH_3I at CVAO parallel to open ocean station S2 (Sect. 4.1.2, Fig. 3a). Atmospheric CH_3I during DRIVE at CVAO (0.7–1.8 ppt) was generally lower than the 1.2–13.8 ppt detected by O'Brien et al. (2009) in a similar season.

Non-biological or indirect biological formation mechanisms in the surface water seem likely since the variability in oceanic CH_3I was not correlated to the measured biological variables. Although a biological source cannot completely be excluded, the abiotic formation thus appears as main driver for variations of its concentration gradient across the air-sea interface with negligible influence from atmospheric CH_3I on oceanic concentrations.

5.1.2 The relative influence of concentration gradient and wind speed on sea-to-air fluxes of CH_3I

Applying the parameterization of Nightingale et al. (2000), sea water concentrations and wind speed were almost equally important as driving factors for the variations in the CH_3I sea-to-air flux for the whole cruise region (Fig. 7) based on their similar regional variability (see the scatter in Fig. 8a and similar error bars at the plot that includes all data points in Figure 8b). Diel variability in fluxes could be mainly ascribed to variations in oceanic CH_3I, since they were much higher than the diel variability in wind speed (Fig. 8a, b). Significant correlations of wind speed with sea-to-air fluxes of CH_3I were only found at two 24h-station. The high correlation to wind speed at S1 was caused by the large variability of the generally low speeds in combination with a relatively constant high concentration gradient. Here we note that although the parameterization of Nightingale et al. (2000) is a commonly applied parameterization for k_w in oceanic trace gas emissions, it might not include all factors influencing sea-to-air fluxes. Stability of the atmosphere and the ocean, sea state, bubble transfer, as well as surfactants might influence the transfer across the air-sea interface as well. Some of these factors are included in the TOGA COARE algorithm representing an alternative method for deriving transfer coefficients, which involves an additional set of meteorological parameters such as air temperature and specific humidity profiles, solar irradiance, downwelling longwave irradiance, and precipitation (Fairall et al., 2003).

Our mean (10^{th}–90^{th} percentile) fluxes of 268 (64–550) in the open ocean and 246 (42–523) pmol m^{-2} h^{-1} in the coastal region are 7.5 and 8.7 lower than the fluxes of Jones et al. (2010) of 2021 (417–4046) and 2154 (321–4096) pmol m^{-2} h^{-1}. Although the spatial resolution of the measurements by Jones et al. (2010) in the same region was higher than during DRIVE, the difference in emission strength can be mainly explained by their large sea water concentrations and very low atmospheric mixing ratios compared to our study. The fluxes reported here were 3.8 times lower than fluxes reported by Richter and Wallace (2004) (958.3 ± 750.0 pmol m^{-2} h^{-1}) using a similar flux parameterization which are a result of higher oceanic CH_3I as well.

5.2 Sea-to-air fluxes of $CHBr_3$ and CH_2Br_2

5.2.1 Oceanic and atmospheric $CHBr_3$ and CH_2Br_2 as drivers of regional and diel variability of the concentration gradient

The oceanic concentrations of both compounds were generally driving factors for their concentration gradients during DRIVE. Only in the open ocean atmospheric $CHBr_3$ and CH_2Br_2 reduced the sea-to-air fluxes significantly (Fig. 6) where the low oceanic concentrations were close to equilibrium with the atmosphere and even led to undersaturation of $CHBr_3$ at S2. The concentration gradient increased towards the Mauritanian upwelling with a much more pronounced increase in oceanic $CHBr_3$ and CH_2Br_2 than in the atmosphere. The oceanic and atmospheric concentrations as well as the concentration gradients of both bromocarbons peaked simultaneously at coastal station S5. Open ocean $CHBr_3$ (1.0–3.8 pmol L^{-1}) and CH_2Br_2 (1.0–2.2 pmol L^{-1}), increasing towards the coast of Mauritania to 8.1–42.4 pmol L^{-1} and

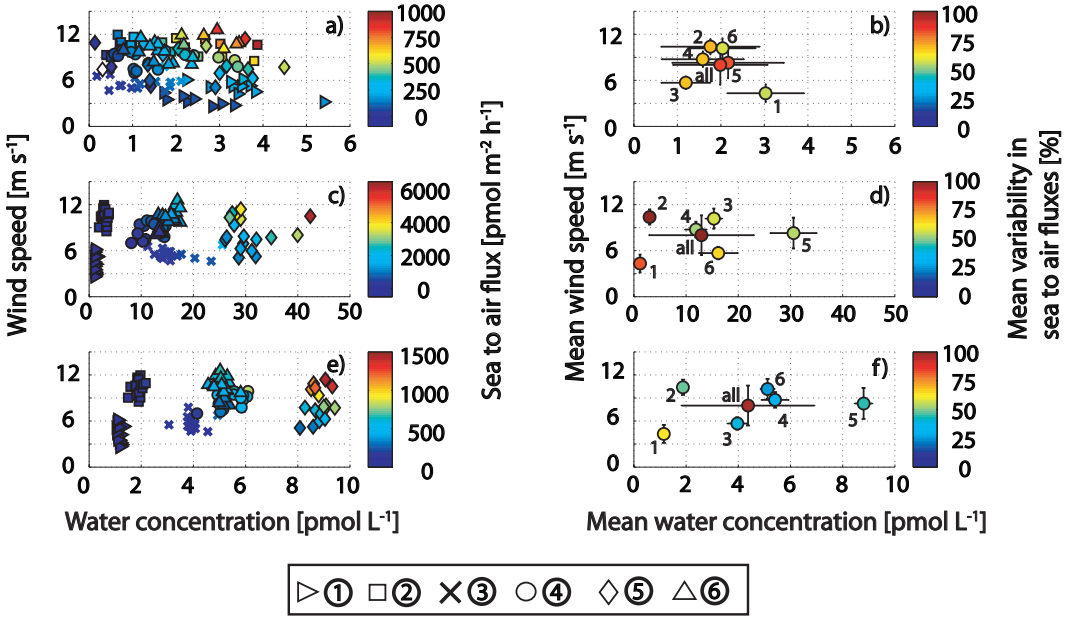

Fig. 8. Left side – wind speed versus CH_3I **(a)**, $CHBr_3$ **(c)** and CH_2Br_2 **(e)** water concentrations. Symbols are filled according to their sea-to-air flux (see color bars). Right side – mean wind speed versus mean CH_3I **(b)**, $CHBr_3$ **(d)** and CH_2Br_2 **(f)** water concentrations with their standard deviations which is expressed in error bars (horizontal for water concentrations and vertical for wind speed) for each diel station (S1–S6) and for all stations together. Symbols are filled with the relative standard deviations of the sea-to-air fluxes (see color bars).

Table 5. Phytoplankton pigments that were found to be significant at $p < 0.05$ and what they are indicative for.

Pigment	Indicative for	$CHBr_3$	CH_2Br_2
Chlorophyll *b*	Chlorophytes	x	x
Chlorophyll *c3*	Haptophytes	x	
Fucoxanthin	Diatoms	x	x
Diatoxanthin		x	
Zeaxanthin	Cyanobacteria	x	
α-carotene	Cryptophytes		x
Alloxanthin			x
Pyrophaephorbide a	Grazing	x	

3.1–9.4 pmol L^{-1}, respectively were in good agreement to earlier studies conducted in the oligotrophic tropical and subtropical Atlantic. Class and Ballschmiter (1988) reported 3.2–23.7 pmol L^{-1} for $CHBr_3$ and 1.7–5.8 pmol L^{-1} for CH_2Br_2 in March, Schall et al. (1997) found 3.2–8.0 for $CHBr_3$ and 1.0–1.8 pmol L^{-1} for CH_2Br_2 in boreal wintertime, while Carpenter et al. (2009) published values from the same season as DRIVE of 2.1–43.6 for $CHBr_3$ and 0.7–8.7 pmol L^{-1} for CH_2Br_2 with the highest values in the Mauritanian upwelling and close to the coast. In contrast to oceanic CH_3I during DRIVE, oceanic $CHBr_3$ and CH_2Br_2 was elevated in the biological active regions and correlated with phytoplankton pigments.

Possible biological sources during DRIVE were identified by using pigments indicative for various phytoplankton groups which were investigated with MLR more thoroughly. However it should be noted that, for example, fucoxanthin, which mainly occurs in diatoms, is also present in other phytoplankton groups to a certain extent (Jeffrey and Vesk, 1997). Production of halocarbons and the occurrence of the phytoplankton pigments may also take place on different time scales, which may obscure or stimulate a correlation. $CHBr_3$ and CH_2Br_2 showed a relationship to *Chlorophytes* and *Diatoms* while $CHBr_3$ also correlated significantly with *Cyanobacteria* and CH_2Br_2 with *Cryptophytes* (Tables 3, 5). Similar biological sources for both bromocarbons are in agreement to previous studies (Manley et al., 1992; Tokarczyk and Moore, 1994). The regional distribution of *Chlorophytes* and $CHBr_3$ and CH_2Br_2 were in best agreement to each other. *Diatoms*, although they were the dominant species in the Mauritanian upwelling and have been shown to produce halocarbons in the laboratory (Moore et al., 1996), appeared not as major contributors to bromocarbons which is in agreement to Quack et al. (2007b). Additionally, pyrophaeophorbide *a* was shown to be significant for the $CHBr_3$ distribution. This chlorophyll degradation product is specific for grazing which could lead to release of bromocarbons (Nightingale et al., 1995) produced within the algae (Moore et al., 1996). The correlations with phytoplankton pigments indicate a potential biological production of $CHBr_3$ and CH_2Br_2, which is also supported by their regional distribution. However, these correlations can neither resolve the rates of production and loss processes of bromocarbons in the ocean, nor their temporal and spatial distribution. Thus,

the correlations found during DRIVE only represent indicators to possible source organisms.

Diel variability in the open ocean for both bromocarbons was very low and increased towards the coast. No relationship of halocarbons to either light, SST or salinity was found during 24 h. Elevated $CHBr_3$ and CH_2Br_2 were usually observed during evening (S3, S4 and S6) and night hours (S5). In contrast, many laboratory and field studies with both macroalgae and phytoplankton have shown maxima of $CHBr_3$ and CH_2Br_2 during the day which was attributed to light induced oxidative stress on the organisms (Ekdahl et al., 1998; Carpenter et al., 2000; Abrahamsson et al., 2004). Bromocarbon production from phytoplankton is still poorly characterized. Elevated bromocarbon production during night may indicate formation during respiration in contrast to light linked production during photosynthesis (Ekdahl et al., 1998; Abrahamsson et al., 2004) or other stress factors such as grazing. Alternatively, $CHBr_3$ and CH_2Br_2 could also be stored in the algal cells during light production and released later during the night time (Ekdahl et al., 1998) which would obscure a correlation to light in the field.

In conclusion, the regional variability of the concentration gradients of both bromocarbons was probably a result of the regional differences in primary production supported by their relationship to SST and phytoplankton pigment data (Sect. 4.2.3).

5.2.2 The relative influence of concentration gradient and wind speed on sea-to-air fluxes of $CHBr_3$ and CH_2Br_2

The regional distribution of sea-to-air fluxes of both bromocarbons was strongly determined by the most likely biologically produced oceanic $CHBr_3$ and CH_2Br_2. The regional variability in oceanic bromocarbons was much larger than the regional variations in wind speed (Fig. 8c–f). However, within individual stations, the variability in oceanic $CHBr_3$ and CH_2Br_2 was mostly lower than the variations in wind speed. At the open ocean stations, only very low oceanic bromocarbons were measured leading to very low concentration gradients and thus to very low sea-to-air fluxes, since the wind speed did not have a large impact on the variability of sea-to-air fluxes. With increasing oceanic $CHBr_3$ and CH_2Br_2 concentrations, the diel impact of changes in wind speed on the sea-to-air flux variability increased which is expressed in high correlation coefficients (Table 4, Fig. 8c, e). This effect was most pronounced for CH_2Br_2 which showed the lowest diel concentration variability of all three halocarbons (see the scatter in Fig. 8e). The influences of wind speed and concentration gradient on the emissions of bromocarbons are discussed based on the parameterization of Nightingale et al. (2000), which may not include all control factors similarly to our discussions concerning CH_3I emissions (Sect. 5.1.2).

Carpenter et al. (2009) derived 8.9 times higher $CHBr_3$ fluxes in the open ocean and 1.3 times higher in the coastal region of mean (10th–90th percentile) 367 (42–625) and 1483 (421–3504) pmol m^{-2} h^{-1} in comparison to our study with 41 (-150 – 222) and 1171 (300 – 2463) pmol m^{-2} h^{-1}. Sea-to-air fluxes of CH_2Br_2 calculated by Carpenter et al. (2009) were 2.4 times higher in the open ocean and in a similar range in the coastal region with 158 (17–288) and 554 (204–917) pmol m^{-2} h^{-1} in comparison to 66 (5–155) and 483 (109–809) pmol m^{-2} h^{-1} (this study) analyzing the same season and region although with higher spatial resolution. This resulted from larger concentration gradients due to their lower atmospheric mixing ratios and comparable ambient parameters.

5.3 Other impact factors on sea-to-air fluxes: MABL height and SST

Wind speed and concentration gradients are direct factors that influence sea-to-air fluxes. Some more indirect factors that could possibly impact the emissions include SST and the MABL through their intensifying or decreasing effect on the concentration gradient. Possible effects of the changes in SST on the solubility of oceanic halocarbons and therewith their concentration gradients were small during DRIVE compared to the variability in sea water concentrations (Fig. 2).

The MABL height has implications for the atmospheric mixing ratios of halocarbons and their sea-to-air fluxes via the concentration or dilution of atmospheric halocarbons, emitted from the oceans, within a decreasing or increasing MABL height (Fuhlbrügge et al., 2013). In order to understand the possible effect of MABL variations, sea-to-air fluxes of all three halocarbons were calculated with minimum and maximum atmospheric mixing ratios associated with high (S1) and low MABL heights (S5) to cover the range of potential fluxes in the study region (Fig. 9). A different concentration distribution caused by other atmospheric conditions can change the $CHBr_3$ and CH_2Br_2 sea-to-air fluxes on average between 19 % (S5) and 4160 % (S1) for $CHBr_3$ and between 7 % (S5) and 1337 % (S1) for CH_2Br_2 (see the lower and upper limits in Fig. 9b–c; the shading implicates the potential range). The effect on the CH_3I fluxes is from 1 % (S1) to 42 % (S4) (Fig. 9a) lower due to its high supersaturation (Fig. 4a). Considering the large MABL height changes occurring within one day above coastal stations, e.g. from 100 to 350 m at S6, the effect of the entailing varying atmospheric mixing ratios on local emissions has to be taken into account when assessing halocarbon sea-to-air fluxes from coastal upwelling regions.

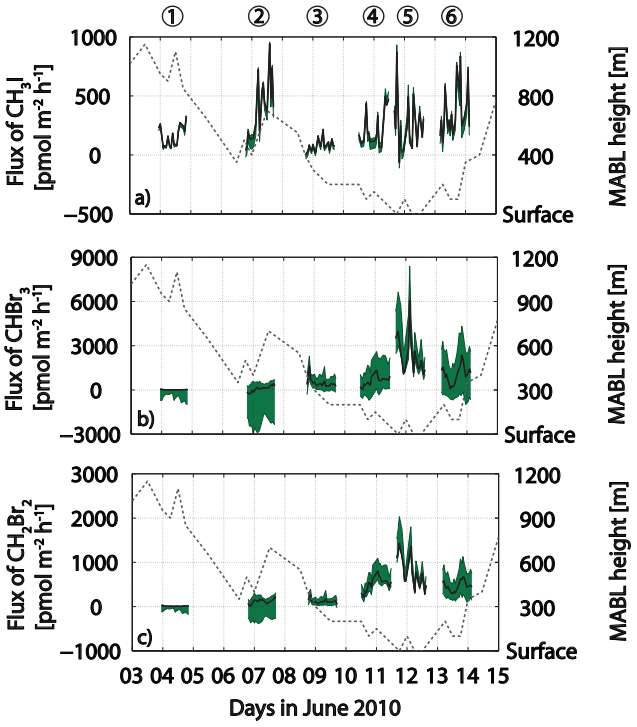

Fig. 9. Sea-to-air fluxes for CH_3I **(a)**, $CHBr_3$ **(b)** and CH_2Br_2 **(c)** during DRIVE and the MABL height, determined by Fuhlbrügge et al. (2013) as the dashed grey line are shown on the right side. The upper and lower value of potential sea-to-air fluxes assuming the lowest MABL (lower range, 3.0 ppt for CH_3I, 3.1 ppt for CH_2Br_2 and 8.9 ppt for $CHBr_3$) and the highest MABL (upper range, 0.6 ppt for CH_3I, 0.9 ppt for CH_2Br_2 and 0.5 ppt for $CHBr_3$) valid for the whole region are shaded in green.

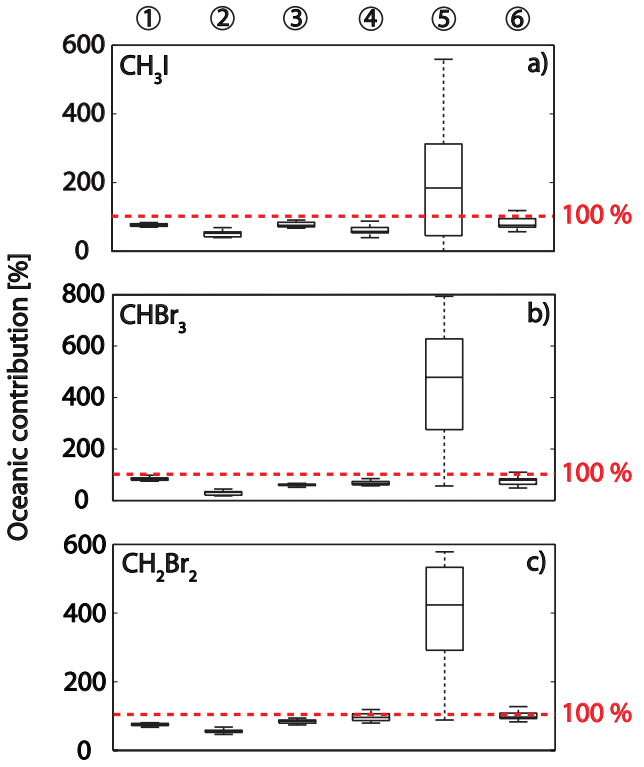

Fig. 10. Oceanic contributions to atmospheric halocarbons assuming a mean distance of 200 km, mean wind speeds, mean sea-to-air fluxes and background mixing ratios for the open ocean (CH_3I = 0.50 ppt, $CHBr_3$ = 0.50 ppt, CH_2Br_2 = 0.75 ppt) and the coastal region (CH_3I = 0.75 ppt, $CHBr_3$ = 3.00 ppt, CH_2Br_2 = 1.80 ppt), and the MABL heights determined by Fuhlbrügge et al. (2013) at every measurement point for CH_3I **(a)**, for $CHBr_3$ **(b)** and for CH_2Br_2 **(c)**, outliers are excluded. The red dashed line marks 100 % in every plot.

5.4 Oceanic influence on atmospheric mixing ratios of CH_3I, $CHBr_3$ and CH_2Br_2

5.4.1 The contribution of the oceanic emissions to the atmospheric mixing ratios

We have shown in the last sections that the sea-to-air fluxes of halocarbons are dominated by the oceanic production and that the sea water concentrations of bromocarbons are increasing towards the coast. In order to understand the importance of sea-to-air fluxes for the atmospheric halocarbon distribution, we calculated their relative contributions to the atmospheric mixing ratios at the individual 24 h-stations. Previous studies assigned the high $CHBr_3$ and CH_2Br_2 mixing ratios above the coastal upwellling to air masses originating from the North West African continent (Quack et al., 2007a) and very low atmospheric bromocarbons to air masses from the northern open ocean (Carpenter et al., 2009; Lee et al., 2010). Air masses during coastal station S5 also arrived from the northern open ocean (Fuhlbrügge et al., 2013) which contradicts the hypothesis that high atmospheric halocarbons could only be accounted for by continental sources.

For our calculations, we apply a fetch of 200 km (the mean distance between the diel stations), sea-to-air fluxes from Sects. 4.1.5 and 4.2.6, according wind speeds and MABL heights (Table 1). The sea-to-air fluxes and the height of the MABL have numerically the same influence on atmospheric mixing ratios since bromocarbons in the atmosphere are within the calculations a product of both. Applying a fetch of 200 km, the air mass travels approximately 7 h until it arrives at the diel stations. Open ocean background values for S1 and S2 were set to 0.50 ppt for CH_3I and $CHBr_3$, and 0.75 ppt for CH_2Br_2, while higher background values of 0.75 ppt for CH_3I, 1.80 ppt for CH_2Br_2 and 3.00 ppt for $CHBr_3$ were assigned to coastal stations S3–S6. We did not include the tropical atmospheric lifetimes of the three halocarbons (7, 24, 123 days for CH_3I, $CHBr_3$, CH_2Br_2; Montzka and Reimann, 2011) since the degradation during the short-term box-calculation has no substantial influence on the results. The oceanic emissions are nearly sufficient to explain most of the atmospheric halocarbons (Fig. 10a–c). Oceanic halocarbon contributions at S1–S6 (except for S5)

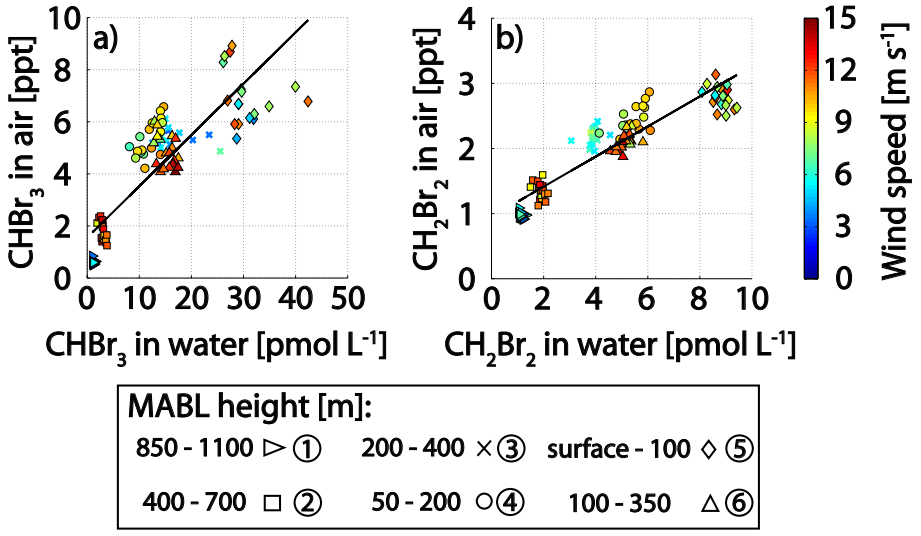

Fig. 11. Correlations of oceanic versus atmospheric halocarbons ($CHBr_3$ in **a** and CH_2Br_2 in **b**) filled with wind speed (see color coding). The black line indicates the regression line for the whole cruise. For the individual correlation coefficients see Table 6.

ranged from 39 to 135 % for CH_3I, between 18 and 126 % for $CHBr_3$ and from 47 to 148 % for CH_2Br_2 with generally lowest contributions at S2 (40–69 % for CH_3I, 18–45 % for $CHBr_3$ and 47–68 % for CH_2Br_2). At S5, the emissions from the assumed 200 km fetch contributed 560 (CH_3I)–800 % ($CHBr_3$) to the observed mixing ratios. At this station high oceanic and atmospheric $CHBr_3$ and CH_2Br_2 coincided with very low MABL heights. These results suggest that (1) atmospheric mixing ratios over the open ocean S1–S2 are derived from regional emissions and distant sources, (2) the source strength in combination with the observed MABL height can nearly maintain the medium range of atmospheric mixing ratios found at S3, S4, and S6, and (3) the high sea-to-air fluxes and low MABL heights leading to the highly elevated atmospheric mixing ratios at S5 are a very local phenomenon, constrained to the boundaries of this station. The large overestimation of mixing ratios within the box model is then a result of the extrapolation of the high sea-to-air fluxes to the fetch of 200 km. Vertical transport has been neglected in this simple model approach, which likely introduces only small errors since the top of the MABL was very stable and isolated above all coastal stations (Fuhlbrügge et al., 2013).

While the Mauritanian upwelling has been identified to contribute to the high atmospheric abundances of all halocarbons in the region, the elevated and highly variable atmospheric mixing ratios of $CHBr_3$ and CH_2Br_2 at Cape Verde can be attributed to local sources. O'Brien et al. (2009) suggested high atmospheric halocarbons at CVAO originating from the coastal region off Mauritania. However, back trajectory analysis revealed air masses at CVAO originating from the open ocean during our investigation (Fuhlbrügge et al., 2013). This together with the considerably lower atmospheric mixing ratios measured at the open ocean stations (0.5 – 2.4 ppt for $CHBr_3$ and 0.9–1.6 ppt for CH_2Br_2) and around the upwelling contradicts upwelling originated halocarbons at Cape Verde during DRIVE. In addition, $CHBr_3$ reached its highest value of the whole campaign at CVAO. Hence, the high and variable atmospheric $CHBr_3$ and CH_2Br_2 at Cape Verde in combination with comparably variable wind speeds suggest local coastal sources for both compounds.

5.4.2 Correlations between oceanic and atmospheric $CHBr_3$ and CH_2Br_2

In contrast to the observations presented in Quack et al. (2007a) and Carpenter et al. (2009), atmospheric $CHBr_3$ and CH_2Br_2 followed the same regional distribution as their oceanic counterparts. Water concentrations and atmospheric mixing ratios of $CHBr_3$ ($R^2 = 0.74$) and CH_2Br_2 ($R^2 = 0.85$) correlated regionally very well during DRIVE (Fig. 11a–b) which has not been observed during the other cruises. This is likely caused by a combination of the stable and isolated marine boundary layer observed over the upwelling, the coinciding high productivity and concentration of the bromocarbons in the upwelling, and the combined effects of air-sea exchange as slowest process (over a considerable fetch) and advection as the fastest (diluting with background air), both influencing the atmospheric signals. We assume biological production of bromocarbons and mixing within the water column also as rapid processes (Ekdahl et al., 1998). Correlations between atmospheric mixing ratios and oceanic concentrations within the individual 24h-stations were only significant at open ocean station S2 for $CHBr_3$ and at coastal stations S4 and S6 for both compounds (Table 6). A diel anti-correlation of atmospheric mixing ratios with water concentrations was also observed at several diel stations (S1, S2, S5,

Table 6. Correlation coefficients R^2 and number of data points n of oceanic versus atmospheric bromocarbons for the whole cruise and each individual station. Bold numbers indicate significant correlations with p <0.05. Italic numbers mark negative correlations.

	Whole cruise	S1 (17.6° N and 24.3° W)	S2 (18.0° N and 21.0° W)	S3 (18.0° N and 18.0° W)	S4 (18.5° N and 16.5° W)	S5 (19.0° N and 16.6° W)	S6 (20.0° N and 17.3° W)
$CHBr_3$	**0.74**	*0.01*	***0.52***	0.01	**0.45**	*0.05*	***0.20***
CH_2Br_2	**0.85**	*0.19*	*0.09*	0.01	**0.40**	*0.18*	**0.28**
n	109	18	19	17	17	18	20

and S6). An explanation for this observation (see Table 6) between the atmospheric and oceanic concentrations on a diel scale is still lacking, since neither wind direction, including land-sea breeze circulation (Fuhlbrügge et al., 2013), nor MABL height variations led to clear correlations.

Positive and negative deviations from the overall good regional correlation of sea water concentrations and atmospheric mixing ratios could also be observed at the individual stations. Atmospheric concentrations can increase with wind speed due to increasing sea-to-air fluxes, while elevated wind speeds also dilute local emissions with background air and vice versa. Thus, low wind speeds in the open ocean led to lower atmospheric mixing ratios at S1 while the higher wind speeds at S2 triggered average mixing ratios (Fig. 11). This may not only be a result of increasing sea-to-air flux and fetch, but may also be partly a result of the reduction of the MABL height. While coastal stations S3, S4 and S6 have similar mean $CHBr_3$ surface water concentrations, S6 showed the largest sea-to-air fluxes of these three stations due to the largest prevailing wind speeds (see Fig. 5), but on average relatively low atmospheric mixing ratios (Fig. 11a, b). We interpret this as intense transport phenomenon and possible dilution of the large sea-to-air fluxes with background air masses due to intensifying winds and increasing MABL height. Although atmospheric mixing ratios for $CHBr_3$ and CH_2Br_2 were highest at S5, they are on average much lower as could be expected from the overall regional correlation and the large sea water concentrations (see the data points below the correlation line in Fig. 11a, b in contrast to most of the data points from other stations that are above the line). We hypothesize regional mixing with background air masses as cause for the lower than average correlation of sea surface $CHBr_3$ and CH_2Br_2 and atmospheric bromocarbons, which supports that the high atmospheric mixing ratios at S5, the high sea-to-air fluxes, and low MABL height are very local phenomena. The good overall correlation between atmospheric and oceanic bromocarbons shows the dominance of sea water production for the atmosphere. The co-correlation of increased productivity and production of bromocarbons during upwelling of cold and nutrient rich water and the high atmospheric mixing ratios in a low and stable MABL over the low sea surface temperature of the upwelled water (Fuhlbrügge et al., 2013) can be explained within the known concepts of wind driven air-sea exchange, advection and MABL variations on a regional scale.

6 Summary and conclusions

We have discussed the temporal and spatial influence of biological productivity, wind speed, MABL height and SST on oceanic emissions and atmospheric mixing ratios of halocarbons in the tropical North East Atlantic.

During DRIVE, oceanic CH_3I neither showed a relationship to phytoplankton pigments nor to cyanobacteria, and its distribution appeared mainly as a result of abiotic or indirect biological formation which seemed to be the main driver of the CH_3I concentration gradient between sea water and air. On a regional scale, neither wind speed nor oceanic CH_3I were dominating the sea-to-air flux, while diel variations in emissions were a result of varying oceanic CH_3I concentrations almost throughout the whole cruise. On the contrary, the oceanic distribution of $CHBr_3$ and CH_2Br_2 and their emissions correlated with phytoplankton pigments which implies a biological source, albeit with no clear diurnal cycles unlike observed in previous studies. The variability in wind speed gained increasing impact on the diel bromocarbon emissions with decreasing distance to the coast, because the diel variability in oceanic $CHBr_3$ and even more pronounced in oceanic CH_2Br_2 was low in comparison to large diel wind speed variations.

MABL height was identified as an additional factor impacting oceanic emissions of halocarbons in the upwelling through its influence on atmospheric halocarbon abundances. Sea-to-air fluxes of CH_3I were hardly influenced by the varying MABL due to its high supersaturation in sea surface water. The sea-to-air fluxes of $CHBr_3$ and CH_2Br_2 however were substantially influenced by atmospheric conditions High atmospheric CH_3I, $CHBr_3$ and CH_2Br_2 mixing ratios at a coastal site on the Cape Verde islands (CVAO) could be attributed to local coastal sources. Regional oceanic bromocarbon emissions from the upwelling, probably driven by biological production, could in combination with varying and low MABL heights and air mass transport explain most of the observed atmospheric halocarbons, contrasting previous hypotheses regarding additional continental bromo-

carbon sources above the upwelling. As a result, the atmospheric bromocarbons showed significant and high overall correlations with the oceanic concentrations, which is caused by the coincidence of oceanic production in upwelled water and low and stable MABLs over the cold upwelled water. We therefore hypothesize that low MABL heights and high sea-to-air fluxes coinciding with high atmospheric mixing ratios could be a common feature in coastal upwelling systems (this study; Fuhlbrügge et al., 2013).

The temporal and spatial development of biological production, wind speed, SST and changes in atmospheric mixing ratios with MABL height will influence the future sea-to-air fluxes and their corresponding atmospheric mixing ratios, as well as their contribution to atmospheric chemical processes. Surface air and water temperature could play a crucial role in the future development of wind speed via the potentially increased land-sea pressure gradients. A potential future increase of SST in the tropical oligotrophic Atlantic (Hoerling et al., 2001) could lead to enhanced oceanic production of CH_3I (Richter, 2004) and in combination with reduced solubility to elevated emissions of CH_3I. An elevation of atmospheric CH_3I with increasing SST and accompanying physical-biological phenomena on a decadal scale has already been shown by Yokouchi et al. (2012) in the tropical and temperate Pacific region. At the same time, the enhancement of eastern boundary upwelling systems accompanied by increasing primary production (Lachkar and Gruber, 2012) could result in higher production of oceanic bromocarbons. Combined with elevated wind speeds (Bakun, 1990), increased emissions of brominated compounds would be the consequence. Hence, the relevance of the tropical upwelling systems with respect to halocarbon emissions will likely increase and the influence of the diel and regional drivers on the emissions may be intensified. To better understand the current and future roles of halocarbon emissions from marine upwelling regions on global ozone changes and atmospheric chemistry, it is important to continue to better quantify the relative roles and interactions of oceanic halocarbon production, wind speed and MABL height, SST and seasonal variations, as well as other relevant forcings in oceanic upwelling regions around the global ocean.

Acknowledgements. The authors would like to thank the chief scientist of the cruise P399/2 Prof Dr Hermann W. Bange, as well as the captain and the crew of the RV *Poseidon* during P399/2 for all their help and support. We are also very grateful to Karen Stange and Gert Petrick for their technical support before and during the campaign. We would like to acknowledge Carolin Löscher for her help with water sampling for pigment analysis and Bettina Taylor for analysis of the flow cytometry samples. The authors thank Christian Müller and Julian Kinzel for their assistance with air sampling at CVAO. We thank Xiaorong Zhu and Leslie Pope for technical assistance in the air canister analyses. Furthermore, we would like to thank Christa Marandino and Susann Tegtmeier for their helpful input. We acknowledge the National Centre for Atmospheric Science (NCAS) for providing the Cape Verde Atmospheric Observatory wind speed data. Additionally, the authors would like to acknowledge NASA for providing satellite MODIS-Aqua data. We thank the anonymous reviewers for very helpful input and corrections. This work was part of the German research project SOPRAN II (grant no. FKZ 03F0611A) funded by the Bundesministerium für Bildung und Forschung (BMBF), and was also supported by the EU project SHIVA (grant no. FP7-ENV-2007-1-226224), as well as NASA UARP Grant NNX09AJ25G.

The service charges for this open access publication have been covered by a Research Centre of the Helmholtz Association.

Edited by: W. T. Sturges

References

Abrahamsson, K., Lorén, A., Wulff, A., and Wangberg, S. A.: Air-sea exchange of halocarbons: The influence of diurnal and regional variations and distribution of pigments, Deep-Sea Res. Part II-Top. Stud. Oceanogr., 51, 2789–2805, doi:10.1016/j.dsr2.2004.09.005, 2004.

Amachi, S., Kamagata, Y., Kanagawa, T., and Muramatsu, Y.: Bacteria mediate methylation of iodine in marine and terrestrial environments, Appl. Environ. Microbiol., 67, 2718–2722, doi:10.1128/aem.67.6.2718-2722.2001, 2001.

Aschmann, J., Sinnhuber, B. M., Chipperfield, M. P., and Hossaini, R.: Impact of deep convection and dehydration on bromine loading in the upper troposphere and lower stratosphere, Atmos. Chem. Phys., 11, 2671–2687, doi:10.5194/acp-11-2671-2011, 2011.

Bakun, A.: Global climate change and intensification of coastal ocean upwelling, Science, 247, 198–201, doi:10.1126/science.247.4939.198, 1990.

Bange, H. W., Atlas, E. L., Bahlmann, E., Baker, A. R., Bracher, A., Cianca, A., Dengler, M., Fuhlbrügge, S., Großmann, K., Hepach, H., Lavric, J., Löscher, C., Krüger, K., Orlikowska, A., Peeken, I., Quack, B., Schafstall, J., Steinhoff, T., Williams, J., and Wittke, F.: Fs poseidon fahrtbericht/cruise report p399 – 2 & 3, Leibniz-Institut für Meereswissenschaften IFM-GEOMAR, Kiel, 74, 2011.

Bell, N., Hsu, L., Jacob, D. J., Schultz, M. G., Blake, D. R., Butler, J. H., King, D. B., Lobert, J. M., and Maier-Reimer, E.: Methyl iodide: Atmospheric budget and use as a tracer of marine convection in global models, J. Geophys. Res.-Atmos., 107, 4340, doi:10.1029/2001jd001151, 2002.

Carpenter, L. J. and Liss, P. S.: On temperate sources of bromoform and other reactive organic bromine gases, J. Geophys. Res.-Atmos., 105, 20539–20547, 2000.

Carpenter, L. J., Malin, G., Liss, P. S., and Kupper, F. C.: Novel biogenic iodine-containing trihalomethanes and other short-lived halocarbons in the coastal east atlantic, Glob. Biogeochem. Cy., 14, 1191–1204, 2000.

Carpenter, L. J., Jones, C. E., Dunk, R. M., Hornsby, K. E., and Woeltjen, J.: Air-sea fluxes of biogenic bromine from the tropical and north atlantic ocean, Atmos. Chem. Phys., 9, 1805–1816, doi:10.5194/acp-9-1805-2009, 2009.

Class, T., and Ballschmiter, K.: Chemistry of organic traces in air viii: Sources and distribution of brom- and bromochloromethanes in marine air and surfacewater of the atlantic ocean, J. Atmos. Chem., 6, 35-46, 1988.

Ekdahl, A., Pedersén, M., and Abrahamsson, K.: A study of the diurnal variation of biogenic volatile halocarbons, Mar. Chem., 63, 1–8, 1998.

Fairall, C. W., Bradley, E. F., Hare, J. E., Grachev, A. A., and Edson, J. B.: Bulk parameterization of air–sea fluxes: Updates and verification for the coare algorithm, J. Clim., 16, 571–591, doi:10.1175/1520-0442(2003)016<0571:bpoasf>,2.0.co;2, 2003.

Fedoseev, A.: Geostrophic circulation of surface waters on the shelf of north-west africa, Rapp. Proc. Verb. Reun. Cons. Inst. Expl. Mer., 159, 32–37, 1970.

Fuhlbrügge, S., Krüger, K., Quack, B., Atlas, E. L., Hepach, H., and Ziska, F.: Impact of the marine atmospheric boundary layer on vsls abundances in the eastern tropical and subtropical north atlantic ocean, Atmos. Chem. Phys., 13, 6345–6357, doi:10.5194/acp-13-6345-2013, 2013.

Fuse, H., Inoue, H., Murakami, K., Takimura, O., and Yamaoka, Y.: Production of free and organic iodine by roseovarius spp, FEMS Microbiology Letters, 229, 189–194, doi:10.1016/s0378-1097(03)00839-5, 2003.

Hagen, E.: Northwest african upwelling scenario, Oceanol. Acta, 24, S113–S128, 2001.

Happell, J. D. and Wallace, D. W. R.: Methyl iodide in the greenland/norwegian seas and the tropical atlantic ocean: Evidence for photochemical production, Geophys. Res. Lett., 23, 2105–2108, doi:10.1029/96gl01764, 1996.

Hoerling, M. P., Hurrell, J. W., and Xu, T. Y.: Tropical origins for recent north atlantic climate change, Science, 292, 90–92, doi:10.1126/science.1058582, 2001.

Hossaini, R., Chipperfield, M. P., Monge-Sanz, B. M., Richards, N. A. D., Atlas, E., and Blake, D. R.: Bromoform and dibromomethane in the tropics: A 3-d model study of chemistry and transport, Atmos. Chem. Phys., 10, 719–735, doi:10.5194/acp-10-719-2010, 2010.

Hossaini, R., Chipperfield, M. P., Feng, W., Breider, T. J., Atlas, E., Montzka, S. A., Miller, B. R., Moore, F., and Elkins, J.: The contribution of natural and anthropogenic very short-lived species to stratospheric bromine, Atmos. Chem. Phys., 12, 371–380, doi:10.5194/acp-12-371-2012, 2012a.

Hossaini, R., Chipperfield, M. P., Dhomse, S., Ordonez, C., Saiz-Lopez, A., Abraham, N. L., Archibald, A., Braesicke, P., Telford, P., Warwick, N., Yang, X., and Pyle, J.: Modelling future changes to the stratospheric source gas injection of biogenic bromocarbons, Geophys. Res. Lett., 39, L20813, doi:10.1029/2012gl053401, 2012b.

Jeffrey, S. W. and Vesk, M.: Introduction to marine phytoplankton and their pigment signatures, in: Phytoplankton pigments in oceanography: Guideline to modern methods., edited by: Jeffrey, S. W., Mantoura, R. F. C., and Wright, S. W., 10, UNESCO Publishing, Paris, 37–84, 1997.

Jones, C. E., Hornsby, K. E., Sommariva, R., Dunk, R. M., Von Glasow, R., McFiggans, G., and Carpenter, L. J.: Quantifying the contribution of marine organic gases to atmospheric iodine, Geophys. Res. Lett., 37, L18804, doi:10.1029/2010gl043990, 2010.

Lachkar, Z. and Gruber, N.: A comparative study of biological production in eastern boundary upwelling systems using an artificial neural network, Biogeosciences, 9, 293–308, doi:10.5194/bg-9-293-2012, 2012.

Lai, S. C., Williams, J., Arnold, S. R., Atlas, E. L., Gebhardt, S., and Hoffmann, T.: Iodine containing species in the remote marine boundary layer: A link to oceanic phytoplankton, Geophys. Res. Lett., 38, L20801, doi:10.1029/2011gl049035, 2011.

Laturnus, F.: Marine macroalgae in polar regions as natural sources for volatile organohalogens, Environ. Sci. Pollut. Res., 8, 103–108, doi:10.1007/bf02987302, 2001.

Lee, J. D., McFiggans, G., Allan, J. D., Baker, A. R., Ball, S. M., Benton, A. K., Carpenter, L. J., Commane, R., Finley, B. D., Evans, M., Fuentes, E., Furneaux, K., Goddard, A., Good, N., Hamilton, J. F., Heard, D. E., Herrmann, H., Hollingsworth, A., Hopkins, J. R., Ingham, T., Irwin, M., Jones, C. E., Jones, R. L., Keene, W. C., Lawler, M. J., Lehmann, S., Lewis, A. C., Long, M. S., Mahajan, A., Methven, J., Moller, S. J., Muller, K., Muller, T., Niedermeier, N., O'Doherty, S., Oetjen, H., Plane, J. M. C., Pszenny, A. A. P., Read, K. A., Saiz-Lopez, A., Saltzman, E. S., Sander, R., von Glasow, R., Whalley, L., Wiedensohler, A., and Young, D.: Reactive halogens in the marine boundary layer (rhamble): The tropical north atlantic experiments, Atmos. Chem. Phys., 10, 1031–1055, doi:10.5194/acp-10-1031-2010, 2010.

Manley, S. L. and Dastoor, M. N.: Methyl-iodide (CH_3I) production by kelp and associated microbes, Mar. Biol., 98, 477–482, 1988.

Manley, S. L., Goodwin, K., and North, W. J.: Laboratory production of bromoform, methylene bromide, and methyl-iodide by macroalgae and distribution in nearshore southern california waters, Limnol. Oceanogr., 37, 1652–1659, 1992.

Martino, M., Mills, G. P., Woeltjen, J., and Liss, P. S.: A new source of volatile organoiodine compounds in surface seawater, Geophys. Res. Lett., 36, L01609, doi:10.1029/2008GL036334, 2009.

McGivern, W. S., Sorkhabi, O., Suits, A. G., Derecskei-Kovacs, A., and North, S. W.: Primary and secondary processes in the photodissociation of chbr3, J. Phys. Chem. A, 104, 10085–10091, doi:10.1021/jp0005017, 2000.

McGregor, H. V., Dima, M., Fischer, H. W., and Mulitza, S.: Rapid 20th-century increase in coastal upwelling off northwest africa, Science, 315, 637–639, doi:10.1126/science.1134839, 2007.

Minas, H. J., Codispoti, L. A., and Dugdale, R. C.: Nutrients and primary production in the upwelling region off northwest africa, Rapp. Proc. Verb. Reun. Cons. Inst. Expl. Mer., 180, 148–183, 1982.

Mittelstaedt, E.: Large-scale circulation along the coast of northwest africa, Rapp. Proc. Verb. Reun. Cons. Inst. Expl. Mer., 180, 50–57, 1982.

Montzka, S. A. and Reimann, S.: Ozone-depleting substances and related chemicals, Chapter 1 in Scientific Assessment of Ozone Depletion: 2010, Global Ozone Research and Monitoring Project, World Meteorological Organization (WMO), Geneva, Report No. 52, 2011.

Moore, R. M. and Zafiriou, O. C.: Photochemical production of methyl-iodide in seawater, J. Geophys. Res.-Atmos., 99, 16415–16420, doi:10.1029/94jd00786, 1994.

Moore, R. M., Geen, C. E., and Tait, V. K.: Determination of henry law constants for a suite of naturally-occurring halo-

genated methanes in seawater, Chemosphere, 30, 1183-1191, doi:10.1016/0045-6535(95)00009-w, 1995a.

Moore, R. M., Tokarczyk, R., Tait, V. K., Poulin, M., and Geen, C. E.: Marine phytoplankton as a natural source of volatile organohalogens, in: Naturally-produced organohalogens, edited by: Grimvall, A., and deLeer, E. W. B., Kluwer Academic Publishers, Dordrecht, The Netherlands, 283–294, 1995b.

Moore, R. M., Webb, M., Tokarczyk, R., and Wever, R.: Bromoperoxidase and iodoperoxidase enzymes and production of halogenated methanes in marine diatom cultures, J. Geophys. Res.-Oceans, 101, 20899–20908, doi:10.1029/96jc01248, 1996.

Moore, R. M. and Groszko, W.: Methyl iodide distribution in the ocean and fluxes to the atmosphere, J. Geophys. Res.-Oceans, 104, 11163–11171, doi:10.1029/1998jc900073, 1999.

Nightingale, P. D., Malin, G., and Liss, P. S.: Production of chloroform and other low-molecular-weight halocarbons by some species of macroalgae, Limnol. Oceanogr., 40, 680–689, 1995.

Nightingale, P. D., Malin, G., Law, C. S., Watson, A. J., Liss, P. S., Liddicoat, M. I., Boutin, J., and Upstill-Goddard, R. C.: In situ evaluation of air-sea gas exchange parameterizations using novel conservative and volatile tracers, Global Biogeochem. Cy., 14, 373–387, doi:10.1029/1999gb900091, 2000.

O'Brien, L. M., Harris, N. R. P., Robinson, A. D., Gostlow, B., Warwick, N., Yang, X., and Pyle, J. A.: Bromocarbons in the tropical marine boundary layer at the cape verde observatory - measurements and modelling, Atmos. Chem. Phys., 9, 9083–9099, doi:10.5194/acp-9-9083-2009, 2009.

O'Dowd, C. D., Jimenez, J. L., Bahreini, R., Flagan, R. C., Seinfeld, J. H., Hameri, K., Pirjola, L., Kulmala, M., Jennings, S. G., and Hoffmann, T.: Marine aerosol formation from biogenic iodine emissions, Nature, 417, 632–636, doi:10.1038/nature00775, 2002.

Pyle, J. A., Warwick, N., Yang, X., Young, P. J., and Zeng, G.: Climate/chemistry feedbacks and biogenic emissions, Philos. Trans. R. Soc. A-Math. Phys. Eng. Sci., 365, 1727–1740, doi:10.1098/rsta.2007.2041, 2007.

Quack, B. and Wallace, D. W. R.: Air-sea flux of bromoform: Controls, rates, and implications, Glob. Biogeochem. Cy., 17, 1023, doi:10.1029/2002gb001890, 2003.

Quack, B., Atlas, E., Petrick, G., Stroud, V., Schauffler, S., and Wallace, D. W. R.: Oceanic bromoform sources for the tropical atmosphere, Geophys. Res. Lett., 31, L23S05, doi:10.1029/2004gl020597, 2004.

Quack, B., Atlas, E., Petrick, G., and Wallace, D. W. R.: Bromoform and dibromomethane above the mauritanian upwelling: Atmospheric distributions and oceanic emissions, J. Geophys. Res.-Atmos., 112, D09312, doi:10.1029/2006jd007614, 2007a.

Quack, B., Peeken, I., Petrick, G., and Nachtigall, K.: Oceanic distribution and sources of bromoform and dibromomethane in the mauritanian upwelling, J. Geophys. Res.-Oceans, 112, C10006, doi:10.1029/2006jc003803, 2007b.

Richter, U.: Factors influencing methyl iodide production in the ocean and its flux to the atmosphere, PhD thesis, Mathematisch-Naturwissenschaftliche Fakultät der Christian-Albrechts-Universität zu Kiel, Christian-Albrechts-Universität zu Kiel, Kiel, 117 pp., 2004.

Richter, U. and Wallace, D. W. R.: Production of methyl iodide in the tropical atlantic ocean, Geophys. Res. Lett., 31, L23S03, doi:10.1029/2004gl020779, 2004.

Saiz-Lopez, A., Plane, J. M. C., Baker, A. R., Carpenter, L. J., von Glasow, R., Martin, J. C. G., McFiggans, G., and Saunders, R. W.: Atmospheric chemistry of iodine, Chem. Rev., 112, 1773–1804, doi:10.1021/cr200029u, 2012.

Salawitch, R. J., Weisenstein, D. K., Kovalenko, L. J., Sioris, C. E., Wennberg, P. O., Chance, K., Ko, M. K. W., and McLinden, C. A.: Sensitivity of ozone to bromine in the lower stratosphere, Geophys. Res. Lett., 32, L05811, doi:10.1029/2004gl021504, 2005.

Schall, C., Heumann, K. G., and Kirst, G. O.: Biogenic volatile organoiodine and organobromine hydrocarbons in the atlantic ocean from 42 degrees N to 72 degrees S, Fresenius J. Anal. Chem., 359, 298–305, 1997.

Schauffler, S. M., Atlas, E. L., Blake, D. R., Flocke, F., Lueb, R. A., Lee-Taylor, J. M., Stroud, V., and Travnicek, W.: Distributions of brominated organic compounds in the troposphere and lower stratosphere, J. Geophys. Res.-Atmos., 104, 21513–21535, 1999.

Smythe-Wright, D., Boswell, S. M., Breithaupt, P., Davidson, R. D., Dimmer, C. H., and Diaz, L. B. E.: Methyl iodide production in the ocean: Implications for climate change, Glob. Biogeochem. Cy., 20, GB3003, doi:10.1029/2005GB002642, 2006.

Solomon, S., Garcia, R. R., and Ravishankara, A. R.: On the role of iodine in ozone depletion, J. Geophys. Res.-Atmos., 99, 20491–20499, doi:10.1029/94JD02028, 1994.

Stemmler, I., Hense, I., Quack, B., and Maier-Reimer, E.: Methyl iodide production in the open ocean, Biogeosciences Discuss., 10, 17549–17595, doi:10.5194/bgd-10-17549-2013, 2013.

Taylor, B. B., Torrecilla, E., Bernhardt, A., Taylor, M. H., Peeken, I., Rottgers, R., Piera, J., and Bracher, A.: Bio-optical provinces in the eastern atlantic ocean and their biogeographical relevance, Biogeosciences, 8, 3609–3629, doi:10.5194/bg-8-3609-2011, 2011.

Tegtmeier, S., Kruger, K., Quack, B., Atlas, E. L., Pisso, I., Stohl, A., and Yang, X.: Emission and transport of bromocarbons: From the west pacific ocean into the stratosphere, Atmos. Chem. Phys., 12, 10633–10648, doi:10.5194/acp-12-10633-2012, 2012.

Tegtmeier, S., Krüger, K., Quack, B., Atlas, E., Blake, D. R., Boenisch, H., Engel, A., Hepach, H., Hossaini, R., Navarro, M. A., Raimund, S., Sala, S., Shi, Q., and Ziska, F.: The contribution of oceanic methyl iodide to stratospheric iodine, Atmos. Chem. Phys., 13, 11869–11886, doi:10.5194/acp-13-11869-2013, 2013.

Tokarczyk, R. and Moore, R. M.: Production of volatile organohalogens by phytoplankton cultures, Geophys. Res. Lett., 21, 285–288, 1994.

Tomczak, M.: The distribution of water masses at the surface as derived from t-s diagram analysis in the cineca area, Rapp. Proc. Verb. Reun. Cons. Inst. Expl. Mer., 180, 48–49, 1982.

Tomczak, M. and Godfrey, J. S.: Regional oceanography: An introduction, 2 ed., Daya Publishing House, Delhi, 2005.

Tran, S., Bonsang, B., Gros, V., Peeken, I., Sarda-Esteve, R., Bernhardt, A., and Belviso, S.: A survey of carbon monoxide and nonmethane hydrocarbons in the arctic ocean during summer 2010, Biogeosciences, 10, 1909–1935, doi:10.5194/bg-10-1909-2013, 2013.

Tsuchiya, M., Talley, L. D., and McCartney, M. S.: An eastern atlantic section from iceland southward across the equator, Deep-Sea Res., 39, 1885–1917, doi:10.1016/0198-0149(92)90004-d, 1992.

Williams, J., Gros, V., Atlas, E., Maciejczyk, K., Batsaikhan, A., Scholer, H. F., Forster, C., Quack, B., Yassaa, N., Sander, R., and Van Dingenen, R.: Possible evidence for a connection between methyl iodide emissions and saharan dust, J. Geophys. Res.-Atmos., 112, D07302, doi:10.1029/2005jd006702, 2007.

Yokouchi, Y., Osada, K., Wada, M., Hasebe, F., Agama, M., Murakami, R., Mukai, H., Nojiri, Y., Inuzuka, Y., Toom-Sauntry, D., and Fraser, P.: Global distribution and seasonal concentration change of methyl iodide in the atmosphere, J. Geophys. Res.-Atmos., 113, D18311, doi:10.1029/2008JD009861, 2008.

Yokouchi, Y., Nojiri, Y., Toom-Sauntry, D., Fraser, P., Inuzuka, Y., Tanimoto, H., Nara, H., Murakami, R., and Mukai, H.: Long-term variation of atmospheric methyl iodide and its link to global environmental change, Geophys. Res. Lett., 39, L23805, doi:10.1029/2012GL053695, 2012.

Ziska, F., Quack, B., Abrahamsson, K., Archer, S. D., Atlas, E., Bell, T., Butler, J. H., Carpenter, L. J., Jones, C. E., Harris, N. R. P., Hepach, H., Heumann, K. G., Hughes, C., Kuss, J., Krüger, K., Liss, P., Moore, R. M., Orlikowska, A., Raimund, S., Reeves, C. E., Reifenhäuser, W., Robinson, A. D., Schall, C., Tanhua, T., Tegtmeier, S., Turner, S., Wang, L., Wallace, D., Williams, J., Yamamoto, H., Yvon-Lewis, S., and Yokouchi, Y.: Global sea-to-air flux climatology for bromoform, dibromomethane and methyl iodide, Atmos. Chem. Phys., 13, 8915–8934, doi:10.5194/acp-13-8915-2013, 2013.

3.3 Manuscript 3

The contribution of oceanic very short lived halocarbons to marine and free troposphere air over the tropical West Pacific

S. Fuhlbrügge[1], B. Quack[1], S. Tegtmeier[1], E. Atlas[2], H. Hepach[1], Q. Shi[3], S. Raimund[1], and K. Krüger[4]

[1] GEOMAR Helmholtz-Zentrum für Ozeanforschung Kiel, Kiel, Germany

[2] Rosenstiel School of Marine and Atmospheric Science (RSMAS), Miami, USA

[3] Department of Oceanography – Dalhousie University, Halifax, Canada

[4] Department of Geosciences, University of Oslo (UiO), Oslo, Norway

Published in: Atmospheric Chemistry and Physics Discuss., Vol. 15, 17887–17943, doi:10.5194/acpd-15-17887-2015, 2015.

Atmos. Chem. Phys. Discuss., 15, 17887–17943, 2015
www.atmos-chem-phys-discuss.net/15/17887/2015/
doi:10.5194/acpd-15-17887-2015

Atmospheric Chemistry and Physics Discussions

The contribution of oceanic halocarbons to marine and free troposphere air over the tropical West Pacific

S. Fuhlbrügge[1], B. Quack[1], S. Tegtmeier[1], E. Atlas[2], H. Hepach[1], Q. Shi[3], S. Raimund[1], and K. Krüger[4]

[1]GEOMAR, Helmholtz Centre for Ocean Research Kiel, Kiel, Germany
[2]Rosenstiel School for Marine and Atmospheric Sciences, Miami, FL, USA
[3]Department of Oceanography – Dalhousie University, Halifax, Canada
[4]University of Oslo, Oslo, Norway

Received: 26 March 2015 – Accepted: 11 June 2015 – Published: 02 July 2015

Correspondence to: K. Krüger (kirstin.krueger@geo.uio.no)

Published by Copernicus Publications on behalf of the European Geosciences Union.

Abstract

Emissions of halogenated very short lived substances (VSLS) from the tropical oceans contribute to the atmospheric halogen budget and affect tropospheric and stratospheric ozone. Here we investigate the contribution of natural oceanic VSLS emissions to the Marine Atmospheric Boundary Layer (MABL) and their transport into the Free Troposphere (FT) over the tropical West Pacific. The study concentrates in particular on ship and aircraft measurements of the VSLS bromoform, dibromomethane and methyl iodide and meteorological parameters during the SHIVA (Stratospheric Ozone: Halogen Impacts in a Varying Atmosphere) campaign in the South China and Sulu Seas in November 2011. Elevated oceanic concentrations of 19.9 (2.80–136.91) pmol L^{-1} for bromoform, 5.0 (2.43–21.82) pmol L^{-1} for dibromomethane and 3.8 (0.55–18.83) pmol L^{-1} for methyl iodide in particular close to Singapore and at the coast of Borneo with high corresponding oceanic emissions of 1486 ± 1718 pmol m^{-2} h^{-1} for bromoform, 405 ± 349 pmol m^{-2} h^{-1} for dibromomethane and 433 ± 482 pmol m^{-2} h^{-1} for methyl iodide characterize this tropical region as a strong source of these compounds. Unexpectedly atmospheric mixing ratios in the MABL were relatively low with 2.08 ± 2.08 ppt for bromoform, 1.17 ± 1.17 ppt for dibromomethane and 0.39 ± 0.09 ppt for methyl iodide. We use meteorological and chemical ship and aircraft observations, FLEXPART trajectory calculations and source-loss estimates to identify the oceanic VSLS contribution to the MABL and to the FT. Our results show that a convective, well-ventilated MABL and intense convection led to the low atmospheric mixing ratios in the MABL despite the high oceanic emissions in coastal areas of the South-China and Sulu Seas. While the accumulated bromoform in the FT above the region origins almost entirely from the local South China Sea area, dibromomethane is largely advected from distant source regions. The accumulated FT mixing ratio of methyl iodide is higher than can be explained with the local oceanic or MABL contributions. Possible reasons, uncertainties and consequences of our observations and model estimates are discussed.

1 Introduction

The contribution of halogens to the atmospheric ozone chemistry is well known. Besides the destruction of stratospheric ozone (Solomon, 1999), halogen radicals (chlorine, bromine, iodine) also affect tropospheric ozone chemistry (Saiz-Lopez and von Glasow, 2012). Halogen radicals are released via photochemical and heterogeneous reaction cycles from organic halogenated trace gases originating from anthropogenic and natural sources, including macro algae, seaweed, phytoplankton and other marine biota. A large number of very short lived brominated and iodinated organic substances are emitted from tropical oceans and coastal regions to the atmosphere (Gschwend et al., 1985; Carpenter and Liss, 2000; Quack and Wallace, 2003; Quack et al., 2007; Liu et al., 2013). In particular, marine emissions of bromoform ($CHBr_3$), dibromomethane (CH_2Br_2) and methyl iodide (CH_3I) are major contributors of organic bromine and iodine to the atmosphere (Montzka and Reimann, 2011). Mean atmospheric lifetimes of the halogenated very short lived substances (VSLS) are 26 days for bromoform, 120 days for dibromomethane (Ko et al., 2003) and 4 days for methyl iodide (Solomon et al., 1994). Climate change could strongly affect marine biota and thereby halogen sources and the oceanic emission strength (Hepach et al., 2014).

Aircraft measurements from Dix et al. (2013) suggest that the halogen-driven ozone loss in the Free Troposphere (FT) is currently underestimated. In particular, significant elevated amounts of the iodine oxide free radical (IO) were found in the FT over the Central Pacific suggesting that iodine has a much larger effect on the FT ozone budget than currently estimated by chemical models. Coinciding with this study, Tegtmeier et al. (2013) projected a higher methyl iodide delivery to the Upper Troposphere/Lower Stratosphere (UTLS) over the tropical West Pacific than previously reported, using an observation based emission climatology by Ziska et al. (2013). Significantly lower amounts of tropospheric and stratospheric ozone are found in chemistry-transport and chemistry climate model runs when taking atmospheric bromine into account (von Glasow et al., 2004; Yang et al., 2005, 2014). Even though the influence of halo-

gens on the tropospheric and stratospheric ozone chemistry is crucial, halogen sources and transport ways are still not fully understood. Deep tropical convective events (Aschmann et al., 2011; Tegtmeier et al., 2013; Carpenter et al., 2014) as well as tropical cyclones, i.e. typhoons (Tegtmeier et al., 2012) are projected to transport the VSLS rapidly from the ocean surface to the upper tropical tropopause layer. The tropical West Pacific is an intense source region for VSLS (Krüger and Quack, 2013). However, only low mean atmospheric mixing ratios were observed for VSLS in the Eastern and Southeast China Seas during ship cruises in 1994 and 2009 (Yokouchi et al., 1997; Quack and Suess, 1999) and through the tropical West Pacific in 2010 (Quack et al., 2011; Brinckmann et al., 2012). None of these previous studies investigated the contribution of oceanic VSLS emissions to the marine atmospheric boundary layer (MABL) and to the FT in this hot spot region with large oceanic sources and strong convective activity.

The SHIVA ("Stratospheric Ozone: Halogen Impacts in a Varying Atmosphere") ship, aircraft and ground-based campaign during November and December 2011 in the Southern South China and Sulu Seas investigated oceanic emission strengths of marine VSLS, as well as their atmospheric transport and chemical transformation from the ocean surface to the upper troposphere. The goal of SHIVA was to improve the prediction of rate, timing and sensitivity of the ozone layer recovery due to climate forcing by combining observations and models. For more details about the SHIVA campaign see the ACP special issue (http://www.atmos-chem-phys.net/special_issue306.html).

In this study, we present campaign data from the research vessel (R/V) *SONNE* and the research aircraft (R/A) *FALCON*. We identify the contribution of oceanic emissions to the MABL and their exchange into the FT applying in-situ observations, trajectory calculations and source-loss estimates. The results are crucial for a better process understanding and for chemical transport model validation (Hossaini et al., 2013; Aschmann and Sinnhuber, 2013). An overview of the data and the methods used in this study is given in Sect. 2. Section 3 provides results from the meteorological observations along the cruise. Section 4 compares atmospheric VSLS measurements derived on R/V *SONNE* and R/A *FALCON* by different gas chromatographic/mass spectromet-

ric (GC/MS) instruments. The contribution of the oceanic emissions to the MABL and FT air is investigated and discussed in Sect. 5 by applying model calculations and the field observations. Finally, a summary of the results is given in Sect. 6.

2 Data and methods

2.1 SHIVA SONNE

2.1.1 Ship cruise

The cruise of R/V *SONNE* started on 15 November 2011 in Singapore and ended on 29 November 2011 in Manila, Philippines (Fig. 1a). The ship crossed the southwest South China Sea towards the northwest coast of Borneo from 16–19 November 2011. From 19–23 November 2011 the ship headed northeast along the northern coast of Borneo towards the Sulu Sea. Two diurnal stations took place on 18 November 2011 at 2.4° N/110.6° E and on 22 November 2011 at 6.0° N/114.8° E. Two meetings between R/V *SONNE* and R/A *FALCON* were carried out on 19 and 21 November 2011, where R/A *FALCON* passed R/V *SONNE* within a distance of about 100 m for several times to get simultaneous measurements of the same air masses. On 24 November 2011 the ship entered the Sulu Sea, and after 4 days transect, R/V *SONNE* reached the Philippine coast.

2.1.2 Aircraft campaign

16 measurement flights were carried out with R/A *FALCON* between 16 November and 11 December 2011 as part of the SHIVA campaign to investigate halogenated VSLS from the surface up to 13 km altitude over the South China and Sulu Seas. Observations were performed between 1 and 8° N, as well as 100 and 122° E, using Miri, Borneo (Malaysia) as the aircraft base. A detailed description of the VSLS measurements and flight tracks can be found in Sala et al. (2014).

2.2 Meteorological observations during SHIVA

2.2.1 Measurements onboard R/V *SONNE*

Meteorological parameters (temperature, air pressure, humidity and wind) were recorded at 20 m height every second on R/V *SONNE*. A 10 min running mean of this data is used for our investigations. An optical disdrometer ("ODM-470") measured the amount and intensity of precipitation during the cruise at 15 m height every minute. To obtain atmospheric profiles of air temperature, relative humidity and wind from the surface to the stratosphere 67 GRAW DFM-09 and 6 GRAW DFM-97 radiosondes were launched every 6 h at standard UTC times (00:00, 06:00, 12:00, 18:00) from the working deck of R/V *SONNE* at about 2 m a.s.l. At the 24 h stations, the launch frequency was increased to 2–3 h to analyse short term diel variations of the atmospheric boundary layer. During the cruise the radiosonde data was integrated in near real time into the Global Telecommunication System (GTS) to improve meteorological reanalyses such as ERA-Interim, which is used as input data for the trajectory calculations (Sect. 5).

2.2.2 Marine atmospheric boundary layer

The MABL is the atmospheric surface layer above the ocean in which trace gas emissions are mixed vertically by convection and turbulence on short time scales of about an hour (Stull, 1988; Seibert et al., 2000). The upper boundary of the MABL is either limited by a stable layer e.g. a temperature inversion or by a significant reduction in air moisture. Determination of the MABL height can be achieved by theoretical approaches, e.g. using critical Bulk Richardson number (Troen and Mahrt, 1986; Vogelezang and Holtslag, 1996; Sorensen, 1998) or by practical approaches summarized in Seibert et al. (2000). An increase with height of the virtual potential temperature, the temperature an air parcel would acquire if adiabatically brought to standard pressure with regard to the humidity of the air parcel, identifies the base of the stable layer, which is typically found between 100 m and 3 km altitude (Stull, 1988). In this study, we use

the height of the base of the stable layer increased by half of the stable layer depth as definition for the MABL height. The height of the MABL is determined from the atmospheric profiles measured by radiosondes launched on board the ship, as described in detail by Fuhlbrügge et al. (2013).

2.2.3 Convective energy

Intense solar insolation and high sea surface temperatures (SST) favour the South China and Sulu Seas for high convective activity. To indicate atmospheric instabilities that can lead to convective events the convective available potential energy (CAPE) (Margules, 1905; Moncrieff and Miller, 1976) is calculated. CAPE is defined as the cumulative buoyant energy of an air parcel from the level of free convection (LFC), the level where the environmental temperature decreases faster than the moist adiabatic lapse rate of a saturated air parcel at the same level, and the equilibrium level (EL), the height at which the air parcel has the same temperature as the environment. CAPE is computed after Eq. (1), with g as the gravitational constant, $T_{\mathrm{v,\,p}}$ as the virtual temperature of an adiabatic ascending air parcel at geometric height z, $T_{\mathrm{v,\,e}}$ as the virtual temperature of the environment at z, z_{LFC} as the height of the level of free convection and z_{EL} as the height of the equilibrium level. CAPE can range from 0 to more than 3 kJ kg^{-1} for very intense thunderstorms (Thompson and Edwards, 2000).

$$\mathrm{CAPE} = \int_{z_{\mathrm{LFC}}}^{z_{\mathrm{EL}}} g \cdot \left(\frac{T_{\mathrm{v,\,p}} - T_{\mathrm{v,\,e}}}{T_{\mathrm{v,\,e}}} \right) \mathrm{d}z \tag{1}$$

2.3 VSLS measurements and flux calculation

For the investigation of VSLS abundances, marine surface air and sea water were sampled synchronously on R/V *SONNE* along the cruise track. From these measurements the oceanic emissions of the compounds during the SHIVA campaign were calculated

(Sect. 2.3.3). Additionally, VSLS abundances in the MABL and the FT were measured by R/A *FALCON*.

2.3.1 Atmospheric samples

Air samples were taken on a 3 hourly basis along the cruise track, and in a 1–2 hourly rhythm during the 24 h stations on R/V *SONNE* resulting in a total of 195 samples during the cruise. The air was pressurized to 2 atm in pre-cleaned stainless steel canisters using a metal bellows pump. The samples were analyzed within 6 months after the cruise at the Rosenstiel School for Marine and Atmospheric Sciences (RSMAS, Miami, Florida) according to Schauffler et al. (1999) with an instrumental precision of ~ 5 %. Further details on the precision and the preparation of the samples and the use of standard gases are described in Montzka et al. (2003) and Fuhlbrügge et al. (2013). On R/A *FALCON* ambient air was analysed in situ by a GhOST-MS (Gas Chromatograph for the Observation of Stratospheric Tracers – coupled with a Mass Spectrometer) by the Goethe University of Frankfurt (GUF). Additionally 700 mL glass flasks were filled with ambient air to a pressure of 2.5 bar with a diaphragm pump using the R/A *FALCON* whole air sampler (WASP) and analysed within 48 h by a ground-based gas chromatography – mass spectrometry (GC/MS) instrument (Agilent 6973) of the University of East Anglia (Worton et al., 2008). During the flights GhOST measurements were conducted approximately every 5 min with a sampling time of 1 min, while WASP samples were taken every 3–15 min with a sampling time of 2 min. Further details on the instrumental precision, intercalibration of both instruments and observations on R/A *FALCON* are given in Sala et al. (2014). Given that the ground-based GC/MS investigated only brominated compounds, methyl iodide data is not available from WASP. Measurements from R/V *SONNE* and R/A *FALCON* were calibrated both with NOAA standards.

2.3.2 Water samples

Sea water samples for dissolved VSLS were taken in-situ on a 3 hourly basis from the moon pool of R/V *SONNE* at a depth of 5 m from a continuously working water pump. Measurements were interrupted between 16 November, 00:00 UTC to 17 November 2011 12:00 UTC due to permission issues in the southwest South China Sea. For the analysis of the water samples, a purge and trap system was attached to a gas chromatograph with mass spectrometric detection in single-ion mode with a precision of 10 % determined from duplicates. The approach is described in detail by Hepach et al. (2014).

2.3.3 Sea–air flux

The sea–air flux (F) of bromoform, dibromomethane and methyl iodide is calculated with k_w as specific transfer coefficient of the compound and Δc as the concentration gradient between the specific water and atmospheric concentrations (Eq. 2). For the determination of k_w, the air–sea gas exchange parameterization of Nightingale et al. (2000) was used and a Schmidt number (Sc) correction to the carbon dioxide derived transfer coefficient k_{CO_2} after Quack and Wallace (2003) was applied for the three gases (Eq. 3).

$$F = k_w \cdot \Delta c \tag{2}$$

$$k_w = k_{CO_2} \cdot \frac{Sc^{-\frac{1}{2}}}{600} \tag{3}$$

Details on deriving the air–sea concentration gradient are further described in Hepach et al. (2014) and references therein.

2.4 Oceanic VSLS contribution to the MABL and FT

2.4.1 Trajectory calculations

For the determination of the air mass transport from the surface to the FT the Lagrangian Particle Dispersion Model FLEXPART of the Norwegian Institute for Air Research in the Department of Atmospheric and Climate Research (Stohl et al., 2005) was used. The model has been extensively evaluated in earlier studies (Stohl et al., 1998; Stohl and Trickl, 1999) and includes parameterizations for turbulence in the atmospheric boundary layer and the FT as well as moist convection (Stohl and Thomson, 1999; Forster et al., 2007). Meteorological input fields are retrieved from the ECMWF (European Centre for Medium-Range Weather Forecasts) assimilation reanalysis product ERA-Interim (Dee et al., 2011) with a horizontal resolution of 1° × 1° and 60 vertical model levels. The ship-based radiosonde measurements (Sect. 2.2.1) were assimilated into ERA-Interim data. The 6 hourly input fields provide air temperature, horizontal and vertical wind, boundary layer height, specific humidity, as well as convective and large scale precipitation. For the trajectory analysis, 80 release points were defined along the cruise track. Time and position of these release events are synchronized with the water and air samples (Sect. 2.3). At these releases, 10 000 trajectories were launched per release point from the ocean surface within a time frame of ±30 min and an area of $\sim 500\,m^2$.

2.4.2 VSLS source-loss estimate in the MABL

A VSLS source-loss estimate for the MABL over the South China and Sulu Seas is obtained by applying the mass balance principle to the oceanic emissions, and to the time scales of air mass transport from FLEXPART and chemical loss. For each release event we define a box of the size given by the in-situ height of the MABL and by the horizontal area of the trajectory releases ($\sim 400\,m^2$ centred on the measurement location). Our VSLS source-loss estimate is based on a steady-state assumption of a constant

VSLS mixing ratio (given by the atmospheric measurements) within this box. The average VSLS delivery and loss calculated for these boxes is denoted as MABL source-loss estimate in this manuscript.

To derive the amount of VSLS delivery to the MABL by oceanic emissions, we consider the specific sea–air flux constant during each trajectory release and the emissions homogeneously distributed in the MABL. The contribution of the sea–air flux to the MABL concentrations of the specific compounds is defined as the Oceanic Delivery (OD). The OD is calculated as the ratio of the VSLS flux out of the ocean (in mol per day) and the total amount of the VSLS in the box (in mol) with the latter derived from the box dimensions and the measured VSLS mixing ratio, given in percentage per day. Another important process determining the VSLS concentrations in the MABL is the loss of MABL air to the FT caused by vertical transport, defined here as COnvective Loss (COL). This loss process is calculated from the mean residence time of the FLEXPART trajectories in the observed MABL during each release, is given as a negative number in percentage per day and equals the loss of VSLS from the MABL to the FT. Chemical loss processes in form of reaction with OH and photolysis can be described by the chemical lifetime of the VSLS in the MABL. Based on tropical MABL lifetime estimates of 16 days for bromoform, 60 days for dibromomethane (Hossaini et al., 2010) and 3 days for methyl iodide (R. Hossaini, personal communication, 2013) the Chemical Loss (CL) is estimated in percentage per day and given as a negative quantity.

Relating the delivery of VSLS from the ocean to the MABL (OD) and the loss of MABL air with the contained VSLS to the FT (COL) results in an Oceanic Delivery Ratio (ODR) (Eq. 4):

$$\mathrm{ODR} = \frac{\mathrm{OD}\,[\%\,\mathrm{day}^{-1}]}{-\mathrm{COL}\,[\%\,\mathrm{day}^{-1}]} = \frac{\text{Sea–Air flux contribution } [\%\,\mathrm{day}^{-1}]}{\text{Loss of MABL air to the FT } [\%\,\mathrm{day}^{-1}]} \quad (4)$$

Similarly, we relate the Chemical Loss in the MABL (CL) to the MABL VSLS loss into the FT (COL) to derive a Chemical Loss Ratio (CLR) (Eq. 5):

$$\mathrm{CLR} = \frac{\mathrm{CL}\,[\%\,\mathrm{day}^{-1}]}{-\mathrm{COL}\,[\%\,\mathrm{day}^{-1}]} = \frac{\text{Loss through chemistry } [\%\,\mathrm{day}^{-1}]}{\text{Loss of MABL air to the FT } [\%\,\mathrm{day}^{-1}]} \quad (5)$$

Assuming steady state in the box, the oceanic delivery, chemical loss and loss to the FT must be balanced by advective transport of air masses in and out of the box. We define the change of the VSLS through advective transport as Advective Delivery (AD) in percentage per day (Eq. 6). Additionally, we define the ratio of change in VSLS caused by advection (AD) to the loss of VSLS out of the MABL to the FT as Advective Delivery Ratio (ADR) in Eq. (7):

$$\mathrm{AD} = -\mathrm{COL} - \mathrm{CL} - \mathrm{OD} \quad (6)$$

$$\mathrm{ADR} = \frac{\mathrm{AD}\,[\%\,\mathrm{day}^{-1}]}{-\mathrm{COL}\,[\%\,\mathrm{day}^{-1}]} = 1 - \mathrm{CLR} - \mathrm{ODR} \quad (7)$$

Note that for the VSLS within the MABL box, COL and CL are loss processes and given as negative numbers while OD and AD (besides a very few exceptions for the latter) are source processes and given as positive numbers. In order to derive the ratios, we have divided CL, OD and AD by −COL and therefore end up with negative ratios for the loss process and positive ratios for the source processes.

In a final step, we relate the source-loss ratios (ODR, CLR and ADR) to the MABL VSLS volume mixing ratio ($\mathrm{VMR_{MABL}}$) in the box (Eq. 8–10), to derive information on the different contributions to the observed mixing ratio. Assuming steady state in the box and a complete loss of all air masses into the FT, we want to estimate how much of newly supplied VSLS results from oceanic delivery ($\mathrm{VMR_{ODR}}$), how much is destroyed

by chemistry (VMR_{CLR}) and how much results from advective transport (VMR_{ADR}).

$$VMR_{ODR} = ODR \cdot VMR_{MABL} \quad (8)$$

$$VMR_{CLR} = CLR \cdot VMR_{MABL} \quad (9)$$

$$VMR_{ADR} = ADR \cdot VMR_{MABL} \quad (10)$$

2.4.3 Oceanic and MABL VSLS contribution to the FT

The cruise covered heterogeneous oceanic regions in the South China Sea. We use a simplified approach to calculate the mean contribution of boundary layer air masses observed on the ship and the oceanic compounds therein to the FT above the South China and Sulu Seas. The contribution is determined as a function of time and altitude based on the distribution of the trajectories released at each measurement location along the ship track. According to R/A *FALCON* observations and our trajectory calculations we assume a well mixed FT within 5° S–20° N, 100–125° E. Observations on R/V *SONNE*, on the other hand, are characterized by large variability and are considered to be representative for the area along the cruise track where the VSLS were measured in the water and atmosphere. We constrain our calculations to this area and define 80 vertical columns along the cruise track. Each column extends horizontally over the area given by the starting points of the trajectories (20 m × 20 m centred on the measurement location) and vertically from the sea surface up to the highest point of R/A *FALCON* observations around 13 km altitude. For each of the 80 trajectory releases along the cruise track, 10 000 trajectories were launched and assigned an identical MABL air parcel containing air with the VSLS mixing ratios observed on R/V *SONNE* during the time of the trajectory release. The volume of the air parcel is given by the in-situ height of the MABL and the horizontal extend of the release box (20 m × 20 m) divided by 10 000 trajectories. The transport of the MABL air parcels is specified by the trajectories, assuming that no mixing occurs between the parcels during the transport. Chemical loss of the VSLS in each air parcel is taken into account through chemical degradation according to their specific tropospheric lifetimes. We average over the vol-

ume and mixing ratios of all trajectories within the South China Sea area independent of their exact horizontal location. Since the VSLS mixing ratios in the FT from the aircraft measurements are representative for the whole South China Sea area, it is for our approach not important where the air parcels reside within this area. Only if trajectories leave the South China Sea area they are not taken into account any longer. Due to the decreasing density of air in the atmosphere with height, the volume of the MABL air parcels expands along the trajectories with increasing altitude. The expanding MABL air parcels take up an increasing fraction of air within the FT column, which is taken into account in our calculations using density profiles from our radiosonde measurements.

We calculate the contribution of oceanic compounds to the FT for 25 layers of 500 m height intervals, situated between 0.5 and 13 km altitude within the column above the measurement location. For each layer, the ratio r_{MABL} of the volume of the MABL air parcels with the VSLS mixing ratio VMR_{MABL} to the whole air volume of the layer is calculated. The ratio of advected FT air with a mixing ratio VMR_{AFT} to the whole air volume of the layer is r_{AFT} respectively, with $r_{MABL} + r_{AFT} = 1$. In our simulation, the FT air with a mixing ratio VMR_{FT} observed by R/A *FALCON* at a specific height is composed of the MABL air parcels and of the advected FT air parcels (Eq. 11):

$$r_{MABL} \cdot VMR_{MABL} + r_{AFT} \cdot VMR_{AFT} = (r_{MABL} + r_{AFT}) \cdot VMR_{FT} \quad (11)$$

The relative Contribution C_{MABL} of VSLS observed in the MABL to the VSLS observed in the FT is computed in altitude steps of 500 m (Eq. 12):

$$C_{MABL}[\%] = 100 \cdot (r_{MABL} \cdot VMR_{MABL})/VMR_{FT} \quad (12)$$

The oceanic Contribution C_{ODR} of the South China Sea to the atmospheric mixing ratios in the FT is computed after Eq. (13):

$$C_{ODR}[\%] = 100 \cdot (r_{MABL} \cdot VMR_{ODR})/VMR_{FT} \quad (13)$$

The simplified approach also allows us to derive mean VSLS mixing ratios accumulated in the FT from both MABL VSLS and oceanic emissions. The FT VSLS mixing ratios are

simulated for each of the 80 releases by initiating a new trajectory release using same meteorological conditions and VSLS MABL observations, when the former MABL air has been transported into the FT, according to the specific residence time in the MABL. The initial FT background mixing ratios are 0 ppt for each VSLS. The accumulated mean mixing ratio of a compound at a specific height is then computed after Eq. (14):

$$VMR_{MFT} = r_{MABL_1} \cdot VMR_{MABL_1} + r_{MABL_2} \cdot VMR_{MABL_2} + \ldots + r_{MABL_i} \cdot VMR_{MABL_i} \quad (14)$$

Here, VMR_{MFT} is the modelled accumulated FT mixing ratio, r_{MABL_i} is the ratio of MABL air parcels in 20 m × 20 m × 500 m layers between 0.5 and 13 km altitude to the total volume of each layer, VMR_{MABL_i} is the mixing ratio in the MABL air parcels including chemical degradation since release from the MABL, i is the number of initiated runs per release. A steady state for the compounds is reached, when variations in their mixing ratios vary less than 1 % between two initiated runs. For bromoform the steady state is reached after 11.0 ± 2.1 days (mean ± σ), 11.8 ± 2.4 days for dibromomethane and 8.0 ± 1.4 days for methyl iodide. The overall mean FT mixing ratio in the South China Sea is derived as the mean from the 80 individually calculated FT mixing ratios determined along the cruise. The oceanic contribution to the FT compounds is calculated with VMR_{ODR} from Eq. (8) inserted as VMR_{MABL} in Eq. (14).

3 Meteorological conditions in the MABL and the FT

3.1 Meteorology along the ship cruise

Moderate to fresh trade winds are dominating the South China and Sulu Seas (Fig. 1a and b), which is reflected by the overall mean wind direction of northeast (50–60°) and a mean wind speed of 5.5 ± 2.9 m s^{-1} during the cruise. The wind observations reveal two different air mass origins. Between 15 and 19 November 2011 a gentle mean wind speed of 3.7 ± 1.8 m s^{-1} with a *northern* wind direction was observed, influenced by a weak low pressure system (not shown here) over the central South China

Sea moving southwest and passing the ship position on 17 November 2011. During 20–29 November 2011 the wind direction changed to *northeast* and the mean wind speed increased to moderate 6.4 ± 3.0 m s^{-1}. A comparison between 6 hourly ERA-Interim wind and a 6 hourly averaged mean of the observed wind on R/V *SONNE* reveals an underestimation of the wind speed by ERA-Interim along the cruise track by 1.6 ± 1.4 m s^{-1} on average (not shown here). The mean deviation of the wind direction between reanalysis and observation is 2 ± 37°. Reanalysis and observed wind speeds correlate with R = 0.76 and the wind directions with R = 0.86, reflecting a good overall agreement between ship observation and ERA-Interim winds. With an observed mean surface air temperature (SAT) of 28.2 ± 0.8 °C and a mean SST of 29.1 ± 0.5 °C the SAT is on average 1.0 ± 0.7 °C below the SST, which benefits convection of surface air (Fig. 2).

3.2 CAPE and humidity

The mean CAPE computed from the radiosonde data is 998 ± 630 J kg^{-1} and typically elevated for tropical regions (Fig. 3). Highest CAPE during the cruise was observed on 16 November 2011 at 12:00 UTC in the southern South China Sea and exceeded 2.9 kJ kg^{-1}, revealing developing convection. ERA-Interim mean CAPE during the cruise was 825 ± 488 J kg^{-1} and about 170 J kg^{-1} lower than observed by the radiosondes.

Precipitation measurements by the optical disdrometer ODM-470 are shown in Fig. 3. Besides a number of small rain events during the cruise, three major convective rain events are evident on 16, 21, and 24 November 2011. The total amount of accumulated rain during the cruise was 52.3 mm. The most intense rain rate of 16.3 mm h^{-1} was observed on 16 November 2011 in the southwest South China Sea. The relatively low total precipitation during the cruise is reflected by negative precipitation anomalies in November 2011 compared to the long term climate mean along the northern coast of Borneo (Climate Diagnostics Bulletin, November 2011, Climate Prediction Center).

Figure 4 shows the time series of the relative humidity measured by the radiosondes launched on R/V *SONNE* from the surface up to the mean height of the cold point tropopause at 17 km. Increased relative humidity within the lower troposphere coincides with the rain fall events observed by the disdrometer on 16, 21, and 24 November 2011 (compare with Fig. 3). Elevated humidity is found on average up to about 6 km, which implies a distinct transport of water vapour to the mid troposphere during the cruise by deep convection or advection of humid air from a nearby convective cell.

3.3 Marine atmospheric boundary layer

Higher SSTs than SATs (Fig. 2) cause unstable atmospheric conditions (negative values) between the surface and about 50–100 m height (Fig. 5). Surface air is heated by warmer surface waters and is enriched with humidity both benefiting moist convection. The stability of the atmosphere increases above 420 ± 120 m and indicates the upper limit of the MABL at this altitude range derived from radiosonde data (Fig. 5). The ERA-Interim MABL height along the cruise track is with 560 ± 130 m systematically higher, but still within the upper range of the MABL height derived from the radiosonde measurements. The unstable conditions of the MABL and the increase of the atmospheric stability above the MABL reflect the characteristics of a convective well ventilated tropical boundary layer. In contrast to cold oceanic upwelling regions with a stable and isolated MABL (Fuhlbrügge et al., 2013), the vertical gradient of the relative humidity measured by the radiosondes (Sect. 3.1) and the height of the MABL do not coincide. This is caused by increased mixing through and above the MABL by turbulence and convection, which leads to the well-ventilated convective MABL.

4 Atmospheric VSLS over the South China and Sulu Seas

4.1 Atmospheric surface observations on R/V *SONNE*

Overall, the three VSLS bromoform, dibromomethane and methyl iodide show a similar pattern of atmospheric mixing ratios (Fig. 6a) along the cruise track with lower atmospheric surface abundances before 21 November 2011, west of Brunei and higher afterwards, which can be attributed to a change in air mass origin as well as an increase of the observed wind speed (Fig. 1). A decrease from 3.4 to 1.2 ppt of bromoform is found at the beginning of the cruise (Fig. 6a) when the ship left Singapore and the coast of the Malaysian Peninsula. On 16–19 November 2011 when the ship passed the southern South China Sea the lower mixing ratios (± standard deviation 1σ) of 1.2 ± 0.3 ppt prevail and also the lowest mixing ratios for bromoform during the whole cruise of 0.8 ppt are found. At the coast of Borneo and the Philippines, the average mixing ratio of bromoform increases to 2.3 ± 1.4 ppt. During the two 24 h stations, the mean mixing ratios are 1.4 ± 0.2 ppt for the first and 2.6 ± 0.4 ppt for the second station. The overall mean bromoform mixing ratio during the cruise is 2.1 ± 1.4 ppt (Table 1) and therefore higher than earlier bromoform observations of 1.2 ppt in January–March 1994 (Yokouchi et al., 1997), 1.1 ppt in September 1994 (Quack and Suess, 1999) and 1.5 ppt in June–July 2009 (Nadzir et al., 2014) further offshore in the South China Sea. The higher atmospheric mixing ratios during the R/V *SONNE* cruise in November 2011 in contrast to the lower mixing ratios in these previous studies may point to stronger local sources, strong seasonal or interannual variations, or even to long-term changes. Dibromomethane shows a mean mixing ratio of 1.2 ± 0.2 ppt (Table 1). Yokouchi et al. (1997) observed a lower mean atmospheric mixing ratio of 0.8 ppt and Nadzir et al. (2014) 1.0 ppt in the South China Sea. An increase of the dibromomethane mixing ratios from 1.0 ± 0.1 ppt to 1.3 ± 0.2 ppt is observed after 21 November 2011 coinciding with an increase of the methyl iodide concentrations from primarily 0.3 ± 0.0 ppt to 0.4 ± 0.1 ppt (Fig. 6a). The highest mixing ratio of methyl iodide was detected in the south western Sulu Sea on 25 November 2011 with 0.8 ppt. The overall mean atmo-

spheric mixing ratio for methyl iodide, of 0.4 ± 0.1 ppt (Table 1) is lower than the mean of 0.6 ppt observed by Yokouchi et al. (1997).

The concentration ratio of dibromomethane and bromoform (Fig. 6b) has been used as an indicator for the age of air masses, after they crossed strong coastal source regions, where a ratio of approximately 0.1 was observed (Yokouchi et al., 2005; Carpenter et al., 2003). The ten times elevated bromoform has a much shorter lifetime, thus degrades more rapidly than dibromomethane, which increases the ratio during transport. Overall, the mean concentration ratio of dibromomethane and bromoform is 0.6 ± 0.2, which suggests that predominantly older air masses are advected over the South China Sea. The highest concentration ratio of 1.2, likely indicating the oldest air mass, is observed on 16 November 2011.

4.2 Oceanic surface concentrations and emissions from R/V *SONNE*

VSLS in the surface sea water along the cruise track show highly variable distributions (Fig. 6c and Table 1). Oceanic bromoform surface concentrations range from 2.8–136.9 pmol L^{-1} with a mean of 19.9 pmol L^{-1} during the cruise, while dibromomethane concentrations range from 2.4–21.8 pmol L^{-1} with a mean of 5.0 pmol L^{-1}. Bromoform and dibromomethane have similar distribution patterns in the sampling region with near shore samples showing typically elevated concentrations. Methyl iodide concentrations range from 0.6–18.8 pmol L^{-1} with a mean of 3.8 pmol L^{-1} and show a different distribution along the ship track than the two bromocarbons, indicating different sources.

High levels of all VSLS are found in waters close to the Malaysian Peninsula, especially in the Singapore Strait on 16 November 2011, likely showing an anthropogenic influence on the VSLS concentrations. VSLS concentrations decrease rapidly when the cruise track leads to open ocean waters. Along the west coast (19–23 November 2011) and north east coast of Borneo (25 November 2011), bromocarbon concentrations are elevated, and especially bromoform concentrations increase in waters influenced by river run.

Oceanic emissions were calculated from synchronized measurements of sea water concentrations and atmospheric mixing ratios, sea surface temperatures and wind speeds, measured on the ship (Sect. 2.3.3). The overall VSLS distribution along the ship track is opposite for the oceanic and atmospheric measurements (Fig. 6a–d). While the sea water concentrations of VSLS generally decrease towards the Sulu Sea, the atmospheric mixing ratios increase, leading to a generally lower concentration gradient of the compounds between sea water and air in the Sulu Sea (not shown here).

Coinciding low VSLS atmospheric background concentrations, high SSTs, elevated oceanic VSLS concentrations and high wind speeds, lead to high emissions of VSLS for the South China and Sulu Sea's (Fig. 6d). In particular, bromoform fluxes are very high and in agreement with coastal fluxes from previous campaigns in tropical source regions (Quack et al., 2007). They often exceed 2000 pmol m^{-2} h^{-1} in the coastal areas and even reach more than 6000 pmol m^{-2} h^{-1} as in the Singapore strait on 15 and on 22 November 2011 at the northwest coast of Borneo, which was also an area of strong convection (Figs. 1, 2, and 6).

4.3 VSLS intercomparison: R/A *FALCON* and R/V *SONNE*

The two profiles of bromocarbon mixing ratios from the surface to 13 km altitude (Sala et al., 2014) and the profile for methyl iodide as observed on R/A *FALCON* with the GhOST and WASP instruments are shown in Fig. 7. Mean bromoform mixing ratios are 1.43 ppt (GhOST) and 1.90 ppt (WASP) in the MABL (0–450 m, determined from meteorological aircraft observations similarly as for the radiosondes, Sect. 2.2.2) and 0.56 ppt (GhOST) and 1.17 ppt (WASP) in the FT (0.45–13 km, Table 1). The GhOST mixing ratios in the MABL are considerably lower than those observed on R/V *SONNE* (2.08 ppt) but higher than the mixing ratios observed by Yokouchi et al. (1997) in January to March 1994, by Quack and Suess (1999) in September 1994 and Nadzir et al. (2014) in June/July 2009 at coastal areas. Open ocean observations of Nadzir et al. (2014) with 1.5 ppt are comparable to GhOST, but lower than WASP observations. A very good agreement of the measurements is given for the longer lived di-

bromomethane with 1.17 ppt (R/V *SONNE*), 1.19 ppt (GhOST) and 1.15 ppt (WASP). Methyl iodide mixing ratios measured by GhOST are 0.59 ± 0.30 ppt within the MABL of 450 m height, which is about 0.2 ppt higher than the values from R/V *SONNE*, but coincide with the observations by Yokouchi et al. (1997). Above the MABL, the average mixing ratio of methyl iodide decreases to 0.26 ± 0.11 ppt (Fig. 7).

Bromoform and dibromomethane concentrations of all instruments in the MABL correlate with $R = 0.83$ (Fig. 8). Bromoform and methyl iodide concentrations correlate with $R = 0.55$ and dibromomethane and methyl iodide with $R = 0.66$; all three correlations are significant at 99 %. Even higher correlations are found if only measurements on R/V *SONNE* are taken into account with $R = 0.92$ for bromoform and dibromomethane, $R = 0.64$ for bromoform and methyl iodide, and $R = 0.77$ for dibromomethane and methyl iodide.

Two case studies for the comparison of R/A *FALCON* and R/V *SONNE* data are obtained from their meetings on 19 and 21 November 2011 (Table 2), when aircraft and ship passed each other within 100 m distance for several times, measuring the same air masses. During both meetings, deviations between the GhOST and WASP instrument on the aircraft are larger for the bromocarbons than the deviation between the WASP and the ship measurements. WASP and the ship data, which agree very well, rely on sampling of air in stainless steel canisters and subsequent analysis with GC/MS while GhOST measures in situ. Whether this offset is systematic for the different methods, needs to be investigated further. The methyl iodide values of the GhOST and air canister data from the ship show larger differences during the second meeting. In the following, a mean of the GhOST and WASP measurements of R/A *FALCON* is used for computations in the free troposphere.

5 Air mass and VSLS transport from the surface to the free troposphere

5.1 Timescales and intensity of vertical transport

Forward trajectories have been computed with FLEXPART starting at sea level along the cruise track between Singapore to Manila. ERA-Interim is used for the meteorological input (Sect. 2.2.1). The FLEXPART runs yield an average MABL residence time of 7.8 ± 3.5 h before the trajectories enter the FT (Fig. 9), reflecting a relatively fast exchange due to the convective well ventilated MABL (Fig. 5). To estimate the loss of air masses out of the South China Sea area between 5° S–20° N and 100–125° E (Sect. 2.4.3) we determine the loss of trajectories out of this area after their release (Fig. 10). After 4 days 88 % of all trajectories released along the cruise track are still within this defined area of the South China Sea, which decreases to 31 % after 10 days. During these ten days 65.1 ± 22.2 % of the trajectories have passed 6 km height and 20.4 ± 9.7 % have passed 13 km height within the area, while 18.5 % of the trajectories re-enter the MABL from the FT. Most intense convection within FLEXPART calculations along the cruise track occurred on 17 and 18 November 2011 in the southern South China Sea (Fig. 9), 22–24 November at the north western coast of Borneo and on 25–26 November in the Sulu Sea. 30–50 % of the trajectories released from the surface at these times ascend to 13 km height within 3–4 days. Discrepancies to CAPE observations on R/V *SONNE* (Fig. 3) are due to the fact that the calculated CAPE describes the stability of the air column that is observed by the radiosondes ascending with weather balloons, while the trajectories simulate the actual movement of the air masses, thus include the convection in other regions after some hours of transport time. Indeed during convective events at the northern coast of Borneo, the majority of trajectories were transported south towards the coast of Borneo where active convection took part. Trajectories launched between 18–22 November during 00:00 and 12:00 UTC each day reveal a longer residence time of up to 5 days in the lower troposphere (Fig. 9). At about 2 km altitude a barrier seems to suppress convection during this time. This agrees with our CAPE observations, showing suppressed convection at about 1.5 km altitude north

of Borneo (Fig. 3), as lowest observed CAPE is predominantly found between 00:00 and 12:00 UTC during these days.

R/V *SONNE* – R/A *FALCON*: identifying observations of the same air mass

To investigate if the same air masses were observed on R/V *SONNE* and on R/A *FALCON* a perfluorocarbon tracer was released on R/V *SONNE* on 21 November 2011, which was indeed detected 25 h later on R/A *FALCON* (Ren et al., 2015). With the trajectory calculations it can be determined which fraction of the air masses investigated on R/V *SONNE* could subsequently be investigated on R/A *FALCON*. Within a horizontal distance of ±20 km and a maximum vertical distance of ±1 km around the position of the aircraft, as well as a time frame of ±3 h of the VSLS air measurements on R/A *FALCON*, 15 % of all launched 80 × 10 000 surface trajectories, marking the air masses on R/V *SONNE*, passed the R/A *FALCON* flight track during the cruise. Allowing a time frame up to 10 days, the amount of trajectories passing the flight track of R/A *FALCON* increases to 77 ± 29 % between 16 November and 11 December 2011. In the following we combine the R/V *SONNE* and R/A *FALCON* measurements to derive the contribution of oceanic VSLS to MABL and FT concentrations based on the observations.

5.2 Contribution of oceanic emissions to VSLS in the MABL

Computed from observations on R/V *SONNE*, the mean sea–air flux during the cruise is 1486±1718 pmol $m^{-2} h^{-1}$ for bromoform, 405±349 pmol $m^{-2} h^{-1}$ for dibromomethane and 433 ± 482 pmol $m^{-2} h^{-1}$ for methyl iodide (Sect. 4.2). The contribution of the flux to the observed atmospheric VSLS concentration in the MABL (Oceanic Delivery, OD), whose height is determined from the radiosondes, is scaled to 1 day (Table 3, Fig. 11). The OD is 116.4 ± 163.6 % day^{-1} to the MABL concentrations for bromoform, 54.2 ± 66.7 % day^{-1} for dibromomethane and 166.5 ± 185.8 % day^{-1} for methyl iodide. In other words, the oceanic source for bromoform is strong enough to fill up the MABL above the measurement location on average about once per day, while for

dibromomethane the emissions are weaker and nearly 2 days would be required until the observed mixing ratios in the MABL are reached. Based on the FLEXPART trajectories, the mean loss of MABL air to the FT during one day (COnvective Loss, COL) is computed to be −307.6 ± 124.3 % day^{-1}. According to the MABL lifetimes of the VSLS the loss due to photolysis and OH, both defined as Chemical Loss (CL) in the MABL is −6.6 % day^{-1} for bromoform, −1.8 % day^{-1} for dibromomethane and −30.7 % day^{-1} for methyl iodide. In order to balance the delivery from the ocean and the loss to the FT and by chemical degradation, an Advective Delivery (AD) of VSLS in and out of the MABL is needed. The AD for bromoform is 197.9 ± 199.7 % day^{-1}, for dibromomethane 255.2 ± 131.9 % day^{-1} and for methyl iodide 171.8 ± 242.3 % day^{-1}. The numbers indicate that, approximately twice as much VSLS would be advected to reach the MABL mixing ratio, if no OD or COL occurred. OD and AD are transported via COL into the FT. Based on the OD and the COL, the Oceanic Delivery Ratio (ODR) is calculated in order to characterize the relative contribution of the local oceanic emissions compared to the loss of MABL air into the FT (Table 3). The average ODR during the cruise is 0.45 ± 0.55 for bromoform, which means that the loss from the MABL to the FT is balanced to 45 % by oceanic emissions along the cruise track. The ODR for dibromomethane is 0.21 ± 0.21 and for methyl iodide 0.74 ± 1.05, respectively, suggesting that the major amount of methyl iodide origins from nearby sources. Similarly to the ODR the CL is related to the COL to derive the Chemical Loss Ratio (CLR) for the VSLS, which is 0.03 ± 0.01 for bromoform, 0.01 ± 0.00 for dibromomethane and 0.12 ± 0.05 for methyl iodide. When compared to the other source and loss processes, the chemical loss appears negligible for all three gases. The ratio of the advective delivery (ADR) relating the AD to the COL is 0.58 ± 0.55 for bromoform, 0.80 ± 0.21 for dibromomethane and 0.38 ± 1.01, implying that most of the observed dibromomethane (80 %) in the MABL is advected from stronger source regions. Applying the ratios to the observed mixing ratios in the MABL gives an estimate of the amount of the VSLS that origin from local oceanic emissions (VMR_{ODR}) that are degraded chemically (VMR_{CLR}) and that are advected (VMR_{ADR}, Table 4). The local ocean emits a concen-

tration that equates to 0.89 ± 1.12 ppt bromoform, 0.25 ± 0.26 ppt dibromomethane and 0.28 ± 0.40 ppt methyl iodide in the MABL. The amount that is destroyed by chemistry in the MABL before the air is transported into the FT accounts to 0.05 ± 0.04 ppt (bromoform), 0.01 ± 0.01 ppt (dibromomethane) and 0.05 ± 0.03 ppt (methyl iodide). Finally 1.18 ± 1.20 ppt of the observed mixing ratios of bromoform, 0.92 ± 0.27 ppt of dibromomethane and 0.14 ± 0.37 ppt of methyl iodide are advected. The average transport from the MABL to the FT ($Flux_{MABL\text{-}FT}$), computed from the MABL concentrations and the trajectory residence time in the MABL, is 4240 ± 1889 pmol m^{-2} h^{-1} for bromoform, 2419 ± 929 pmol m^{-2} h^{-1} for dibromomethane and 865 ± 373 pmol m^{-2} h^{-1} for methyl iodide. Calculations with the ERA-Interim MABL height, which is on average 140 m higher than the radiosonde derived one, leads to very similar estimates (Appendix 1).

Since the wind is a driving factor for oceanic emissions and advection of VSLS, changes in wind speed are assumed to affect atmospheric VSLS mixing ratios in the MABL during this cruise. Significant correlations are found between wind speed and the observed mixing ratios of all three VSLS in the MABL with correlation coefficients of $R = 0.55$ (bromoform), $R = 0.57$ (dibromomethane) and $R = 0.56$ (methyl iodide), respectively. The according amount of mixing ratios that origin from the oceanic emissions (VMR_{ODR}) correlate significantly to the wind speed with $R = 0.52$, $R = 0.72$ and $R = 0.62$, respectively. On the opposite, VMR_{ADR}, which is calculated as the residual from VMR_{ODR}, is negative correlated to the wind speed with $R = -0.21$, $R = -0.32$ and $R = -0.53$. The correlations reveal that the contribution of oceanic emissions to MABL VSLS increase for higher wind speeds, while the advective contribution decreases.

5.3 Oceanic contribution to the FT

5.3.1 Identification of MABL air and their contained VSLS in the FT

With a simplified approach (method description in Sect. 2.4.3) we are able to estimate the contribution of MABL air and regional marine sources observed on R/V *SONNE* to the FT. Individual MABL air masses during the cruise contribute on average over 20 %

to the lowest FT air right after they leave 0.5 km altitude (Fig. 12). Within 2–6 days after crossing that level an observed MABL air mass contributes up to 15 % depending on the height. A decrease of the contribution with height down to 3 % occurs until 8 km altitude. Above this height, the contribution of the MABL air masses increases again to over 5 % as a result of the density driven extension of the air parcels. The temporal decrease due to the transport of trajectories out of the predefined South China and Sulu Seas area (Fig. 10) is visible after three days.

The average contribution of VSLS from the MABL air to the FT mixing ratio (c_{MABL}) between 2 and 11 km altitude within 10 days after release is with 1–28 % highest for bromoform followed by 1–12 % for dibromomethane and only 0–5 % for the short-lived methyl iodide (coloured contours in Fig. 12). For all compounds, the largest contributions of > 25 % are found between 0.5 and 2 km height within the first 2 days after release due to occasional fresh entrainment of MABL air. Above 8 km altitude, the average contribution of the individual MABL VSLS releases increase again to > 11 % (bromoform), > 5 % (dibromomethane) and > 3 % (methyl iodide), due to the density driven extension of the MABL air parcels with height. The chemical degradation of methyl iodide, according to its short tropospheric lifetime of 4 days is visible already 2 days after release, when its contribution decreases to < 7 % within 0.5–2.5 km altitude and to < 2.5 % above 2.5 km altitude. To identify the contribution of the oceanic emissions to the FT VSLS during the cruise, the VMR_{ODR} of each compound is used as the initial mixing ratio in the MABL air mass. The mean contribution of marine compounds from the South China Sea to the FT air varies with time and altitude, but is generally higher for bromoform with 1–13 % than for methyl iodide with 0–4 %. This is not surprising, considering the longer lifetime of bromoform compared to methyl iodide, although the relative contribution of oceanic emissions to MABL air (Sect. 5.2) was identified to be higher for methyl iodide (74 %) than for bromoform (45 %). The low mean regional marine contribution of dibromomethane to the observed MABL mixing ratio of 21 % is also reflected in its mean oceanic contribution of only 0–3 % to the FT air masses.

5.3.2 Accumulated VSLS in the free troposphere

By simulating a steady transport of MABL air masses into the FT, mean accumulated VSLS mixing ratios in the FT along and during the cruise were computed (Fig. 13) as described in 2.4.3. The simulated FT mixing ratios of bromoform and dibromomethane from the observed MABL (VMR_{MABL}) decrease on average from 1.8 and 1.1 ppt at 0.5 km height to 0.7 ppt respectively 0.6 ppt at 7 km height and increase again above 8 km up to 0.9 ppt (bromoform) and 0.8 ppt (dibromomethane). Simulated methyl iodide shows a decrease from 0.21 ppt at 0.5 km to 0.06 ppt at 3 km. Above this altitude, the simulated mixing ratios of methyl iodide are quite constant 0.06 ppt.

To estimate the accumulated FT mixing ratios solely from oceanic emissions, the VMR_{ODR} is used as the initial MABL mixing ratio (Fig. 13). The simulated FT mixing ratios using either VMR_{MABL} or VMR_{ODR} as input reveal a similar vertical pattern, since both simulations are based on the same meteorology and trajectories. While FT mixing ratios based on VMR_{MABL} and VMR_{ODR} are similar for methyl iodide (due to the large oceanic contribution to the MABL mixing ratios), FT mixing ratios from VMR_{ODR} are on average $\sim$ 0.5 ppt lower for bromoform and $\sim$ 0.6 ppt dibromomethane than from VMR_{MABL}. Comparing the simulated VMR_{MABL} FT mixing ratios with the observed FT mixing ratios from R/A *FALCON* reveals stronger vertical variations for the simulations in contrast to the observations. Bromoform is overestimated in the VMR_{MABL} simulation between 0.5 and 7 km altitude, as well as between 9 and 12 km. Simulated dibromomethane in the FT based on VMR_{MABL} underestimates the observed mixing ratios between 3 and 12 km height. In particular, the maximum between 6 and 9 km height is not reflected in the simulations. However, observations of both bromocarbons are within 1σ of the FT simulations with MABL air. The methyl iodide simulations show a distinct underestimation of the observed FT mixing ratios. In Sect. 4.3 we have shown that methyl iodide measured in same air masses by R/V *SONNE* and R/A *FALCON* was 51 % higher for the aircraft (Table 2). Adjusting all R/A *FALCON* values by this identified offset to R/V *SONNE* reveals a better agreement between observed and simulated FT mixing ratios (Fig. 13).

5.3.3 Discussion

The simulations show how local oceanic emissions and advection of remote air can explain the observed FT mixing ratios (Fig. 13). Local oceanic emissions of bromoform from the South China Sea contribute about 60 % to the FT mixing ratios. However, simulations based on the MABL mixing ratios clearly overestimate the observations in the FT. In order to explain the FT bromoform profiles from the aircraft observations, we need to take into account advection from other FT regions within the South China Sea. This FT advection leads to lower bromoform than the convection out of the MABL along the cruise track. The bromoform found in the MABL originates to 45 % from local sources along the ship track. Accordingly, advection from strong source regions, possibly along the coast, is necessary to explain the remaining 55 % of the bromoform abundance. The fact that the MABL bromoform observed along the cruise track is too high for the local emissions and also too high for the FT profiles above the South China Sea, suggests that the local MABL observations are impacted by additional stronger source regions and may not be representative for the whole region. Observations of lower atmospheric bromoform mixing ratios by Yokouchi et al. (1997), Quack and Suess (1999) and Nadzir et al. (2014) in the South China Sea (Sect. 4.1) confirm this assumption.

Dibromomethane in the FT derived from MABL abundances matches the aircraft observations quite well, indicating that dibromomethane observations in the MABL along the cruise track are representative for the region. While in the FT, advection of air masses with different mixing ratios is not necessary to explain the observed dibromomethane, the situation is reversed in the MABL. Significant advection of dibromomethane-rich air is necessary to explain the observations in the MABL, since only low oceanic sources were observed during the cruise. The impact of advection on the dibromomethane mixing ratio is enhanced by its relatively long tropospheric lifetime of 120 days.

In contrast to bromoform and dibromomethane, the simulated mixing ratios of methyl iodide in the FT are strongly underestimated no matter whether observed MABL mixing ratios or oceanic emissions are used. Due to its short tropospheric life time of 4 days methyl iodide is rapidly degraded during the transport into the FT. The offset between the simulated and observed FT methyl iodide could be caused by additional strong sources of methyl iodide in the South China Sea area. Furthermore, modelling or measurement uncertainties may add to this offset, which we all discuss in the following:

The simulations use constant atmospheric lifetimes for each compound and neglect variations with altitude which could impact the simulated abundances. However, the altitude variations of methyl iodide in the MABL and FT are around 0.5 days (WMO, 2015) and thus are quite small. Therefore it seems unlikely that the lifetime estimate causes a large underestimation of the FT methyl iodide. Deficiencies in the meteorological input fields and the FLEXPART model, in particular in the boundary layer and in the convection parameterizations would affect all compounds and their contribution to the FT concentrations in a similar way and thus seems to be unlikely as well. Ship and aircraft measurements reveal instrumental offsets, while observing the same air masses, which cannot be resolved due to the different applied calibration scales (Sect. 4.3). When we adjust for a constant factor, by which observations of methyl iodide in the MABL differed between R/V *SONNE* and R/A *FALCON*, the simulated and observed FT mixing ratios match better. Thus, an instrumental offset causing, at least partially, the calculated discrepancy for methyl iodide appears likely (Sect. 2.3.1).

Another explanation for the elevated methyl iodide in the FT is advection of fresh air with elevated methyl iodide mixing ratio in the FT from e.g. South East Asia or the Philippines. These areas are known to comprise strong sources for atmospheric methyl iodide from e.g. rice plantation (Redeker et al., 2003; Lee-Taylor and Redeker, 2005). In combination with convective activity over land, which is common in this area (Hendon and Woodberry, 1993), the high observed FT mixing ratios of methyl iodide could be explained, despite the low oceanic contribution during the cruise. The low observed MABL mixing ratios of methyl iodide on R/V *SONNE* may thus also not be representative for the area. Yokouchi et al. (1997) observed higher atmospheric methyl iodide mixing ratios in the South China Sea. Finally, the method of our simplified approach includes uncertainties as well. Since observational studies quantifying the oceanic contribution to atmospheric abundances of VSLS are quite rare, it is difficult to evaluate our findings at the moment and more studies for different oceanic regimes should be carried out to validate our results.

6 Summary

The contribution of oceanic VSLS emissions to marine atmospheric boundary layer (MABL) and free troposphere (FT) air during the SHIVA campaign in November 2011 in the South China and Sulu Seas was investigated in this study. Meteorological parameters were measured near the ocean surface and in the troposphere by regular radiosonde launches on R/V *SONNE* during the cruise. Oceanic VSLS emissions were determined from atmospheric and sea surface water concentration observations. The transport from the surface through the MABL into the FT was computed with the trajectory model FLEXPART.

The ship cruise was dominated by north-easterly winds with a characteristic moderate mean wind speed of $5.5\,\mathrm{m\,s^{-1}}$. The radiosonde launches revealed the high convective potential of the South China and Sulu Seas with an average convective available potential energy (CAPE) of $998 \pm 629\,\mathrm{J\,kg^{-1}}$ and a convective, well ventilated, weakly developed MABL with an average height of $420 \pm 120\,\mathrm{m}$ during the cruise. 800 000 forward trajectories, launched from the ocean surface along the cruise track, show a rapid exchange of MABL air with the FT within 7.8 h. This study concentrates on the three very short lived substances bromoform, dibromomethane and methyl iodide which are known to impact tropospheric and stratospheric ozone. On the one hand, the observations on R/V *SONNE* reveal high mean ocean surface concentrations and emissions for bromoform ($19.94\,\mathrm{pmol\,L^{-1}}$ and $1486\,\mathrm{pmol\,m^{-2}\,h^{-1}}$), dibromomethane ($4.99\,\mathrm{pmol\,L^{-1}}$ and $405\,\mathrm{pmol\,m^{-2}\,h^{-1}}$) and methyl iodide ($3.82\,\mathrm{pmol\,L^{-1}}$ and $433\,\mathrm{pmol\,m^{-2}\,h^{-1}}$) in com-

parison to other oceanic source regions. Atmospheric mixing ratios in the MABL, on the other hand, are relatively low compared to earlier campaigns with mean values of 2.08 ppt bromoform, 1.17 ppt dibromomethane, and 0.39 ppt methyl iodide. The contribution of the oceanic VSLS emissions to their MABL concentrations was evaluated by simple source-loss estimations, resulting in an Oceanic Delivery Ratio (ODR). The ODR for bromoform is computed to be 0.45, revealing that bromoform mixing ratios in the MABL above the marginal seas originated on average to 45 % from local oceanic sources. The ODR for dibromomethane is 21 % and for methyl iodide 74 % indicating that the long-lived dibromomethane is largely advected in the MABL, while the short-lived methyl iodide originates mainly from the local ocean.

We extend our analysis to the FT using VSLS profiles obtained from observations on the research aircraft (R/A) *FALCON* above the South China Sea. The average contribution of a single MABL air release to the FT mixing ratios (Sect. 5.3.1) is up to 28 % (bromoform), 12 % (dibromomethane) and 5 % (methyl iodide). The mean contributions of the local oceanic VSLS to the FT within this MABL air release are up to 13 % (bromoform), 3 % (dibromomethane) and 4 % (methyl iodide). In order to estimate if the accumulated contribution from the single MABL air releases is sufficient to explain the accumulated VSLS mixing ratios observed in the FT, we simulate a steady transport of observed MABL air masses, respectively, oceanic emissions into the FT above the South China Sea. The simulations for bromoform based on the volume mixing ratios in the MABL (VMR_{MABL}) overestimated the observations in the FT, while the simulations based on the local oceanic emissions of bromoform from the South China Sea (VMR_{ODR}) explained about 60 % of the observed FT mixing ratio. In the MABL the local oceanic emissions along the cruise track can also explain half of the bromoform which is also too high for the FT observations. Thus, we conclude that the observed mixing ratios of bromoform in the MABL are influenced by stronger local sources and may not be representative for the whole South China Sea where we expect generally lower values.

Dibromomethane in the FT, simulated from observed MABL mixing ratios, shows a good agreement between observations and simulations. It is most likely mixed in the FT with advected air masses containing similar dibromomethane mixing ratios. Methyl iodide in the FT is strongly underestimated in the simulations, using both the observed MABL mixing ratios and the oceanic emissions. The disagreement points either to an unresolved offset between the ship and aircraft data, or to an underestimation of representative methyl iodide MABL mixing ratios and to additional methyl iodide sources, e.g. rice plantations in South East Asia that were not covered by the ship cruise.

Our investigations show how oceanic emissions of VSLS in a strong oceanic source region contribute to the observed atmospheric mixing ratios in the MABL. Furthermore, the contributions of these atmospheric mixing ratios and the local oceanic VSLS therein to the VSLS, observed in the FT above this source region, are derived. The results reveal strong links between oceanic emissions, atmospheric mixing ratios, MABL conditions and prevailing convective activity in the troposphere. The methods should be applied to other oceanic regions to derive a better process understanding of the contributions of air–sea gas exchange on atmospheric abundances. For the detection of future climate change effects on ocean surface trace gas emissions and their influence on atmospheric chemistry and composition it is important to study the complex interplay between oceanic sources and emissions, meteorology, atmospheric mixing ratios, and transport to the upper atmosphere.

Acknowledgements. This work was supported by the EU project SHIVA under grant agreement no. FP7-ENV-2007-1-226224 and by the BMBF grants SHIVA-SONNE 03G0218A and SOPRAN II FKZ 03F0611A. We thank the authorities of Malaysia and the Philippines for the permissions to work in their territorial waters, as well as the SHIVA coordinators Klaus Pfeilsticker and Marcel Dorf and all other SHIVA contributors. We acknowledge the European Centre for medium range weather forecast (ECMWF) for the provision of ERA-Interim reanalysis data and the Lagrangian particle dispersion model FLEXPART used in this publication. We would also like to thank for the support, the captain and crew of R/V *SONNE* and the pilot in command and crew of R/A *FALCON* as well as the Projektträger Jülich (PTJ) and the Deutscher Wetterdienst (DWD). E. Atlas was supported by grant #NNX12AH02G from the NASA Upper

Atmosphere Research Program. We thank X. Zhu and L. Pope for technical support of canister analysis.

References

Aschmann, J. and Sinnhuber, B.-M.: Contribution of very short-lived substances to stratospheric bromine loading: uncertainties and constraints, Atmos. Chem. Phys., 13, 1203–1219, doi:10.5194/acp-13-1203-2013, 2013.

Aschmann, J., Sinnhuber, B.-M., Chipperfield, M. P., and Hossaini, R.: Impact of deep convection and dehydration on bromine loading in the upper troposphere and lower stratosphere, Atmos. Chem. Phys., 11, 2671–2687, doi:10.5194/acp-11-2671-2011, 2011.

Brinckmann, S., Engel, A., Bönisch, H., Quack, B., and Atlas, E.: Short-lived brominated hydrocarbons – observations in the source regions and the tropical tropopause layer, Atmos. Chem. Phys., 12, 1213–1228, doi:10.5194/acp-12-1213-2012, 2012.

Carpenter, L. and Liss, P.: On temperate sources of bromoform and other reactive organic bromine gases, J. Geophys. Res.-Atmos., 105, 20539–20547, doi:10.1029/2000JD900242, 2000.

Carpenter, L., Liss, P., and Penkett, S.: Marine organohalogens in the atmosphere over the Atlantic and Southern Oceans, J. Geophys. Res.-Atmos., 108, 4256, doi:10.1029/2002JD002769, 2003.

Carpenter, L. J., Reimann, S., Burkholder, J. B., Clerbaux, C., Hall, B. D., Hossaini, R., Laube, J. C., and Yvon-Lewis, S. A.: Update on Ozone-Depleting Substances (ODSs) and other gases of interest to the Montreal Protocol, in: Scientific Assessment of Ozone Depletion: 2014, edited by: Engel, A. and Montzka, S. A., World Meteorological Organization, Geneva, 2014.

Dee, D., Uppala, S., Simmons, A., Berrisford, P., Poli, P., Kobayashi, S., Andrae, U., Balmaseda, M., Balsamo, G., Bauer, P., Bechtold, P., Beljaars, A., van de Berg, L., Bidlot, J., Bormann, N., Delsol, C., Dragani, R., Fuentes, M., Geer, A., Haimberger, L., Healy, S., Hersbach, H., Holm, E., Isaksen, L., Kallberg, P., Kohler, M., Matricardi, M., McNally, A., Monge-Sanz, B., Morcrette, J., Park, B., Peubey, C., de Rosnay, P., Tavolato, C., Thepaut, J., and Vitart, F.: The ERA-Interim reanalysis: configuration and performance of the data assimilation system, Q. J. Roy. Meteor. Soc., 137, 553–597, doi:10.1002/qj.828, 2011.

Dix, B., Baidara, S., Bresch, J., Hall, S., Schmidt, K., Wang, S., and Volkamer, R.: Detection of iodine monoxide in the tropical free troposphere, P. Natl. Acad. Sci. USA, 110, 2035–2040, doi:10.1073/pnas.1212386110, 2013.

Forster, C., Stohl, A., and Seibert, P.: Parameterization of convective transport in a Lagrangian particle dispersion model and its evaluation, J. Appl. Meteorol. Clim., 46, 403–422, doi:10.1175/JAM2470.1, 2007.

Fuhlbrügge, S., Krüger, K., Quack, B., Atlas, E., Hepach, H., and Ziska, F.: Impact of the marine atmospheric boundary layer conditions on VSLS abundances in the eastern tropical and subtropical North Atlantic Ocean, Atmos. Chem. Phys., 13, 6345–6357, doi:10.5194/acp-13-6345-2013, 2013.

Gschwend, P., Macfarlane, J., and Newman, K.: Volatile halogenated organic-compounds released to seawater from temperate marine macroalgae, Science, 227, 1033–1035, doi:10.1126/science.227.4690.1033, 1985.

Hendon, H. and Woodberry, K.: The diurnal cycle of tropical convection, J. Geophys. Res.-Atmos., 98, 16623–16637, doi:10.1029/93JD00525, 1993.

Hepach, H., Quack, B., Ziska, F., Fuhlbrügge, S., Atlas, E. L., Krüger, K., Peeken, I., and Wallace, D. W. R.: Drivers of diel and regional variations of halocarbon emissions from the tropical North East Atlantic, Atmos. Chem. Phys., 14, 1255–1275, doi:10.5194/acp-14-1255-2014, 2014.

Hossaini, R., Chipperfield, M. P., Monge-Sanz, B. M., Richards, N. A. D., Atlas, E., and Blake, D. R.: Bromoform and dibromomethane in the tropics: a 3-D model study of chemistry and transport, Atmos. Chem. Phys., 10, 719–735, doi:10.5194/acp-10-719-2010, 2010.

Hossaini, R., Mantle, H., Chipperfield, M. P., Montzka, S. A., Hamer, P., Ziska, F., Quack, B., Krüger, K., Tegtmeier, S., Atlas, E., Sala, S., Engel, A., Bönisch, H., Keber, T., Oram, D., Mills, G., Ordóñez, C., Saiz-Lopez, A., Warwick, N., Liang, Q., Feng, W., Moore, F., Miller, B. R., Marécal, V., Richards, N. A. D., Dorf, M., and Pfeilsticker, K.: Evaluating global emission inventories of biogenic bromocarbons, Atmos. Chem. Phys., 13, 11819–11838, doi:10.5194/acp-13-11819-2013, 2013.

Ko, M. K. W., Poulet, G., and Blake, D. R.: Very Short-Lived Halogen and Sulfur Substances, Scientific Assessment of Ozone Depletion: 2002, Global Ozone Research and Monitoring Project, Chapter 2, report No. 47, World Meteorological Organization, Geneva, 2003.

Krüger, K. and Quack, B.: Introduction to special issue: the *TransBrom Sonne* expedition in the tropical West Pacific, Atmos. Chem. Phys., 13, 9439–9446, doi:10.5194/acp-13-9439-2013, 2013.

Lee-Taylor, J. and Redeker, K.: Reevaluation of global emissions from rice paddies of methyl iodide and other species, Geophys. Res. Lett., 32, L15801, doi:10.1029/2005GL022918, 2005.

Liu, Y., Yvon-Lewis, S., Thornton, D., Butler, J., Bianchi, T., Campbell, L., Hu, L., and Smith, R.: Spatial and temporal distributions of bromoform and dibromomethane in the Atlantic Ocean and their relationship with photosynthetic biomass, J. Geophys. Res.-Oceans, 118, 3950–3965, doi:10.1002/jgrc.20299, 2013.

Margules, M.: Über die Energie der Stürme, K. K. Zentralanstalt für Meteorologie und Erdmagnetismus in Wien, Vienna, 1–26, 1905.

Moncrieff, M. and Miller, M.: Dynamics and simulation of tropical cumulonimbus and squall lines, Q. J. Roy. Meteor. Soc., 102, 373–394, doi:10.1002/qj.49710243208, 1976.

Montzka, S., Butler, J., Hall, B., Mondeel, D., and Elkins, J.: A decline in tropospheric organic bromine, Geophys. Res. Lett., 30, 1826, doi:10.1029/2003GL017745, 2003.

Montzka, S. A. and Reimann, S.: Ozone-depleting substances and related chemicals, Scientific Assessment of Ozone Depletion: 2010, Global Ozone Research and Monitoring Project – Report No. 52, Geneva, Switzerland, 2011.

Mohd Nadzir, M. S., Phang, S. M., Abas, M. R., Abdul Rahman, N., Abu Samah, A., Sturges, W. T., Oram, D. E., Mills, G. P., Leedham, E. C., Pyle, J. A., Harris, N. R. P., Robinson, A. D., Ashfold, M. J., Mead, M. I., Latif, M. T., Khan, M. F., Amiruddin, A. M., Banan, N., and Hanafiah, M. M.: Bromocarbons in the tropical coastal and open ocean atmosphere during the 2009 Prime Expedition Scientific Cruise (PESC-09), Atmos. Chem. Phys., 14, 8137–8148, doi:10.5194/acp-14-8137-2014, 2014.

Nightingale, P., Malin, G., Law, C., Watson, A., Liss, P., Liddicoat, M., Boutin, J., and Upstill-Goddard, R.: In situ evaluation of air–sea gas exchange parameterizations using novel conservative and volatile tracers, Global Biogeochem. Cy., 14, 373–387, doi:10.1029/1999GB900091, 2000.

Quack, B. and Suess, E.: Volatile halogenated hydrocarbons over the western Pacific between 43 and 4° N, J. Geophys. Res.-Atmos., 104, 1663–1678, doi:10.1029/98JD02730, 1999.

Quack, B. and Wallace, D.: Air–sea flux of bromoform: controls, rates, and implications, Global Biogeochem. Cy., 17, 1023, doi:10.1029/2002GB001890, 2003.

Quack, B., Atlas, E., Petrick, G., and Wallace, D.: Bromoform and dibromomethane above the Mauritanian upwelling: atmospheric distributions and oceanic emissions, J. Geophys. Res.-Atmos., 112, D09312, doi:10.1029/2006JD007614, 2007.

Quack, B., Krüger, K., Atlas, E., Tegtmeier, S., Großmann, K., Rex, M., von Glasow, R., Sommariva, R., and Wallace, D.: Halocarbon sources and emissions over the Western Pacific, oral presentation, EGU General Assembly, 5 April 2011, Vienna, Austria, 2011.

Redeker, K., Meinardi, S., Blake, D., and Sass, R.: Gaseous emissions from flooded rice paddy agriculture, J. Geophys. Res.-Atmos., 108, 4386, doi:10.1029/2002JD002814, 2003.

Ren, Y., Baumann, R., and Schlager, H.: An airborne perfluorocarbon tracer system and its first application for a Lagrangian experiment, Atmos. Meas. Tech., 8, 69–80, doi:10.5194/amt-8-69-2015, 2015.

Saiz-Lopez, A. and von Glasow, R.: Reactive halogen chemistry in the troposphere, Chem. Soc. Rev., 41, 6448–6472, doi:10.1039/c2cs35208g, 2012.

Sala, S., Bönisch, H., Keber, T., Oram, D. E., Mills, G., and Engel, A.: Deriving an atmospheric budget of total organic bromine using airborne in situ measurements from the western Pacific area during SHIVA, Atmos. Chem. Phys., 14, 6903–6923, doi:10.5194/acp-14-6903-2014, 2014.

Schauffler, S., Atlas, E., Blake, D., Flocke, F., Lueb, R., Lee-Taylor, J., Stroud, V., and Travnicek, W.: Distributions of brominated organic compounds in the troposphere and lower stratosphere, J. Geophys. Res.-Atmos., 104, 21513–21535, doi:10.1029/1999JD900197, 1999.

Seibert, P., Beyrich, F., Gryning, S., Joffre, S., Rasmussen, A., and Tercier, P.: Review and intercomparison of operational methods for the determination of the mixing height, Atmos. Environ., 34, 1001–1027, doi:10.1016/S1352-2310(99)00349-0, 2000.

Solomon, S.: Stratospheric ozone depletion: a review of concepts and history, Rev. Geophys., 37, 275–316, doi:10.1029/1999RG900008, 1999.

Solomon, S., Garcia, R., and Ravishankara, A.: On the role of iodine in ozone depletion, J. Geophys. Res.-Atmos., 99, 20491–20499, doi:10.1029/94JD02028, 1994.

Sorensen, J.: Sensitivity of the DERMA long-range gaussian dispersion model to meteorological input and diffusion parameters, Atmos. Environ., 32, 4195–4206, doi:10.1016/S1352-2310(98)00178-2, 1998.

Stohl, A. and Thomson, D.: A density correction for Lagrangian particle dispersion models, Bound.-Lay. Meteorol., 90, 155–167, doi:10.1023/A:1001741110696, 1999.

Stohl, A. and Trickl, T.: A textbook example of long-range transport: Simultaneous observation of ozone maxima of stratospheric and North American origin in the free troposphere over Europe, J. Geophys. Res.-Atmos., 104, 30445–30462, doi:10.1029/1999JD900803, 1999.

Stohl, A., Hittenberger, M., and Wotawa, G.: Validation of the Lagrangian particle dispersion model FLEXPART against large-scale tracer experiment data, Atmos. Environ., 32, 4245–4264, doi:10.1016/S1352-2310(98)00184-8, 1998.

Stohl, A., Forster, C., Frank, A., Seibert, P., and Wotawa, G.: Technical note: The Lagrangian particle dispersion model FLEXPART version 6.2, Atmos. Chem. Phys., 5, 2461–2474, doi:10.5194/acp-5-2461-2005, 2005.

Stull, R.: An Introduction to Boundary Layer Meteorology, Kluwer Academic Publishers, Dordrecht, 1988.

Tegtmeier, S., Krüger, K., Quack, B., Atlas, E. L., Pisso, I., Stohl, A., and Yang, X.: Emission and transport of bromocarbons: from the West Pacific ocean into the stratosphere, Atmos. Chem. Phys., 12, 10633–10648, doi:10.5194/acp-12-10633-2012, 2012.

Tegtmeier, S., Krüger, K., Quack, B., Atlas, E., Blake, D. R., Boenisch, H., Engel, A., Hepach, H., Hossaini, R., Navarro, M. A., Raimund, S., Sala, S., Shi, Q., and Ziska, F.: The contribution of oceanic methyl iodide to stratospheric iodine, Atmos. Chem. Phys., 13, 11869–11886, doi:10.5194/acp-13-11869-2013, 2013.

Thompson, R. and Edwards, R.: An overview of environmental conditions and forecast implications of the 3 May 1999 tornado outbreak, Weather Forecast., 15, 682–699, doi:10.1175/1520-0434(2000)015<0682:AOOECA>2.0.CO;2, 2000.

Troen, I. and Mahrt, L.: A simple-model of the atmospheric boundary-layer: Sensitivity to surface evaporation, Bound.-Lay. Meteorol., 37, 129–148, doi:10.1007/BF00122760, 1986.

Vogelezang, D. and Holtslag, A.: Evaluation and model impacts of alternative boundary-layer height formulations, Bound.-Lay. Meteorol., 81, 245–269, doi:10.1007/BF02430331, 1996.

von Glasow, R., von Kuhlmann, R., Lawrence, M. G., Platt, U., and Crutzen, P. J.: Impact of reactive bromine chemistry in the troposphere, Atmos. Chem. Phys., 4, 2481–2497, doi:10.5194/acp-4-2481-2004, 2004.

WMO: Scientific Assessment of Ozone Depletion: 2014, Global Ozone Research and Monitoring Project, Geneva, Switzerland, 2015.

Worton, D., Mills, G., Oram, D., and Sturges, W.: Gas chromatography negative ion chemical ionization mass spectrometry: application to the detection of alkyl nitrates and halocarbons

in the atmosphere, J. Chromatogr. A, 1201, 112–119, doi:10.1016/j.chroma.2008.06.019, 2008.

Yang, X., Cox, R., Warwick, N., Pyle, J., Carver, G., O'Connor, F., and Savage, N.: Tropospheric bromine chemistry and its impacts on ozone: a model study, J. Geophys. Res.-Atmos., 110, D23311, doi:10.1029/2005JD006244, 2005.

Yang, X., Abraham, N. L., Archibald, A. T., Braesicke, P., Keeble, J., Telford, P. J., Warwick, N. J., and Pyle, J. A.: How sensitive is the recovery of stratospheric ozone to changes in concentrations of very short-lived bromocarbons?, Atmos. Chem. Phys., 14, 10431–10438, doi:10.5194/acp-14-10431-2014, 2014.

Yokouchi, Y., Mukai, H., Yamamoto, H., Otsuki, A., Saitoh, C., and Nojiri, Y.: Distribution of methyl iodide, ethyl iodide, bromoform, and dibromomethane over the ocean (east and southeast Asian seas and the western Pacific), J. Geophys. Res.-Atmos., 102, 8805–8809, doi:10.1029/96JD03384, 1997.

Yokouchi, Y., Hasebe, F., Fujiwara, M., Takashima, H., Shiotani, M., Nishi, N., Kanaya, Y., Hashimoto, S., Fraser, P., Toom-Sauntry, D., Mukai, H., and Nojiri, Y.: Correlations and emission ratios among bromoform, dibromochloromethane, and dibromomethane in the atmosphere, J. Geophys. Res.-Atmos., 110, D23309, doi:10.1029/2005JD006303, 2005.

Table 1. Mean ± standard deviation and range ([ ]) of atmospheric mixing ratios observed on R/V *SONNE* and R/A *FALCON* (GhOST-MS and WASP GC/MS) in the MABL and the FT, water concentrations observed by R/V *SONNE* and computed the sea–air flux. MABL and FT mixing ratios for bromoform and dibromomethane on R/A *FALCON* are adopted from Sala et al. (2014). The R/A *FALCON* MABL height was set to 450 m. The last line gives the sea–air flux computed from R/V *SONNE* mixing ratios for all three compounds.

				Bromoform	Dibromomethane	Methyl iodide
Atmosph. mixing ratios [ppt]	R/V *SONNE*			2.08 ± 1.36 [0.79–5.07]	1.17 ± 0.19 [0.71–1.98]	0.39 ± 0.09 [0.19–0.78]
	R/A *FALCON*	GhOST	MABL	1.43 ± 0.53 [0.42–3.42]	1.19 ± 0.21 [0.58–1.89]	0. 59 ± 0.30 [0.29–3.23]
			FT	0.56 ± 0.17 [0.16–2.15]	0.87 ± 0.12 [0.56–1.54]	0.26 ± 0.11 [0.08–0.80]
		WASP	MABL	1.90 ± 0.55 [0.99–3.78]	1.15 ± 0.14 [0.85–1.59]	/
			FT	1.17 ± 0.50 [0.43–3.22]	0.88 ± 0.14 [0.46–1.36]	/
Water concentrations [pmol L^{-1}]				19.94 ± 17.90 [2.80–136.91]	4.99 ± 2.59 [2.43–21.82]	3.82 ± 2.43 [0.55–18.84]
Sea–air flux [pmol m^{-2} h^{-1}]				1486 ± 1718 [−8–13 149]	405 ± 349 [16–2210]	433 ± 482 [13–2980]

Table 2. Mean atmospheric mixing ratios of bromoform, dibromomethane and methyl iodide observed on R/V *SONNE* and R/A *FALCON* during two case studies on 19 November 2011 at 3.2° N and 112.5° E and on 21 November 2011 at 4.6° N and 113.0° E.

		Bromoform [ppt]	Dibromomethane [ppt]	Methyl iodide [ppt]
19 Nov 2011	R/V *SONNE*	1.37	0.99	0.29
	R/A *FALCON*: GhOST/WASP	1.02/1.37	0.94/1.03	0.45/–
21 Nov 2011	R/V *SONNE*	2.05	1.08	0.28
	R/A *FALCON*: GhOST/WASP	1.63/2.00	1.31/1.08	0.82/–

Table 3. Mean ± standard deviation of Oceanic Delivery (OD), COnvective Loss (COL), Chemical Loss (CL), Advective Delivery (AD), Oceanic Delivery Ratio (ODR), Chemical Loss Ratio (CLR), Advective Delivery Ratio (ADR) for bromoform ($CHBr_3$), dibromomethane (CH_2Br_2) and methyl iodide (CH_3I).

	OD [% day^{-1}]	COL [% day^{-1}]	CL [% day^{-1}]	AD [% day^{-1}]	ODR	CLR	ADR
$CHBr_3$	116.4 ± 163.6	−307.6 ± 124.3	−6.6	197.9 ± 199.7	0.45 ± 0.55	−0.03 ± 0.01	0.58 ± 0.55
CH_2Br_2	54.2 ± 66.7	−307.6 ± 124.3	−1.8	255.2 ± 131.9	0.21 ± 0.21	−0.01 ± 0.00	0.80 ± 0.21
CH_3I	166.5 ± 185.8	−307.6 ± 124.3	−30.7	171.8 ± 242.3	0.74 ± 1.05	−0.12 ± 0.05	0.38 ± 1.01

Table 4. Mean ± standard deviation of observed Volume Mixing Ratios in the MABL on R/V *SONNE* (VMR_{MABL}) vs. the amount of VMR originating from oceanic emissions (VMR_{ODR}), chemically degraded according to the specific lifetime (VMR_{CLR}), originating from advection (VMR_{ADR}) and the Flux from the MABL into the FT ($Flux_{MABL\text{-}FT}$) for bromoform ($CHBr_3$), dibromomethane (CH_2Br_2) and methyl iodide (CH_3I).

	VMR_{MABL} [ppt]	VMR_{ODR} [ppt]	VMR_{CLR} [ppt]	VMR_{ADR} [ppt]	$Flux_{MABL\text{-}FT}$ [pmol m^{-2} h^{1}]
$CHBr_3$	2.08 ± 1.36	0.89 ± 1.12	−0.05 ± 0.04	1.18 ± 1.20	4240 ± 1889
CH_2Br_2	1.17 ± 0.19	0.25 ± 0.26	−0.01 ± 0.01	0.92 ± 0.27	2419 ± 929
CH_3I	0.39 ± 0.09	0.28 ± 0.40	−0.05 ± 0.03	0.14 ± 0.37	865 ± 373

Table 5. Correlation coefficients between wind speed and VSLS MABL mixing ratios (VMR_{MABL}), the Oceanic Delivery (OD), the COnvective Loss to the FT (COL), the Advective Delivery (AD), computed as the residual of OD, and the mixing ratios originating from the OD (VMR_{ODR}) and from the AD (VMR_{ADR}). Bold numbers are significant at the 95 % (p value).

Wind speed	Bromoform	Dibromomethane	Methyl iodide
VMR_{MABL}	**0.55**	**0.57**	**0.56**
OD	**0.31**	**0.48**	**0.52**
COL		**−0.33**	
AD	−0.04	0.06	**−0.28**
VMR_{ODR}	**0.52**	**0.72**	**0.62**
VMR_{ADR}	−0.21	**−0.32**	**−0.53**

Table A1. As Table 3 and Table 4 using ERA-Interim MABL height.

	OD [% day^{-1}]	COL [% day^{-1}]	CL [% day^{-1}]	AD [% day^{-1}]	ODR	CLR	ADR	VMR_{ODR} [ppt]	VMR_{CLR} [ppt]	VMR_{ADR} [ppt]	MABL-FT Flux [pmol m^{-2} h^{1}]
$CHBr_3$	87.0 ± 124.5	−224.9 ± 70.7	−6.6	144.5 ± 143.1	0.43 ± 0.56	−0.03 ± 0.01	0.60 ± 0.55	0.88 ± 1.18	−0.07 ± 0.04	1.24 ± 1.20	4251 ± 1907
CH_2Br_2	39.3 ± 40.3	−224.9 ± 70.7	−1.8	187.4 ± 83.2	0.20 ± 0.21	−0.01 ± 0.00	0.81 ± 0.21	0.24 ± 0.26	−0.01 ± 0.00	0.93 ± 0.27	2456 ± 921
CH_3I	135.2 ± 195.0	−224.9 ± 70.7	−30.7	120.4 ± 220.8	0.73 ± 1.06	−0.15 ± 0.05	0.42 ± 1.03	0.28 ± 0.39	−0.06 ± 0.03	0.15 ± 0.37	799 ± 356

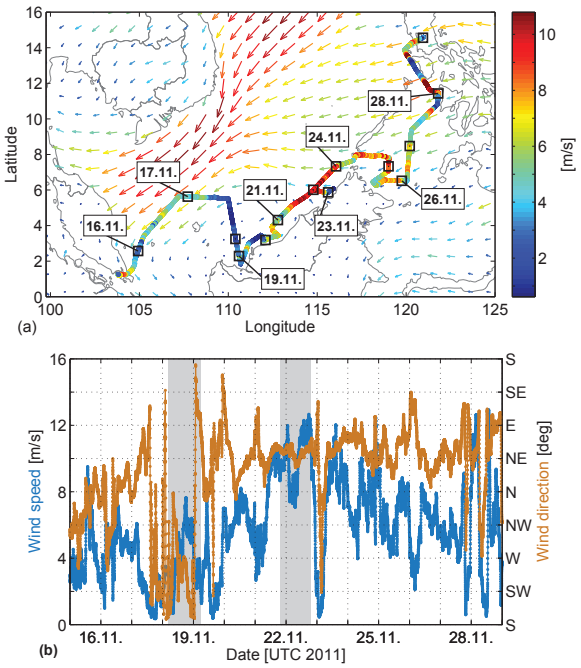

Figure 1. (a) ERA-Interim mean wind field 15–30 November 2011 (arrows) and 10 min running mean of wind speed observed on R/V *SONNE* as the cruise track. The black squares show the ships position at 00:00 UTC each day. **(b)** Time series of wind speed (blue) and wind direction (ocher) measured on R/V *SONNE*. The data are averaged by a 10 min running mean. The two shaded areas (light grey) in the background show the 24 h stations.

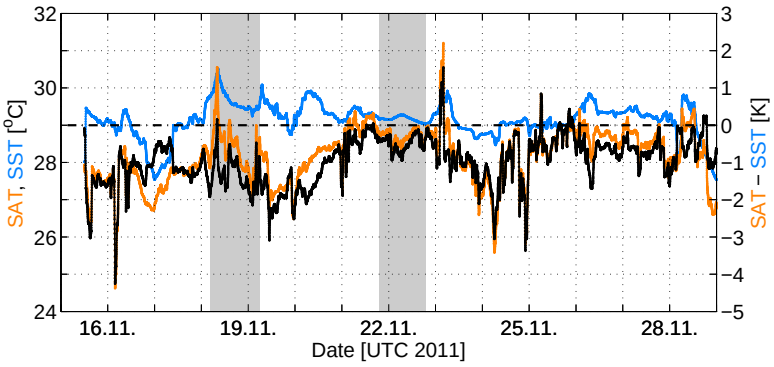

Figure 2. Time series of SAT (10 min running mean, orange) and SST (10 min running mean, blue) on the left and the difference of SAT and SST (10 min running mean, right scale). For the temperature difference, the 0 K line is given by dashed line. The two shaded areas (light grey) in the background show the 24 h stations.

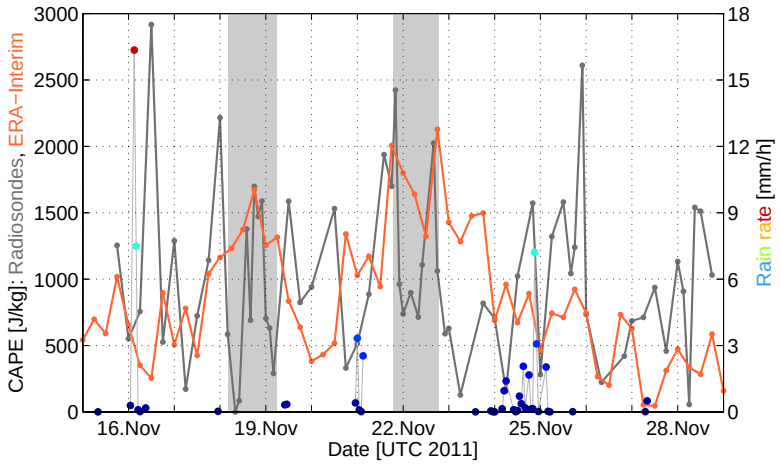

Figure 3. Left scale: convective available potential energy (CAPE) from radiosondes on R/V *SONNE* (grey) and ERA-Interim (orange). Right scale: Rain rate (colored dots) during the cruise, observed by an optical disdrometer (ODM 470) on R/V *SONNE*. The two shaded areas (light grey) in the background show the 24 h stations.

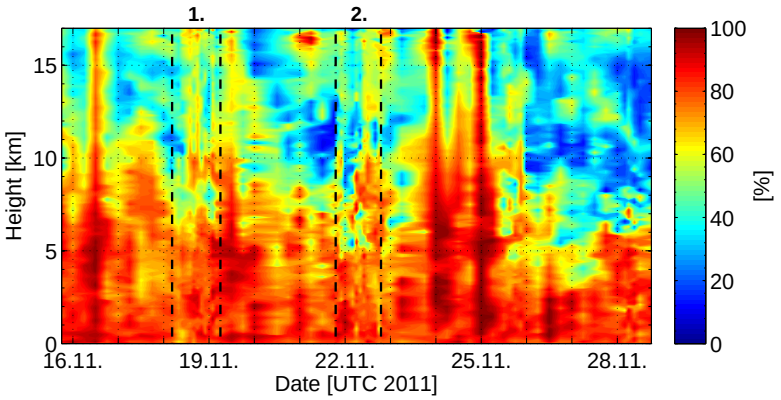

Figure 4. Relative humidity by radiosondes up to 17 km height, the mean cold point tropopause level. The dashed lines and the two numbers above the figure indicate the two 24 h stations.

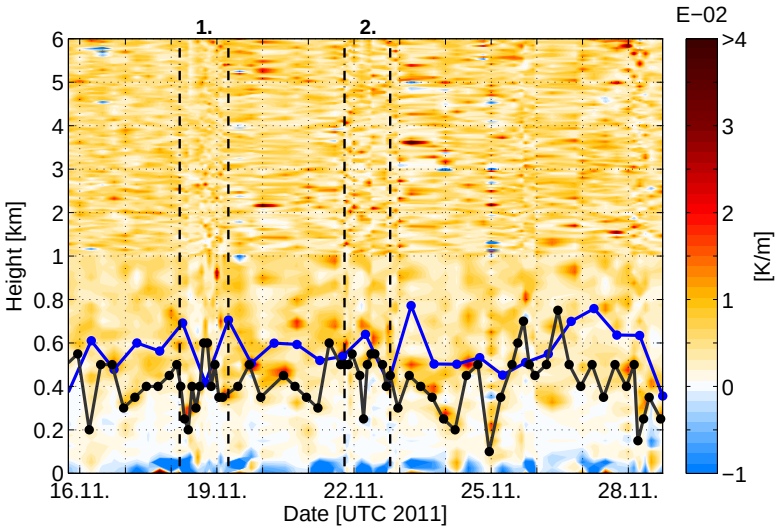

Figure 5. Virtual potential temperature gradient as indicator for atmospheric stability (red for stable, white for neutral and blue for unstable) with MABL height from radiosondes (black curve) and from ERA-Interim (blue curve). The *y* axis is non-linear. The lower 1 km is enlarged to display the stability around the MABL height. The dashed lines and the two numbers above the figure indicate the two 24 h stations.

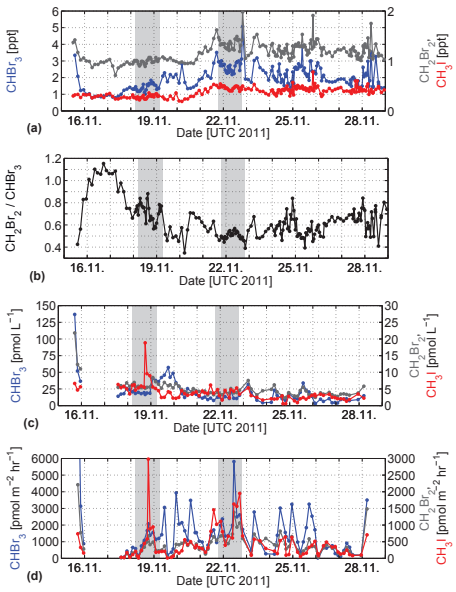

Figure 6. (a) Atmospheric mixing ratios of bromoform ($CHBr_3$, blue), dibromomethane (CH_2Br_2, dark grey) and methyl iodide (CH_3I, red) measured on R/V *SONNE*. **(b)** Concentration ratio of dibromomethane and bromoform on R/V *SONNE*. **(c)** Water concentrations of methyl iodide, bromoform and dibromomethane measured on R/V *SONNE*. **(d)** Emissions of methyl iodide, bromoform and dibromomethane from atmospheric and water samples measured on R/V *SONNE*. The two shaded areas (light grey) in the background show the 24 h stations.

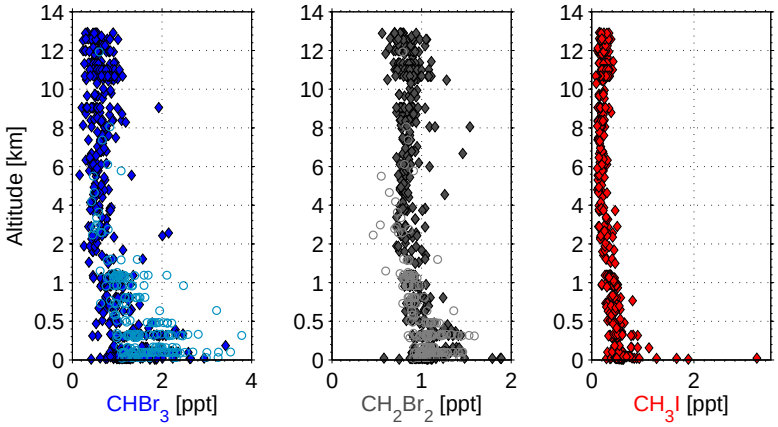

Figure 7. Vertical distribution bromoform ($CHBr_3$, blue), dibromomethane (CH_2Br_2, grey) and methyl iodide (CH_3I, red) mixing ratios measured by GhOST (diamonds) and WASP (circles) on R/A *FALCON*. Methyl iodide was only measured by GhOST. The lower 2 km are non-linear displayed.

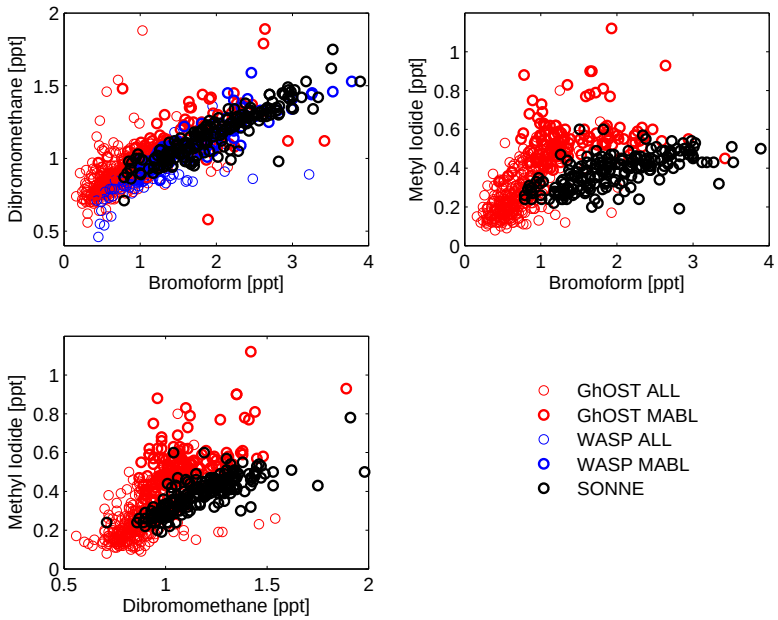

Figure 8. Correlation of bromoform and dibromomethane (upper left), bromoform and methyl iodide (upper right), and dibromomethane and methyl iodide (lower left) from GhOST and WASP for all heights (ALL) and only within the MABL (MABL) and from R/V *SONNE*.

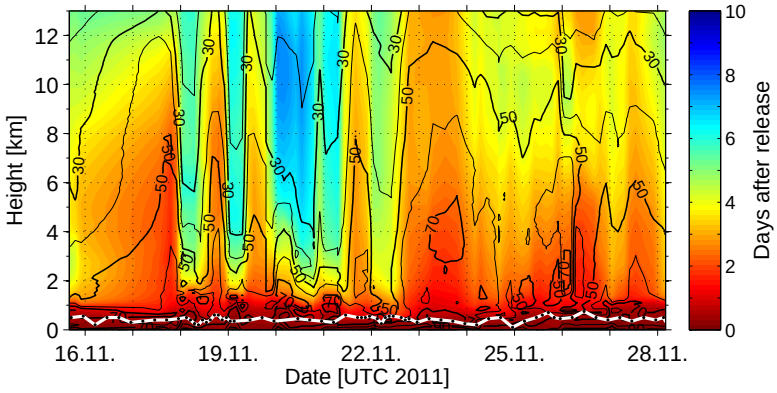

Figure 9. Forward trajectory runs along the cruise track with FLEXPART using ERA-Interim data. The black contour lines show the mean amount of trajectories (in %) reaching this height within the specific time (colour shading). The white line indicates the radiosonde MABL height.

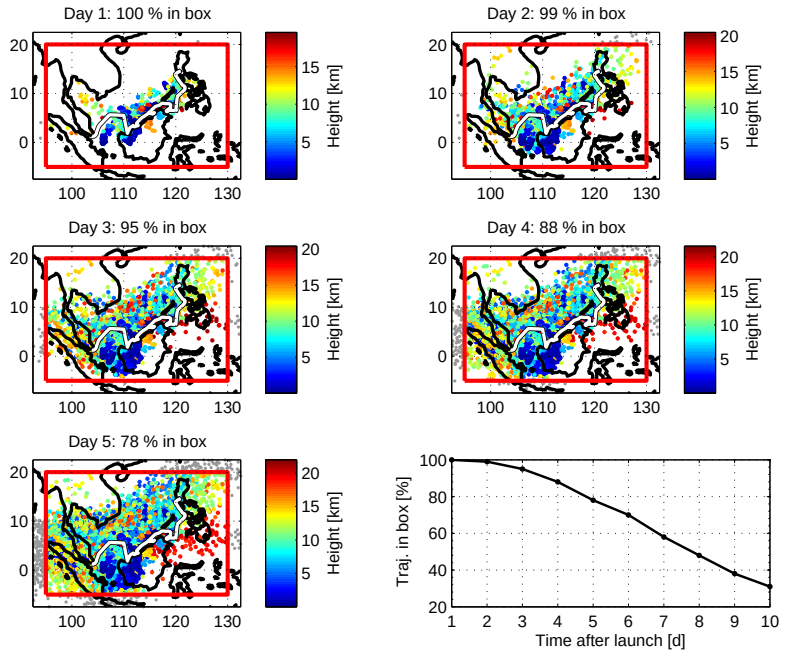

Figure 10. Horizontal distribution, altitude and amount of trajectories with time during the cruise. The red box represents the South China and Sulu Seas area. The lower right plot shows the amount of trajectories that remain in the box with time from all trajectory releases.

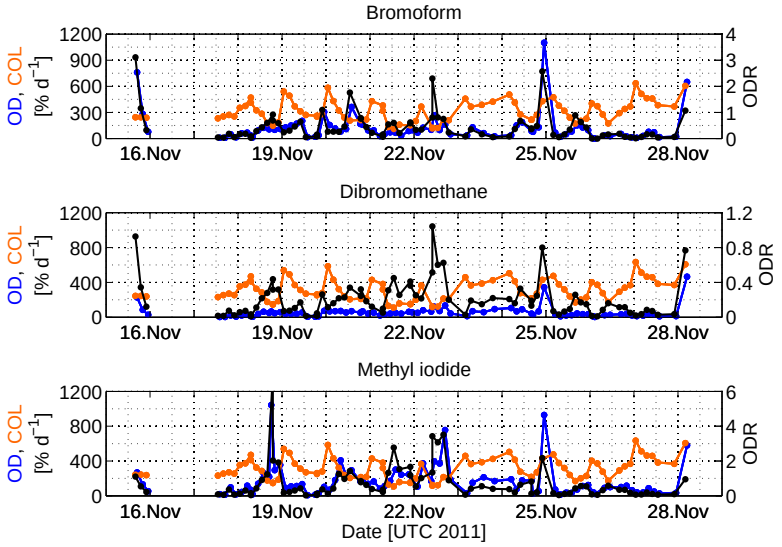

Figure 11. Time series of oceanic delivery (OD) to MABL concentration in % day^{-1} (blue), COnvective Loss (COL) from the MABL to the FT in % day^{-1} (orange) and the Oceanic Delivery Ratio (ODR, black) for bromoform (upper plot), dibromomethane (centre plot) and methyl iodide (lower plot).

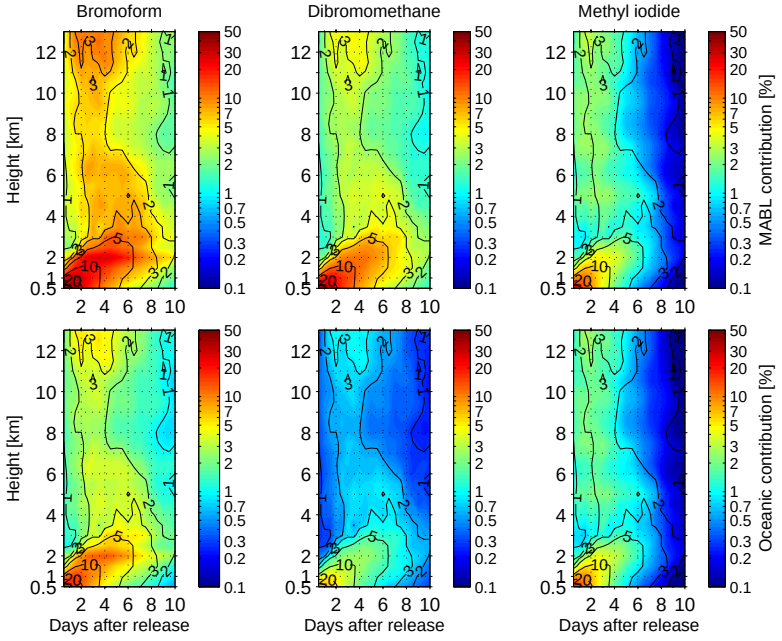

Figure 12. Mean MABL air contribution (upper plots) and oceanic contribution (lower plots) to observed FT mixing ratios observed by R/A *FALCON* for three VSLS. The black contour lines show the mean portion of MABL air masses in the FT [%], the colours show the oceanic contribution to the observed compounds in the FT, at specific height and day after release [%] including chemical degradation, the loss out of the South China Sea area with time and the vertical density driven extension of MABL air masses. The scale of the coloured contour is logarithmic.

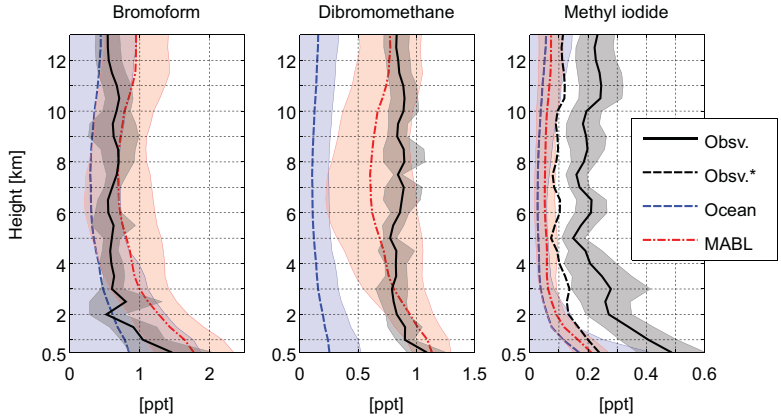

Figure 13. Mean FT mixing ratios (solid lines) and 1 standard deviation (shaded areas) observed by R/A *FALCON* (Obsv., black) vs. simulated mean FT mixing ratios from MABL air (MABL, red) and oceanic emissions (Ocean, blue) observed by R/V *SONNE*. R/A *FALCON* observations have been adjusted for methyl iodide (Obsv.*, dashed black) according measurements deviations during the meetings of R/V *SONNE* and R/A *FALCON* (compare Table 2; Sect. 4.3).

3.4 Manuscript 4

Observation of the Variations of Very Short-Lived Halocarbon Emissions in Tropical Coastal Marine Boundary Layer

J. Sentian[1], C. T. Xiang[1], H. C. Jing[1], B. Quack[2], S. Fuhlbrügge[2], K. Krüger[2*], and E. Atlas[3]

[1] Faculty of Science and Natural Resource, Universiti Malaysia Sabah, Sabah, Malaysia

[2] GEOMAR Helmholtz-Zentrum für Ozeanforschung Kiel, Kiel, Germany

[3] Rosenstiel School of Marine and Atmospheric Science (RSMAS), Miami, USA

[*] now at Department of Geosciences, University of Oslo (UiO), Oslo, Norway

Published in: Advanced Science Letters, Vol. 21, 144-149, doi:10.1166/asl.2015.5856, 2015.

Advanced Science Letters
Vol. 21, 144–149, 2015

Observation of the Variations of Very Short-Lived Halocarbon Emissions in Tropical Coastal Marine Boundary Layer

Justin Sentian[1], Chen Tian Xiang[1], Huang Chen Jing[1], Birgit Quack[2], Steffen Fuhlbrügge[2], Kristin Krüger[2], and Elliot Atlas[3]

[1]*Faculty of Science and Natural Resource, Universiti Malaysia Sabah, 84000 Kota Kinabalu, Sabah, Malaysia*
[2]*GEOMAR Helmholtz-Zentrum für Ozeanforschung Kiel, Wischhofstr. 1-3, 24148 Kiel, Germany*
[3]*The Rosenstiel School of Marine and Atmospheric Science, 4600 Rickenbacker Causeway, Miami, FL 33149-1098, USA*

Halocarbons (methyl iodide, bromoform and dibromomethane) are produced naturally and the source has been found to be largely from the ocean. In recent years, the role of very short-lived halocarbons in the atmospheric chemistry has attracted many researchers in this field. Dissolved halocarbons in sea water and atmospheric halocarbons were taken at 73 different positions across South China Sea and Sulu Sea during the SHIVA measurement campaign on RV SONNE cruise from Singapore to Manila on the 15 to 29 November 2011. Both water and canister samples of air were analyzed on two different purge-and-trap (PT) gas chromatographic systems. Significant levels of halocarbons were observed during day-time and night-time in the tropical marine boundary layer. All of the halocarbons show higher concentrations at the coastal area compare to the location in the open sea.

Keywords: Halocarbons, SHIVA Campaign, Sea-to-Air Flux, Tropical, Marine Boundary Layer.

1. INTRODUCTION

Over the past 30 years, research interest on the reactive halogen species effects on the ozone depletion has significantly increased.[1,2] In recent years, the role of very short-lived halocarbons (VSLS) in the atmospheric chemistry has become the focus of investigation.[2,3] VSLSs are substances that have atmospheric lifetimes comparable to or less than average tropospheric transport time scales of about 6 months. Studies[1,2] have shown that these reactive halocarbons originate in the marine boundary layer[4,5] and are transported to the upper troposphere and lower stratosphere. Stratospheric halogen loading is maintained by transport of source gases followed by their degradation in the stratosphere and transport of intermediate products and inorganic halogens produced in the troposphere.[2] Tropospheric inorganic halogens can be derived from the degradation of VSLSs or from inorganic halogen sources.[6] At the same time, bromine and iodine atoms released from these compounds by photolysis and oxidation can take part in catalytic ozone destroying cycles in both the troposphere and stratosphere[1,2,7] while iodine also participates in aerosol formation.[6]

Spatial and temporal variability in VSLS halocarbons production and sea-to-air flux of the short-lived halogenated trace gases create strong varying marine and atmospheric distributions and thus also varying stratospheric contributions.[7] However, the current understanding on impact of these natural ozone depleting substances is still highly uncertain and such that potential future changes in the mechanisms that regulate their emissions to the atmosphere, their transport, and their chemical processing are still largely unknown.[1,8] Therefore, the oceanic emissions have the potential to cause surprises in the future evolution of the ozone layer in a changing climate, unless they are better understood.[9,10] The measurements were thus needed to improve the understanding of future stratospheric halogen loading and therewith ozone depletion.[1] The results of the observation of these VSLS halocarbons will surely enhance the understanding of the spatial and temporal variation of the VSLS in the tropical marine boundary layer.

SHIVA (Stratospheric ozone: Halogen Impacts in a Varying Atmosphere) measurement campaign combines ship-borne (RV SONNE), aircraft-based and local boat measurements in and over the South China Sea and the Sulu Sea and around the coast of Malaysian Borneo from 15 to 29 November 2011. The campaign is within the frame work of the European project,

*Author to whom correspondence should be addressed.

1936-6612/2015/21/144/006 doi:10.1166/asl.2015.5856

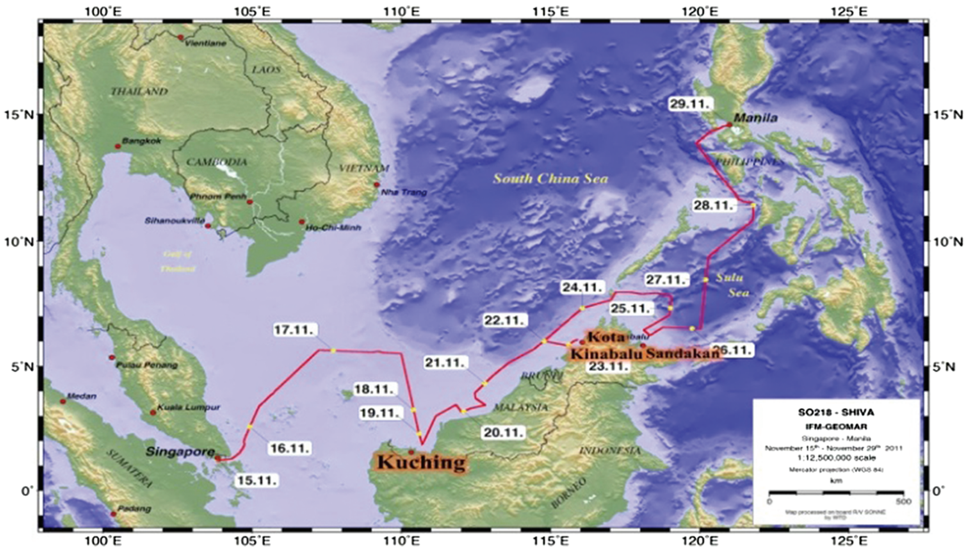

Fig. 1. The RV Sonne ship track leading from Singapore to manila during the measurement campaign.

which was organized and conducted by the Leibniz-Institute of Marine Sciences (IFM-GEOMAR) in collaboration with other European universities and Malaysian universities (University Malaysia Sabah, University Malaya and University Malaysia Sarawak).

2. METHODOLOGY

The measurement of the dissolved halocarbons in seawater during the SHIVA measurement campaign, seawater samples were taken at 73 different positions along a cruise track (Fig. 1) using a submerged water pump under the RV SONNE research vessel's keel. There were additional of 10 CTD stations with 24-bottle CTD rosette (10-L-Niskin bottles). The seawater samples at each station were collected in the entire water column with focus on surface layer, chlorophyll maximum layer and lower layers. The atmospheric halocarbons were also collected in a 2L stainless steel canister, being pressurized to 2 bars for RSMAS with a metal bellows pump by every 6 hours. During the cruise, the RV SONNE vessel approached the coastline near Kuching, Kota Kinabalu as well as Sandakan and performed the seawater and air sampling with the aim of comparing the results with samples taken in the offshore track.

During the cruise, both seawater and canister samples of air were analyzed using two different purge-and-trap (PT) gas chromatographic systems; one used an electron capture detector (ECD) and one used a mass-spectrometric detector (GC44 MS), where the halocarbons were quantified in single ion mode.

$$\frac{k_w}{k_{CO_2}} = \frac{Sc^{-(1/2)}}{660} \tag{1}$$

Quantification of volatiles was performed by external liquid standards. Liquid standards were diluted in seawater and treated like a normal sample.[8,9] After analysis, halocarbon concentrations were determined in water and air was used for sea-to-air fluxes calculations.

The sea-to-air fluxes of the methyl iodide (CH_3I), bromoform ($CHBr_3$) and dibromomethane (CH_2Br_2) were calculated using the air-sea gas exchange parameterization.[5] Schmidt number (Sc) corrections for the compound specific transfer coefficients k_w were derived with the transfer coefficient k_{CO_2} of CO_2^8 (Eq. (1)).

The air-sea concentration gradient was derived from all simultaneous water (c_w) and air (c_{atm}) measurements calculated with the Henry's law constants H of Moore and coworkers[3] in order to obtain the theoretical equilibrium concentration c_{atm}/H (Eq. (2)). The saturation anomaly S has been calculated from the concentration gradient as the percentage of the equilibrium concentration (Eq. (3)).

$$F = k_w \cdot \left(c_w - \frac{c_{atm}}{H}\right) \tag{2}$$

$$S = \left(\left(c_w - \frac{c_{atm}}{H}\right) \cdot 100\right) \cdot \left(\frac{c_{atm}}{H}\right) \tag{3}$$

Water temperature and salinity were continuously recorded using the vessel's thermosalinograph. Air pressure and wind speed were determined by sensors on the compass deck at a height 25.5 m. The wind speed measurement was corrected to 10 m values. Ten minute averages of the water temperature, salinity, air pressure and wind speed have been included in the calculations.

3. RESULTS AND DISCUSSION

VSLS halocarbon measurements (seawater and atmospheric air samples) during the campaign are shown in Table I.

Table I. Halocarbon measurements (water and air) and sea-to-air fluxes during SHIVA measurement campaign

VSLS	Air sample (ppt)	Water sample (pmol L^{-1})	Sea-to-air flux (pmol $m^{-2}h^{-1}$)	Wind speed (m/s)
CH_3I	0.38	3.82	433.04	5.9 (0.3–13.5)
[Range]	0.19–0.55	0.55–18.84	13.08–1979	
$CHBr_3$	2.02	19.94	1486.13	
[Range]	1.00–5.07	2.80–136.91	7.52–13149	
CH_2Br_2	1.16	4.99	405.17	
[Range]	0.90–0.55	0.55–18.84	13.08–2979	

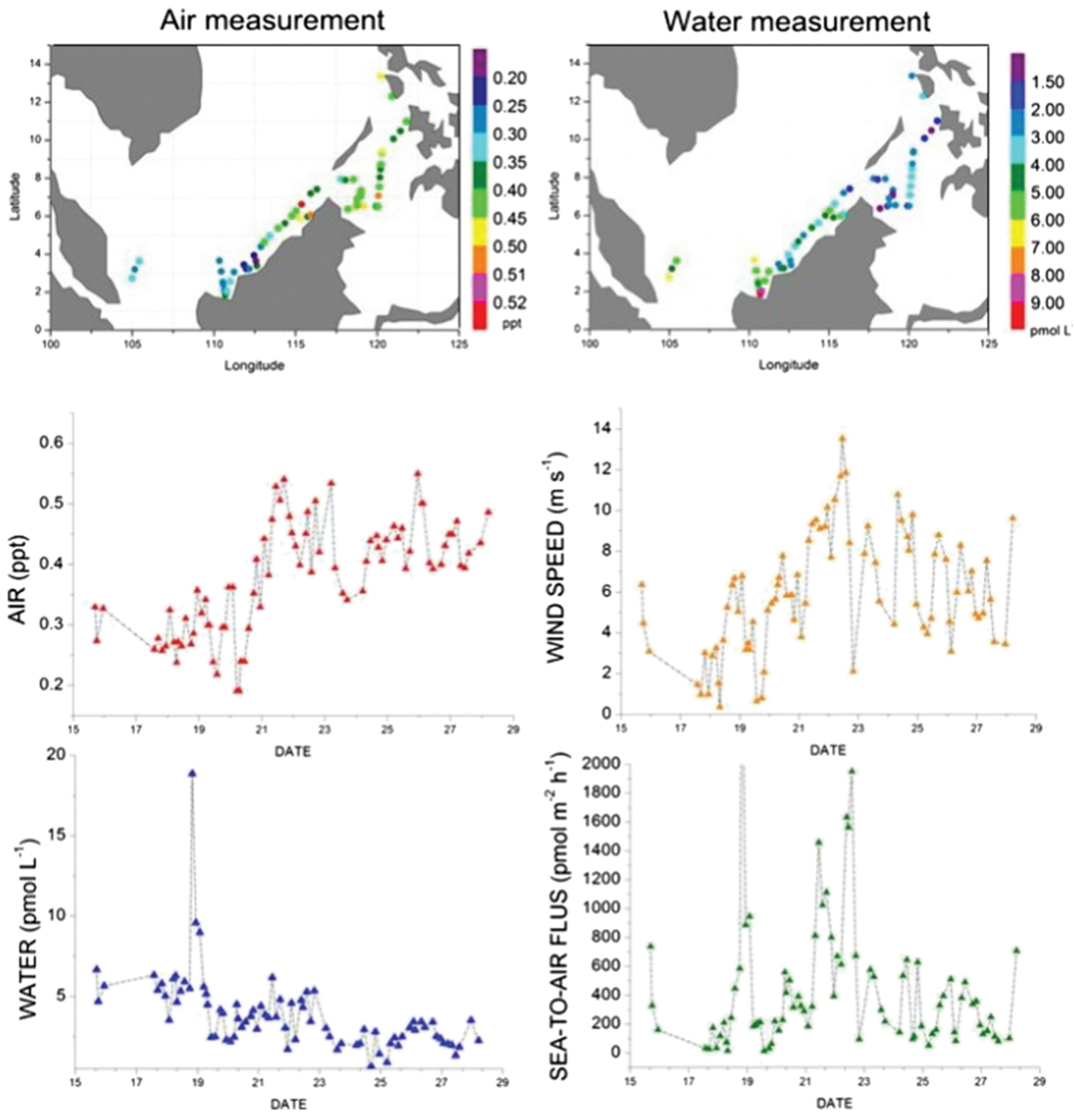

Fig. 2. The regional distribution and variation of CH_3I in the air sample (red), water sample (blue) and sea-to-air flux (green) during the measurement campaign.

3.1. Methyl Iodide (CH_3I)

As shown in Table I, the concentration of methyl iodide (CH_3I) in seawater samples is between 0.55 and 18.84 pmol L^{-1} with an average of 3.82 pmol L^{-1}. In comparison with those samples which were taken near the coastline in Kuching, in Kota Kinabalu and Sandakan, the concentration of CH_3I in coastal areas was relatively higher than those in the open sea. The average concentration of CH_3I in seawater samples near Kuching was 5.19 pmol L^{-1} while in Kota Kinabalu and Sandakan were 4.27 pmol L^{-1} and 3.05 pmol L^{-1} respectively. Higher concentrations near the coastline may be attributed by the presence of microalgae as positively indicated by higher productivity (i.e., high concentration of chlorophyll). Meanwhile, the air measurements also showed the same trend, as the air samples near the coastal areas were observed to be higher (0.2–0.5 ppt) than the locations offshore.

During the measurement campaign, methyl iodide in the air showed three peaks of concentration (Fig. 2) located offshore of Kota Kinabalu (0.53 and 0.54 ppt) and offshore of Sandakan in Sulu Sea (east coast of Sabah) (about 0.55 ppt). Similar peak trends and locations were also observed in water samples. This observation suggests that fluxes of CH_3I from seawater into the marine boundary layer are eminent. Analysis of the sea-to-air fluxes of methyl iodide (CH_3I) (Fig. 2) was also found to be higher during those peaks with the highest flux of 1979 pmol m^{-2} h^{-1}. The wind speed also shows positive effects on the sea-to-air exchange, where higher wind speeds were observed during the peak fluxes. This is in comparison with the other two VSLS halocarbons ($CHBr_3$ and CH_2Br_2) as described in the following showed low sea-to-air flux as well as the dual variation. During the three coastal samplings, the maximum concentrations of CH_3I in the surface water were found

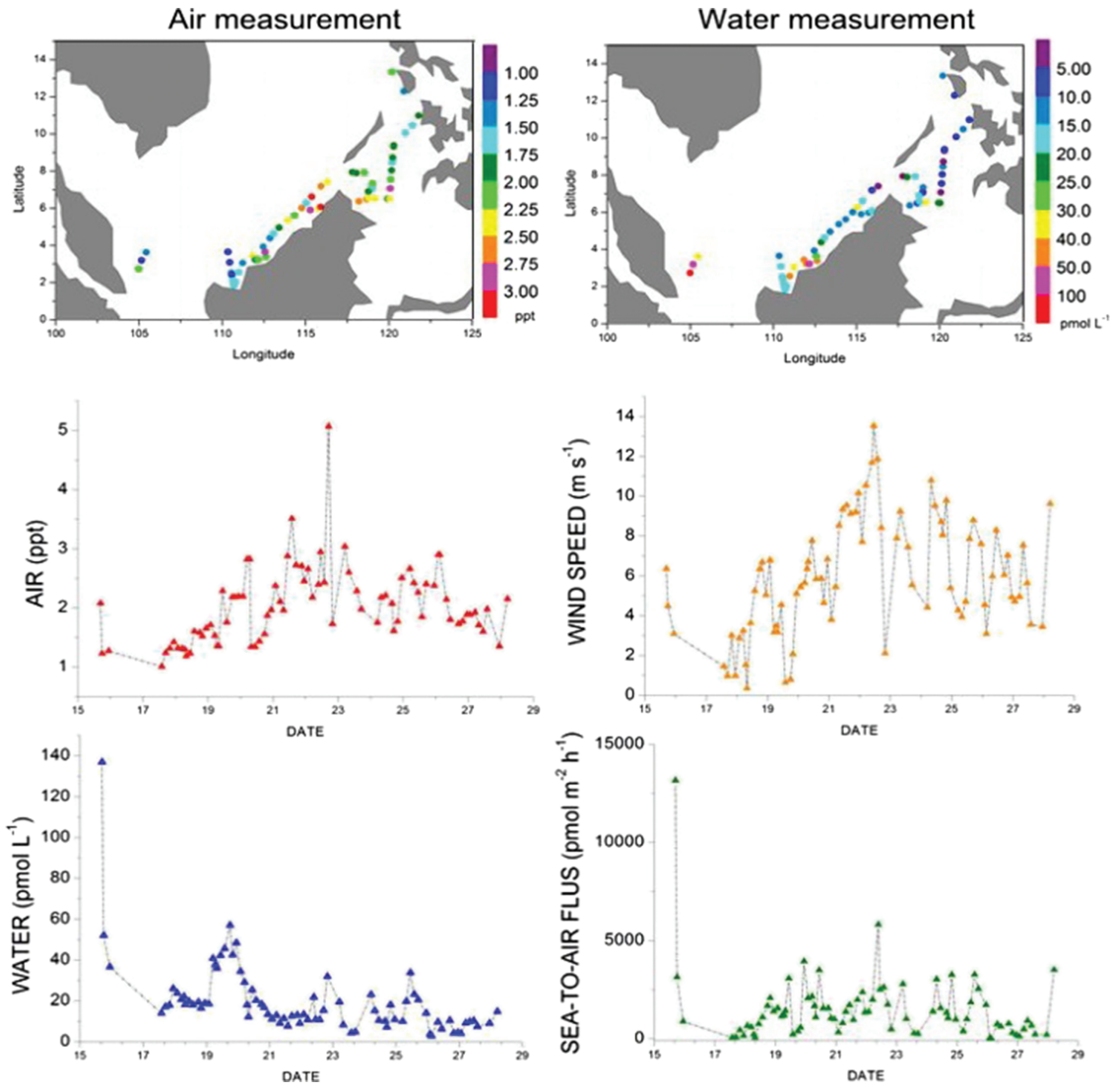

Fig. 3. The regional distribution and variation of the air (red), water sample (blue), sea-to-air flux (green) of $CHBr_3$ during the measurement campaign.

in the morning hours and elevation in the afternoon. Hence, no overall diurnal cycle could be detected.

3.2. Bromoform ($CHBr_3$) and Dibromomethane (CH_2Br_2)

The bromoform ($CHBr_3$) distribution is highly variable along the cruise track. Near the shore (Kuching, Kota Kinabalu and Sandakan), seawater samples showed typically elevated concentrations of brominated compounds while samples off shore generally contain lower halocarbons concentrations. The highest concentration near the coastline for both halocarbon compounds were 21.86 pmol L^{-1} ($CHBr_3$) and 4.81 pmol L^{-1}(CH_2Br_2), respectively (Figs. 3 and 4). The seawater measurement of $CHBr_3$ and CH_2Br_2 concentrations were relatively lower in the offshore with average concentrations of 7.50 pmol L^{-1} ($CHBr_3$) and 3.35 pmol L^{-1} (CH_2Br_2), respectively. Both halocarbon compounds also have a peak during the beginning of the cruise at Singapore coastal water with concentrations of 136.91 pmol L^{-1} ($CHBr_3$) and 21.82 pmol L^{-1} (CH_2Br_2). The higher concentration near the shore may be related to such high productivity as indicated by high concentration of chlorophyll.

The atmospheric halocarbon showed the same trends as those in seawater samples. The concentrations near the coastline were relatively higher than those offshores. The highest concentrations for $CHBr_3$ near coastline were 2.82 ppt (Kuching), 5.07 ppt (Kota Kinabalu) and 2.89 ppt (Sandakan) while for CH_2Br_2 value of atmospheric $CHBr_3$ were lower; 0.44 ppt and 0.05 ppt for CH_2Br_2 at the open sea area. Similarly for CH_2Br_2, the highest reading appeared at the coastal regions near Kota Kinabalu, 1.07 ppt (Kuching), 1.98 ppt (Kota Kinabalu) and 1.44 ppt (Sandakan).

Investigation into sea-to-air flux showed that high fluxes were observed near the coastline for both halocarbon compounds notably near Kuching, Kota Kinabalu and Sandakan (Figs. 3 and 4). These may lead to a significant halogen contribution in the upper troposphere and lower stratosphere. The sea-to-air fluxes for $CHBr_3$ and CH_2Br_2 are in the range of 7.52 to 13149 pmol m^{-2} h^{-1} and 16.0 to 2209.61 pmol m^{-2} h^{-1},

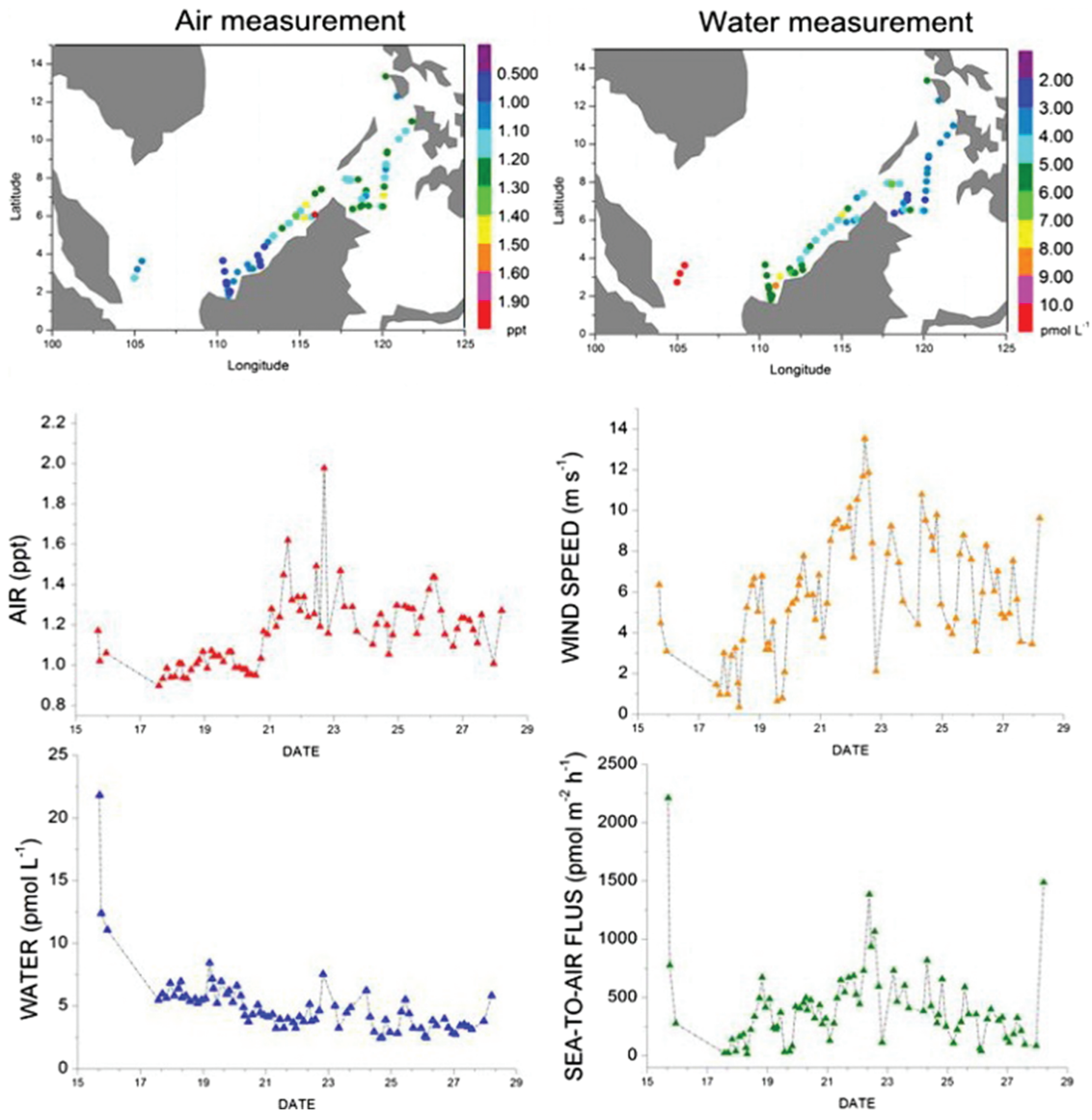

Fig. 4. The regional distribution and variation of CH_2Br_2 in air samples (red), seawater samples (blue) and sea-to-air flux (green) during the measurement campaign.

respectively. Higher fluxes into the atmosphere have also been observed to be associated with high wind speed (Figs. 3 and 4).

4. CONCLUSIONS

The observations of VSLS halocarbons along the cruise track in the tropical marine boundary layer in South China Sea and Sulu Sea have shown high spatial variability, hinting at multiple sources and sinks. All three VSLS halocarbons showed a higher concentration near the coastal areas than the open sea. Bromoform ($CHBr_3$) was found to be the most concentrated halocarbon in seawater as well as in the tropical marine boundary layer. The regional pattern between seawater and atmospheric concentration for the three halocarbons showed a concentration gradient between the South China Sea and Sulu Sea. Halocarbon concentrations in seawater were relative higher in South China Sea than Sulu Sea while the concentrations of halocarbons in the air were observed to higher in Sulu Sea than South China Sea. Sea-to-air fluxes were also found to be much greater in South China Sea than Sulu Sea, which may be attributed to local meteorological conditions.

Acknowledgment: We gratefully acknowledge funding from the European Union and collaboration works from various European and Malaysian universities and institutions during the SHIVA (Stratospheric ozone: Halogen Impacts in a Varying Atmosphere) Measurement Campaign.

References and Notes

1. S. A. McKeen and S. C. Liu, *Geophys. Res. Lett.* 20, 2363 **(1993)**.
2. R. M. Moore, R. Tokarczyk, V. K. Tait, M. Poulin, and C. E. Geen, Marine phytoplankton as a natural source of volatile organohalogens. Naturally-produced organohalogens, Dordrecht, The Netherlands **(1995b)**, pp. 283–294.

3. R. M. Moore, C. E. Geen, and V. K. Tait, *Chemosphere* 30, 1183 **(1995a)**.
4. C. D. O'Dowd, *J. Geophys. Res.* 106, 1545 **(2001)**.
5. B. Quack, E. Atlas, G. Petrick, and D. W. R. Wallace, *J. Geophys. Res-Atmos.* 112, D09312 **(2007a)**.
6. B. Quack and D. W. R. Wallace, *Global Biogeochem.* 17, 1023 **(2003)**.
7. S. A. Montzka and S. Reimann, Ozone-Depleting Substances (ODSs) and Related Chemicals, Chapter 1 in Scientific Assessment of Ozone Depletion: 2010, World Meteorological Organization, Switzerland, Geneva **(2011)**.
8. F. Schweitzer, P. Mirabel, and C. George, *J. Atmos. Chem.* 34, 101 **(1999)**.
9. P. D. Nightingale, G. Malin, C. S. Law, A. J. Watson, P. S. Liss, M. I. Liddicoat, J. Boutin, and R. C, Upstill-Goddard, *Global Biogeochem.* 14, 373 **(2000)**.
10. B. Quack, I. Peeken, G. Petrick, and K. Nachtigall, *J. Geophys. Res-Oceans* 112, C10006 **(2007b)**.
11. B. Quack and K. Kruger, SHIVA RV SONNE Cruise report, Cruise SO218 **(2001)** EU-Grant: 224644.

Received: 15 June 2014. Accepted: 30 October 2014.

3.5 Manuscript 5

Meteorological constraints on oceanic halocarbons above the Peruvian Upwelling

S. Fuhlbrügge[1], B. Quack[1], E. Atlas[2], A. Fiehn[1], H. Hepach[1], K. Krüger[3] and F. Ziska[1]

[1] GEOMAR Helmholtz-Zentrum für Ozeanforschung Kiel, Kiel, Germany

[2] Rosenstiel School of Marine and Atmospheric Science (RSMAS), Miami, USA

[3] Department of Geosciences, University of Oslo (UiO), Oslo, Norway

Published in: Atmospheric Chemistry and Physics Discuss., Vol. 15, 20597-20628, doi:10.5194/acpd-15-20597-2015, 2015.

Atmos. Chem. Phys. Discuss., 15, 20597–20628, 2015
www.atmos-chem-phys-discuss.net/15/20597/2015/
doi:10.5194/acpd-15-20597-2015

Atmospheric Chemistry and Physics Discussions

Meteorological constraints on oceanic halocarbons above the Peruvian Upwelling

S. Fuhlbrügge[1], B. Quack[1], E. Atlas[2], A. Fiehn[1], H. Hepach[1], and K. Krüger[3]

[1]GEOMAR, Helmholtz Centre for Ocean Research Kiel, Kiel, Germany
[2]Rosenstiel School for Marine and Atmospheric Sciences, Miami, FL, USA
[3]University of Oslo, Oslo, Norway

Received: 23 June 2015 – Accepted: 6 July 2015 – Published: 31 July 2015

Correspondence to: K. Krüger (kirstin.krueger@geo.uio.no)

Published by Copernicus Publications on behalf of the European Geosciences Union.

Abstract

Halogenated very short lived substances (VSLS) are naturally produced in the ocean and emitted to the atmosphere. Recently, oceanic upwelling regions in the tropical East Atlantic were identified as strong sources of brominated halocarbons to the atmosphere. During a cruise of R/V *METEOR* in December 2012 the oceanic sources and emissions of various halogenated trace gases and their mixing ratios in the marine atmospheric boundary layer (MABL) were investigated above the Peruvian Upwelling for the first time. This study presents novel observations of the three VSLS bromoform, dibromomethane and methyl iodide together with high resolution meteorological measurements and Lagrangian transport modelling. Although relatively low oceanic emissions were observed, except for methyl iodide, surface atmospheric abundances were elevated. Radiosonde launches during the cruise revealed a low, stable MABL and a distinct trade inversion above acting both as strong barriers for convection and trace gas transport in this region. Significant correlations between observed atmospheric VSLS abundances, sea surface temperature, relative humidity and MABL height were found. We used a simple source-loss estimate to identify the contribution of oceanic emissions to observed atmospheric concentrations which revealed that the observed marine VSLS abundances were dominated by horizontal advection below the trade inversion. The observed VSLS variations can be explained by the low emissions and their accumulation under different MABL and trade inversion conditions. This study confirms the importance of oceanic upwelling and trade wind systems on creating effective transport barriers in the lower atmosphere controlling the distribution of VSLS abundances above ocean upwelling regions.

1 Introduction

Short-lived halocarbons from the oceans contribute to reactive atmospheric halogens, which are involved in tropospheric and stratospheric ozone depletion, aerosol forma-

tion, and more chemical cycles, influencing the fate of pollutants and climate (McGivern et al., 2000; Saiz-Lopez and von Glasow, 2012; Simpson et al., 2015). Recent studies have identified open ocean upwelling areas in the Atlantic as large source regions for a number of brominated and iodinated oceanic trace gases (Quack et al., 2004, 2007; O'Brien et al., 2009; Raimund et al., 2011; Hepach et al., 2015a). Their sources are related to biological and chemical processes in the productive waters of the upwelling. The compounds are emitted from the ocean and are horizontally transported and vertically mixed in the marine atmospheric boundary layer (MABL) (Carpenter et al., 2010). In the Mauritanian upwelling, it was found that besides oceanic sources meteorological conditions strongly influenced the atmospheric mixing ratio of the marine compounds bromoform ($CHBr_3$), dibromomethane (CH_2Br_2) and also methyl iodide (CH_3I) (Hepach et al., 2014). Especially the combination of a pronounced low MABL above cold upwelling waters with high concentrations and emissions of the compounds caused elevated atmospheric mixing ratios. In return, these atmospheric mixing ratios also reduce the marine emissions through a decrease of the sea–air concentration gradient (Fuhlbrügge et al., 2013). Similar relationships would be expected for other oceanic upwelling areas, where not only the oceanic emissions, but also meteorological conditions in the lowermost atmosphere, i.e., the height, type and structure of the boundary layer and trade inversion, determine the VSLS contribution to atmospheric chemical processes. The intense oceanic upwelling in the Southeast Pacific off the coast of Peru transports large amounts of subsurface waters to the ocean surface and creates one of the highest productive oceanic regions worldwide (Codispoti et al., 1982). The Peruvian Upwelling is therefore a potentially intense source region for halogenated VSLS, e.g. bromoform ($CHBr_3$), dibromomethane (CH_2Br_2) and methyl iodide (CH_3I) (Yokouchi et al., 1999; Butler et al., 2007; Carpenter et al., 2009). Indeed, Schönhardt et al. (2008) detected elevated IO columns during September and November 2005 along the Peruvian coast with the SCIAMACHY satellite instrument and implied elevated iodine source gases from the Peruvian Upwelling.

Although, recent studies investigated halocarbons in the East Pacific (Yokouchi et al., 2008; Mahajan et al., 2012; Saiz-Lopez et al., 2012; Martin et al., 2013; Liu et al., 2013) few studies concentrated on the Peruvian Upwelling in the Southeast Pacific. Only measurements of methyl iodide exist in this region, revealing atmospheric abundances of 7 ppt (Rasmussen et al., 1982). Observations of bromocarbons above the Peruvian Upwelling are lacking.

In this study we present a high resolution dataset of meteorological parameters, oceanic concentrations, emissions and atmospheric abundances of VSLS along the Peruvian coast and in the Upwelling. Not much is known of the oceanic source strength of the VSLS and the meteorological influence on the marine trace gas distribution and abundances in this region. The goal of this study is to assess the influence of oceanic upwelling and meteorological conditions on the atmospheric VSLS abundances above the Peruvian Upwelling, and the contribution of the local oceanic emissions, respectively the MABL mixing ratios, to free tropospheric VSLS concentrations.

The paper is structured as following. Section 2 gives an overview of the data and methods we use in this study. Section 3 presents the results from our atmospheric and oceanic observations and analyses the contribution from oceanic VSLS emissions to the MABL, as well as meteorological constrains on the observations. Section 4 discusses the results, before the study is summarized in Sect. 5.

2 Data and methods

The cruise M91 on R/V *METEOR* from 1 to 26 December 2012 started and ended in Lima, Peru (Fig. 1a). The ship reached the most northern position during the cruise on 3 December 2012 at 5° S. In the following three weeks the ships headed southward and reached its southern most position at 16° S on 21 December 2012. During this time the track alternated between open ocean sections and sections very close to the Peruvian coast in the cold upwelling waters to collect coastal as well as open ocean data. Diurnal variations were observed during 6 stations along the cruise track (Fig. 2).

2.1 Meteorological observations

Meteorological measurements of surface air temperature (SAT), sea surface temperature (SST), relative humidity, air pressure, wind speed and direction were taken every second at about 25 m height on R/V *METEOR* and averaged to 10 min intervals for our investigations. Atmospheric profiles of temperature, wind and humidity were obtained by 98 radiosonde launches at standard UTC time (00:00, 06:00, 12:00, 18:00 UTC) and additionally 3 hourly during the diurnal stations along the cruise track, using Vaisala RS92 radiosondes. Due to permission limitations, radiosondes could not be launched within 12 NM of the Peruvian coast. The collected radiosonde data was integrated in near real time into the Global Telecommunication System (GTS) to improve meteorological reanalysis (e.g. ERA-Interim) and operational European Centre for Medium Range Weather Forecast models (opECMWF).

2.2 MABL height

The radiosonde data are used to identify the height of the MABL, which is the atmospheric surface layer above the ocean in which trace gas emissions are mixed horizontally on a short time scale of an hour or less by convection and turbulence (Stull, 1988). Two different kinds of MABL can be distinguished, the convective and the stable MABL, which can be characterized by the gradient of the virtual potential temperature θ_v. A negative or neutral gradient reveals an unstable convective layer, while a positive gradient reveals a stable atmospheric layer. In case of an increase of the virtual potential temperature from the surface, mixing in the MABL is suppressed. The upper limit of the convective MABL is set by a *stable layer*, e.g., a temperature inversion or a significant reduction in air moisture and is typically found above open ocean regions between 100 m and 3 km height (Stull, 1988; Seibert et al., 2000). For the determination of this *stable layer* above the convective MABL, we use the practical approach described in Seibert et al. (2000) and compute the virtual potential temperature during the radiosonde ascent whose increase with altitude indicates the base of a *stable layer*.

In this study the base of this *stable layer* increased by half of this *stable layer* depth is the definition for the MABL height. Over oceanic upwelling regions this stable layer can even descend to the ocean surface (e.g. Höflich et al., 1972; Fuhlbrügge et al., 2013).

2.2.1 Relative humidity

Estimates for atmospheric surface stability and MABL conditions in oceanic upwelling region can also be obtained from variations of the surface humidity. While the absolute humidity determines the amount of water in a specific volume of air, the relative humidity is the ratio of the partial pressure of water vapour to the equilibrium vapour pressure at the observed temperature. Variations of the SAT therefore directly influence the relative humidity at the surface. A decrease of the SAT due to cold upwelling water leads to an increase of the relative humidity, while the absolute humidity stays constant or even decreases due to condensation of water vapour once the relative humidity reaches 100 % and the air is saturated with water vapour. An elevated relative humidity in this oceanic region therefore points to stable layers with suppressed mixing of surface air and to a low and stable MABL height.

2.2.2 Estimation of MABL height above the upwelling

To estimate the MABL height above upwelling areas close to the coast, where radiosonde launches were permitted (Sect. 2.1) a multiple linear regression was applied. Using observed meteorological parameters revealing significant correlations (see Sect. 3.5) with the observed MABL height, relative humidity (x_1), SAT (x_2), SST (x_3) and wind speed (x_4), along the cruise we obtained the following Eq. (1):

$$\begin{aligned} &\text{MABL height} = b_1 x_1 + b_2 x_2 + b_3 x_3 + b_4 x_4 \\ &\text{with } b_1 = -0.0117; b_2 = 0.0202; b_3 = 0.0467; b_4 = 0.0089 \end{aligned} \quad (1)$$

2.3 Atmospheric VSLS measurements

A total of 198 air samples were collected 3 hourly during the cruise at about 20 m height on the 5th superstructure deck of R/V *METEOR.* The air samples were pressurized to 2 atm in pre-cleaned stainless steel canisters with a metal bellows pump and were analyzed at the Rosenstiel School for Marine and Atmospheric Sciences (RSMAS, Miami, Florida) within 6 months after the cruise. Details about the analysis, the instrumental precision and the preparation of the samples are described in Schauffler et al. (1999) and Fuhlbrügge et al. (2013). The atmospheric mixing ratios were calculated with a NOAA standard (SX3573) from GEOMAR.

2.4 Oceanic concentrations and sea–air flux

102 water samples were taken in-situ on a 3 hourly basis from the moon pool of R/V *METEOR* at a depth of 6.8 m from a continuously working water pump after 9 December 2012. The samples were then analysed for bromoform, dibromomethane and methyl iodide and other halogenated trace gases by a purge and trap system, attached to a gas chromatograph combined with an ECD (electron capture detector) with a precision of 10 % determined from duplicates. The approach is described in detail by Hepach et al. (2014).

2.4.1 Sea–air flux

The sea–air flux (F) of bromoform, dibromomethane and methyl iodide is calculated with k_w as transfer coefficient and Δc as concentration gradient between the water and equilibrium water concentration determined from the atmospheric concentrations (Eq. 2). The transfer coefficient was determined by the air–sea gas exchange parameterization of Nightingale et al. (2000) after a Schmidt number (Sc) correction for the

three gases (Eq. 3).

$$F = k_w \cdot \Delta c \tag{2}$$

$$k_w = k_{CO_2} \cdot \frac{Sc^{-\frac{1}{2}}}{600} \tag{3}$$

Details on deriving the air–sea concentration gradient and emissions are further described in Hepach et al. (2014) and references therein.

2.5 Trajectory calculations

The Lagrangian Particle Dispersion Model FLEXPART of the Norwegian Institute for Air Research in the Department of Atmospheric and Climate Research (Stohl et al., 2005) was used to analyse the air mass origins and the transport of surface air masses along the cruise track to the free troposphere. FLEXPART has been evaluated in previous studies (Stohl et al., 1998; Stohl and Trickl, 1999). The model includes moist convection and turbulence parameterizations in the atmospheric boundary layer and free troposphere (Stohl and Thomson, 1999; Forster et al., 2007). We use the ECMWF (European Centre for Medium-Range Weather Forecasts) reanalysis product ERA-Interim (Dee et al., 2011) with a horizontal resolution of $1^\circ \times 1^\circ$ and 60 vertical model levels as meteorological input fields, providing air temperature, horizontal and vertical winds, boundary layer height, specific humidity, as well as convective and large scale precipitation with a 6 hourly temporal resolution. Due to the spatial resolution of ERA-Interim data along the Peruvian coast defining the land–sea mask of our trajectory calculations, 98 out of 140 release points for the forward and backward trajectory calculations were analysed along the cruise track. At each these release points 10 000 forward and 50 backward trajectories were launched within ±30 min and ∼ 20 m distance to the ship positions from the ocean surface. Time and position of the release events are synchronized with air samples taken on R/V *METEOR* (Sect. 2.3).

2.6 Oceanic contribution to MABL VSLS abundances

To obtain an estimate of the contribution of local oceanic sources to the atmospheric mixing ratios in the lowermost atmosphere above the Peruvian upwelling we apply a mass balance concept to the oceanic emissions, to the time scales of air mass transport and to the chemical loss (Fuhlbrügge et al., 2015). First we define a box above each release event with a size of $\sim 400\,m^2$ around the measurement location and the height of the MABL and assume a steady-state observed VSLS mixing ratio within the box. During each trajectory release event we assume the specific sea–air flux to be constant and the emissions to be homogeneously mixed within the box. Then the contribution of the sea–air flux is computed as the ratio of the VSLS flux from the ocean into the MABL (in mol per day) and the total amount of VSLS in the box (in mol) and is defined as the Oceanic Delivery (OD) and OD is given in percentage per day. In addition to the delivery of oceanic VSLS to the box, the loss of VSLS out of the box into the free troposphere is defined as the COnvective Loss (COL) and is derived from the mean residence time derived from the FLEXPART trajectories in the box during each release event. Since this process is a loss process, COL is given as a negative quantity and in percentage per day. The chemical degradation of VSLS by OH and photolysis in the MABL is considered by the chemical lifetime of each compound in the MABL. We use lifetimes of 16 days for bromoform and 60 days for dibromomethane (Hossaini et al., 2010) and 3 days for methyl iodide (R. Hossaini, personal communication, 2013), representative for the tropical boundary layer. The Chemical Loss (CL) acts as loss process as well and is given as a negative quantity in percentage per day. We further assume a steady state in the box. OD, COL and CL must therefore be balanced by an advective transport of air masses in and out of the box. The change of the VSLS through advective transport is defined as Advective Delivery (AD) and given in percentage per day.

By relating OD to COL, we receive an Oceanic Delivery Ratio (ODR) (Eq. 4):

$$\mathrm{ODR} = \frac{\mathrm{OD}\,[\%\,d^{-1}]}{-\mathrm{COL}\,[\%\,d^{-1}]} = \frac{\text{Sea–air flux contribution}\,[\%\,d^{-1}]}{\text{Loss of box air to the FT}\,[\%\,d^{-1}]} \quad (4)$$

Similarly, the Chemical Loss in the box (CL), respectively, the change in VSLS due to advection (AD) are related to COL to get the Chemical Loss Ratio (CLR) and the Advective Delivery Ratio (ADR) with ADR = 1 – CLR – ODR. Since CL, OD and AD are divided by –COL, ratios for source processes are positive and negative for loss processes (Fuhlbrügge et al., 2015).

3 Observations on R/V *METEOR*

3.1 Meteorological observations

The Peruvian coast is dominated by the Southern Hemisphere trade wind regime with predominantly southeast winds (Fig. 1). The Andes, which are known to act as a barrier to zonal wind in this region, affect the horizontal air mass transport along the coast (Fig. 1b–d). The steeply sloping mountains at the coast form strong winds parallel to the South American coastline (Garreaud and Munoz, 2005), leading to distinct wind-driven oceanic upwelling of cold water along the coast. The 10-day backward trajectories reveal predominantly near-shore air masses with coastal influence and marine air masses (Fig. 1). The average wind direction observed on R/V *METEOR* during the cruise is $160^\circ \pm 34^\circ$ (mean $\pm\,\sigma$) with a moderate average wind speed of $6.2 \pm 2.2\,ms^{-1}$ (Fig. 2b). ERA-Interim reveals similar winds along the cruise track with a mean wind speed of $5.6 \pm 1.8\,ms^{-1}$ and a mean wind direction of $168^\circ \pm 21^\circ$ (not shown here). The divergence of the wind driven Ekman transport along the Peruvian coast leads to the observed oceanic upwelling of cold waters. This upwelling is observed for several times near the coast where both, SST and SAT rapidly drop to less than 18 °C (Fig. 2a). The impact of the cold upwelling water on the observed air masses is also visible in the

observed humidity fields (Fig. 2c). Here, the decreasing SAT reduces the amount of water vapour that the surface air is able to contain, leading to an increase of the relative humidity. The decreasing SAT and increasing relative humidity above the oceanic upwelling indicate a stable atmospheric surface layer, in which vertical mixing is suppressed. The absolute humidity stays constant or even decreases above the oceanic upwelling due to condensation of water vapour when surface air cools and becomes saturated, which coincides with fog observations on the ship above the upwelling regions. A decrease of the absolute humidity outside the upwelling points to a change in advected air masses for example between 9 and 11 December, but also on 19 December 2012 (Fig. 2c).

3.2 VSLS observations and oceanic emissions

Bromoform concentrations in the ocean surface range from 0.2–21.5 pmol L^{-1} with a mean of $6.6 \pm 5.5 (1\sigma)$ pmol L^{-1} during the cruise (Fig. 2d, Table 1). Dibromomethane concentrations range from 0.2–12.7 pmol L^{-1} with a mean of 4.3 ± 3.4 pmol L^{-1} and methyl iodide concentrations range from 1.1–35.4 pmol L^{-1} with a mean of 9.8 ± 6.3 pmol L^{-1}. Samples taken in the upwelling areas show elevated concentrations compared to the open ocean for all compounds. For further discussion on the distribution of the oceanic halocarbons, see Hepach et al. (2015a).

Mixing ratios of atmospheric bromoform range from 1.53–5.85 ppt during the cruise with an overall moderate mean of 2.91 ± 0.68 ppt (Table 1). Elevated mixing ratios of > 3 ppt are generally found above the oceanic upwelling areas close to the Peruvian coast, while these concentrations are hardly measured outside the oceanic upwelling (Fig. 2e). Highest bromoform mixing ratios (> 4 ppt) are observed on 23 and 24 December 2012 at 15.3° S and 75.4° W. Dibromomethane mixing ratios range between 0.82 and 2.04 ppt with an overall low mean of 1.25 ± 0.26 ppt. The atmospheric bromocarbons correlate with each other with $R = 0.79$ (Table 3). Like bromoform, also dibromomethane mixing ratios are elevated above the oceanic upwelling areas, except for 8 December 2012, where an increase is also found outside the upwelling. The con-

centration ratio of dibromomethane and bromoform can be used as an indicator for the age of bromocarbon sources along the coast. Low ratios of about 0.1 have been observed and are interpreted as the emission ratios of macro algae (Yokouchi et al., 2005; Carpenter et al., 2003). The shorter mean boundary layer lifetime of bromoform (16 days) in contrast to dibromomethane (60 days) after Hossaini et al. (2010) leads to an increase of the ratio as long as the air mass is not enriched with fresh bromoform. During the cruise the concentration ratio shows a gradient from the North to the South, with a mean of 0.44 ± 0.07 (Fig. 2f). Thus, we find relatively remote air masses in the North with a concentration ratio of 0.70 on 5 December and lowest ratios down to 0.31 on 24 December 2012, which implies an intensification of fresh sources towards the South that is also reflected by elevated water concentrations. Atmospheric methyl iodide along the cruise track ranges between 0.61 and 3.21 ppt with an overall elevated mean of 1.54 ± 0.49 ppt generally maximizing over the oceanic upwelling regions (Fig. 2e). Correlations of methyl iodide with the bromocarbons result in $R = 0.79$ for bromoform and $R = 0.66$ for dibromomethane (Table 3).

Oceanic emissions during the cruise were calculated from the synchronized measurements of sea water concentrations and atmospheric mixing ratios, sea surface temperatures and wind speeds, measured on R/V *METEOR* (Sect. 2.4.1). Oceanic concentrations and atmospheric mixing ratios of each compound are weakly or not at all correlated ($R_{\text{bromoform}} = 0.00$, $R_{\text{dibromomethane}} = 0.29$ and $R_{\text{methyl iodide}} = 0.34$). Mean sea–air fluxes during the cruise are 130 ± 554 pmol m^{-2} h^{-1} (bromoform), 273 ± 334 pmol m^{-2} h^{-1} (dibromomethane) and 954 ± 697 pmol m^{-2} h^{-1} (methyl iodide) (Fig. 2g, Table 1). The low bromocarbon emissions are probably caused by the observed elevated VSLS atmospheric concentrations, relatively low oceanic VSLS concentrations and low wind speeds and SSTs. On the other site, the high concentrations of methyl iodide in the surface waters lead to high oceanic emissions and elevated atmospheric mixing ratios. Further investigations of the distributions and sources of iodinated compounds during this cruise are carried out by Hepach et al. (2015b).

3.3 Lower atmosphere conditions

The atmospheric conditions in the lower troposphere, in particular the stability of the lowermost atmosphere and the height of the MABL, are obtained from radiosonde data launched along the cruise track. The relative humidity shows a strong vertical gradient at ∼ 1 km height (Fig. 3a). At this altitude, the relative humidity drops rapidly from over 75 % to less than 50 % which indicates a decrease in total humidity and/or an increase in air temperature due to suppressed mixing. The barrier for convective activity in this height, known as the trade inversion (Höflich, 1972), is typically found over the eastern side of tropical oceans within the lower 3 km above the surface and caused by the large-scale descending of air masses in the Hadley Cell (Riehl, 1954, 1979). This trade inversion is also reflected in the meridional wind observed by the radiosondes (Fig. 3b). Air masses below ∼ 1 km altitude have a strong positive meridional wind component due to the Southeast trade winds in this region, which is also visible in the forward trajectories (Fig. 1c and d). The back flow of the trade winds in the Hadley Cell to the subtropics causes a predominantly Northerly wind above ∼ 1 km height. The intense increase of θ_v in combination with the relative humidity decrease and the wind shear at ∼ 1 km height identifies this level as a strong vertical transport barrier (Fig. 3c). However, the low SAT above the cold upwelling water creates additional stable layers below the trade inversion. In particular above the upwelling, these stable layers can reach the surface and lead to very low MABL heights, e.g., on 3, 8 or 17 December 2012 and a reduction in vertical surface air exchange. Meteorological observers on board the ship witnessed fog coinciding with the elevated relative humidity above upwelling regions lasting for almost 20 h on 15–16 December 2012, confirming the suppressed mixing within the MABL. The mean MABL height from the radiosonde observations is 370 ± 170 m (ERA-Interim 376 ± 169 m). Since the relative humidity, SAT, SST and wind speed are good indicators for the MABL conditions in this oceanic region and these meteorological parameters show significant correlations with the observed MABL height (Table 3), we use a multiple linear regression based

on these parameters to estimate the MABL height above the upwelling (Sect. 2.2.2). With the regressed MABL heights above the upwelling, the mean MABL height during the cruise decreases to 307 ± 177 m and reveals the expected low mean MABL heights above cold upwelling regions of 158 ± 79 m and down to even 10 m as was previously observed above the Mauritanian Upwelling (Fuhlbrügge et al., 2013). A 12 hourly ERA-Interim MABL height revealed an average height of 376 ± 169 m along the cruise track. The effects of the MABL and trade inversions transport barriers result in supressed transport to the free troposphere (Fig. 3d).

We interpret the observations as the following. In the region of the Peruvian Upwelling, compounds emitted from the ocean and observed at the marine surface are first homogeneously distributed within the MABL during a couple of hours, before advection transport them further within the second transport barrier of the lowermost atmosphere the trade wind inversion. For air masses above or close to oceanic upwelling regions, the MABL height is the first weak transport barrier on short time scales (hours), while the trade inversions acts as the second more pronounced barrier for vertical transport on long time scales (days).

3.4 Contribution of oceanic emissions to observed VSLS abundances in the MABL

We estimate the contribution of oceanic emissions to mixing ratios within the MABL and below the trade inversion with a VSLS source-loss estimate (Table 2). The loss of VSLS out of the MABL box is $-341.7\,\%\,d^{-1}$ and equal for all compounds, since it is computed from the loss of trajectories out of the box. The loss is based on a mean residence time of the FLEXPART trajectories of 7 h in the observed MABL height during the cruise. The ratio of the OD of each compound and the COL results in the particular ODR. The ODR reveals that on average only 3 % of the observed atmospheric bromoform in the MABL origins from nearby oceanic emissions and that 97 % are advected. Local oceanic emissions of dibromomethane contribute about 11 % of the observed abundances in the MABL, while methyl iodide emissions contribute with 31 %, which

is far less compared to observations in other source regions with high convection as in the South China and Sulu Seas (Fuhlbrügge et al., 2015). While the surface air masses can leave the MABL within hours, they are suppressed from entering the free troposphere through the trade inversion barrier. Adapting an average trade inversion height of 1.1 km as the transport barrier for surface air masses into the free troposphere reveals an average residence time of the FLEXPART trajectories of 41 h below this trade inversion height. The atmospheric VSLS below the trade inversion originate to 12 % from oceanic emissions (ODR) for bromoform, to 37 % for dibromomethane and to 103 % for methyl iodide. The increased residence time of air masses below the trade inversion, reflected by the FLEXPART trajectories, leads to a stronger enrichment of air masses with VSLS from the oceanic emissions, reflected by OD, compared to the MABL box. However, the low sea–air fluxes of bromoform and dibromomethane are by far not strong enough to lead to the observed mixing ratios. Oceanic emissions of methyl iodide could explain the atmospheric mixing ratios below the trade inversion (ODR), but the chemical degradation can destroy up to 72 % (CLR) of the observed amount within the residence time of the air masses below the trade inversion. Since the oceanic delivery is very low for the bromocarbons and the elevated oceanic delivery of methyl iodide is nearly compensated by the chemical degradation, observed VSLS abundances of all three compounds are mostly advected during the cruise, which is reflected by high ADRs within the MABL and below the trade inversion (Table 2).

3.5 Meteorological constrains on atmospheric VSLS in the MABL

Fuhlbrügge et al. (2013) identified the influence of meteorological conditions, in particular of MABL height variations on VSLS abundances in the tropical Northeast Atlantic above the Mauritanian Upwelling, and suggested a general correlation of MABL conditions and VSLS abundances over oceanic upwelling regions. Indeed, we also find significant high correlations between meteorological parameters and the abundances of bromoform, dibromomethane and methyl iodide (Table 3) along the Peruvian coast. The predominantly moderate winds during the cruise are negatively correlated with the

atmospheric VSLS (bromoform $R = -0.38$, dibromomethane $R = -0.53$, and methyl iodide $R = -0.33$) and positively correlated with the MABL height ($R = 0.44$) implying that VSLS abundances tend to be elevated during periods of lower wind speeds, which in return lead to less mixing of surface air and therefore to lower MABL heights, in particular on 11, 15–17 and 24 December 2012. SAT and SST both correlate with atmospheric VSLS. Bromoform correlates with SAT and SST with $R = -0.50$, respectively $R = -0.57$. Correlation coefficients between methyl iodide, SAT and SST are slightly lower with $R = -0.37$ and $R = -0.42$, while dibromomethane has the strongest negative correlation to SAT ($R = -0.78$) and SST ($R = -0.81$). Generally high correlations between a meteorological parameter and the VSLS are found for the relative humidity with $R = 0.74$, $R = 0.77$ and $R = 0.67$ (bromoform, dibromomethane and methyl iodide). Correlation coefficients between the MABL height and the VSLS are slightly lower with $R = -0.55$, $R = -0.61$, respectively $R = -0.45$. Since SAT and SST impact the MABL, which affects the relative humidity, these correlation coefficients are correlated with each other.

The results reveal that the MABL properties (height and character) influence the VSLS abundances at the marine surface, although not as distinct as above the Mauritanian Upwelling (Fuhlbrügge et al., 2013). A comparison between the observations from the Peruvian Upwelling and the Mauritanian Upwelling (Fig. 4) shows that the variance of the former may explain the lower correlation. Reasons for this are discussed in the following.

4 Discussion

The observations reveal a significant correlation between the MABL height and atmospheric VSLS abundances above the Peruvian Upwelling. However, the correlation coefficients between the determined MABL height and the atmospheric VSLS are not as high as above the Mauritanian Upwelling during the DRIVE campaign (Fuhlbrügge et al., 2013). Reasons might be the large area of the investigated region in the North-

east Atlantic Ocean during the DRIVE campaign (25° latitude × 10° longitude) in contrast to this study along the Peruvian coast (12° latitude × 2 ° longitude). M91 observations therefore involve less variability of covered oceanic regimes of open ocean and coastal upwelling, VSLS concentrations and meteorological parameters, in particular of the MABL height, than the DRIVE observations. The Andes along South America lead to predominantly southerly winds along the West coast line with minor continental influence, while the Mauritanian Upwelling is influenced by both, maritime and continental air masses. The latter can lead to strong surface inversions above the Mauritanian Upwelling and strongly suppressed mixing of surface air. Although our investigations revealed low MABL heights close to the Peruvian coast, the distinct surface inversions as observed above the Mauritanian Upwelling are not present in the available radiosonde data for this Peruvian Upwelling region. In addition, the relatively low sea–air fluxes of bromoform and dibromomethane, caused by moderate winds and small concentration gradients between the surface ocean and the surface atmosphere, as well as the short lifetime of methyl iodide lead to an insufficient enrichment of VSLS in the atmosphere. The observed air masses therefore contain VSLS mixing ratios which are predominantly advected. This is confirmed by our computed ADR (Sect. 3.4). The backward trajectories reveal air masses originating from the open ocean, which are transported along the coast for about 5 days until they reach the ship. In combination with the distinct trade inversion acting as strong barrier to the vertical mixing of trace gases, air-masses along the coast travel close to the surface where they can be enriched with local emissions before they are observed on-board. In addition, the in-situ observed oceanic emissions along the cruise track of R/V *METEOR* therefore cause small variations to the accumulated background mixing ratios of the advected air masses. This leads to lower correlation coefficients between the MABL height and the VSLS abundances compared to the Mauritanian Upwelling.

Although the oceanic emissions are already well mixed within days below the trade inversion, methyl iodide mixing ratios indicate a positive correlation with the trade inversion height, which is unexpected. The correlation coefficient might be artificial, as we

observe elevated methyl iodide above the upwelling, where trade wind inversion heights are missing but can be assumed to be low (Riehl, 1954), which is also indicated by the correlation coefficients with SAT and SST. Nevertheless, this circumstance should be taken into account in future studies.

After the air masses are observed on R/V *METEOR*, the 10 day FLEXPART forward trajectories reveal a near-surface transport towards the equator (Fig. 1c and d). These trajectories predominantly stay below 1 km altitude due to the horizontal extent of the trade inversion. The contribution of oceanic VSLS emissions from the Peruvian Upwelling to the free troposphere above this region is therefore strongly suppressed by the trade inversion (Fig. 3d). A contribution of oceanic emissions from the Peruvian Upwelling to the free troposphere is only achieved in the ITCZ after a transport time of 5–8 days, where the VSLS abundances are transported into higher altitudes. These transport paths may also explain the elevated methyl iodide observed by Yokouchi et al. (2008) at San Cristobal, Galapagos and the elevated IO of Schönhardt et al. (2008) and Dix et al. (2013) in the tropical East Pacific. The elevated mixing ratios of methyl iodide are further investigated by Hepach et al. (2015b). It has to be noted that the determined low contribution of oceanic emissions and boundary layer air to the free troposphere in this region is only representative for normal El Niño Southern Oscillation conditions as it was observed in December 2012 (http://www.cpc.ncep.noaa.gov/products/analysis_monitoring/enso_disc_nov2012/ensodisc.pdf). Since the Walker Circulation is reversed during El Niño, upwelling along the Peruvian coast is known to be suppressed and convective activity enhanced (Philander, 1989).

5 Summary

This study investigated the contribution of oceanic VSLS emissions to their abundances in the lowermost atmosphere as well as meteorological constrains on this contribution above both, oceanic upwelling regions and open ocean along the Peruvian coast during December 2012. Meteorological data were measured on R/V *METEOR* near the ocean

surface and by radiosondes launched up to the stratosphere. Oceanic VSLS emissions along the cruise track were determined from air and water samples taken near the ocean surface. To investigate the transport of the observed air masses, FLEXPART forward and backward trajectories were computed.

Oceanic upwelling was observed close to the Peruvian coast by SST decreases to 15 °C caused by the wind driven Ekman transport along the coast line with observed moderate wind speeds of $6.2 \pm 2.2\,\mathrm{ms}^{-1}$. The oceanic upwelling coincided with elevated relative humidity including the formation of low level fog. On average a low, stable MABL height of 307 ± 177 m was determined from radiosonde launches and multiple linear regressions during the cruise. A decrease of the MABL height from the open ocean towards the coast was observed. The radiosonde launches also revealed a distinct trade inversion at 1.1 ± 0.3 km height. This study concentrates on the three halogenated VSLS: bromoform, dibromomethane and methyl iodide. Except for methyl iodide, oceanic emissions were low with $130 \pm 554\,\mathrm{pmol\,m}^{-2}\,\mathrm{h}^{-1}$ for bromoform, $273 \pm 334\,\mathrm{pmol\,m}^{-2}\,\mathrm{h}^{-1}$ for dibromomethane, and $954 \pm 697\,\mathrm{pmol\,m}^{-2}\,\mathrm{h}^{-1}$ for methyl iodide. Despite the low oceanic emissions, the atmospheric mixing ratios of the compounds were elevated with 2.9 ± 0.7 ppt (bromoform), 1.3 ± 0.3 ppt (dibromomethane) and 1.5 ± 0.5 ppt (methyl iodide). According to our FLEXPART ERA-Interim trajectory calculations, the average residence time of surface air masses in the observed MABL was 7 h. Once these air masses left the MABL, they were suppressed in their vertical movement by the trade inversion, which was reflected by an average residence time of 41 h below the trade inversion. This additional distinct inversion layer evolved as the dominant transport barrier for MABL air into the free troposphere and led to an accumulation of air masses and the VSLS abundances therein observed during the cruise. With a simple source-loss estimate we computed the ratio between the contribution of oceanic emissions and advection to the loss of air into the free troposphere. The oceanic emissions along the cruise track explained on average only 12 % for bromoform and 37 % for dibromomethane, but 103 % for methyl iodide of the observed VSLS abundances. Considering the chemical degradation of the compounds

during the residence time of the trajectories below the trade inversion, a residual advective transport of 104 % (bromoform), 68 % (dibromomethane) and 69 % (methyl iodide) was necessary to explain the observed atmospheric VSLS mixing ratios. The elevated atmospheric VSLS observed on R/V *METEOR* were therefore largely advected and enriched along the Peruvian coast. Nevertheless, significant correlation coefficients between the MABL height and atmospheric abundances of bromoform ($R = -0.55$), dibromomethane ($R = -0.61$), respectively methyl iodide ($R = -0.45$) reveal an impact of the low oceanic emissions on the atmospheric VSLS abundances. The lower correlation between the MABL height and the atmospheric VSLS in this oceanic region compared to the Mauritanian Upwelling was identified to be caused by less variability of oceanic regimes and more stable atmospheric regimes during this cruise.

Our study confirms that MABL height and characteristics is generally related with atmospheric VSLS abundances above oceanic upwelling regions. Additionally, a widespread trade inversion can lead to a near-surface accumulation of the VSLS which impacts oceanic emissions and therefore feedback on VSLS concentrations in the lower atmosphere. The double transport barrier phenomena should be investigated in future studies of other oceanic upwelling regions as well.

Acknowledgements. This study was supported by the BMBF grant SOPRAN II FKZ 03F0611A. We acknowledge the authorities of Peru for the permissions to work in their territorial waters. We thank the European Centre for medium range weather forecast (ECMWF) for the provision of ERA-Interim reanalysis data and the Lagrangian particle dispersion model FLEXPART used in this publication. We also like to thank the captain and crew of R/V *METEOR*, and the Deutscher Wetterdienst (DWD) for the support.

References

Butler, J., King, D., Lobert, J., Montzka, S., Yvon-Lewis, S., Hall, B., Warwick, N., Mondeel, D., Aydin, M., and Elkins, J.: Oceanic distributions and emissions of short-lived halocarbons, Global Biogeochem. Cy., 21, GB1023, doi:10.1029/2006GB002732, 2007.

Carpenter, L., Liss, P., and Penkett, S.: Marine organohalogens in the atmosphere over the Atlantic and Southern Oceans, J. Geophys. Res.-Atmos., 108, 4256, doi:10.1029/2002JD002769, 2003.

Carpenter, L. J., Jones, C. E., Dunk, R. M., Hornsby, K. E., and Woeltjen, J.: Air-sea fluxes of biogenic bromine from the tropical and North Atlantic Ocean, Atmos. Chem. Phys., 9, 1805–1816, doi:10.5194/acp-9-1805-2009, 2009.

Carpenter, L., Fleming, Z., Read, K., Lee, J., Moller, S., Hopkins, J., Purvis, R., Lewis, A., Muller, K., Heinold, B., Herrmann, H., Fomba, K., van Pinxteren, D., Muller, C., Tegen, I., Wiedensohler, A., Muller, T., Niedermeier, N., Achterberg, E., Patey, M., Kozlova, E., Heimann, M., Heard, D., Plane, J., Mahajan, A., Oetjen, H., Ingham, T., Stone, D., Whalley, L., Evans, M., Pilling, M., Leigh, R., Monks, P., Karunaharan, A., Vaughan, S., Arnold, S., Tschritter, J., Pohler, D., Friess, U., Holla, R., Mendes, L., Lopez, H., Faria, B., Manning, A., and Wallace, D.: Seasonal characteristics of tropical marine boundary layer air measured at the Cape Verde Atmospheric Observatory, J. Atmos. Chem., 67, 87–140, doi:10.1007/s10874-011-9206-1, 2010.

Codispoti, L. A., Dugdale, R. C., and Minas, H. J.: A comparison of the nutrient regimes off northwest Africa, Peru and Baja California, Rapport et Procés-verbaux des réunions, Conseil permanent International pour l'Exploration de la Mer, 180, 184–201, 1982.

Dix, B., Baidara, S., Bresch, J., Hall, S., Schmidt, K., Wang, S., and Volkamer, R.: Detection of iodine monoxide in the tropical free troposphere, P. Natl. Acad. Sci. USA, 110, 2035–2040, doi:10.1073/pnas.1212386110, 2013.

Forster, C., Stohl, A., and Seibert, P.: Parameterization of convective transport in a Lagrangian particle dispersion model and its evaluation, J. Appl. Meteorol. Clim., 46, 403–422, doi:10.1175/JAM2470.1, 2007.

Fuhlbrügge, S., Krüger, K., Quack, B., Atlas, E., Hepach, H., and Ziska, F.: Impact of the marine atmospheric boundary layer conditions on VSLS abundances in the eastern tropical and subtropical North Atlantic Ocean, Atmos. Chem. Phys., 13, 6345–6357, doi:10.5194/acp-13-6345-2013, 2013.

Fuhlbrügge, S., Quack, B., Tegtmeier, S., Atlas, E., Hepach, H., Shi, Q., Raimund, S., and Krüger, K.: The contribution of oceanic halocarbons to marine and free troposphere air over the tropical West Pacific, Atmos. Chem. Phys. Discuss., 15, 17887–17943, doi:10.5194/acpd-15-17887-2015, 2015.

Garreaud, R. and Munoz, R.: The low-level jet off the west coast of subtropical South America: structure and variability, Mon. Weather Rev., 133, 2246–2261, doi:10.1175/MWR2972.1, 2005.

Hepach, H., Quack, B., Ziska, F., Fuhlbrügge, S., Atlas, E. L., Krüger, K., Peeken, I., and Wallace, D. W. R.: Drivers of diel and regional variations of halocarbon emissions from the tropical North East Atlantic, Atmos. Chem. Phys., 14, 1255–1275, doi:10.5194/acp-14-1255-2014, 2014.

Hepach, H., Quack, B., Raimund, S., Fischer, T., Atlas, E. L., and Bracher, A.: Halocarbon emissions and sources in the equatorial Atlantic Cold Tongue, Biogeosciences Discuss., 12, 5559–5608, doi:10.5194/bgd-12-5559-2015, 2015a.

Hepach, H., Quack, B., Tegtmeier, S., Engel, A., Bracher, A., Fuhlbrügge, S., Raimund, S., Lampel, J., L., G., and Krüger, K.: Contributions of biogenic halogenated compounds from the Peruvian upwelling to the tropical troposphere, in preparation, 2015b.

Höflich, O.: The meteorological effects of cold upwelling water areas, Geoforum, 3, 35–46, doi:10.1016/0016-7185(72)90084-X, 1972.

Hossaini, R., Chipperfield, M. P., Monge-Sanz, B. M., Richards, N. A. D., Atlas, E., and Blake, D. R.: Bromoform and dibromomethane in the tropics: a 3-D model study of chemistry and transport, Atmos. Chem. Phys., 10, 719–735, doi:10.5194/acp-10-719-2010, 2010.

Liu, Y., Yvon-Lewis, S., Thornton, D., Butler, J., Bianchi, T., Campbell, L., Hu, L., and Smith, R.: Spatial and temporal distributions of bromoform and dibromomethane in the Atlantic Ocean and their relationship with photosynthetic biomass, J. Geophys. Res.-Oceans, 118, 3950–3965, doi:10.1002/jgrc.20299, 2013.

Mahajan, A. S., Gómez Martín, J. C., Hay, T. D., Royer, S.-J., Yvon-Lewis, S., Liu, Y., Hu, L., Prados-Roman, C., Ordóñez, C., Plane, J. M. C., and Saiz-Lopez, A.: Latitudinal distribution of reactive iodine in the Eastern Pacific and its link to open ocean sources, Atmos. Chem. Phys., 12, 11609–11617, doi:10.5194/acp-12-11609-2012, 2012.

Martin, J., Mahajan, A., Hay, T., Prados-Roman, C., Ordonez, C., MacDonald, S., Plane, J., Sorribas, M., Gil, M., Mora, J., Reyes, M., Oram, D., Leedham, E., and Saiz-Lopez, A.: Iodine chemistry in the eastern Pacific marine boundary layer, J. Geophys. Res.-Atmos., 118, 887–904, doi:10.1002/jgrd.50132, 2013.

McGivern, W., Sorkhabi, O., Suits, A., Derecskei-Kovacs, A., and North, S.: Primary and secondary processes in the photodissociation of $CHBr_3$, J. Phys. Chem.-US, 104, 10085–10091, doi:10.1021/jp0005017, 2000.

Nightingale, P., Malin, G., Law, C., Watson, A., Liss, P., Liddicoat, M., Boutin, J., and Upstill-Goddard, R.: In situ evaluation of air–sea gas exchange parameterizations using novel conservative and volatile tracers, Global Biogeochem. Cy., 14, 373–387, doi:10.1029/1999GB900091, 2000.

O'Brien, L. M., Harris, N. R. P., Robinson, A. D., Gostlow, B., Warwick, N., Yang, X., and Pyle, J. A.: Bromocarbons in the tropical marine boundary layer at the Cape Verde Observatory – measurements and modelling, Atmos. Chem. Phys., 9, 9083–9099, doi:10.5194/acp-9-9083-2009, 2009.

Philander, G.: El-Nino and La-Nina, Am. Sci., 77, 451–459, 1989.

Quack, B., Atlas, E., Petrick, G., Stroud, V., Schauffler, S., and Wallace, D.: Oceanic bromoform sources for the tropical atmosphere, Geophys. Res. Lett., 31, L23S05, doi:10.1029/2004GL020597, 2004.

Quack, B., Atlas, E., Petrick, G., and Wallace, D.: Bromoform and dibromomethane above the Mauritanian upwelling: atmospheric distributions and oceanic emissions, J. Geophys. Res.-Atmos., 112, D09312, doi:10.1029/2006JD007614, 2007.

Raimund, S., Quack, B., Bozec, Y., Vernet, M., Rossi, V., Garçon, V., Morel, Y., and Morin, P.: Sources of short-lived bromocarbons in the Iberian upwelling system, Biogeosciences, 8, 1551–1564, doi:10.5194/bg-8-1551-2011, 2011.

Rasmussen, R., Khalil, M., Gunawardena, R., and Hoyt, S.: Atmospheric methyl-iodide (CH_3I), J. Geophys. Res.-Oc. Atm., 87, 3086–3090, doi:10.1029/JC087iC04p03086, 1982.

Riehl, H.: Tropical Meteorology, McGraw-Hill, New York-London, 1954.

Riehl, H.: Climate and Weather in the Tropics, Academic Press, London, 1979.

Saiz-Lopez, A. and von Glasow, R.: Reactive halogen chemistry in the troposphere, Chem. Soc. Rev., 41, 6448–6472, doi:10.1039/c2cs35208g, 2012.

Saiz-Lopez, A., Lamarque, J.-F., Kinnison, D. E., Tilmes, S., Ordóñez, C., Orlando, J. J., Conley, A. J., Plane, J. M. C., Mahajan, A. S., Sousa Santos, G., Atlas, E. L., Blake, D. R., Sander, S. P., Schauffler, S., Thompson, A. M., and Brasseur, G.: Estimating the climate significance of halogen-driven ozone loss in the tropical marine troposphere, Atmos. Chem. Phys., 12, 3939–3949, doi:10.5194/acp-12-3939-2012, 2012.

Schauffler, S., Atlas, E., Blake, D., Flocke, F., Lueb, R., Lee-Taylor, J., Stroud, V., and Travnicek, W.: Distributions of brominated organic compounds in the troposphere and lower stratosphere, J. Geophys. Res.-Atmos., 104, 21513–21535, doi:10.1029/1999JD900197, 1999.

Schönhardt, A., Richter, A., Wittrock, F., Kirk, H., Oetjen, H., Roscoe, H. K., and Burrows, J. P.: Observations of iodine monoxide columns from satellite, Atmos. Chem. Phys., 8, 637–653, doi:10.5194/acp-8-637-2008, 2008.

Seibert, P., Beyrich, F., Gryning, S., Joffre, S., Rasmussen, A., and Tercier, P.: Review and intercomparison of operational methods for the determination of the mixing height, Atmos. Environ., 34, 1001–1027, doi:10.1016/S1352-2310(99)00349-0, 2000.

Simpson, W., Brown, S., Saiz-Lopez, A., Thornton, J., and von Glasow, R.: Tropospheric halogen chemistry: sources, cycling, and impacts, Chem. Rev., 4035–4062, doi:10.1021/cr5006638, 2015.

Stohl, A. and Thomson, D.: A density correction for Lagrangian particle dispersion models, Bound.-Lay. Meteorol., 90, 155–167, doi:10.1023/A:1001741110696, 1999.

Stohl, A. and Trickl, T.: A textbook example of long-range transport: simultaneous observation of ozone maxima of stratospheric and North American origin in the free troposphere over Europe, J. Geophys. Res.-Atmos., 104, 30445–30462, doi:10.1029/1999JD900803, 1999.

Stohl, A., Hittenberger, M., and Wotawa, G.: Validation of the Lagrangian particle dispersion model FLEXPART against large-scale tracer experiment data, Atmos. Environ., 32, 4245–4264, doi:10.1016/S1352-2310(98)00184-8, 1998.

Stohl, A., Forster, C., Frank, A., Seibert, P., and Wotawa, G.: Technical note: The Lagrangian particle dispersion model FLEXPART version 6.2, Atmos. Chem. Phys., 5, 2461–2474, doi:10.5194/acp-5-2461-2005, 2005.

Stull, R.: An Introduction to Boundary Layer Meteorology, Kluwer Academic Publishers, Dordrecht, 1988.

Yokouchi, Y., Li, H., Machida, T., Aoki, S., and Akimoto, H.: Isoprene in the marine boundary layer (southeast Asian Sea, eastern Indian Ocean, and Southern Ocean): comparison with dimethyl sulfide and bromoform, J. Geophys. Res.-Atmos., 104, 8067–8076, doi:10.1029/1998JD100013, 1999.

Yokouchi, Y., Hasebe, F., Fujiwara, M., Takashima, H., Shiotani, M., Nishi, N., Kanaya, Y., Hashimoto, S., Fraser, P., Toom-Sauntry, D., Mukai, H., and Nojiri, Y.: Correlations and emission ratios among bromoform, dibromochloromethane, and dibromomethane in the atmosphere, J. Geophys. Res.-Atmos., 110, D23309, doi:10.1029/2005JD006303, 2005.

Yokouchi, Y., Osada, K., Wada, M., Hasebe, F., Agama, M., Murakami, R., Mukai, H., Nojiri, Y., Inuzuka, Y., Toom-Sauntry, D., and Fraser, P.: Global distribution and seasonal concentra-

tion change of methyl iodide in the atmosphere, J. Geophys. Res.-Atmos., 113, D18311, doi:10.1029/2008JD009861, 2008.

Table 1. Oceanic concentrations, atmospheric mixing ratios and sea–air fluxes of bromoform ($CHBr_3$), dibromomethane (CH_2Br_2), the concentration ratio of bromoform and dibromomethane and methyl iodide (CH_3I) observed during the cruise. Values are given in mean $\pm 1\sigma$ [range].

	$CHBr_3$	CH_2Br_2	$CH_2Br_2/CHBr_3$	CH_3I
Oceanic concentration [pmol L^{-1}]	6.6 ± 5.5 [0.2–21.5]	4.3 ± 3.4 [0.2–12.7]	0.9 ± 0.8 [0.1–4.2]	9.8 ± 6.3 [1.1–35.4]
Atmospheric mixing ratio [ppt]	2.9 ± 0.7 [1.5–5.9]	1.3 ± 0.3 [0.8–2.0]	0.4 ± 0.1 [0.3–0.7]	1.5 ± 0.5 [0.6–3.2]
Sea–air flux [pmol m^{-2} h^{-1}]	130 ± 554 [−550–2201]	273 ± 334 [−128–1321]	0.4 ± 8.6 [−24.5–48.9]	954 ± 697 [21–4687]

Table 2. Mean $\pm 1\sigma$ of Oceanic Delivery (OD), Advective Delivery (AD), Chemical Loss (CL), COnvective Loss (COL), Oceanic Delivery Ratio (ODR), Advective Delivery Ratio (ADR) and Chemical Loss Ratio (CLR) of bromoform ($CHBr_3$), dibromomethane (CH_2Br_2) and methyl iodide (CH_3I). Parameters have been computed for a box with the vertical extension of the MABL height (MABLH) and a mean trade inversion height of 1.1 km (TIH).

		OD [% d^{-1}]	AD [% d^{-1}]	CL [% d^{-1}]	COL [% d^{-1}]	ODR	ADR	CLR
$CHBr_3$	MABLH	10.2 ± 31.2	347.5 ± 114.3	−6.6	−341.7 ± 118.2	0.03 ± 0.09	0.99 ± 0.09	−0.02 ± 0.01
	TIH	4.4 ± 13.6	52.3 ± 24.3	−6.6	−58.5 ± 27.4	0.12 ± 0.45	1.04 ± 0.44	−0.16 ± 0.07
CH_2Br_2	MABLH	36.0 ± 43.5	317.0 ± 117.2	−1.8	−341.7 ± 118.2	0.11 ± 0.12	0.90 ± 0.12	−0.01 ± 0.00
	TIH	15.3 ± 18.6	36.5 ± 27.4	−1.8	−58.5 ± 27.4	0.37 ± 0.61	0.67 ± 0.61	−0.04 ± 0.02
CH_3I	MABLH	96.2 ± 53.7	276.2 ± 122.6	−30.7	−341.7 ± 118.2	0.31 ± 0.18	0.79 ± 0.17	−0.10 ± 0.04
	TIH	41.1 ± 23.0	39.5 ± 34.2	−30.7	−58.5 ± 27.4	1.03 ± 0.78	0.69 ± 0.66	−0.72 ± 0.31

Table 3. Spearman correlation coefficients (R) of meteorological parameters, MABL height and trade inversion height correlated with atmospheric bromoform ($CHBr_3$), dibromomethane (CH_2Br_2) and methyl iodide (CH_3I). MABL height* is the determined MABL height from the radiosonde launches, complimented by the regressed MABL height (Sect. 3.3). Bold coefficients have a p value of < 0.05.

	MABL height	MABL height*	Trade inversion	$CHBr_3$	CH_2Br_2	CH_3I
Wind speed	**0.35**	**0.44**	−0.06	**−0.38**	**−0.53**	**−0.33**
SAT	**0.65**	**0.79**	**0.24**	**−0.50**	**−0.78**	**−0.37**
SST	**0.66**	**0.80**	**0.23**	**−0.57**	**−0.81**	**−0.42**
SAT – SST	**−0.39**	**−0.47**	−0.11	**0.38**	**0.48**	**0.30**
Rel. humidity	**−0.77**	**−0.81**	−0.06	**0.74**	**0.77**	**0.67**
MABL height*	–	–	0.08	**−0.55**	**−0.61**	**−0.45**
$CHBr_3$	**−0.55**	**−0.60**	−0.03	–	**0.79**	**0.79**
CH_2Br_2	**−0.61**	**−0.72**	−0.02	**0.79**	–	**0.66**
CH_3I	**−0.45**	**−0.50**	**0.30**	**0.79**	**0.66**	–

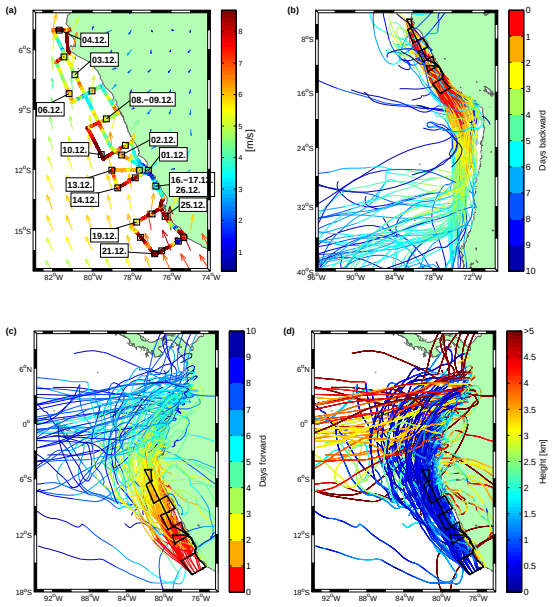

Figure 1. (a) 10 min mean of wind speed observed on R/V *METEOR* displayed along the cruise track; monthly mean (December 2012) of 10 m wind speed and direction from ERA-Interim displayed as arrows. **(b)** Extract from 10-day FLEXPART backward trajectories coloured according to the time until they reach the specific ship position on the cruise track of R/V *METEOR* (black). **(c)** Extract from 10-day FLEXPART forward trajectories coloured according to the time since they were released. **(d)** Same as **(c)** coloured according to the height (km) of the trajectories.

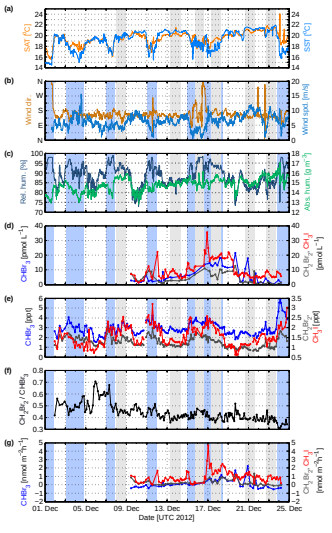

Figure 2. Observations during 1–25 December 2012 on R/V *METEOR*. Diurnal stations are indicated by grey background shades. **(a)** 10 min mean of the SAT (orange) and the SST (blue) in °C. According to SST decrease, upwelling regions are marked with a light blue background shade in Fig. 2b–e. **(b)** 10 min mean of wind direction in cardinal directions (ocher) and wind speed in $m\,s^{-1}$ (blue). **(c)** 10 min mean of relative humidity in % (dark blue) and absolute humidity in $g\,m^{-3}$ (green). **(d)** Oceanic surface concentrations of bromoform ($CHBr_3$, blue), dibromomethane (CH_2Br_2, dark grey) and methyl iodide (CH_3I, red) in $pmol\,L^{-1}$. **(e)** Atmospheric mixing ratios of bromoform, dibromomethane and methyl iodide in ppt. **(f)** Concentration ratio of dibromomethane and bromoform. **(g)** Sea–air flux for bromoform, dibromomethane and methyl iodide in $pmol\,m^{-2}\,h^{-1}$.

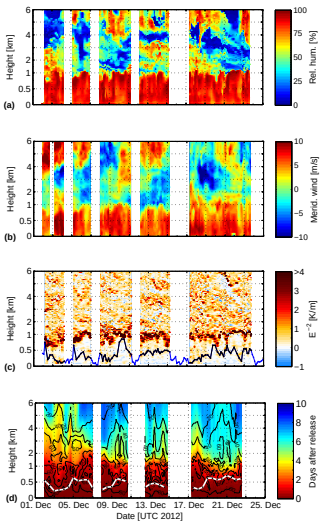

Figure 3. Radiosonde observations of the lower 6 km of the atmosphere between 2 and 24 December 2012 on R/V *METEOR*. Shown are **(a)** the relative humidity in %, **(b)** the meridional wind in $m\,s^{-1}$ and **(c)** the gradient of the virtual potential temperature in $E^{-2}\,K\,m^{-1}$ in combination with the determined MABL height (black) and the complimented MABL height above the oceanic upwelling from the multiple linear regressions (blue). **(d)** Distribution of 10-day FLEXPART forward trajectories. The black contour lines give the amount of trajectories in percentage that reach a specific altitude within the 10 days. The elapsed time in days until these trajectories reach this height is reflected by the colour shading. The white line shows the ERA-Interim MABL height at the ship position. Trajectory analyses gaps close to the coast are whitened (Sect. 2.5). The *y* axes are non-linear.

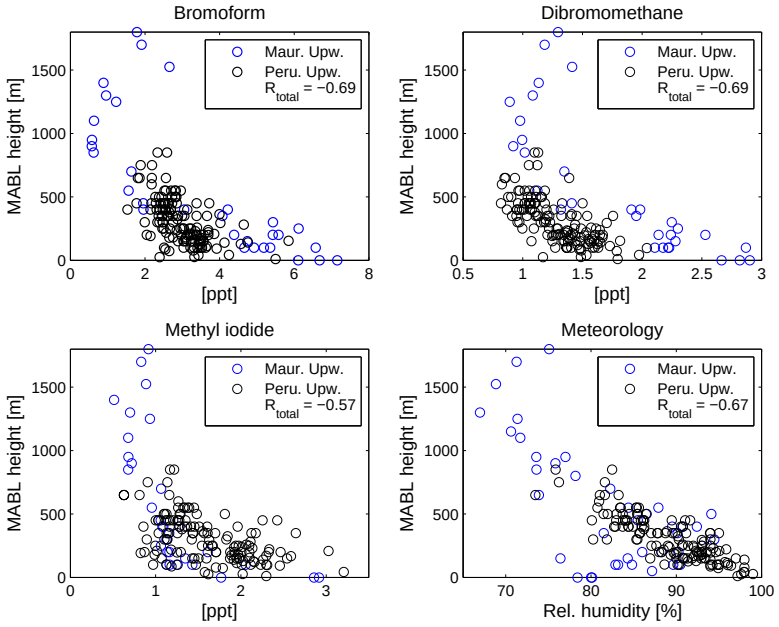

Figure 4. Scatter plots of atmospheric mixing ratios of bromoform, dibromomethane, methyl iodide and relative humidity vs. MABL height. Blue circles reflect observations from the Mauritanian Upwelling (Fuhlbrügge et al., 2013) and black circles from this study. R_{total} gives the Spearman correlation coefficients for both data sets together.

3.6 Manuscript 6

Biogenic halocarbons from the Peruvian upwelling region as tropospheric halogen source

H. Hepach[1], B. Quack[1], S. Tegtmeier[1], A. Engel[1], A. Bracher[2], S. Fuhlbrügge[1], L. Galgani[1], E. L. Atlas[3], J. Lampel[4*], U. Frieß[4] and K. Krüger[5]

[1] GEOMAR Helmholtz-Zentrum für Ozeanforschung Kiel, Kiel, Germany

[2] Alfred-Wegener-Institut (AW) – Helmholtz-Zentrum für Polar und Meeresforschung, Bremerhaven, Germany

[3] Rosenstiel School of Marine and Atmospheric Science (RSMAS), Miami, USA

[4] Institut für Umweltphysik, Universität Heidelberg, Heidelberg, Germany

[5] Department of Geosciences, University of Oslo (UiO), Oslo, Norway

[*] now at Max-Planck-Institute für Chemie, Mainz, Germany

Published in: Atmospheric Chemistry and Physics Discuss., doi:10.5194/acp-2016-39, 2016.

Atmos. Chem. Phys. Discuss., doi:10.5194/acp-2016-39, 2016
Manuscript under review for journal Atmos. Chem. Phys.
Published: 14 March 2016

Atmospheric Chemistry and Physics Discussions

Biogenic halocarbons from the Peruvian upwelling region as tropospheric halogen source

Helmke Hepach[1], Birgit Quack[1], Susann Tegtmeier[1], Anja Engel[1], Astrid Bracher[2], Steffen Fuhlbrügge[1], Luisa Galgani[1], Elliot Atlas[3], Johannes Lampel[4,5], Udo Frieß[4], and Kirstin Krüger[6]

Correspondence to: H. Hepach (hhepach@geomar.de)

[1] GEOMAR Helmholtz Centre for Ocean Research Kiel, Germany

[2] Alfred Wegener Institute (AWI), Helmholtz Centre for Polar and Marine Research Bremerhaven, Germany and Institute of Environmental Physics, University of Bremen, Germany

[3] Rosenstiel School of Marine and Atmospheric Science (RSMAS), University of Miami, USA

[4] Institute of Environmental Physics, University of Heidelberg, Germany

[5] now at Max Planck Institute for Chemistry, Mainz, Germany

[6] Department of Geosciences, University of Oslo, Oslo, Norway

Atmos. Chem. Phys. Discuss., doi:10.5194/acp-2016-39, 2016
Manuscript under review for journal Atmos. Chem. Phys.
Published: 14 March 2016

Atmospheric Chemistry and Physics Discussions

Abstract

Halocarbons, halogenated short-chained hydrocarbons, are produced naturally in the oceans by biological and chemical processes. They are emitted from surface seawater into the atmosphere, where they take part in numerous chemical processes such as ozone destruction and the oxidation of mercury and dimethyl sulfide. Here we present oceanic and atmospheric halocarbon data for the Peruvian upwelling obtained during the M91 cruise onboard the research vessel *Meteor* in December 2012. Surface waters during the cruise were characterized by moderate concentrations of bromoform ($CHBr_3$) and dibromomethane (CH_2Br_2) correlating with diatom biomass derived from marker pigment concentrations, which suggests this phytoplankton group as likely source. Concentrations measured for the iodinated compounds methyl iodide (CH_3I) of up to 35.4 pmol L^{-1}, chloroiodomethane (CH_2ClI) of up to 58.1 pmol L^{-1} and diiodomethane (CH_2I_2) of up to 32.4 pmol L^{-1} in water samples were much higher than previously reported for the tropical Atlantic upwelling systems. Iodocarbons also correlated with the diatom biomass and even more significantly with dissolved organic matter (DOM) components measured in the surface water. Our results suggest a biological source of these compounds as significant driving factor for the observed large iodocarbon concentrations. Elevated atmospheric mixing ratios of CH_3I (up to 3.2 ppt), CH_2ClI (up to 2.5 ppt) and CH_2I_2 (3.3 ppt) above the upwelling were correlated with seawater concentrations and high sea-to-air fluxes. The enhanced iodocarbon production in the Peruvian upwelling contributed significantly to tropospheric iodine levels.

1 Introduction

Brominated and iodinated short-lived organic compounds (halocarbons) from the oceans contribute to tropospheric and stratospheric chemistry (von Glasow et al., 2004; Saiz-Lopez et al., 2012b; Carpenter and Reimann, 2014). They are significant carriers of iodine and bromine into the marine atmospheric boundary layer (Salawitch, 2006; Jones et al., 2010; Yokouchi et al., 2011; Saiz-Lopez et al., 2012b), where they and their degradation products may also be involved in aerosol and ultra-fine particle formation (O'Dowd et al., 2002; Burkholder et al., 2004). Furthermore, the short-lived organic compounds are a source for bromine and iodine in the free troposphere, and thus play an important role for ozone chemistry and other processes such as the oxidation of several atmospheric constituents (Saiz-Lopez et al., 2012a). Numerous modelling studies over the last years have shown that brominated short-lived compounds and their degradation products can be entrained into the stratosphere and enhance

Atmos. Chem. Phys. Discuss., doi:10.5194/acp-2016-39, 2016
Manuscript under review for journal Atmos. Chem. Phys.
Published: 14 March 2016

Atmospheric Chemistry and Physics Discussions

the halogen-driven ozone destruction (Carpenter and Reimann, 2014; Hossaini et al., 2015). Recently, it was suggested that also oceanic iodine in organic or inorganic form can contribute to the stratospheric halogen loading, however only in small amounts due to its strong degradation (Tegtmeier et al., 2013; Saiz-Lopez et al., 2015).

While different source and sink processes determine the distribution of halocarbons in the oceanic surface water, the underlying mechanisms are largely unresolved. Biological activity plays a role for the production of bromoform ($CHBr_3$), dibromomethane (CH_2Br_2), methyl iodide (CH_3I), chloroiodomethane (CH_2ClI) and diiodomethane (CH_2I_2) (Gschwend et al., 1985; Tokarczyk and Moore, 1994; Moore et al., 1996), while CH_3I also originates from photochemical reactions with dissolved organic matter (DOM) (Moore and Zafiriou, 1994; Bell et al., 2002; Shi et al., 2014).

Biologically mediated halogenation of DOM (Lin and Manley, 2012; Liu et al., 2015) and bromination of compounds such as β-diketones via enzymes such as bromoperoxidase (BPO) within or outside the algal cells (Theiler et al., 1978) are among the potentially important production processes of $CHBr_3$ and CH_2Br_2. Air-sea gas exchange into the atmosphere is the most important sink for both compounds (Quack and Wallace, 2003; Hepach et al., 2015).

The biological formation of CH_3I has been investigated during laboratory and field studies (Scarratt and Moore, 1998; Amachi et al., 2001; Fuse et al., 2003; Smythe-Wright et al., 2006; Brownell et al., 2010; Hughes et al., 2011) identifying phyto- and bacterioplankton as producers, revealing large variability in biological production rates. However, biogeochemical modelling studies suggest that photochemistry may be more important for global CH_3I production (Stemmler et al., 2014). Due to their much shorter lifetime in surface water and the atmosphere, fewer studies investigated production processes of CH_2I_2 and CH_2ClI. CH_2I_2 has been suggested to be produced both by phytoplankton (Moore et al., 1996) and bacteria (Fuse et al., 2003; Amachi, 2008). The main source for CH_2ClI is likely its production during the photolysis of CH_2I_2 with a yield of 35 % based on a laboratory study (Jones and Carpenter, 2005). CH_2ClI has also been detected in phytoplankton cultures (Tokarczyk and Moore, 1994) where it may originate from direct production or also from CH_2I_2 conversion. The main sink for both CH_2I_2 and CH_2ClI is their photolytic destruction in the surface ocean resulting in lifetimes of less than 10 min (CH_2I_2) and 9 h (CH_2ClI), respectively, in the tropical ocean (Jones and Carpenter, 2005; Martino et al., 2006). Other sinks for these three iodocarbons are air-sea gas exchange and chloride substitution. The latter may play an important role for CH_3I in low latitudes at low wind speeds (Zafiriou, 1975; Jones and Carpenter, 2007).

Atmos. Chem. Phys. Discuss., doi:10.5194/acp-2016-39, 2016
Manuscript under review for journal Atmos. Chem. Phys.
Published: 14 March 2016

Atmospheric Chemistry and Physics Discussions

Oceanic measurements of natural halocarbons are sparse (Ziska et al., 2013), but reveal that especially tropical and subtropical upwelling systems are potentially important source regions (Quack et al., 2007a; Raimund et al., 2011). Previously observed high tropospheric iodine monoxide (IO) levels in the tropical East Pacific have been related to short-lived iodinated compounds in surface waters (Schönhardt et al., 2008; Dix et al., 2013). However, iodocarbon fluxes have not been considered high enough to explain observed IO concentrations (Jones et al., 2010; Mahajan et al., 2010; Grossmann et al., 2013; Lawler et al., 2014), and recent global modelling studies suggested abiotic sources contributing on average about 75 % to the IO budget (Prados-Roman et al., 2015). Such abiotic sources could be emissions of hypoiodous acid (HOI) and molecular iodine (I_2) as recently confirmed by a laboratory study (Carpenter et al., 2013).

This paper characterizes the Peruvian upwelling region between 5.0° S, 82.0° W and 16.2° S, 76.8° W with regard to the two brominated compounds $CHBr_3$ and CH_2Br_2 and the iodinated compounds CH_3I, CH_2ClI and CH_2I_2 in water and atmosphere. The latter two compounds were measured for the first time in this region. Possible oceanic sources based on the analysis of phytoplankton species composition and different DOM components were evaluated and identified. Sea-to-air fluxes of these halogenated compounds were derived and their contribution to the tropospheric iodine loading above the tropical East Pacific by combining halocarbon and IO measurements and model calculations were estimated.

2 Methods

The M91 cruise of the RV *Meteor* from December 1 to 26, 2012 investigated the surface ocean and atmosphere of the Peruvian upwelling region (Bange, 2013). From the northernmost location of the cruise at 5.0° S and 82.0° W, the ship moved to the southernmost position at 16.2° S and 76.8° W with several transects perpendicular to the coast, alternating between open ocean and coastal upwelling (Fig. 1). All underway measurements were taken from a continuously operating pump in the ship's hydrographic shaft from a depth of 6.8 m. Sea surface temperature (SST) and sea surface salinity (SSS) were measured continuously with a SeaCAT thermosalinograph from Seabird Electronics (SBE).

Deep samples were taken from 4 to 10 depths between 1 and 2000 m from 12 L Niskin bottles attached to a 24-bottle-rosette sampler equipped with a CTD and an oxygen sensor from SBE. Halocarbon samples were collected at 24 of the total 98 casts. The uppermost sample from the depth profiles (between 1 and 10 m) was included in the surface water measurements.

Atmos. Chem. Phys. Discuss., doi:10.5194/acp-2016-39, 2016
Manuscript under review for journal Atmos. Chem. Phys.
Published: 14 March 2016

Atmospheric Chemistry and Physics Discussions

2.1 Analysis of halocarbon samples

Halocarbon samples were taken three hourly from sea surface water and air. Surface water samples were analyzed on board with a purge and trap system attached to a GC-MS (combined gas chromatography and mass spectrometry) described in more detail in Hepach et al. (2014). The depth profile samples were analyzed with a similar setup: a purge and trap system was attached to a GC equipped with an ECD (electron capture detector). The precision of the measurements lay within 10 % for all five halocarbons determined from duplicates and both systems were calibrated using the same liquid standards in methanol. Halocarbon measurements in seawater started only on December 9 due to set up problems. Atmospheric halocarbon samples were taken on the monkey deck at a height of 20 m using a metal bellows pump from December 1, and were analyzed at the Rosenstiel School of Marine and Atmospheric Science (RSMAS) as described in Schauffler et al. (1998). For further details of atmospheric measurements see Fuhlbrügge et al. (2015a). Quantification was achieved using the NOAA standard SX3573 from GEOMAR.

2.2 Biological parameters

Phytoplankton composition was derived from pigment concentrations. Samples were taken in parallel with the halocarbon samples in the sea surface and up to six samples in depths between 3 and 200 m. Water was filtered with GF/F filters, which were stored at -80 °C until analysis after shock-freezing in liquid nitrogen. Pigments as described in Taylor et al. (2011) were analyzed using a HPLC technique according to Barlow et al. (1997). We used the diagnostic pigment analysis by Vidussi et al. (2001), subsequently refined by Uitz et al. (2006) by introducing pigment specific weight coefficients, to determine the chlorophyll *a* (Chl *a*) concentration of seven groups of phytoplankton which are assumed to build up the entire phytoplankton community in ocean waters. Identified phytoplankton groups include diatoms, chlorophytes, dinoflagellates, haptophytes, cyanobacteria, cryptophytes and chrysophytes. Total chlorophyll a (TChl *a*) concentrations were calculated from the sum of the pigment concentrations of monovinyl Chl *a*, divinyl Chl *a* and chlorophyllide *a*.

Samples for the identification of DOM components were taken at 37 stations from a rubber boat from subsurface water at approximately 20 cm (further called “subsurface”). All samples were processed onboard and analyzed back in the home laboratory. Samples were analyzed for dissolved and total organic carbon (DOC and TOC), total dissolved nitrogen (TDN), total nitrogen (TN), total, dissolved and particulate high molecular weight (HMW, >1kDa)

Atmos. Chem. Phys. Discuss., doi:10.5194/acp-2016-39, 2016
Manuscript under review for journal Atmos. Chem. Phys.
Published: 14 March 2016

Atmospheric Chemistry and Physics Discussions

combined carbohydrates (TCCHO, DCCHO and PCCHO) applying a high-temperature catalytic oxidation method using a TOC analyzer (TOC-V_{CSH}) from Shimadzu, as well as total, dissolved and particulate combined HMW uronic acids (TURA, DURA and PURA), i.e. galacturonic acid and glucuronic acid. These were analyzed by High Performance Anion Exchange Chromatography coupled with Pulsed Amperometric Detection (HPAEC-PAD) after Engel and Händel (2011). For a more detailed description of both the sampling method and analysis see Engel and Galgani (2015).

2.3 Correlation analysis

Correlation analyses between all halocarbons, biological proxies and ambient parameters were carried out using Matlab® for all collocated surface and depth samples. All datasets were tested for normal distribution using the Lilliefors-test. Since most of the data were not distributed normally, Spearman's rank correlation (hereinafter called r_s) was used. All correlations with a significance level of smaller than 5 % ($p < 0.05$) were regarded as significant.

2.4 Calculation of sea-to-air fluxes

Sea-to-air fluxes F of halocarbons were calculated according to equation 1 with k_w as the gas exchange coefficient parameterized according to Nightingale et al. (2000), c_w the water concentrations from the halocarbon underway measurements, c_{atm} from the simultaneous atmospheric measurements and H as the Henry's law constant to derive the equilibrium concentration.

$$F = k_w \cdot (c_w - \frac{c_{atm}}{H}) \quad (1)$$

The gas exchange coefficient usually applied to derive carbon dioxide fluxes was adjusted for halocarbons using Schmidt number corrections as calculated in Quack and Wallace (2003), and Henry's law coefficients as reported for each of the compounds by Moore et al. (1995) were applied. Wind speed and air pressure were averaged to 10 min intervals for the calculation of the instantaneous fluxes.

2.5 FLEXPART simulations of tropospheric iodine

The atmospheric transport of the iodocarbons from the oceanic surface into the Marine Atmospheric Boundary Layer (MABL) was simulated with the Lagrangian particle dispersion

Atmos. Chem. Phys. Discuss., doi:10.5194/acp-2016-39, 2016
Manuscript under review for journal Atmos. Chem. Phys.
Published: 14 March 2016

Atmospheric Chemistry and Physics Discussions

model FLEXPART (Stohl et al., 2005) which has been used extensively in studies of long-range and mesoscale transport (Stohl and Trickl, 1999). FLEXPART is an off-line model driven by external meteorological fields. It includes parameterizations for moist convection, turbulence in the boundary layer, dry deposition, scavenging, and the simulation of chemical decay. We simulate trajectories of a multitude of air parcels describing transport and chemical decay of the emitted oceanic iodocarbons. For each data point of the observed sea-to-air flux, 100000 air parcels were released over the duration of the M91 cruise from a 0.1° x 0.1° grid box at the ocean surface centered at the measurement location. We used FLEXPART version 9.2 and the runs are driven by the ECMWF reanalysis product ERA-Interim (Dee et al., 2011) given at a horizontal resolution of 1° x 1° on 60 model levels. Transport, dispersion and convection of the air parcels are calculated from the 6-hourly fields of horizontal and vertical wind, temperature, specific humidity, convective and large scale precipitation and others. The chemical decay of the iodocarbons was prescribed by their atmospheric lifetime which was set to 4 days, 9 hours and 10 min for CH_3I, CH_2ClI, and CH_2I_2, respectively, according to current estimates (Jones and Carpenter, 2005; Martino et al., 2006; Carpenter and Reimann, 2014). After degradation of the iodocarbons, the released iodine was simulated as inorganic iodine (I_y) tracer with a prescribed lifetime in the marine boundary layer of two days (personal communication R. von Glasow). Thus we did not include detailed tropospheric iodine chemistry, explicit removal of HOI, HI, $IONO_2$, and I_xO_y through scavenging or heterogeneous recycling of HOI, $IONO_2$, and INO_2 on aerosols (Saiz-Lopez et al., 2014). In order to estimate the uncertainties arising from this simplification, we conducted two additional simulations, one with a very short lifetime of one day and one with a longer lifetime of three days. Following model simulations of halogen chemistry for air masses from different oceanic regions in Sommariva and von Glasow (2012), IO corresponds to 20 % of the I_y budget in the marine boundary layer on a daytime average. The IO to I_y ratio shows moderate changes with daytime resulting in highest IO proportion at sunrise (~ 30 %) and lowest IO proportion around noon (~ 15 %) (see Fig. S6 in Sommariva and von Glasow (2012)). The ratio shows only very small variations for different air mass origins and thus the chemical conditions such as ozone and nitrogen species concentrations. Additionally, the ratio does not change much with altitude within the marine boundary layer. Based on the above estimates from Sommariva and von Glasow (2012), we used the IO to I_y ratio as a function of daytime to estimate IO from I_y every 3 hours. Daily averages of the IO abundance were compared to the MAX-DOAS IO measurements on board described in the next section.

Atmos. Chem. Phys. Discuss., doi:10.5194/acp-2016-39, 2016
Manuscript under review for journal Atmos. Chem. Phys.
Published: 14 March 2016

Atmospheric Chemistry and Physics Discussions

2.6 MAX-DOAS Measurements of IO

Multi-AXis Diffential Optical Absorption Spectroscopy (MAX-DOAS) (Hönninger, 2002; Platt and Stutz, 2008) observations were conducted continuously at daytime from November 30 to December 25 2012 in order to quantify tropospheric abundances of IO, BrO, HCHO, Glyoxal, NO_2 and HONO along the cruise track, and for aerosol profiles also of O_4. The MAX-DOAS instrument and the measurement procedure are described in Grossmann et al. (2013) and Lampel et al. (2015).

The primary quantity derived from MAX-DOAS measurements is the differential slant column density (dSCD), which represents the difference in path-integrated concentrations between two measurements in off-axis and zenith direction. From the MAX-DOAS observations of O_4 dSCD aerosol extinction profiles to estimate the quality of visibility were inferred using an optimal estimation approach described in Frieß et al. (2006) and Yilmaz (2012) after applying a correction factor of 1.25 to the O_4 dSCDs (Clémer et al., 2010). IO was analyzed in the spectral range from 418 – 438 nm following the settings in Lampel et al. (2015). IO was found up to 6 times above the detection limit (twice the measurement error).

3 The tropical East Pacific – general description and state during M91

The tropical East Pacific is characterized by one of the strongest and most productive all-year-prevailing eastern boundary upwelling systems of the world (Bakun and Weeks, 2008). Temperatures drop to less than 16 °C when cold water from the Humboldt current is transported to the surface due to Ekman transport caused by strong equatorward winds (Tomczak and Godfrey, 2005), which is also connected with an upward transport of nutrients (Chavez et al., 2008). As a consequence of the enhanced nutrient supply and the high solar insolation, phytoplankton blooms, indicated by high Chl *a* values, can be observed at the surface especially in the boreal winter months (Echevin et al., 2008). A strong oxygen minimum zone (OMZ) is formed due to enhanced primary production, sinking particles and weak circulation (Karstensen et al., 2008).

Low SSTs of mean (min – max) 19.4 (15.0 – 22.4) °C and high TChl *a* values of on average 1.80 (0.06 – 12.65) µg L^{-1} (Table 1, Fig. 1) were measured during our cruise. Diatoms were dominating the TChl *a* concentration in the surface water with a mean of 1.66 (0.00 – 10.47) µg Chl *a* L^{-1}, followed by haptophytes (mean: 0.25 µg Chl *a* L^{-1}), chlorophytes (mean: 0.19 µg Chl *a* L^{-1}), cyanobacteria (mean: 0.09 µg Chl *a* L^{-1}), dinoflagellates (mean: 0.08 µg Chl *a* L^{-1}), cryptophytes (mean: 0.03 µg Chl *a* L^{-1}), and finally chrysophytes (mean: 0.03 µg Chl *a*

Atmos. Chem. Phys. Discuss., doi:10.5194/acp-2016-39, 2016
Manuscript under review for journal Atmos. Chem. Phys.
Published: 14 March 2016

Atmospheric Chemistry and Physics Discussions

L^{-1}). Diatoms were observed at all stations with concentrations above 0.5 µg Chl *a* L^{-1} to contribute more than 50 % of the algal biomass. They correlated very well with TChl *a* (Table 2) and with cryptophytes, which were elevated in very similar regions. Abundance of these phytoplankton groups was strongly anticorrelated with SST and SSS, indicating a close conjunction with the colder and more saline upwelling waters. Nutrients (nitrate, nitrite, ammonium and phosphate) were also measured during the cruise (see Czeschel et al. (2015) for further information). A weak anticorrelation of phytoplankton group with the ratio of dissolved inorganic nitrogen and phosphate (sum of nitrate, nitrite and ammonium divided by phosphate, DIN:DIP) (Table 2) indicated that diatoms and cryptophytes were more abundant in aged upwelling, where nutrients were already slightly depleted or used up. The TChl *a* maximum was generally found in the surface ocean except for four stations with overall low TChl *a* (< 0.5 µg L^{-1}) where a subsurface maximum around 30 and 50 m was identified.

All regions with SSTs below the mean of 19.4 °C are considered as upwelling in the following sections for identifying different significant regions for halocarbon production. Based on this criterion, four upwelling regions (I – IV) close to the coast were classified (Fig. 1). The most intense upwelling (lowest SSTs, high nutrient concentrations) appeared in the northernmost region of the cruise track, region I, while higher TChl *a* and lower nutrients indicate a fully developed bloom in the southern part of the cruise (upwelling regions III and IV). Upwelling region II was characterized by a lower DIN:DIP ratio in contrast to region I. SSS with a mean of 34.95 (34.10 and 35.50) is lowest in upwelling region IV, which is likely influenced by local river input such as the rivers Pisco, Cañete and Matagente, and may explain the observed low salinities due to enhanced fresh water input in boreal winter (Bruland et al., 2005).

4 Halocarbons in the surface water and depth profiles during M91

4.1 Halocarbon distribution in surface water

Measurements of halocarbons in the tropical East Pacific are very sparse and no data were available for the Peruvian upwelling system before our campaign. Sea surface concentrations of $CHBr_3$ with a mean of 6.6 (0.2 – 21.5) and of CH_2Br_2 of 4.3 (0.2 – 12.7) pmol L^{-1} were measured during M91 (Table 1, Fig. 2). These values are low in comparison to 44.7 pmol L^{-1} $CHBr_3$ in tropical upwelling systems in the Atlantic, while our measurements of CH_2Br_2 compare better to these upwelling systems, from which maximum concentrations of 9.4 pmol

Atmos. Chem. Phys. Discuss., doi:10.5194/acp-2016-39, 2016
Manuscript under review for journal Atmos. Chem. Phys.
Published: 14 March 2016

Atmospheric Chemistry and Physics Discussions

L^{-1} were reported (Quack et al., 2007a; Carpenter et al., 2009; Hepach et al., 2014, 2015). $CHBr_3$ (0.2– 20.7 pmol L^{-1}) and CH_2Br_2 (0.7 – 6.5 pmol L^{-1}) concentrations in the tropical East Pacific open ocean and Chilean coastal waters during a cruise from Punta Arenas, Chile to Seattle, USA in April 2010 (Liu et al., 2013) compare well to our data. Some measurements also exist for the tropical West Pacific with on average 0.5 to 3 times the $CHBr_3$ and 0.2 to 1 times the CH_2Br_2 during our cruise with the high average originating from a campaign close to the coast with macroalgal and anthropogenic sources (Krüger and Quack, 2013; Fuhlbrügge et al., 2015b). $CHBr_3$ and CH_2Br_2 have been proposed to have similar sources (Moore et al., 1996; Quack et al., 2007b). However, during our cruise, the correlation between the two compounds was comparatively weak (r_s = 0.56), consistent with the findings of Liu et al. (2013), who ascribed the weaker correlation of these two compounds to formation in a common ecosystem rather than to the exact same biological sources. Maxima of CH_2Br_2 were observed in both upwelling regions III and IV, while $CHBr_3$ was highest in the most southerly upwelling IV (Fig. 2).

While we found the Peruvian upwelling and the adjacent waters to be only a moderate source region for bromocarbons, iodocarbons were observed in high concentration of 10.9 (0.4 – 58.1) for CH_2ClI, 9.8 (1.1 – 35.4) for CH_3I and 7.7 (0.2 – 32.4) pmol L^{-1} for CH_2I_2 (Table 1, Fig. 3a). These concentrations identify the Peruvian upwelling as a significant source region of iodocarbons, especially considering the very short lifetimes of CH_2I_2 (10 min) and CH_2ClI (9 h) in tropical surface water (Jones and Carpenter, 2005). Hot spots were upwelling regions III and even more the less fresh upwelling of region IV (Fig. 2 and 3).

The occurrence of CH_3I in the tropical oceans (up to 36.5 pmol L^{-1}) has previously been attributed to a predominantly photochemical source (Richter and Wallace, 2004; Jones et al., 2010), explaining its global hot spots in the subtropical gyres and close to the tropical western boundaries of the continents (Ziska et al., 2013; Stemmler et al., 2014). Previous measurements in the East Pacific obtained concentrations of up to 21.7 and of up to 8.8 pmol L^{-1} (Butler et al., 2007), but not directly in the upwelling.

No oceanic observations of CH_2ClI and CH_2I_2 have been published so far for the tropical East Pacific. Concentrations of CH_2ClI of up to 24.5 pmol L^{-1} were measured in the tropical and subtropical Atlantic ocean (Abrahamsson et al., 2004; Chuck et al., 2005; Jones et al., 2010) and up to 17.1 pmol L^{-1} for CH_2I_2 (Jones et al., 2010; Hepach et al., 2015), which is lower but in the range of our measurements from the Peruvian upwelling.

Atmos. Chem. Phys. Discuss., doi:10.5194/acp-2016-39, 2016
Manuscript under review for journal Atmos. Chem. Phys.
Published: 14 March 2016

Correlations between the compounds indicate similar sources for all measured halocarbons, except for CH_2Br_2, with upwelling region IV as hot spot area (Fig. 2). The strongest correlation was found for CH_3I with CH_2ClI (r_s = 0.83). CH_2I_2 and CH_2ClI are often found to correlate very well with each other (Tokarczyk and Moore, 1994; Moore et al., 1996; Archer et al., 2007), mostly attributed to the formation of CH_2ClI during photolysis of CH_2I_2. In comparison, the weaker correlation between CH_2ClI and CH_2I_2 (r_s = 0.59) during our cruise may be the result of additional sources for CH_2ClI (see also section 5).

4.2 Halocarbon distribution in depth profiles

Depth profiles of halocarbons reveal maxima at the surface and around the Chl *a* maximum, usually attributed to biological production of these compounds. $CHBr_3$ and CH_2Br_2 profiles (not shown) showed distinct maxima in the deeper Chl *a* maximum during large part of the cruise, while some profiles were characterized by elevated concentrations in the surface usually associated with upwelling water. Both kinds of profiles are consistent with previous studies finding maxima in the deeper water column in the open ocean and surface maxima in upwelling regions (Yamamoto et al., 2001; Quack et al., 2004; Hepach et al., 2015). During the northern part of M91 (upwelling III), CH_2Br_2 in the water column was more elevated than $CHBr_3$, while during the remaining part of the cruise, $CHBr_3$ was usually higher.

Though most of the stations were characterized by subsurface maxima of iodocarbons, which were mostly located between 10 and 50 m (see example in Fig. 4, upper panel), surface maxima were often observed in upwelling region IV (see example in Fig. 4, lower panel), the region with highest iodocarbon concentrations. Profiles with surface maxima were generally characterized by much higher concentrations of these compounds. Similarly to very low CH_2I_2 concentrations in the surface in the northern part of the measurements, it was also hardly detected in the deeper water in this region (Fig. 4, upper panel). Surface maxima in depth profiles of CH_3I and CH_2ClI were connected to surface maxima of several phytoplankton species, mainly diatoms (r_s = 0.57 and 0.62). Direct and indirect biological and photochemical formation account as possible sources for these maxima. CH_2I_2 was usually strongly depleted in the surface in contrast to the deeper layers due to its rapid photolysis, which may also have been a source for surface CH_2ClI. Subsurface maxima occurred both below and within the mixed layer (see the example in Fig. 4d indicated by the temperature-, salinity- and density profiles). Maxima in the mixed layer probably appear because of very fast production (Hepach et al., 2015), while maxima below the mixed layer are supported by accumulation due to reduced mixing.

Atmos. Chem. Phys. Discuss., doi:10.5194/acp-2016-39, 2016
Manuscript under review for journal Atmos. Chem. Phys.
Published: 14 March 2016

All five halocarbons were strongly depleted in waters below 50 m. These deeper layers were also characterized by very low oxygen values, known as strong OMZ below the biologically active layers (Karstensen et al., 2008). A possible reason for the strong depletion of the halocarbons is their bacterial mediated reductive dehalogenation occurring under anaerobic conditions (Bouwer et al., 1981; Tanhua et al., 1996).

5 Relationship of surface halocarbons to environmental parameters

Physical and chemical parameters as well as biological proxies such as TChl *a* and phytoplankton group composition were investigated using correlation analysis in order to investigate marine sources of halocarbons.

5.1 Potential bromocarbon sources

Bromocarbons were weakly, but significantly anticorrelated with SSS and SST (r_s between -0.29 and -0.57), indicating sources in the upwelled water (Table 2). They showed a positive correlation with diatoms (r_s = 0.58 for both compounds), the dominant phytoplankton group in the region. Diatoms have already been found to be involved in bromocarbon production in several laboratory and field studies (Tokarczyk and Moore, 1994; Moore et al., 1996; Quack et al., 2007b; Hughes et al., 2013). Thus, these findings are in agreement with current assumptions that diatoms may contribute directly or indirectly to bromocarbon production. During M91, CH_2Br_2 was more abundant in cooler, nutrient-rich water than $CHBr_3$, leading to a stronger correlation with TChl *a* and SST, indicating an additional source associated with fresh upwelling. No significant correlations were found for bromocarbons with polysaccharidic DOM (Table 3), implying that DOM components analyzed during the cruise were not involved in bromocarbon production, at least not in the upper water column.

5.2 Iodinated compounds and phyotplankton

In general, the iodocarbons correlated stronger with biological parameters than the bromocarbons. Diatoms were found to correlate very strongly with all three iodocarbons (r_s = 0.73 with CH_3I, r_s = 0.79 with CH_2ClI and r_s = 0.72). Weak but significant anticorrelations with DIN:DIP and SST suggest that iodocarbons were associated with cool and slightly DIN depleted water. The occurrence of large amounts of iodocarbons seemed to be associated with an established diatom bloom. The production of CH_3I, CH_2ClI and CH_2I_2 by a number of diatom species has been observed in several studies before (Moore et al., 1996; Manley and

Atmos. Chem. Phys. Discuss., doi:10.5194/acp-2016-39, 2016
Manuscript under review for journal Atmos. Chem. Phys.
Published: 14 March 2016

de la Cuesta, 1997), consistent with our findings. The very high correlation of cryptophytes with iodocarbons was likely based on the co-occurrence of these species with diatoms (Table 2 and description in section 3).

5.3 Iodinated compounds and DOM

Correlations of the three iodinated compounds to polysaccharidic DOM components in subsurface water revealed a strong relationship of the iodocarbon abundance with polysaccharides and in particular uronic acids (Table 3). CH_3I and CH_2ClI showed strong correlations with particulate uronic acids (both r_s = 0.84), total uronic acids (r_s = 0.83 and 0.88) and dissolved polysaccharides (r_s = 0.82 and 0.90). The correlations of CH_2I_2 with polysaccharides were less strong, but significant (r_s = 0.68 with particulate, r_s = 0.66 with total and r_s = 0.55 with dissolved). The above listed DOM components were also significantly correlated to diatoms (r_s = 0.68 with polysaccharides and r_s = 0.75 with uronic acids), which were a potential source for the accumulated organic matter in the subsurface. The exact composition of surface water DOM is determined by the phytoplankton species producing the DOM. Polysaccharides with uronic acids as an important constituent have for example been shown to contribute largely to the DOM pool in a diatom rich region (Engel et al., 2012).

Hill and Manley (2009) tested several diatom species for their production of halocarbons in a laboratory study, and suggested that a major formation pathway for polyhalogenated compounds may actually not be from direct algal production, but rather indirectly through their release of hypoiodous (HOI) and hypobromous acid (HOBr), which then react with the present DOM (Liu et al., 2015). The formation of HOI and HOBr within the algae is enzymatic with possible chloroperoxidase (CPO), BPO and iodoperoxidase (IPO) involvement. While CPO and BPO may produce both HOBr and HOI, IPO only leads to HOI. Moore et al. (1996) suggested that the occurrence of BPO and IPO in the phytoplankton cells may be highly species dependent. This leads to the assumption that diatoms abundant in the Peruvian upwelling contained more IPO than BPO, which could explain the higher abundance of iodocarbons relative to bromocarbons during M91.

The formation of CH_3I through DOM may be different than the production of CH_2ClI and CH_2I_2. While CH_2I_2 is suggested to be formed via haloform-type reactions (Carpenter et al., 2005), CH_3I is produced using a methyl-radical source (White, 1982). The relationship of CH_3I with DOM can be the result of both photochemical and biological production pathways: DOM, which was observed in high concentrations in the biologically productive waters, can

Atmos. Chem. Phys. Discuss., doi:10.5194/acp-2016-39, 2016
Manuscript under review for journal Atmos. Chem. Phys.
Published: 14 March 2016

act as the methyl-radical source during photochemical production of CH_3I (Bell et al., 2002). A second possible biological pathway of methyl iodide production takes place via bacteria and micro algae, which can utilize methyl transferases in their cells. HOI plays a significant role in this production pathway by providing the iodine to the methyl group (Yokouchi et al., 2014).

In conclusion, the Peruvian upwelling was a strong source for the iodocarbons CH_3I, CH_2ClI and CH_2I_2, and a weaker source for the bromocarbons $CHBr_3$ and CH_2Br_2. We propose a formation mechanism for this region as described in Fig. 5 based on measurements of short-lived halocarbons and biological parameters during M91. Diatoms, which can contain the necessary enzymes for halocarbon formation, were identified as important source based on their strong correlations with the bromo- and iodocarbons and with polysaccharidic DOM. The very good correlations of iodocarbons with polysaccharides and uronic acids are a hint that these DOM components may have been important substrates for iodocarbon production potentially produced from the present diatoms. The higher iodocarbon concentrations can likely be explained by phytoplankton species containing more IPO than BPO, leading to a stronger production of iodocarbons. Additionally, the particular type of DOM may also have regulated the production of specific halocarbons (Liu et al., 2015), in this case CH_3I, CH_2ClI and CH_2I_2.

One interesting feature of our analysis is the fact that CH_2I_2 when compared to the other two iodocarbons showed weaker correlations with the polysaccharides possibly due to its shorter surface water lifetime. Moreover, CH_2I_2 and CH_2ClI showed weaker correlations in the Peruvian upwelling than during other cruises in the tropical Atlantic, namely MSM18/3 (Hepach et al., 2015) and DRIVE (Hepach et al., 2014). Combining the two arguments of a short CH_2I_2 lifetime and only a weak correlation between CH_2I_2 and CH_2ClI, this may indicate an additional source for CH_2ClI similar to CH_3I, explaining why CH_3I and CH_2ClI correlate much better with each other than with CH_2I_2.

6 From the ocean to the atmosphere

6.1 Sea-to-air fluxes of iodocarbons

Due to high oceanic iodocarbon concentrations measured in sea surface water of the Peruvian upwelling and despite the moderate prevailing wind speeds of 6.17 (0.42 – 15.47) m s^{-1}, high iodocarbon sea-to-air fluxes were calculated in contrast to the rather low bromocarbon

Atmos. Chem. Phys. Discuss., doi:10.5194/acp-2016-39, 2016
Manuscript under review for journal Atmos. Chem. Phys.
Published: 14 March 2016

Atmospheric Chemistry and Physics Discussions

emissions during this M91 cruise (Fuhlbrügge et al., 2015a). The highest average fluxes of the three iodocarbons of 954 (21 – 4686) were calculated for CH_3I, followed by 834 (-24 – 5652) for CH_2ClI, and finally 504 (-126 – 2546) pmol m^{-2} h^{-1} for CH_2I_2 (Table 1). These were on average 4 to 7 times higher than $CHBr_3$ and 2 to 4 times higher than the CH_2Br_2 sea-to-air fluxes during the cruise.

Our estimated fluxes of CH_3I are in the range of emissions calculated for the tropical and subtropical Atlantic of 625 to 2154 pmol m^{-2} h^{-1} (Chuck et al., 2005; Jones et al., 2010). Moore and Groszko (1999), who performed a study between 40° N and 40° S close to our investigation region but not covering the Peruvian upwelling, calculated on average 666 pmol m^{-2} h^{-1}, which is 0.7 times our flux. Sea-to-air fluxes of CH_2ClI from the same studies were reported to range on average between 250 and 1138 pmol m^{-2} h^{-1} with the largest fluxes originating from the Mauritanian upwelling region. These are 0.3 to 1.4 times the fluxes we calculated, showing that the Peruvian upwelling region is at the top end of oceanic CH_2ClI emissions. We are only aware of two studies focusing on emissions of CH_2I_2 from the Atlantic tropical ocean (Jones et al., 2010; Hepach et al., 2015) which are on average 0.2, respectively 1.4 times the fluxes from the tropical East Pacific. The larger sea-to-air fluxes reported in Hepach et al. (2015) from the equatorial Atlantic cold tongue are mainly a result of much lower atmospheric mixing ratios there, increasing the concentration gradient, and additionally higher wind speeds, increasing the exchange coefficient k_w.

Summarizing this section, the large production of iodocarbons in the Peruvian upwelling led to enhanced emissions of these compounds to the troposphere despite very low wind speeds. An additional factor influencing halocarbon emissions is the low height and insolation of the MABL, where halocarbons accumulate above the air-sea interface. The large sea-to-air fluxes and low wind speeds should result in high tropospheric iodocarbons, which was indeed observed and is discussed in the following section.

6.2 Atmospheric iodocarbons

Atmospheric mixing ratios of the three iodocarbons were elevated during M91 with up to 3.2 ppt for CH_3I, up to 2.5 ppt for CH_2ClI and up to 3.3 ppt for CH_2I_2 (Table 1), likely a result of the strong production and emissions of these compounds.

CH_3I data were generally elevated in comparison to other eastern Pacific measurements of up to 2.1 ppt CH_3I (Butler et al., 2007), but lower than in the tropical central and East Atlantic around the equator, characterized by higher atmospheric CH_3I of over 5 ppt (Ziska et al.,

Atmos. Chem. Phys. Discuss., doi:10.5194/acp-2016-39, 2016
Manuscript under review for journal Atmos. Chem. Phys.
Published: 14 March 2016

Atmospheric Chemistry and Physics Discussions

2013). Both CH_2ClI and CH_2I_2 were also elevated in comparison to previous oceanic measurements, where e.g. 0.01 to 0.99 ppt CH_2ClI were measured for remote locations in the Atlantic and Pacific (Chuck et al., 2005; Varner et al., 2008) and only up to 0.07 ppt were reported for CH_2I_2 at a remote site in the Pacific (Yokouchi et al., 2011). Coastal areas with high macroalgal abundance were characterized by high CH_2ClI of up to 3.4 ppt (Varner et al., 2008) and up to 3.1 ppt CH_2I_2 (Carpenter et al., 1999; Peters et al., 2005), while 19.8 ppt (Peters et al., 2005) were measured at Mace Head, Ireland and Lilia, Brittany in the North Atlantic.

The different atmospheric lifetimes of the three iodocarbons, ranging between 4 d (CH_3I), 9 h (CH_2ClI) and 10 min (CH_2I_2) (Carpenter and Reimann, 2014), partly explain the observed differences in their distributions. Although atmospheric CH_3I was generally elevated in regions of high oceanic CH_3I (Fig. 3) in upwelling regions III and IV, the atmospheric and oceanic data did not show a significant correlation. The CH_3I lifetime of several days allows atmospheric CH_3I to mix within the MABL, possibly masking a correlation between local source regions and elevated mixing ratios.

The two shorter-lived iodinated compounds CH_2ClI and CH_2I_2 generally showed a stronger influence of local marine sources. Both species correlate significantly with their oceanic concentrations with $r_s = 0.60$ (CH_2ClI) and $r_s = 0.64$ (CH_2I_2). Oceanic CH_2ClI and CH_2I_2 were emitted into the boundary layer where they could accumulate during night (see comparison with global radiation in Fig. 3b), and were rapidly degraded during day time via photolysis, which is their main sink in the troposphere (Carpenter and Reimann, 2014). Moderate average wind speeds in the upwelling regions (Fig. 6) and stable atmospheric boundary layer conditions (Fuhlbrügge et al., 2015a) supported the accumulation of these compounds.

The Peruvian upwelling was in general characterized by elevated atmospheric iodocarbons as a result of their large sea-to-air fluxes caused by strong biological production. The upwelling could sustain elevated atmospheric levels of e.g. CH_3I, could trap iodocarbons and their degradation products in a stable MABL, and may have therefore contributed significantly to the tropospheric inorganic iodine budget, which is discussed in the following.

6.3 Contributions to tropospheric iodine

After their emission from the ocean and their chemical degradation in the marine boundary layer, iodocarbons contribute to the atmospheric inorganic iodine budget, I_y. The importance of this contribution compared to abiotic sources is currently under debate and analyzed for

Atmos. Chem. Phys. Discuss., doi:10.5194/acp-2016-39, 2016
Manuscript under review for journal Atmos. Chem. Phys.
Published: 14 March 2016

Atmospheric Chemistry and Physics Discussions

various oceanic environments (Mahajan et al., 2010; Grossmann et al., 2013; Prados-Roman et al., 2015). So far, no correlations of IO with the organic iodine precursor species have been observed (Grossmann et al., 2013) and correlations between IO and Chl *a* were often found to be negative (Mahajan et al., 2012; Gómez Martín et al., 2013). Chemical modelling studies, undertaken to explain the contributions of organic and inorganic oceanic iodine sources, simulated that only a small fraction of the atmospheric IO stems from the organic precursors with estimates of about 25 % on a global average (Prados-Roman et al., 2015). Both arguments, the missing correlations and the small contributions, indicate that the organic source gas emissions play a minor role for the atmospheric iodine budget. Given the special conditions of the Peruvian upwelling with cold nutrient rich waters, the strong iodocarbon sources and a stable MABL and trade inversion, it is of interest to analyze the local contributions to the atmosphere in this region and to compare with estimates from other oceanic environments.

We focus our analysis on the section of the cruise where MAX-DOAS measurements of IO and simultaneous iodocarbon measurements in the surface water and atmosphere were made (roughly south of 10° S). Tropospheric VCDs of IO in the range of 2.5 – 6.0 $\times 10^{12}$ molec cm^{-2} were inferred from the MAX-DOAS measurements. Similar VCDs of IO were reported by Schönhardt et al. (2008) based on remote satellite measurements from SCIAMACHY. Volume mixing ratios of IO along the cruise track (Fig. 7a) derived from the MAX-DOAS measurements show a pronounced variability and maxima close to upwelling regions II and IV. Daytime averaged IO volume mixing ratios are displayed in Fig. 7b and range between 0.8 ppt (on December 12 and December 22) and 1.5 ppt (on December 26). Overall the daytime IO abundance in the MABL above the Peruvian upwelling was relatively high compared to measurements from the nearby Galapagos islands (~ 0.4 ppt) (Gómez Martín et al., 2013) and from other tropical oceans such as the Malaspina 2010 circumnavigation (0.4 – 1 ppt) (Prados-Roman et al., 2015). Other measurement campaigns such as the Cape Verde measurements (Read et al., 2008) or the TransBrom Sonne in the West Pacific (Grossmann et al., 2013) found similar IO mixing ratios with values above 1 ppt, but significantly lower IO VCDs in case of the latter.

The M91 cruise track crisscrossed the waters between the coast and 200 km offshore multiple times, providing a comprehensive set of measurements over a confined area (see Fig. 7a) and allowing us to analyze the relation between IO and organic precursors. Assuming constant emissions over the cruise period we can link the oceanic sources with atmospheric IO observations at locations reached after hours to days of atmospheric transport. Therefore, we

Atmos. Chem. Phys. Discuss., doi:10.5194/acp-2016-39, 2016
Manuscript under review for journal Atmos. Chem. Phys.
Published: 14 March 2016

released FLEXPART trajectories from all sea surface measurement locations continuously over the whole measurement time period from December 8 to December 26 loaded with the oceanic organic iodine as prescribed by the observed iodocarbon emissions. Based on the simulations of transport and chemical decay described in Section 2.5, we derived organic and inorganic iodine mixing ratios individually for each air parcel. Mixing with air parcels impacted by other source regions was not taken into account. FLEXPART-based IO originating from organic precursors was derived as mean values over all air parcels in the MABL coinciding with the MAX-DOAS measurement locations within an area of 5 km x 5 km. Simplifying assumptions of a prescribed inorganic iodine lifetime (2 days) and IO to I_y ratio (0.15 to 0.3) were made to derive the IO mixing ratios. Uncertainties were estimated based on additional runs with varying atmospheric lifetime of inorganic iodine (1 – 3 days).

For the first part of the cruise from December 8 to December 18, FLEXPART-derived IO mixing ratio estimates at the MAX-DOAS measurement locations (red line in Fig. 7b and c) explain between 40 and 70 % (55 % on average) of the measured IO assuming a lifetime for inorganic iodine of 2 days. As a consequence, about 0.5 ppt of IO is expected to originate from other, likely inorganic, iodine sources. For the scenario of a shorter I_y lifetime (one day), we find that the organic sources explain about 30 % of the IO and for a relatively long lifetime (three days), 80 % can be explained. In general, the air masses were transported along the coast in northwest direction and organic sources contribute to the IO budget along this transport path. Most of the IO results from CH_2ClI (Fig. 7c) which was transported some hours northwestwards (lifetime of 9 hours) before contributing to the atmospheric inorganic iodine budget.

For the second part of the cruise from December 19 to December 26, the amount of IO estimated from organic precursors was much smaller and often close to zero. This very small organic contribution was caused by two facts. First, the instantaneous sources during the last part of the cruise were much smaller (Fig. 6b – d) and second, further southward situated sources, which also influence the iodine abundance in the cruise track region were not analyzed and thus not included in the simulations. Because of missing information on the source strength and distribution southwards of the cruise track, a proper comparison is only possible for the first part of the cruise before December 19. However, given that the MAX-DOAS measurements of IO remained relatively high during the second part of the cruise, it is likely that additional significant organic iodine sources existed further southwards. This assumption is also supported by the fact that atmospheric CH_3I mixing ratios remained relatively high during the second part of the cruise (50 % compared to the earlier part, see Fig.

Atmos. Chem. Phys. Discuss., doi:10.5194/acp-2016-39, 2016
Manuscript under review for journal Atmos. Chem. Phys.
Published: 14 March 2016

3b) while the water concentrations were close to zero. Consequently, a source region of CH_3I must have existed further southwards contributing to the observed mixing ratios of CH_3I and IO after some hours to days of atmospheric transport.

While the contribution of organic iodine to IO during the first part of the cruise is considerably higher than found in other regions, the amount of inorganic iodine precursors of 0.5 ppt necessary to explain total IO is very similar to the one derived in other studies (Prados-Roman et al., 2015). The higher organic contribution was consistent with the fact that there was an overall higher IO abundance compared to most other campaigns. Instantaneous IO and organic source gas emissions during M91 were not directly correlated. However, taking the transport within the first hours and days into account enables us to explain a considerable part of the atmospheric IO variations with the variability of the oceanic organic sources (Fig. 7b). Overall, we conclude that for the Peruvian upwelling region with special conditions in the ocean and atmosphere, higher iodocarbon sources lead to larger IO abundances while the absolute inorganic contribution is similar to other regions.

7 Conclusions

The Peruvian upwelling at the west coast of South America was characterized for halocarbons for the first time during the M91 cruise. We measured moderate concentrations of the bromocarbons $CHBr_3$ and CH_2Br_2, while we observed exceptionally high concentrations of the iodocarbons CH_3I, CH_2ClI and CH_2I_2 in the surface seawater.

$CHBr_3$ and CH_2Br_2 were significantly correlated with TChl *a* and diatoms, suggesting biological formation of these compounds. Higher correlations of diatoms were found with the three iodocarbons, and even stronger correlations of the iodocarbons with the DOM components polysaccharides and uronic acids were observed. The polyhalogenated compounds CH_2ClI and CH_2I_2 were potentially formed via these DOM components with the likely involvement of diatoms. CH_3I may have been formed via photochemistry from the large pool of observed DOM and/or biologically via methyl transferases in micro algae and bacteria. The production of iodocarbons from DOM via the proposed mechanisms seems to have exceeded the bromocarbon production in the region in contrast to several previous studies in tropical Atlantic upwelling regions (Hepach et al., 2014, 2015).

Depth profiles showed subsurface maxima, common in the open ocean, and very pronounced and elevated surface maxima in regions of highest underway iodocarbon concentrations. The

Atmos. Chem. Phys. Discuss., doi:10.5194/acp-2016-39, 2016
Manuscript under review for journal Atmos. Chem. Phys.
Published: 14 March 2016

Atmospheric Chemistry and Physics Discussions

surface water was always depleted in CH_2I_2 with respect to the underlying water column due to its very rapid photolysis. The OMZ at depth was strongly depleted in all five measured halocarbons, suggesting an effective sink in the oxygen depleted waters.

The high oceanic iodocarbon concentrations and elevated emissions also led to elevated atmospheric mixing ratios in the marine boundary layer. Atmospheric CH_2ClI and CH_2I_2 showed clear diurnal cycles, accumulating during night and decreasing rapidly during day time. Despite previous suggestions that the tropospheric iodine loading is mainly a product from direct emission of HOI and I_2, we calculated important contributions of iodocarbons to the observed IO levels. Using FLEXPART, we estimated a contribution of combined iodocarbon fluxes to IO of 30 to 80 % assuming an inorganic iodine lifetime between 1 and 3 days. This contribution of organoiodine is much higher than previously assumed (Prados-Roman et al., 2015), suggesting that iodocarbons therefore may contribute significantly to tropospheric iodine levels in regions of strong iodocarbon production mediated by phytoplankton (diatoms) and bacteria.

Our observations reveal several uncertainties which need to be addressed in the future to better constrain the halocarbon budget and understand its role in a changing climate. Further studies of upwelling regions need to be performed in different seasons and years, since these regions are impacted by synoptic and climatic conditions, which are expected to have an impact on the strength of halocarbon emissions. A regular monitoring and better knowledge of halocarbon sources and emissions is severely needed, since these have numerous implications for atmospheric processes such as ozone chemistry and aerosol formation, which have been investigated in several atmospheric modeling studies. These studies have mostly applied Chl *a* as proxy for halocarbon emissions. However, the potential involvement of DOM in the production of both iodo- and bromocarbons and the often weak correlation to Chl *a* in the field raises the question whether Chl *a* is a suitable parameter to estimate halocarbon concentrations. Laboratory studies are therefore crucial to help identifying more adequate parameters for predicting halocarbons in the ocean. Associated with the involvement of DOM in iodocarbon production is the occurrence of the relevant DOM components in large concentrations in the sea surface microlayer (SML) (Engel and Galgani, 2015). The SML has been shown to cover a wide range of oceanic regions (Wurl et al., 2011), which could represent a significant additional source to atmospheric iodocarbons. The potential of the SML to produce CH_2I_2 has been previously suggested by Martino et al. (2009), who proposed that HOI converted from iodide in the SML may react with the present DOM, which may apply to CH_2ClI and CH_3I as well. Furthermore, the SML is in direct contact to the

Atmos. Chem. Phys. Discuss., doi:10.5194/acp-2016-39, 2016
Manuscript under review for journal Atmos. Chem. Phys.
Published: 14 March 2016

atmosphere, and the direct exposure to light may enhance halocarbon emissions (see also Fig. 5). The influence of these halocarbon emissions on the tropospheric halogen loading is still very much under debate, and our results underline the importance to constrain the actual contribution of these compounds to tropospheric halogen chemistry.

Acknowledgements

We thank the chief scientist of the cruise M91 Hermann Bange, as well as the captain and the crew of the RV *Meteor* for their support. We would like to acknowledge Sonja Wiegmann for pigment analysis, Kerstin Nachtigall for nutrient measurements, and Stefan Raimund and Sebastian Flöter for helping with halocarbon measurements. This work was part of the German research projects SOPRAN II (grant no. FKZ 03F0611A) and III (grant no. FKZ 03F0662A) funded by the Bundesministerium für Bildung und Forschung (BMBF). Astrid Bracher's contribution was funded by the Total Foundation project „Phytoscope".

Atmos. Chem. Phys. Discuss., doi:10.5194/acp-2016-39, 2016
Manuscript under review for journal Atmos. Chem. Phys.
Published: 14 March 2016

Tables

Table 1. Environmental parameters, as well as halocarbons in water, air and sea-to-air fluxes during the cruise. Means of sea surface temperature (SST), sea surface salinity (SSS) and wind speed are for 10-min-averages.

Parameter		Unit	Mean (min - max)
SST		°C	19.4 (15.0 - 22.4)
SSS			34.95 (34.10 - 35.50)
TChl *a*		µg L^{-1}	1.80 (0.06 - 12.65)
Wind speed		m s^{-1}	6.17 (0.42 - 15.47)
$CHBr_3$	Water	pmol L^{-1}	6.6 (0.2 - 21.5)
	Air	ppt	2.9 (1.5 - 5.9)
	Sea-to-air flux	pmol m^{-2} h^{-1}	130 (-550 - 2201)
CH_2Br_2	Water	pmol L^{-1}	4.3 (0.2 - 12.7)
	Air	ppt	1.3 (0.8 - 2.0)
	Sea-to-air flux	pmol m^{-2} h^{-1}	273 (-128 - 1321)
CH_3I	Water	pmol L^{-1}	9.8 (1.1 - 35.4)
	Air	ppt	1.5 (0.6 - 3.2)
	Sea-to-air flux	pmol m^{-2} h^{-1}	954 (21 - 4686)
CH_2ClI	Water	pmol L^{-1}	10.9 (0.4 - 58.1)

Atmos. Chem. Phys. Discuss., doi:10.5194/acp-2016-39, 2016
Manuscript under review for journal Atmos. Chem. Phys.
Published: 14 March 2016

Atmospheric Chemistry and Physics Discussions

	Air	ppt	0.4 (0 - 2.5)
	Sea-to-air flux	pmol m^{-2} h^{-1}	834 (-28 - 5652)
	Water	pmol L^{-1}	7.7 (0.2 - 32.4)
CH_2I_2	Air	ppt	0.2 (0 - 3.3)
	Sea-to-air flux	pmol m^{-2} h^{-1}	504 (-126 - 2546)

Atmos. Chem. Phys. Discuss., doi:10.5194/acp-2016-39, 2016
Manuscript under review for journal Atmos. Chem. Phys.
Published: 14 March 2016

Table 2. Spearman's rank correlation coefficients of correlations of halocarbon with several ambient parameters, as well as biological proxies. Bold numbers indicate correlations that are significant with $p < 0.05$ with a sample number of 107 for all environmental data and 46 for all phytoplankton and nutrient data considering all collocated surface data.

	$CHBr_3$	CH_2Br_2	CH_3I	CH_2ClI	CH_2I_2	SST	SSS	Global radiation	Diatoms	Crypto-phytes	Dino-flagellates	TChl *a*
DIN:DIP	-0.26	-0.34	**-0.38**	**-0.30**	-0.32	0.00	**0.41**	0.13	-0.18	-0.17	-0.10	-0.08
TChl *a*	**0.48**	**0.56**	**0.73**	**0.74**	**0.70**	**-0.82**	**-0.77**	-0.20	**0.93**	**0.85**	**0.33**	
Dino-flagellates	0.15	0.28	0.15	0.17	0.21	-0.23	-0.22	-0.01	**0.38**	0.26		
Crypto-phytes	**0.38**	**0.54**	**0.61**	**0.61**	**0.64**	**-0.74**	**-0.79**	-0.18	**0.73**			
Diatoms	**0.58**	**0.58**	**0.73**	**0.79**	**0.72**	**-0.76**	**-0.72**	-0.18				
Global radiation	0.14	-0.10	-0.22	-0.03	-0.08	**0.20**	0.12					
SSS	**-0.44**	**-0.48**	**-0.75**	**-0.69**	**-0.45**	**0.68**						
SST	**-0.29**	**-0.57**	**-0.52**	**-0.62**	**-0.58**							
CH_2I_2	**0.60**	0.43	**0.66**	**0.59**								
CH_2ClI	**0.64**	**0.70**	**0.83**									
CH_3I	**0.66**	**0.46**										

Atmospheric Chemistry and Physics Discussions
Open Access
EGU

Atmos. Chem. Phys. Discuss., doi:10.5194/acp-2016-39, 2016
Manuscript under review for journal Atmos. Chem. Phys.
Published: 14 March 2016

Atmospheric Chemistry and Physics Discussions

CH_2Br_2	**0.56**

Atmos. Chem. Phys. Discuss., doi:10.5194/acp-2016-39, 2016
Manuscript under review for journal Atmos. Chem. Phys.
Published: 14 March 2016

Atmospheric Chemistry and Physics Discussions

Table 3. Correlations of halocarbons with combined high molecular weight (HMW) carbohydrates (CCHO) and uronic acids (URA) from subsurface samples (T – total, d – dissolved, P – particulate) with a sample number of 29 for each variable.

	$CHBr_3$	CH_2Br_2	CH_3I	CH_2ClI	CH_2I_2
TCCHO	0.15	0.28	**0.78**	**0.82**	**0.66**
dCCHO	0.39	0.48	**0.82**	**0.90**	**0.55**
PCCHO	-0.06	-0.10	**0.61**	**0.64**	**0.68**
TURA	0.31	0.34	**0.83**	**0.88**	**0.52**
dURA	-0.18	0.42	**0.48**	**0.79**	**0.50**
PURA	0.37	0.22	**0.84**	**0.84**	**0.54**

Atmos. Chem. Phys. Discuss., doi:10.5194/acp-2016-39, 2016
Manuscript under review for journal Atmos. Chem. Phys.
Published: 14 March 2016

Atmospheric Chemistry and Physics Discussions

Figures

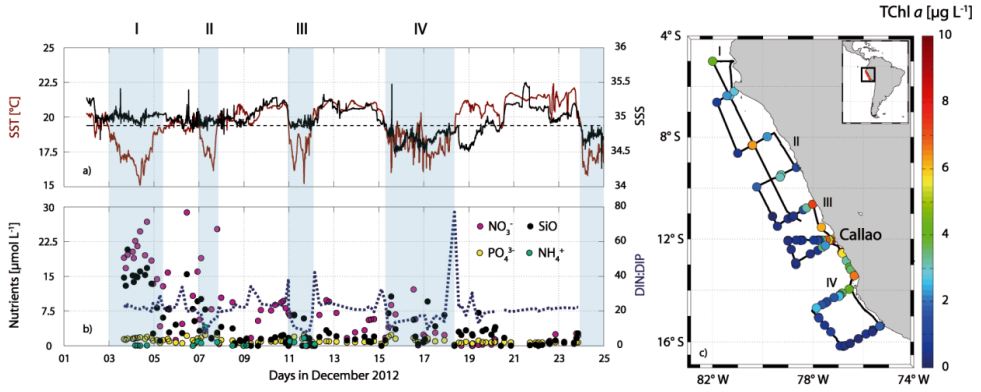

Fig. 1. Ambient parameters during the M91 cruise: SST (dark red) and sea surface salinity (SSS) (black) in a) with the dashed line as the mean SST. Nutrients (purple is nitrate – NO_3^-, yellow is phosphate – PO_4^{3-}, black is silicate – SiO_2, light cyan is ammonium – NH_4^+) with the N to P ratio (dark blue dashed line) are shown in b). Total chlorophyll *a* (TChl *a*) is shown in the map in c). The light blue shaded areas stand for the regions where SST is below the mean, indicating upwelling of cold water.

Atmos. Chem. Phys. Discuss., doi:10.5194/acp-2016-39, 2016
Manuscript under review for journal Atmos. Chem. Phys.
Published: 14 March 2016

Atmospheric Chemistry and Physics Discussions

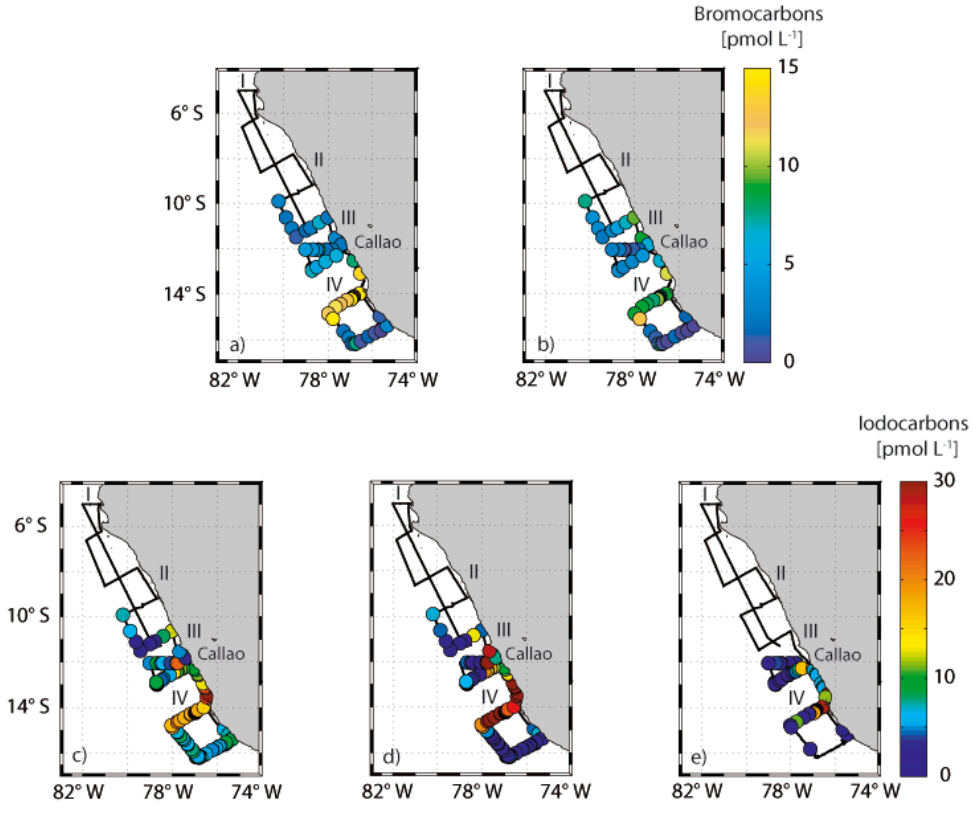

1

Atmos. Chem. Phys. Discuss., doi:10.5194/acp-2016-39, 2016
Manuscript under review for journal Atmos. Chem. Phys.
Published: 14 March 2016

Atmospheric Chemistry and Physics Discussions

Fig. 2. Halocarbon surface water measurements are shown in a) and b) for the bromocarbons (note the colorbar oin the upper panel) with a – $CHBr_3$ and b – CH_2Br_2. Iodocarbons can be found in c) – e) (note the colorbar in the lower panel) with c – CH_3I, d – CH_2ClI and e – CH_2I_2.

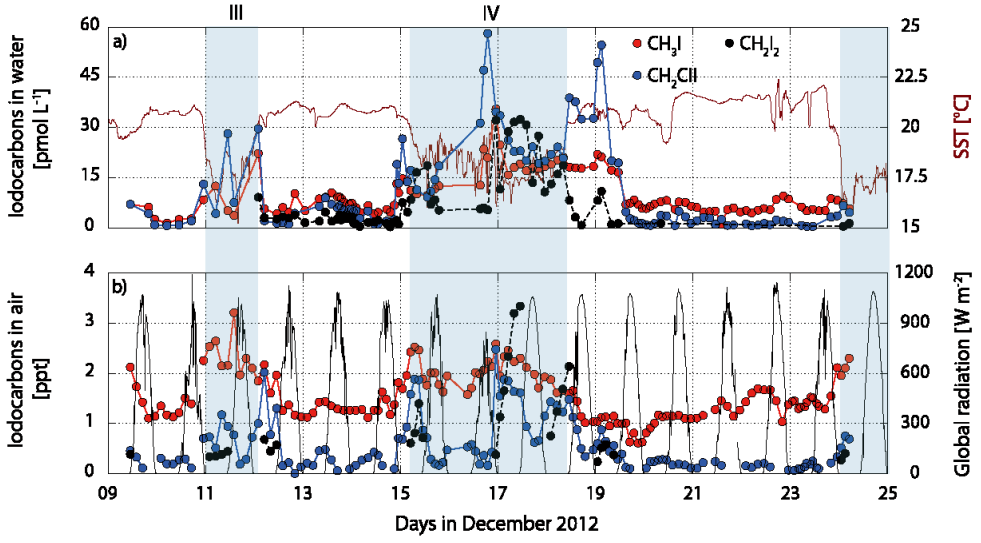

Fig. 3. Surface water measurements of iodocarbons are presented in a) with CH_3I in red, CH_2ClI in blue and CH_2I_2 in black on the left side along with SST (dark red) on the right side. Additionally, atmospheric mixing ratios of CH_3I (red), CH_2ClI (blue) and CH_2I_2 (grey) on the left side together with global radiation (black) on the right side are depicted in b). Note that all times are in UTC.

Atmos. Chem. Phys. Discuss., doi:10.5194/acp-2016-39, 2016
Manuscript under review for journal Atmos. Chem. Phys.
Published: 14 March 2016

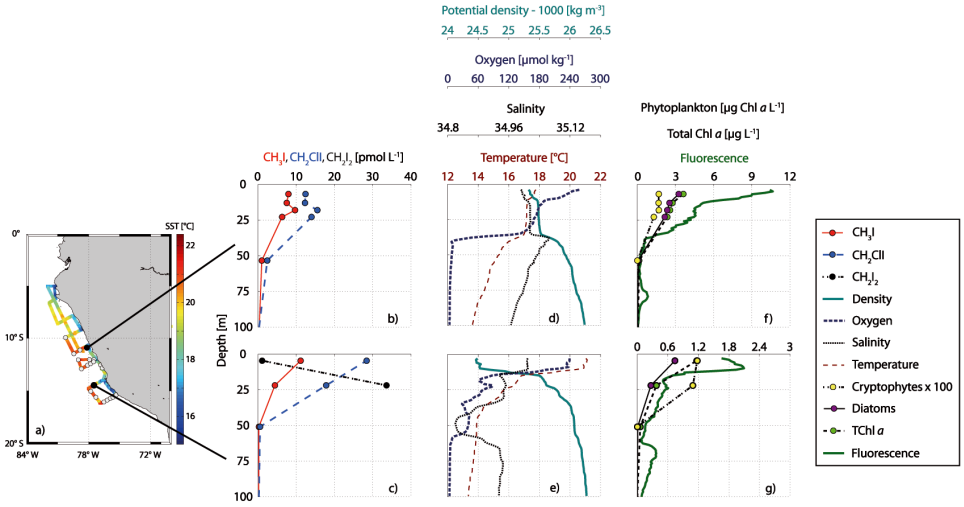

Fig. 4. A cruise map including all CTD stations and SST is shown in a), while selected depth profiles of iodocarbons can be seen in a) – b), together with ambient parameters such as potential density (cyan), oxygen (dark blue), salinity (black) and temperature (dark red) in d) – e), as well as phytoplankton groups (cryptophytes and diatoms), total chlorophyll a and fluorescence in f) – g). CH_2I_2 was undetectable at the first station (see also consistence with surface data).

Atmos. Chem. Phys. Discuss., doi:10.5194/acp-2016-39, 2016
Manuscript under review for journal Atmos. Chem. Phys.
Published: 14 March 2016

Atmospheric Chemistry and Physics Discussions

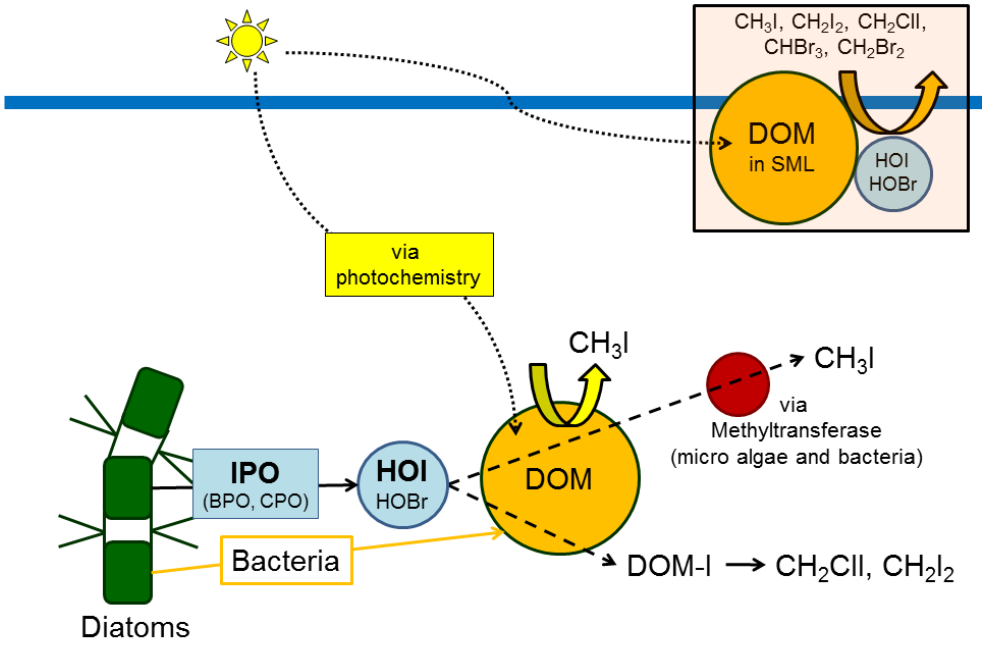

1

2 Fig. 5. Proposed mechanisms for formation of iodocarbons – release of HOI with the help
3 ofvia iodoperoxiases (IPO) and reaction with DOM (dissolved organic matter (DOM) via
4 iodine binding to DOM (DOM-I) to form CH_2ClI and CH_2I_2. CH_3I formation via
5 photochemistry and/or biological formation via methyltransferases. The box indicates
6 potential formation of halocarbons from DOM in the sea surface microlayer SML.

7

31

Atmos. Chem. Phys. Discuss., doi:10.5194/acp-2016-39, 2016
Manuscript under review for journal Atmos. Chem. Phys.
Published: 14 March 2016

Atmospheric Chemistry and Physics Discussions

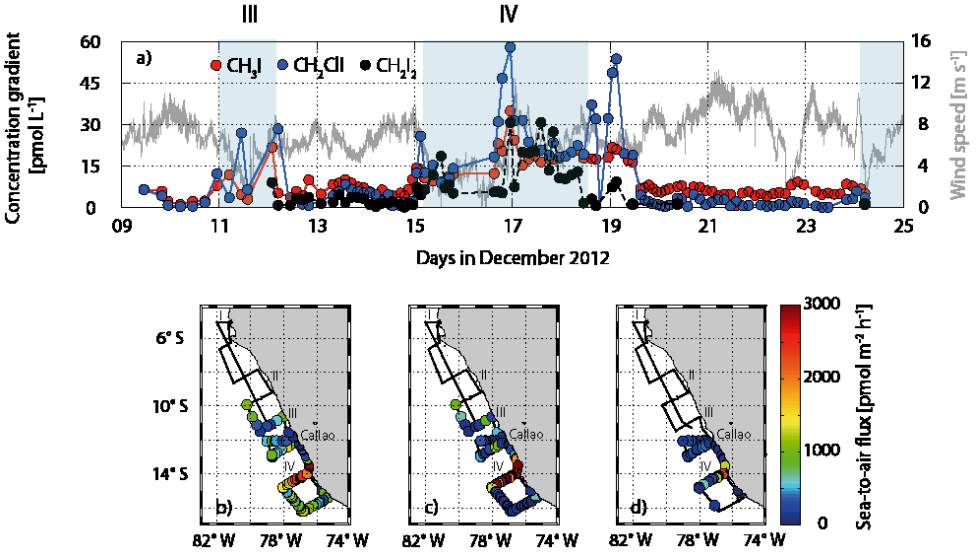

Fig. 6. The concentration gradient of CH_3I, CH_2ClI and CH_2I_2 along with wind speed (grey) is shown in a), while the sea-to-air flux is depicted in b) for CH_3I, c) for CH_2ClI and d) for CH_2I_2. Note the color bar on the right.

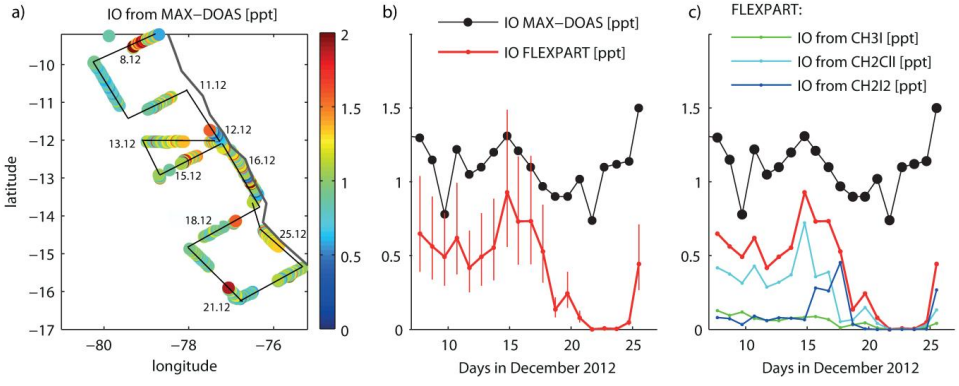

Fig. 7. MAX-DOAS measurements of IO during the M91 campaign along the cruise track are shown a). Daytime averaged IO values from MAX-DOAS and coincident FLEXPART values are provided in b). The vertical bars correspond to uncertainties associated with the inorganic iodine lifetime in the MABL (1 – 3 days) and the daytime fraction of IO to I_y (0.15 to 0.3).

Atmos. Chem. Phys. Discuss., doi:10.5194/acp-2016-39, 2016
Manuscript under review for journal Atmos. Chem. Phys.
Published: 14 March 2016

Atmospheric Chemistry and Physics Discussions

Contributions of the three oceanic iodocarbon sources to the modelled FLEXPART IO are also given in c).

Atmos. Chem. Phys. Discuss., doi:10.5194/acp-2016-39, 2016
Manuscript under review for journal Atmos. Chem. Phys.
Published: 14 March 2016

Atmospheric Chemistry and Physics Discussions

References

Abrahamsson, K., Lorén, A., Wulff, A., and Wangberg, S. A.: Air-sea exchange of halocarbons: the influence of diurnal and regional variations and distribution of pigments, Deep-Sea Res. Part II-Top. Stud. Oceanogr., 51, 2789-2805, 10.1016/j.dsr2.2004.09.005, 2004.

Amachi, S., Kamagata, Y., Kanagawa, T., and Muramatsu, Y.: Bacteria mediate methylation of iodine in marine and terrestrial environments, Applied and Environmental Microbiology, 67, 2718-2722, 10.1128/aem.67.6.2718-2722.2001, 2001.

Amachi, S.: Microbial contribution to global iodine cycling: volatilization, accumulation, reduction, oxidation, and sorption of iodine, Microbes Environ., 23, 269-276, 10.1264/jsme2.ME08548, 2008.

Archer, S. D., Goldson, L. E., Liddicoat, M. I., Cummings, D. G., and Nightingale, P. D.: Marked seasonality in the concentrations and sea-to-air flux of volatile iodocarbon compounds in the western English channel, J. Geophys. Res.-Oceans, 112, 10.1029/2006jc003963, 2007.

Bakun, A., and Weeks, S. J.: The marine ecosystem off Peru: what are the secrets of its fishery productivity and what might its future hold?, Prog. Oceanogr., 79, 290-299, http://dx.doi.org/10.1016/j.pocean.2008.10.027, 2008.

Bange, H. W.: Surface ocean - lower atmosphere study (solas) in the upwelling region of Peru, Bremerhaven, 69, 2013.

Barlow, R. G., Cummings, D. G., and Gibb, S. W.: Improved resolution of mono- and divinyl chlorophylls a and b and zeaxanthin and lutein in phytoplankton extracts using reverse phase c-8 hplc, Marine Ecology Progress Series, 161, 303-307, 10.3354/meps161303, 1997.

Bell, N., Hsu, L., Jacob, D. J., Schultz, M. G., Blake, D. R., Butler, J. H., King, D. B., Lobert, J. M., and Maier-Reimer, E.: Methyl iodide: atmospheric budget and use as a tracer of marine convection in global models, J. Geophys. Res.-Atmos., 107, 434010.1029/2001jd001151, 2002.

Bouwer, E. J., Rittmann, B. E., and McCarty, P. L.: Anaerobic degradation of halogenated 1- and 2-carbon organic compounds, Environ. Sci. Technol., 15, 596-599, 10.1021/es00087a012, 1981.

Brownell, D. K., Moore, R. M., and Cullen, J. J.: Production of methyl halides by prochlorococcus and synechococcus, Glob. Biogeochem. Cycles, 24, GB2002, 10.1029/2009gb003671, 2010.

Bruland, K. W., Rue, E. L., Smith, G. J., and DiTullio, G. R.: Iron, macronutrients and diatom blooms in the Peru upwelling regime: brown and blue waters of Peru, Mar. Chem., 93, 81-103, 10.1016/j.marchem.2004.06.011, 2005.

Burkholder, J. B., Curtius, J., Ravishankara, A. R., and Lovejoy, E. R.: Laboratory studies of the homogeneous nucleation of iodine oxides, Atmos. Chem. Phys., 4, 19-34, 10.5194/acp-4-19-2004, 2004.

Butler, J. H., King, D. B., Lobert, J. M., Montzka, S. A., Yvon-Lewis, S. A., Hall, B. D., Warwick, N. J., Mondeel, D. J., Aydin, M., and Elkins, J. W.: Oceanic distributions and emissions of short-lived halocarbons, Glob. Biogeochem. Cycles, 21, Gb1023

10.1029/2006gb002732, 2007.

Carpenter, L. J., Sturges, W. T., Penkett, S. A., Liss, P. S., Alicke, B., Hebestreit, K., and Platt, U.: Short-lived alkyl iodides and bromides at Mace Head, Ireland: links to biogenic sources and halogen oxide production, J. Geophys. Res.-Atmos., 104, 1679-1689, 1999.

Carpenter, L. J., Hopkins, J. R., Jones, C. E., Lewis, A. C., Parthipan, R., Wevill, D. J., Poissant, L., Pilote, M., and Constant, P.: Abiotic source of reactive organic halogens in the sub-arctic atmosphere?, Environ. Sci. Technol., 39, 8812-8816, 10.1021/es050918w, 2005.

Carpenter, L. J., Jones, C. E., Dunk, R. M., Hornsby, K. E., and Woeltjen, J.: Air-sea fluxes of biogenic bromine from the tropical and north Atlantic ocean, Atmos. Chem. Phys., 9, 1805-1816, 10.5194/acp-9-1805-2009, 2009.

Carpenter, L. J., MacDonald, S. M., Shaw, M. D., Kumar, R., Saunders, R. W., Parthipan, R., Wilson, J., and Plane, J. M. C.: Atmospheric iodine levels influenced by sea surface emissions of inorganic iodine, Nat. Geosci., 6, 108-111, 10.1038/ngeo1687, 2013.

Carpenter, L. J., and Reimann, S.: Ozone-depleting substances (odss) and other gases of interest to the montreal protocol, chapter 1 in scientific assessment of ozone depletion, World Meteorological Institution (WMO), Geneva, Report No. 55, 2014.

Chavez, F. P., Bertrand, A., Guevara-Carrasco, R., Soler, P., and Csirke, J.: The northern humboldt current system: brief history, present status and a view towards the future, Prog. Oceanogr., 79, 95-105, http://dx.doi.org/10.1016/j.pocean.2008.10.012, 2008.

Chuck, A. L., Turner, S. M., and Liss, P. S.: Oceanic distributions and air-sea fluxes of biogenic halocarbons in the open ocean, J. Geophys. Res.-Oceans, 110, C10022 10.1029/2004jc002741, 2005.

Clémer, K., Van Roozendael, M., Fayt, C., Hendrick, F., Hermans, C., Pinardi, G., Spurr, R., Wang, P., and De Mazière, M.: Multiple wavelength retrieval of tropospheric aerosol optical properties from maxdoas measurements in Beijing, Atmos. Meas. Tech., 3, 863-878, 10.5194/amt-3-863-2010, 2010.

Czeschel, R., Stramma, L., Weller, R. A., and Fischer, T.: Circulation, eddies, oxygen, and nutrient changes in the eastern tropical south Pacific ocean, Ocean Sci., 11, 455-470, 10.5194/os-11-455-2015, 2015.

Dee, D. P., Uppala, S. M., Simmons, A. J., Berrisford, P., Poli, P., Kobayashi, S., Andrae, U., Balmaseda, M. A., Balsamo, G., Bauer, P., Bechtold, P., Beljaars, A. C. M., van de Berg, L., Bidlot, J., Bormann, N., Delsol, C., Dragani, R., Fuentes, M., Geer, A. J., Haimberger, L., Healy, S. B., Hersbach, H., Hólm, E. V., Isaksen, L., Kållberg, P., Köhler, M., Matricardi, M., McNally, A. P., Monge-Sanz, B. M., Morcrette, J. J., Park, B. K., Peubey, C., de Rosnay, P., Tavolato, C., Thépaut, J. N., and Vitart, F.: The era-interim reanalysis: configuration and performance of the data assimilation system, Quarterly Journal of the Royal Meteorological Society, 137, 553-597, 10.1002/qj.828, 2011.

Dix, B., Baidara, S., Bresch, J. F., Hall, S. R., Schmidt, K. S., Wang, S. Y., and Volkamer, R.: Detection of iodine monoxide in the tropical free troposphere, Proc. Natl. Acad. Sci. U. S. A., 110, 2035-2040, 10.1073/pnas.1212386110, 2013.

Echevin, V., Aumont, O., Ledesma, J., and Flores, G.: The seasonal cycle of surface chlorophyll in the Peruvian upwelling system: a modelling study, Prog. Oceanogr., 79, 167-176, 10.1016/j.pocean.2008.10.026, 2008.

Engel, A., and Handel, N.: A novel protocol for determining the concentration and composition of sugars in particulate and in high molecular weight dissolved organic matter (hmw-dom) in seawater, Mar. Chem., 127, 180-191, 10.1016/j.marchem.2011.09.004, 2011.

Engel, A., and Galgani, L.: The organic sea surface microlayer in the upwelling region off Peru and implications for air-sea exchange processes, Biogeosciences Discuss., 12, 10579-10619, 10.5194/bgd-12-10579-2015, 2015.

Frieß, U., Monks, P. S., Remedios, J. J., Rozanov, A., Sinreich, R., Wagner, T., and Platt, U.: Max-doas o4 measurements: a new technique to derive information on atmospheric aerosols: 2. modeling studies, Journal of Geophysical Research: Atmosphere, 111, D14203, 10.1029/2005JD006618,, 2006.

Fuhlbrügge, S., Quack, B., Atlas, E., Fiehn, A., Hepach, H., and Krüger, K.: Meteorological constraints on oceanic halocarbons above the Peruvian upwelling, Atmos. Chem. Phys. Discuss., 15, 20597-20628, 10.5194/acpd-15-20597-2015, 2015a.

Fuhlbrügge, S., Quack, B., Tegtmeier, S., Atlas, E., Hepach, H., Shi, Q., Raimund, S., and Krüger, K.: The contribution of oceanic halocarbons to marine and free troposphere air over the tropical west Pacific, Atmos. Chem. Phys. Discuss., 15, 17887-17943, 10.5194/acpd-15-17887-2015, 2015b.

Fuse, H., Inoue, H., Murakami, K., Takimura, O., and Yamaoka, Y.: Production of free and organic iodine by roseovarius spp, FEMS Microbiology Letters, 229, 189-194, 10.1016/s0378-1097(03)00839-5, 2003.

Gómez Martín, J. C. G., Mahajan, A. S., Hay, T. D., Prados-Roman, C., Ordonez, C., MacDonald, S. M., Plane, J. M. C., Sorribas, M., Gil, M., Mora, J. F. P., Reyes, M. V. A., Oram, D. E., Leedham, E., and Saiz-Lopez, A.: Iodine chemistry in the eastern Pacific marine boundary layer, J. Geophys. Res.-Atmos., 118, 887-904, 10.1002/jgrd.50132, 2013.

Grossmann, K., Friess, U., Peters, E., Wittrock, F., Lampel, J., Yilmaz, S., Tschritter, J., Sommariva, R., von Glasow, R., Quack, B., Kruger, K., Pfeilsticker, K., and Platt, U.: Iodine monoxide in the western Pacific marine boundary layer, Atmos. Chem. Phys., 13, 3363-3378, 10.5194/acp-13-3363-2013, 2013.

Gschwend, P. M., Macfarlane, J. K., and Newman, K. A.: Volatile halogenated organic compounds released to seawater from temperate marine macroalgae, Science, 227, 1033-1035, 10.1126/science.227.4690.1033, 1985.

Hepach, H., Quack, B., Ziska, F., Fuhlbrügge, S., Atlas, E. L., Krüger, K., Peeken, I., and Wallace, D. W. R.: Drivers of diel and regional variations of halocarbon emissions from the

tropical north east Atlantic, Atmos. Chem. Phys., 14, 1255-1275, 10.5194/acp-14-1255-2014, 2014.

Hepach, H., Quack, B., Raimund, S., Fischer, T., Atlas, E. L., and Bracher, A.: Halocarbon emissions and sources in the equatorial Atlantic cold tongue, Biogeosciences, 12, 6369-6387, 10.5194/bg-12-6369-2015, 2015.

Hill, V. L., and Manley, S. L.: Release of reactive bromine and iodine from diatoms and its possible role in halogen transfer in polar and tropical oceans, Limnol. Oceanogr., 54, 812-822, 10.4319/lo.2009.54.3.0812, 2009.

Hossaini, R., Chipperfield, M. P., Montzka, S. A., Rap, A., Dhomse, S., and Feng, W.: Efficiency of short-lived halogens at influencing climate through depletion of stratospheric ozone, Nat. Geosci., 8, 186-190, 10.1038/ngeo2363, 2015.

Hughes, C., Franklin, D. J., and Malin, G.: Iodomethane production by two important marine cyanobacteria: prochlorococcus marinus (ccmp 2389) and synechococcus sp (ccmp 2370), Mar. Chem., 125, 19-25, 10.1016/j.marchem.2011.01.007, 2011.

Hughes, C., Johnson, M., Utting, R., Turner, S., Malin, G., Clarke, A., and Liss, P. S.: Microbial control of bromocarbon concentrations in coastal waters of the western Antarctic peninsula, Mar. Chem., 151, 35-46, 10.1016/j.marchem.2013.01.007, 2013.

Jones, C. E., and Carpenter, L. J.: Solar photolysis of CH_2I_2, CH_2ICl, and CH_2IBr in water, saltwater, and seawater, Environ. Sci. Technol., 39, 6130-6137, 10.1021/es050563g, 2005.

Jones, C. E., and Carpenter, L. J.: Chemical destruction of CH_3I, C_2H_5I, 1-C_3H_7I, and 2-C_3H_7I in saltwater, Geophys. Res. Lett., 34, 10.1029/2007gl029775, 2007.

Jones, C. E., Hornsby, K. E., Sommariva, R., Dunk, R. M., Von Glasow, R., McFiggans, G., and Carpenter, L. J.: Quantifying the contribution of marine organic gases to atmospheric iodine, Geophys. Res. Lett., 37, L1880410.1029/2010gl043990, 2010.

Karstensen, J., Stramma, L., and Visbeck, M.: Oxygen minimum zones in the eastern tropical Atlantic and Pacific oceans, Prog. Oceanogr., 77, 331-350, 10.1016/j.pocean.2007.05.009, 2008.

Krüger, K., and Quack, B.: Introduction to special issue: the TransBrom Sonne expedition in the tropical west Pacific, Atmos. Chem. Phys., 13, 9439-9446, 10.5194/acp-13-9439-2013, 2013.

Lampel, J., Frieß, U., and Platt, U.: The impact of vibrational raman scattering of air on doas measurements of atmospheric trace gases, Atmos. Meas. Tech., 8, 3767-3787, 10.5194/amt-8-3767-2015, 2015.

Lawler, M. J., Mahajan, A. S., Saiz-Lopez, A., and Saltzman, E. S.: Observations of I_2 at a remote marine site, Atmos. Chem. Phys., 14, 2669-2678, 10.5194/acp-14-2669-2014, 2014.

Lin, C. Y., and Manley, S. L.: Bromoform production from seawater treated with bromoperoxidase, Limnol. Oceanogr., 57, 1857-1866, 10.4319/1o.2012.57.06.1857, 2012.

Liu, Y. N., Yvon-Lewis, S. A., Thornton, D. C. O., Campbell, L., and Bianchi, T. S.: Spatial distribution of brominated very short-lived substances in the eastern Pacific, J. Geophys. Res.-Oceans, 118, 2318-2328, 10.1002/jgrc.20183, 2013.

Liu, Y. N., Thornton, D. C. O., Bianchi, T. S., Arnold, W. A., Shields, M. R., Chen, J., and Yvon-Lewis, S. A.: Dissolved organic matter composition drives the marine production of brominated very short-lived substances, Environ. Sci. Technol., 49, 3366-3374, 10.1021/es505464k, 2015.

Mahajan, A. S., Plane, J. M. C., Oetjen, H., Mendes, L., Saunders, R. W., Saiz-Lopez, A., Jones, C. E., Carpenter, L. J., and McFiggans, G. B.: Measurement and modelling of tropospheric reactive halogen species over the tropical Atlantic ocean, Atmos. Chem. Phys., 10, 4611-4624, 10.5194/acp-10-4611-2010, 2010.

Mahajan, A. S., Gómez Martín, J. C., Hay, T. D., Royer, S. J., Yvon-Lewis, S., Liu, Y., Hu, L., Prados-Roman, C., Ordóñez, C., Plane, J. M. C., and Saiz-Lopez, A.: Latitudinal distribution of reactive iodine in the eastern Pacific and its link to open ocean sources, Atmos. Chem. Phys., 12, 11609-11617, 10.5194/acp-12-11609-2012, 2012.

Manley, S. L., and de la Cuesta, J. L.: Methyl iodide production from marine phytoplankton cultures, Limnol. Oceanogr., 42, 142-147, 10.4319/lo.1997.42.1.0142, 1997.

Martino, M., Liss, P. S., and Plane, J. M. C.: Wavelength-dependence of the photolysis of diiodomethane in seawater, Geophys. Res. Lett., 33, 10.1029/2005gl025424, 2006.

Martino, M., Mills, G. P., Woeltjen, J., and Liss, P. S.: A new source of volatile organoiodine compounds in surface seawater, Geophys. Res. Lett., 36, 10.1029/2008gl036334, 2009.

Moore, R. M., and Zafiriou, O. C.: Photochemical production of methyl-iodide in seawater, J. Geophys. Res.-Atmos., 99, 16415-16420, 10.1029/94jd00786, 1994.

Moore, R. M., Geen, C. E., and Tait, V. K.: Determination of henry law constants for a suite of naturally-occurring halogenated methanes in seawater, Chemosphere, 30, 1183-1191, 10.1016/0045-6535(95)00009-w, 1995.

Moore, R. M., Webb, M., Tokarczyk, R., and Wever, R.: Bromoperoxidase and iodoperoxidase enzymes and production of halogenated methanes in marine diatom cultures, J. Geophys. Res.-Oceans, 101, 20899-20908, 10.1029/96jc01248, 1996.

Moore, R. M., and Groszko, W.: Methyl iodide distribution in the ocean and fluxes to the atmosphere, J. Geophys. Res.-Oceans, 104, 11163-11171, 10.1029/1998jc900073, 1999.

Nightingale, P. D., Malin, G., Law, C. S., Watson, A. J., Liss, P. S., Liddicoat, M. I., Boutin, J., and Upstill-Goddard, R. C.: In situ evaluation of air-sea gas exchange parameterizations using novel conservative and volatile tracers, Glob. Biogeochem. Cycles, 14, 373-387, 10.1029/1999gb900091, 2000.

O'Dowd, C. D., Jimenez, J. L., Bahreini, R., Flagan, R. C., Seinfeld, J. H., Hameri, K., Pirjola, L., Kulmala, M., Jennings, S. G., and Hoffmann, T.: Marine aerosol formation from biogenic iodine emissions, Nature, 417, 632-636, 10.1038/nature00775, 2002.

Peters, C., Pechtl, S., Stutz, J., Hebestreit, K., Honninger, G., Heumann, K. G., Schwarz, A., Winterlik, J., and Platt, U.: Reactive and organic halogen species in three different European coastal environments, Atmos. Chem. Phys., 5, 3357-3375, 2005.

Prados-Roman, C., Cuevas, C. A., Hay, T., Fernandez, R. P., Mahajan, A. S., Royer, S. J., Galí, M., Simó, R., Dachs, J., Großmann, K., Kinnison, D. E., Lamarque, J. F., and Saiz-Lopez, A.: Iodine oxide in the global marine boundary layer, Atmos. Chem. Phys., 15, 583-593, 10.5194/acp-15-583-2015, 2015.

Quack, B., and Wallace, D. W. R.: Air-sea flux of bromoform: controls, rates, and implications, Glob. Biogeochem. Cycles, 17, 10.1029/2002gb001890, 2003.

Quack, B., Atlas, E., Petrick, G., Stroud, V., Schauffler, S., and Wallace, D. W. R.: Oceanic bromoform sources for the tropical atmosphere, Geophys. Res. Lett., 31, 10.1029/2004gl020597, 2004.

Quack, B., Atlas, E., Petrick, G., and Wallace, D. W. R.: Bromoform and dibromomethane above the Mauritanian upwelling: atmospheric distributions and oceanic emissions, J. Geophys. Res.-Atmos., 112, 10.1029/2006jd007614, 2007a.

Quack, B., Peeken, I., Petrick, G., and Nachtigall, K.: Oceanic distribution and sources of bromoform and dibromomethane in the Mauritanian upwelling, J. Geophys. Res.-Oceans, 112, 10.1029/2006jc003803, 2007b.

Raimund, S., Quack, B., Bozec, Y., Vernet, M., Rossi, V., Garcon, V., Morel, Y., and Morin, P.: Sources of short-lived bromocarbons in the Iberian upwelling system, Biogeosciences, 8, 1551-1564, 10.5194/bg-8-1551-2011, 2011.

Read, K. A., Mahajan, A. S., Carpenter, L. J., Evans, M. J., Faria, B. V. E., Heard, D. E., Hopkins, J. R., Lee, J. D., Moller, S. J., Lewis, A. C., Mendes, L., McQuaid, J. B., Oetjen, H., Saiz-Lopez, A., Pilling, M. J., and Plane, J. M. C.: Extensive halogen-mediated ozone destruction over the tropical Atlantic ocean, Nature, 453, 1232-1235, 10.1038/nature07035, 2008.

Richter, U., and Wallace, D. W. R.: Production of methyl iodide in the tropical Atlantic ocean, Geophys. Res. Lett., 31, 10.1029/2004gl020779, 2004.

Saiz-Lopez, A., Lamarque, J. F., Kinnison, D. E., Tilmes, S., Ordonez, C., Orlando, J. J., Conley, A. J., Plane, J. M. C., Mahajan, A. S., Santos, G. S., Atlas, E. L., Blake, D. R., Sander, S. P., Schauffler, S., Thompson, A. M., and Brasseur, G.: Estimating the climate significance of halogen-driven ozone loss in the tropical marine troposphere, Atmos. Chem. Phys., 12, 3939-3949, 10.5194/acp-12-3939-2012, 2012a.

Saiz-Lopez, A., Plane, J. M. C., Baker, A. R., Carpenter, L. J., von Glasow, R., Martin, J. C. G., McFiggans, G., and Saunders, R. W.: Atmospheric chemistry of iodine, Chem. Rev., 112, 1773-1804, 10.1021/cr200029u, 2012b.

Saiz-Lopez, A., Fernandez, R. P., Ordóñez, C., Kinnison, D. E., Gómez Martín, J. C., Lamarque, J. F., and Tilmes, S.: Iodine chemistry in the troposphere and its effect on ozone, Atmos. Chem. Phys., 14, 13119-13143, 10.5194/acp-14-13119-2014, 2014.

Saiz-Lopez, A., Baidar, S., Cuevas, C. A., Koenig, T. K., Fernandez, R. P., Dix, B., Kinnison, D. E., Lamarque, J. F., and Rodriguez-LLoveras, T. L.: Injection of iodine to the stratosphere, Geophys. Res. Lett., 42, 6852-6859, 10.1002/2015GL064796, 2015.

Salawitch, R. J.: Atmospheric chemistry - biogenic bromine, Nature, 439, 275-277, 10.1038/439275a, 2006.

Scarratt, M. G., and Moore, R. M.: Production of methyl bromide and methyl chloride in laboratory cultures of marine phytoplankton II, Mar. Chem., 59, 311-320, 10.1016/s0304-4203(97)00092-3, 1998.

Schauffler, S. M., Atlas, E. L., Flocke, F., Lueb, R. A., Stroud, V., and Travnicek, W.: Measurements of bromine containing organic compounds at the tropical tropopause, Geophys. Res. Lett., 25, 317-320, 10.1029/98GL00040, 1998.

Schönhardt, A., Richter, A., Wittrock, F., Kirk, H., Oetjen, H., Roscoe, H. K., and Burrows, J. P.: Observations of iodine monoxide columns from satellite, Atmos. Chem. Phys., 8, 637-653, 10.5194/acp-8-637-2008, 2008.

Shi, Q., Marandino, C., Petrick, G., Quack, B., and Wallace, D.: A time series of incubation experiments to examine the production and loss of CH_3I in surface seawater, J. Geophys. Res.-Oceans, 119, 8242-8254, 10.1002/2014jc010223, 2014.

Smythe-Wright, D., Boswell, S. M., Breithaupt, P., Davidson, R. D., Dimmer, C. H., and Diaz, L. B. E.: Methyl iodide production in the ocean: implications for climate change, Glob. Biogeochem. Cycles, 20, 10.1029/2005gb002642, 2006.

Sommariva, R., and von Glasow, R.: Multiphase halogen chemistry in the tropical Atlantic ocean, Environ. Sci. Technol., 46, 10429-10437, 10.1021/es300209f, 2012.

Stemmler, I., Hense, I., Quack, B., and Maier-Reimer, E.: Methyl iodide production in the open ocean, Biogeosciences, 11, 4459-4476, 10.5194/bg-11-4459-2014, 2014.

Stohl, A., and Trickl, T.: A textbook example of long-range transport: simultaneous observation of ozone maxima of stratospheric and North American origin in the free troposphere over Europe, J. Geophys. Res.-Atmos., 104, 30445-30462, 10.1029/1999jd900803, 1999.

Stohl, A., Forster, C., Frank, A., Seibert, P., and Wotawa, G.: Technical note: the lagrangian particle dispersion model flexpart version 6.2, Atmos. Chem. Phys., 5, 2461-2474, 10.5194/acp-5-2461-2005, 2005.

Tanhua, T., Fogelqvist, E., and Basturk, O.: Reduction of volatile halocarbons in anoxic seawater, results from a study in the Black Sea, Mar. Chem., 54, 159-170, 10.1016/0304-4203(96)00005-9, 1996.

Taylor, B. B., Torrecilla, E., Bernhardt, A., Taylor, M. H., Peeken, I., Rottgers, R., Piera, J., and Bracher, A.: Bio-optical provinces in the eastern Atlantic ocean and their biogeographical relevance, Biogeosciences, 8, 3609-3629, 10.5194/bg-8-3609-2011, 2011.

Tegtmeier, S., Krüger, K., Quack, B., Atlas, E., Blake, D. R., Boenisch, H., Engel, A., Hepach, H., Hossaini, R., Navarro, M. A., Raimund, S., Sala, S., Shi, Q., and Ziska, F.: The contribution of oceanic methyl iodide to stratospheric iodine, Atmos. Chem. Phys., 13, 11869-11886, 10.5194/acp-13-11869-2013, 2013.

Theiler, R., Cook, J. C., and Hager, L. P.: Halohydrocarbon synthesis by bromoperoxidase, Science, 202, 1094-1096, 10.1126/science.202.4372.1094, 1978.

Tokarczyk, R., and Moore, R. M.: Production of volatile organohalogens by phytoplankton cultures, Geophys. Res. Lett., 21, 285-288, 10.1029/94GL00009, 1994.

Tomczak, M., and Godfrey, J. S.: Regional oceanography: an introduction, 2 ed., Daya Publishing House, Delhi, 2005.

Uitz, J., Claustre, H., Morel, A., and Hooker, S. B.: Vertical distribution of phytoplankton communities in open ocean: an assessment based on surface chlorophyll, J. Geophys. Res.-Oceans, 111, 10.1029/2005jc003207, 2006.

Varner, R. K., Zhou, Y., Russo, R. S., Wingenter, O. W., Atlas, E., Stroud, C., Mao, H., Talbot, R., and Sive, B. C.: Controls on atmospheric chloroiodomethane (CH_2ClI) in marine environments, J. Geophys. Res.-Atmos., 113, D10303

10.1029/2007jd008889, 2008.

Vidussi, F., Claustre, H., Manca, B. B., Luchetta, A., and Marty, J. C.: Phytoplankton pigment distribution in relation to upper thermocline circulation in the eastern Mediterranean Sea during winter, J. Geophys. Res.-Oceans, 106, 19939-19956, 10.1029/1999jc000308, 2001.

von Glasow, R., von Kuhlmann, R., Lawrence, M. G., Platt, U., and Crutzen, P. J.: Impact of reactive bromine chemistry in the troposphere, Atmos. Chem. Phys., 4, 2481-2497, 10.5194/acp-4-2481-2004, 2004.

White, R. H.: Analysis of dimethyl sulfonium compounds in marine-algae, J. Mar. Res., 40, 529-536, 1982.

Wurl, O., Wurl, E., Miller, L., Johnson, K., and Vagle, S.: Formation and global distribution of sea-surface microlayers, Biogeosciences, 8, 121-135, 10.5194/bg-8-121-2011, 2011.

Yamamoto, H., Yokouchi, Y., Otsuki, A., and Itoh, H.: Depth profiles of volatile halogenated hydrocarbons in seawater in the Bay of Bengal, Chemosphere, 45, 371-377, 10.1016/s0045-6535(00)00541-5, 2001.

Yilmaz, S.: Retrieval of atmospheric aerosol and trace gas vertical profiles using multi-axis differential optical absorption spectroscopy, Institut für Umweltphysik, Universität Heidelberg, Heidelberg, Heidelberg, 2012.

Yokouchi, Y., Saito, T., Ooki, A., and Mukai, H.: Diurnal and seasonal variations of iodocarbons (CH_2ClI, CH_2I_2, CH_3I, and C_2H_5I) in the marine atmosphere, J. Geophys. Res.-Atmos., 116, 10.1029/2010jd015252, 2011.

Yokouchi, Y., Ooki, A., Hashimoto, S., and Itoh, H.: A study on the production and emission of marine-derived volatile halocarbons, in: Western pacific air-sea interactions study, edited by: Uematsu, M., Yokouchi, Y., Watanabe, Y. W., Takeda, S., and Yamanaka, Y., TERRAPUB, Okusawa, 1-25, 2014.

Zafiriou, O. C.: Reaction of methyl halides with seawater and marine aerosols, J. Mar. Res., 33, 75-81, 1975.

Ziska, F., Quack, B., Abrahamsson, K., Archer, S. D., Atlas, E., Bell, T., Butler, J. H., Carpenter, L. J., Jones, C. E., Harris, N. R. P., Hepach, H., Heumann, K. G., Hughes, C., Kuss, J., Krüger, K., Liss, P., Moore, R. M., Orlikowska, A., Raimund, S., Reeves, C. E., Reifenhäuser, W., Robinson, A. D., Schall, C., Tanhua, T., Tegtmeier, S., Turner, S., Wang, L., Wallace, D., Williams, J., Yamamoto, H., Yvon-Lewis, S., and Yokouchi, Y.: Global sea-to-air flux climatology for bromoform, dibromomethane and methyl iodide, Atmos. Chem. Phys., 13, 8915-8934, 10.5194/acp-13-8915-2013, 2013.

4. Synthesis and Outlook

This thesis investigated the influences of source regions, marine emissions and meteorological conditions on atmospheric VSLS, in particular bromoform, dibromomethane and methyl iodide. For this, ship-based observations and transport modelling were employed in the six adjacent manuscripts. The research area covered the tropical and subtropical Northeast Atlantic and the tropical West and Southeast Pacific including ocean upwelling, coastal areas and open ocean regimes. The following questions were addressed in this thesis and are summarized in the following synthesis:

1. **What are the sources for elevated atmospheric VSLS in oceanic upwelling regimes?**

Two different oceanic upwelling regimes along Mauritania and Peru were investigated and identified to be important natural source regions for atmospheric VSLS. High oceanic concentrations led to elevated oceanic emissions and atmospheric mixing ratios of bromoform, dibromomethane and methyl iodide. Previous studies showed that the atmospheric mixing ratios were too high to be explained only by oceanic emissions and revealed the need for an additional VSLS source. This source

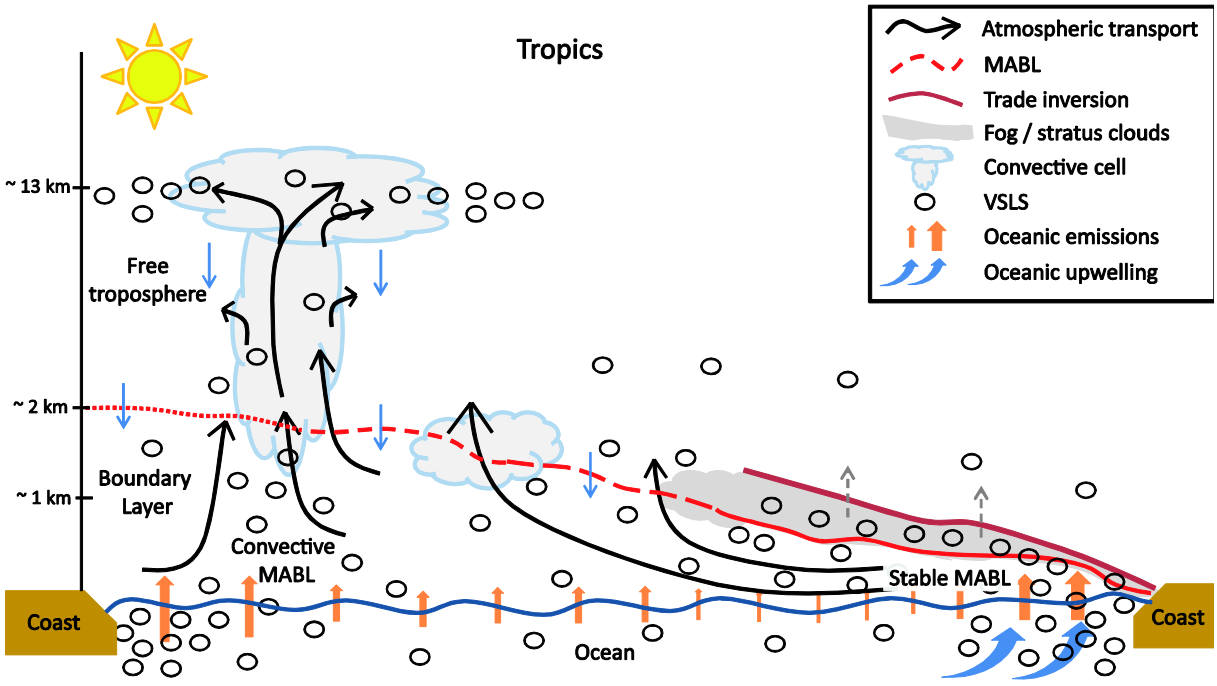

Figure 4-1: Schematic scheme for the tropics: Oceanic emissions from oceanic upwelling regions are trapped below the MABL and trade inversion. Once the concentration gradient between the MABL and the surface water decreases, the oceanic emissions decrease as well. In contrast within convective regions, surface air masses are transported rapidly to the free and upper troposphere and can therefore lead to lower VSLS concentrations in the MABL.

was not found by the investigations of this thesis; however, the results showed that atmospheric conditions, in addition to elevated oceanic emissions, strongly contributed to elevated atmospheric VSLS mixing ratios. In particular, a stable MABL together with a trade inversion was identified to play an important role for VSLS in the lowermost atmosphere above oceanic upwelling regions in the tropics.

2. **How do meteorological conditions influence atmospheric VSLS?**

Oceanic VSLS that are emitted into the atmosphere are first mixed within the MABL. The intensity of their distribution to the free troposphere was identified to depend strongly on the oceanic and atmospheric regimes. Above oceanic upwelling intense atmospheric surface inversions caused by warm and moist air flow above cold upwelling water can, in case of low wind speeds, lead to a very stable, low and isolated MABL with suppressed vertical mixing. In this case, the surface air masses are trapped at the ground and are strongly enriched by oceanic VSLS emissions. The trade inversions (at ~1 km height) above oceanic upwelling regions were identified as an additional vertical transport barrier for the VSLS in this thesis. In particular along the Peruvian coast, the meteorological and geographical conditions led to a predominantly meridional flow of VSLS enriched surface air masses below the trade inversion. The suppressed mixing was also reflected in elevated atmospheric humidity, which shows a significant anti-correlation at the surface to the MABL height and a strong decrease in the vertical profiles at the height of the trade inversion. In contrast, tropical open ocean regions with high sea surface temperatures (SSTs) as was observed in the South China and Sulu Seas during early winter monsoon conditions benefit a convective, instable, well ventilated MABL with pronounced vertical air mass transport through it, which was reflected by elevated humidity in the free troposphere. The convective conditions distributed the VSLS emissions rapidly within the MABL and the free troposphere and transported them even to the upper troposphere. Thus, surface VSLS observations in these regions revealed low atmospheric mixing ratios despite elevated oceanic emissions.

3. **Which factors influence the spatial and temporal variability of VSLS emissions and atmospheric concentrations?**

This thesis revealed that different oceanic and atmospheric regimes lead to a strong regional variability of VSLS emissions and atmospheric mixing ratios. Geographical conditions, like the Andes as a zonal wind barrier, or the Sahara desert as heat provider, shape the atmospheric and oceanic regimes and their interaction. Observations of VSLS emissions and atmospheric concentrations revealed spatial variations between open ocean, coastal and oceanic upwelling regimes in the tropical and subtropical oceans with highest emissions in the South China and Sulu Seas and highest

atmospheric concentrations above the Mauritanian upwelling. Diurnal variations of VSLS emissions and atmospheric abundances were observed in all oceanic regimes. These variations were mainly influenced by variations in oceanic concentrations, wind speed, height and stability of the MABL and wind direction, e.g. due to sea-breezes. The wind speed, MABL height and lower atmospheric stability affect the atmospheric mixing ratios which in return affect the oceanic emissions through the influence on the concentration gradient between sea water and atmosphere.

Outlook

The findings of this thesis are based on new observations and estimates, which show that the characteristic of the MABL in combination with oceanic emissions and coastal sources regulate the halogen budget of the atmosphere. The result, that different oceanic, atmospheric and geographical regimes lead to varying VSLS emissions and atmospheric abundances opens additional questions and directs future research needs. A consolidation of the findings, e.g. the contribution of oceanic emissions to the atmospheric budgets can only be achieved by filling the large spatial and temporal data gaps in many open ocean, coastal and upwelling regions of the world's oceans, which would also help to improve existing global VSLS emission budgets and the estimates of their contribution to the tropospheric and stratospheric halogen budget. Since climate changes are expected to impact marine VSLS production and emissions in the future, an improved VSLS climatology would also contribute to better estimates of oceanic future emissions. Since the oceanic emissions are a major parameter of this thesis and are calculated from other parameters, e.g. oceanic and atmospheric concentrations and wind speed, the applicability of the computed fluxes should be validated by direct flux measurements of bromoform, dibromomethane and methyl iodide. This technique is not available yet, but should be developed as new detection capabilities arise. Another factor influencing the results of this thesis is the accuracy of the atmospheric transport calculations, which was simulated with the Lagrangian transport model FLEXPART using ERA-Interim reanalysis. Comparing the projected vertical atmospheric mixing ratio profiles of VSLS from oceanic in-situ observations with the aircraft atmospheric VSLS abundances in the tropical West Pacific revealed promising results. Further developments in transport modelling (e.g. boundary layer and convection parameterizations) and in global meteorological reanalysis (e.g. SPARC Reanalysis Intercomparison Project, SRIP) are needed and will lead to improvements of the understanding of the contribution of oceanic VSLS emissions to the atmospheric abundances.

5. Bibliography

Aron, R.: Mixing height - an inconsistent indicator of potential air-pollution concentrations, Atmospheric Environment, 17, 2193-2197, 10.1016/0004-6981(83)90215-9, 1983.

Aron, R.: Mixing height - an inconsistent indicator of potential air-pollution concentrations - reply, Atmospheric Environment, 19, 1732-1733, 10.1016/0004-6981(85)90226-4, 1985.

Aschmann, J., Sinnhuber, B., Atlas, E., and Schauffler, S.: Modeling the transport of very short-lived substances into the tropical upper troposphere and lower stratosphere, Atmospheric Chemistry and Physics, 9, 9237-9247, 2009.

Aschmann, J., Sinnhuber, B., Chipperfield, M., and Hossaini, R.: Impact of deep convection and dehydration on bromine loading in the upper troposphere and lower stratosphere, Atmospheric Chemistry and Physics, 11, 2671-2687, 10.5194/acp-11-2671-2011, 2011.

Ashfold, M., Harris, N., Atlas, E., Manning, A., and Pyle, J.: Transport of short-lived species into the Tropical Tropopause Layer, Atmospheric Chemistry and Physics, 12, 6309-6322, 10.5194/acp-12-6309-2012, 2012.

Bell, N., Hsu, L., Jacob, D., Schultz, M., Blake, D., Butler, J., King, D., Lobert, J., and Maier-Reimer, E.: Methyl iodide: Atmospheric budget and use as a tracer of marine convection in global models, Journal of Geophysical Research-Atmospheres, 107, 10.1029/2001JD001151, 2002.

Brinckmann, S., Engel, A., Bonisch, H., Quack, B., and Atlas, E.: Short-lived brominated hydrocarbons - observations in the source regions and the tropical tropopause layer, Atmospheric Chemistry and Physics, 12, 1213-1228, 10.5194/acp-12-1213-2012, 2012.

Butler, J., King, D., Lobert, J., Montzka, S., Yvon-Lewis, S., Hall, B., Warwick, N., Mondeel, D., Aydin, M., and Elkins, J.: Oceanic distributions and emissions of short-lived halocarbons, Global Biogeochemical Cycles, 21, 10.1029/2006GB002732, 2007.

Carpenter, L., Wevill, D., Hopkins, J., Dunk, R., Jones, C., Hornsby, K., and McQuaid, J.: Bromoform in tropical Atlantic air from 25 degrees N to 25 degrees S, Geophysical Research Letters, 34, 10.1029/2007GL029893, 2007.

Carpenter, L., Jones, C., Dunk, R., Hornsby, K., and Woeltjen, J.: Air-sea fluxes of biogenic bromine from the tropical and North Atlantic Ocean, Atmospheric Chemistry and Physics, 9, 1805-1816, 2009.

Carpenter, L., and Reimann, S.: Chapter 1: Update on Ozone-Depleting Substances (ODSs) and Other Gases of Interest to the Montreal Protocol, in: Scientific Assessment of Ozone Depletion 2014, Vienna, 2015.

Chubachi, S.: Preliminary result of ozone observations at Syowa station from February 1982 to January 1983, Memoirs of National Institute of Polar Research. Special Issue, 13 - 19, 1984.

Chuck, A., Turner, S., and Liss, P.: Oceanic distributions and air-sea fluxes of biogenic halocarbons in the open ocean, Journal of Geophysical Research-Oceans, 110, 10.1029/2004JC002741, 2005.

Class, T., and Ballschmiter, K.: Chemistry of organic traces in air: 8. Sources and distribution of bromochloromethanes and bromochloromethanes in marine air and surfacewater of the Atlantic Ocean, Journal of Atmospheric Chemistry, 6, 35-46, 10.1007/BF00048330, 1988.

Colling, A.: Ocean circulation, 2nd ed., Open University Course Team, 2001.

Crutzen, P.: Ozone production rates in an oxygen-hydrogen-nitrogen oxide atmosphere, Journal of Geophysical Research, 76, 7311-&, 10.1029/JC076i030p07311, 1971.

Dee, D., Uppala, S., Simmons, A., Berrisford, P., Poli, P., Kobayashi, S., Andrae, U., Balmaseda, M., Balsamo, G., Bauer, P., Bechtold, P., Beljaars, A., van de Berg, L., Bidlot, J., Bormann, N., Delsol, C., Dragani, R., Fuentes, M., Geer, A., Haimberger, L., Healy, S., Hersbach, H., Holm, E., Isaksen, L., Kallberg, P., Kohler, M., Matricardi, M., McNally, A., Monge-Sanz, B., Morcrette, J., Park, B., Peubey, C., de Rosnay, P., Tavolato, C., Thepaut, J., and Vitart, F.: The ERA-Interim reanalysis: configuration and performance of the data assimilation system, Quarterly Journal of the Royal Meteorological Society, 137, 553-597, 10.1002/qj.828, 2011.

Dorf, M., Butler, J., Butz, A., Camy-Peyret, C., Chipperfield, M., Kritten, L., Montzka, S., Simmes, B., Weidner, F., and Pfeilsticker, K.: Long-term observations of stratospheric bromine reveal slow down in growth, Geophysical Research Letters, 33, 10.1029/2006GL027714, 2006.

Farman, J. C., Gardiner, B. G., and Shanklin, J. D.: Large losses of total ozone in Antarctica reveal seasonal ClOx/NOx interaction, Nature, 315, 207-210, 10.1038/315207a0, 1985.

Fogelqvist, E.: Carbon-tetrachloride, tetrachloroethylene, 1,1,1-trichloroethane and bromoform in arctic seawater, Journal of Geophysical Research-Oceans, 90, 9181-9193, 10.1029/JC090iC05p09181, 1985.

Forster, C., Stohl, A., and Seibert, P.: Parameterization of convective transport in a Lagrangian particle dispersion model and its evaluation, Journal of Applied Meteorology and Climatology, 46, 403-422, 10.1175/JAM2470.1, 2007.

Fuhlbrügge, S., Krüger, K., Quack, B., Atlas, E., Hepach, H., and Ziska, F.: Impact of the marine atmospheric boundary layer conditions on VSLS abundances in the eastern tropical and subtropical North Atlantic Ocean, Atmospheric Chemistry and Physics, 13, 6345-6357, 10.5194/acp-13-6345-2013, 2013.

Fuhlbrügge, S., Quack, B., Atlas, E., Fiehn, A., Hepach, H., and Krüger, K.: Meteorological constraints on oceanic halocarbons above the Peruvian Upwelling, Atmos. Chem. Phys. Discuss., 15, 20597–20628, 10.5194/acpd-15-20597-2015, 2015a.

Fuhlbrügge, S., Quack, B., Tegtmeier, S., Atlas, E., Hepach, H., Shi, Q., Raimund, S., and Krüger, K.: The contribution of oceanic very short lived halocarbons to marine and free troposphere air over the tropical West Pacific, Atmos. Chem. Phys. Discuss., 15, 17887-17943, 10.5194/acpd-15-17887-2015, 2015b.

Garbe, C. S., Rutgersson, A., Boutin, J., de Leeuw, G., Delille, B., Fairall, C. W., Gruber, N., Hare, J. E., Ho, D. T., Johnson, M. T., Nightingale, P. D., Pettersson, H., Piskozub, J., Sahlée, E., Tsai, W.-T., Ward, B., Woolf, D. K., and Zappa, C. J.: Transfer across the air-sea interface, in: Ocean-atmosphere interactions of gases and particles, in: Ocean-Atmosphere Interactions of Gases and Particles, edited by: Liss, P. S., and Johnson, M. T., Springer Earth System Sciences, Norwhich, UK, 55-112, 2014.

Garratt, J.: The internal boundary-layer - a review, Boundary-Layer Meteorology, 50, 171-203, 10.1007/BF00120524, 1990.

Gschwend, P., Macfarlane, J., and Newman, K.: Volatile halogenated organic-compounds released to seawater from temperate marine macroalgae, Science, 227, 1033-1035, 10.1126/science.227.4690.1033, 1985.

Happell, J., and Wallace, D.: Methyl iodide in the Greenland/Norwegian Seas and the tropical Atlantic Ocean: Evidence for photochemical production, Geophysical Research Letters, 23, 2105-2108, 10.1029/96GL01764, 1996.

Hayduk, W., and Laudie, H.: Prediction of diffusion-coefficients for nonelectrolytes in dilute aqueous-solutions, Aiche Journal, 20, 611-615, 10.1002/aic.690200329, 1974.

Hepach, H., Quack, B., Ziska, F., Fuhlbrügge, S., Atlas, E., Krüger, K., Peeken, I., and Wallace, D. W. R.: Drivers of diel and regional variations of halocarbon emissions from the tropical North East Atlantic, Atmos. Chem. Phys., 14, 10.5194/acp-14-1255-2014, 2014.

Hepach, H., Quack, B., Tegtmeier, S., Engel, A., Bracher, A., Fuhlbrügge, S., Raimund, S., Lampel, J., L., G., and Krüger, K.: Contributions of biogenic halogenated compounds from the Peruvian upwelling to the tropical troposphere, to be submitted, 2015.

Holton, J., and Hakim, G.: Chapter 5: The Planetary Boundary Layer, in: An Introduction to Dynamic Meteorology, 5th ed., Elsevier Inc., Oxford, 2012.

Holzworth, C.: Estimates of mean maximum mixing depths in the contiguous United States, Monthly Weather Review, 92, 235-242, 1964.

Holzworth, C.: Mixing depths, wind speeds and air pollution potential for selected locations in the United States, Journal of Applied Meteorology, 6, 1039-1044, 1967.

Holzworth, C.: Mixing depths, wind speeds, and potential for urban pollution throughout the contiguous United States, EPA, Office of Air Programs Publ. AP-101, 118pp., 1972.

Hossaini, R., Chipperfield, M., Monge-Sanz, B., Richards, N., Atlas, E., and Blake, D.: Bromoform and dibromomethane in the tropics: a 3-D model study of chemistry and transport, Atmospheric Chemistry and Physics, 10, 719-735, 10.5194/acp-10-719-2010, 2010.

Hossaini, R., Chipperfield, M., Dhomse, S., Ordonez, C., Saiz-Lopez, A., Abraham, N., Archibald, A., Braesicke, P., Telford, P., Warwick, N., Yang, X., and Pyle, J.: Modelling future changes to the stratospheric source gas injection of biogenic bromocarbons, Geophysical Research Letters, 39, 10.1029/2012GL053401, 2012.

Hughes, C., Franklin, D., and Malin, G.: Iodomethane production by two important marine cyanobacteria: Prochlorococcus marinus (CCMP 2389) and Synechococcus sp (CCMP 2370), Marine Chemistry, 125, 19-25, 10.1016/j.marchem.2011.01.007, 2011.

Höflich, O.: The meteorological effects of cold upwelling water areas, Geoforum, 3, 35-46, 10.1016/0016-7185(72)90084-X, 1972.

IHO: Limits of Ocean and Seas, 3rd Edition, International Hydrographic Organization, Monaco, Monte Carlo, 1953.

Kerkweg, A., Jockel, P., Warwick, N., Gebhardt, S., Brenninkmeijer, C., and Lelieveld, J.: Consistent simulation of bromine chemistry from the marine boundary layer to the stratosphere - Part 2: Bromocarbons, Atmospheric Chemistry and Physics, 8, 5919-5939, 2008.

Ko, M. K. W., and Poulet, G.: Chapter 2: Very Short-Lived Halogen and Sulfur Substances, in: Scientific Assessment of Ozone Depletion: 2002, 2003.

Krüger, K., and Quack, B.: Introduction to special issue: the TransBrom Sonne expedition in the tropical West Pacific, Atmospheric Chemistry and Physics, 13, 9439-9446, 10.5194/acp-13-9439-2013, 2013.

Law, K. S., and Sturges, W. T.: Chapter 2: Halogenated Very Short-Lived Substances, in: Scientific Assessment of Ozone Depletion: 2006, 2007.

Leedham, E., Hughes, C., Keng, F., Phang, S., Malin, G., and Sturges, W.: Emission of atmospherically significant halocarbons by naturally occurring and farmed tropical macroalgae, Biogeosciences, 10, 3615-3633, 10.5194/bg-10-3615-2013, 2013.

Liang, Q., Stolarski, R., Kawa, S., Nielsen, J., Douglass, A., Rodriguez, J., Blake, D., Atlas, E., and Ott, L.: Finding the missing stratospheric Br-y: a global modeling study of CHBr3 and CH2Br2, Atmospheric Chemistry and Physics, 10, 2269-2286, 2010.

Liao, L., Belleza, D., and Geraldino, P.: Marine algae of the Sulu Sea Islands, Philippines II: annotated list of the brown seaweeds (Phaeophyceae) from the Cuyo Islands, Phytotaxa, 152, 1-17, 2013.

Liss, P., and Slater, P.: Flux of gases across the air-sea interface, Nature, 247, 181-184, 10.1038/247181a0, 1974.

Lovelock, J. E.: Atmospheric fluorine compounds as indicators of air movements, Nature, 230, 379-&, 10.1038/230379a0, 1971.

Lovelock, J. E., and Maggs, R. J.: Halogenated hydrocarbons in and over Atlantic, Nature, 241, 194-196, 10.1038/241194a0, 1973.

Manley, S., and Dastoor, M.: Methyl-iodide (CH3I) production by kelp and assoviated microbes, Marine Biology, 98, 477-482, 10.1007/BF00391538, 1988.

Manley, S. L., and de la Cuesta, J. L.: Methyl iodide production from marine phytoplankton cultures, Limnology and Oceanography, 42, 142-147, 1997.

Mann, K., and Lazier, J.: Dynamics of Marine Ecosystems: Biological-Physical Interactions in the Oceans, Blackwell Publishing Ltd., Oxford, 2006.

McGivern, W., Francisco, J., and North, S.: Investigation of the atmospheric oxidation pathways of bromoform: Initiation via OH/Cl reactions, Journal of Physical Chemistry a, 106, 6395-6400, 10.1021/jp0255886, 2002.

McGivern, W., Kim, H., Francisco, J., and North, S.: Investigation of the atmospheric oxidation pathways of bromoform and dibromomethane: Initiation via UV photolysis and hydrogen abstraction, Journal of Physical Chemistry a, 108, 7247-7252, 10.1021/jp0311613, 2004.

Mittelstaedt, E.: Upwelling regions, in: Landoldt-Börnstein, New Series, edited by: Sündermann, J., Springer Verlag, Berlin, 135-166, 1986.

Molina, M. J., and Rowland, F. S.: Stratospheric sink for chlorofluoromethanes - chlorine atomic-catalysed destruction of ozone, Nature, 249, 810-812, 10.1038/249810a0, 1974.

Montzka, S. A., and Reimann, S.: Chapter 1: Ozone-depleting substances (ODSs) and related chemicals, in: Scientific Assessment of Ozone Depletion: 2010, Global Ozone Research and Monitoring Project – Report No. 52, Geneva, Switzerland, 2011.

Moore, R., and Tokarczyk, R.: Volatile biogenic halocarbons in the northwest Atlantic, Global Biogeochemical Cycles, 7, 195-210, 10.1029/92GB02653, 1993.

Moore, R., and Zafiriou, O.: Photochemical production of methyl iodide in seawater, Journal of Geophysical Research-Atmospheres, 99, 16415-16420, 10.1029/94JD00786, 1994.

Moore, R., Geen, C., and Tait, V.: Determination of Henry's law constants for a suite of naturally-occurring halogenated methanes in seawater, Chemosphere, 30, 1183-1191, 10.1016/0045-6535(95)00009-W, 1995a.

Moore, R., Tokarczyk, R., Tait, V., Poulin, M., and Geen, C.: Marine phytoplankton as a natural source of volatile organohalogens, Naturally-Produced Organohalogens, 283-294, 1995b.

Morton, B.: The marine biology of the South China Sea, Hong Kong University Press, Hong Kong, 1993.

Morton, B., and Blackmore, G.: South China sea, Marine Pollution Bulletin, 42, 1236-1263, 10.1016/S0025-326X(01)00240-5, 2001.

Nadzir, M., Phang, S., Abas, M., Rahman, N., Abu Samah, A., Sturges, W., Oram, D., Mills, G., Leedham, E., Pyle, J., Harris, N., Robinson, A., Ashfold, M., Mead, M., Latif, M., Khan, M., Amiruddin, A., Banan, N., and Hanafiah, M.: Bromocarbons in the tropical coastal and open ocean atmosphere during the 2009 Prime Expedition Scientific Cruise (PESC-09), Atmospheric Chemistry and Physics, 14, 8137-8148, 10.5194/acp-14-8137-2014, 2014.

Nightingale, P., Malin, G., and Liss, P.: Production of chloroform and other low-molecular-weight halocarbons by some species of macroalgae, Limnology and Oceanography, 40, 680-689, 1995.

Nightingale, P.: Air-Sea Gas Exchange, in: Surface Ocean - Lower Atmosphere Processes, edited by: Le Quéré, C., and Saltzman, E., American Geophysical Union, Washington, 69-97, 2009.

O'Brien, L., Harris, N., Robinson, A., Gostlow, B., Warwick, N., Yang, X., and Pyle, J.: Bromocarbons in the tropical marine boundary layer at the Cape Verde Observatory - measurements and modelling, Atmospheric Chemistry and Physics, 9, 9083-9099, 10.5194/acp-9-9083-2009, 2009.

Ordonez, C., Lamarque, J., Tilmes, S., Kinnison, D., Atlas, E., Blake, D., Santos, G., Brasseur, G., and Saiz-Lopez, A.: Bromine and iodine chemistry in a global chemistry-climate model: description and

evaluation of very short-lived oceanic sources, Atmospheric Chemistry and Physics, 12, 1423-1447, 10.5194/acp-12-1423-2012, 2012.

Palmer, C., and Reason, C.: Relationships of surface bromoform concentrations with mixed layer depth and salinity in the tropical oceans, Global Biogeochemical Cycles, 23, 10.1029/2008GB003338, 2009.

Pawson, S., and Steinbrecht, W.: Chapter 2: Update on global ozone: Past, Present, and Future, in: Scientific Assessment of Ozone Depletion 2014, Vienna, 2015.

Penkett, S., Jones, B., Rycroft, M., and Simmons, D.: An interhemisperic comparison of the concentrations of bromine compounds in the atmosphere, Nature, 318, 550-553, 10.1038/318550a0, 1985.

Pyle, J., Ashfold, M., Harris, N., Robinson, A., Warwick, N., Carver, G., Gostlow, B., O'Brien, L., Manning, A., Phang, S., Yong, S., Leong, K., Ung, E., and Ong, S.: Bromoform in the tropical boundary layer of the Maritime Continent during OP3, Atmospheric Chemistry and Physics, 11, 529-542, 10.5194/acp-11-529-2011, 2011.

Quack, B., and Suess, E.: Volatile halogenated hydrocarbons over the western Pacific between 43 degrees and 4 degrees N, Journal of Geophysical Research-Atmospheres, 104, 1663-1678, 10.1029/98JD02730, 1999.

Quack, B., and Wallace, D.: Air-sea flux of bromoform: Controls, rates, and implications, Global Biogeochemical Cycles, 17, 10.1029/2002GB001890, 2003.

Quack, B., Atlas, E., Petrick, G., Stroud, V., Schauffler, S., and Wallace, D.: Oceanic bromoform sources for the tropical atmosphere, Geophysical Research Letters, 31, 10.1029/2004GL020597, 2004.

Quack, B., Atlas, E., Petrick, G., and Wallace, D.: Bromoform and dibromomethane above the Mauritanian upwelling: Atmospheric distributions and oceanic emissions, Journal of Geophysical Research-Atmospheres, 112, 10.1029/2006JD007614, 2007a.

Quack, B., Peeken, I., Petrick, G., and Nachtigall, K.: Oceanic distribution and sources of bromoform and dibromomethane in the Mauritanian upwelling, Journal of Geophysical Research-Oceans, 112, 10.1029/2006JC003803, 2007b.

Raimund, S., Quack, B., Bozec, Y., Vernet, M., Rossi, V., Garcon, V., Morel, Y., and Morin, P.: Sources of short-lived bromocarbons in the Iberian upwelling system, Biogeosciences, 8, 1551-1564, 10.5194/bg-8-1551-2011, 2011.

Read, K., Mahajan, A., Carpenter, L., Evans, M., Faria, B., Heard, D., Hopkins, J., Lee, J., Moller, S., Lewis, A., Mendes, L., McQuaid, J., Oetjen, H., Saiz-Lopez, A., Pilling, M., and Plane, J.: Extensive halogen-mediated ozone destruction over the tropical Atlantic Ocean, Nature, 453, 1232-1235, 10.1038/nature07035, 2008.

Reeves, C., Penkett, S., Bauguitte, S., Law, K., Evans, M., Bandy, B., Monks, P., Edwards, G., Phillips, G., Barjat, H., Kent, J., Dewey, K., Schmitgen, S., and Kley, D.: Potential for photochemical ozone formation in the troposphere over the North Atlantic as derived from aircraft observations during ACSOE, Journal of Geophysical Research-Atmospheres, 107, 10.1029/2002JD002415, 2002.

Saiz-Lopez, A., Plane, J., Baker, A., Carpenter, L., von Glasow, R., Martin, J., McFiggans, G., and Saunders, R.: Atmospheric Chemistry of Iodine, Chemical Reviews, 112, 1773-1804, 10.1021/cr200029u, 2012.

Saiz-Lopez, A., Fernandez, R., Ordonez, C., Kinnison, D., Martin, J., Lamarque, J., and Tilmes, S.: Iodine chemistry in the troposphere and its effect on ozone, Atmospheric Chemistry and Physics, 14, 13119-13143, 10.5194/acp-14-13119-2014, 2014.

Salawitch, R., Weisenstein, D., Kovalenko, L., Sioris, C., Wennberg, P., Chance, K., Ko, M., and McLinden, C.: Sensitivity of ozone to bromine in the lower stratosphere, Geophysical Research Letters, 32, 10.1029/2004GL021504, 2005.

Salawitch, R.: Atmospheric chemistry - Biogenic bromine, Nature, 439, 275-277, 10.1038/439275a, 2006.

Sander, R.: Compilation of Henry's Law Constants for Inorganic and Organic Species of Potential Importance in Environmental Chemistry, Air Chemistry Department Max-Planck Institute of Chemistry, Mainz3.0, 1999.

Seibert, P., Beyrich, F., Gryning, S., Joffre, S., Rasmussen, A., and Tercier, P.: Mixing height determination for dispersion modelling. COST710 Working Group 2, 1997.

Seibert, P., Beyrich, F., Gryning, S., Joffre, S., Rasmussen, A., and Tercier, P.: Review and intercomparison of operational methods for the determination of the mixing height, Atmospheric Environment, 34, 1001-1027, 10.1016/S1352-2310(99)00349-0, 2000.

Sentian, J., Xiang, C., Jing, H., Quack, B., Fuhlbrügge, S., Krüger, K., and E, A.: Observation of the Variations of Very Short-Lived Halocarbon Emissions in Tropical Coastal Marine Boundary Layer, Advanced Science Letters, 21, 144-149, 10.1166/asl.2015.5856, 2015.

Simpson, W., Brown, S., Saiz-Lopez, A., Thornton, J., and von Glasow, R.: Tropospheric Halogen Chemistry: Sources, Cycling, and Impacts, Chemical Reviews Article ASAP, 4035-4062, 10.1021/cr5006638, 2015.

Sinnhuber, B., and Folkins, I.: Estimating the contribution of bromoform to stratospheric bromine and its relation to dehydration in the tropical tropopause layer, Atmospheric Chemistry and Physics, 6, 4755-4761, 2006.

Stevenson, D., Young, P., Naik, V., Lamarque, J., Shindell, D., Voulgarakis, A., Skeie, R., Dalsoren, S., Myhre, G., Berntsen, T., Folberth, G., Rumbold, S., Collins, W., MacKenzie, I., Doherty, R., Zeng, G., van Noije, T., Strunk, A., Bergmann, D., Cameron-Smith, P., Plummer, D., Strode, S., Horowitz, L., Lee, Y., Szopa, S., Sudo, K., Nagashima, T., Josse, B., Cionni, I., Righi, M., Eyring, V., Conley, A., Bowman, K., Wild, O., and Archibald, A.: Tropospheric ozone changes, radiative forcing and attribution to emissions in the Atmospheric Chemistry and Climate Model Intercomparison Project (ACCMIP), Atmospheric Chemistry and Physics, 13, 3063-3085, 10.5194/acp-13-3063-2013, 2013.

Stohl, A., and Thomson, D.: A density correction for Lagrangian particle dispersion models, Boundary-Layer Meteorology, 90, 155-167, 10.1023/A:1001741110696, 1999.

Stohl, A., Forster, C., Frank, A., Seibert, P., and Wotawa, G.: Technical note: The Lagrangian particle dispersion model FLEXPART version 6.2, Atmospheric Chemistry and Physics, 5, 2461-2474, 2005.

Stull, R.: An Introduction to Boundary Layer Meteorology, Kluwer Academic Publishers, Dordrecht, 1988.

Sørensen, J., Rasmussen, A., and Svensmark, H.: Forecast of atmospheric boundary layer height utilised for ETEX real-time dispersion modelling, Physics and Chemistry of the Earth, 21, 435-439, 1996.

Tarazona, J., and Arntz, W.: The Peruvian Coastal Upwelling System, in: Coastal Marine Ecosystems of Latin America, Springer Verlag, 229-244, 2001.

Tomczak, M., and Godfrey, J.: Regional Oceanography: an Introduction, 2nd ed., Daya Publishing House, 2003.

Troen, I., and Mahrt, L.: A simple-model of the atmospheric boundary-layer: Sensitivity to surface evaporation, Boundary-Layer Meteorology, 37, 129-148, 10.1007/BF00122760, 1986.

Vogelezang, D., and Holtslag, A.: Evaluation and model impacts of alternative boundary-layer height formulations, Boundary-Layer Meteorology, 81, 245-269, 10.1007/BF02430331, 1996.

von Bezold, W.: Zur Thermodynamik der Atmosphaere. Zweite Mittheilung. Potentielle Temperatur. Verticaler Temperaturgradient. Zusammengesetzte Convection., Sitzungsberichte der Königlich Preussischen Akademie der Wissenschaften zu Berlin, 1189–1206, 1888.

von Glasow, R., von Kuhlmann, R., Lawrence, M., Platt, U., and Crutzen, P.: Impact of reactive bromine chemistry in the troposphere, Atmospheric Chemistry and Physics, 4, 2481-2497, 2004.

von Glasow, R., and Crutzen, P.: Tropospheric Halogen Chemistry, edited by: Holland, H. D. and Turekian, K. K., Treatise on Geochemistry Update 1, 4.02, 1–67, 2007.

Wanninkhof, R., Asher, W., Ho, D., Sweeney, C., and McGillis, W.: Advances in Quantifying Air-Sea Gas Exchange and Environmental Forcing, Annual Review of Marine Science, 1, 213-244, 10.1146/annurev.marine.010908.163742, 2009.

Warwick, N., Pyle, J., Carver, G., Yang, X., Savage, N., O'Connor, F., and Cox, R.: Global modeling of biogenic bromocarbons, Journal of Geophysical Research-Atmospheres, 111, 10.1029/2006JD007264, 2006.

Weinhold, B.: Ozone nation - EPA standard panned by the people, Environmental Health Perspectives, 116, A302-A305, 2008.

Wilke, C. R., and Chang, P.: Correlation of diffusion coefficients in dilute solutions, Aiche J., 1, 264-270, 10.1002/aic.690010222, 1955.

Yang, X., Cox, R., Warwick, N., Pyle, J., Carver, G., O'Connor, F., and Savage, N.: Tropospheric bromine chemistry and its impacts on ozone: A model study, Journal of Geophysical Research-Atmospheres, 110, 10.1029/2005JD006244, 2005.

Yang, X., Abraham, N., Archibald, A., Braesicke, P., Keeble, J., Telford, P., Warwick, N., and Pyle, J.: How sensitive is the recovery of stratospheric ozone to changes in concentrations of very short-lived bromocarbons?, Atmospheric Chemistry and Physics, 14, 10431-10438, 10.5194/acp-14-10431-2014, 2014.

Yokouchi, Y., Hasebe, F., Fujiwara, M., Takashima, H., Shiotani, M., Nishi, N., Kanaya, Y., Hashimoto, S., Fraser, P., Toom-Sauntry, D., Mukai, H., and Nojiri, Y.: Correlations and emission ratios among bromoform, dibromochloromethane, and dibromomethane in the atmosphere, Journal of Geophysical Research-Atmospheres, 110, 10.1029/2005JD006303, 2005.

Ziemianski, M., Grabowski, W., and Moncrieff, M.: Explicit convection over the western Pacific warm pool in the community atmospheric model, Journal of Climate, 18, 1482-1502, 10.1175/JCLI3345.1, 2005.

Ziska, F., Quack, B., Abrahamsson, K., Archer, S., Atlas, E., Bell, T., Butler, J., Carpenter, L., Jones, C., Harris, N., Hepach, H., Heumann, K., Hughes, C., Kuss, J., Kruger, K., Liss, P., Moore, R., Orlikowska, A., Raimund, S., Reeves, C., Reifenhauser, W., Robinson, A., Schall, C., Tanhua, T., Tegtmeier, S., Turner, S., Wang, L., Wallace, D., Williams, J., Yamamoto, H., Yvon-Lewis, S., and Yokouchi, Y.: Global sea-to-air flux climatology for bromoform, dibromomethane and methyl iodide, Atmospheric Chemistry and Physics, 13, 8915-8934, 10.5194/acp-13-8915-2013, 2013.

Zuta, S., and Guillén, O.: Oceanograffa de las aguas costeras del Perü, Instituto del Mar del Peru, Callao, Peru, 157-324, 1970.

6. Lists

6.1 Figures

6.2 Tables

Danksagung

Zu allererst möchte ich mich bei meinen beiden Betreuerinnen Frau Prof. Dr. Kirstin Krüger und Frau Dr. Birgit Quack, für das in mich gesetzte Vertrauen und die Unterstützung diese Arbeit zu meistern, bedanken. Danke auch an Herrn Prof. Dr. Hermann Bange für die hilfreichen Anmerkungen während der ISOS-Treffen.

Mein Dank gilt auch Frau Prof. Dr. Christa Marandino für die Bereitschaft als Zweitgutachterin zu fungieren, sowie Herrn Prof. Dr. Martin Frank für Leitung der Prüfungskommission.

Desweiteren gilt mein Dank auch der gesamten AG Krüger und der AG Halocarbons für die vergangenen 4 Jahre. Danke für die schöne Zeit und die zahllosen Male, in denen ihr mich mit hilfreichem Feedback versorgt habt (namentlich sortiert): Alina, Doreen, Franzi, Helmke, Matt, Severin, Sinikka, Susi und Viky.

Für das Korrekturlesen der vorherigen Seiten danke ich dir ganz herzlich Hannah.

Zusätzlich danke ich auch den Kollegen des FB1 Maritime Meteorologie und des FB2 Chemische Ozeanographie. Außerdem danke ich den Fahrtleitern Hermann, Kicki und Birgit, den Kapitänen, der Crew und der wissenschaftlichen Crew von FS SONNE und FS Meteor.

Dank gilt natürlich auch meinen Eltern und Verwandten, sowie Robi, Chris, Jessi, Dirk, Rainer, Claudia, Paddy, Swantje, Frode und Oli für die Motivation und Unterstützung während der gesamten Zeit.

Diese Doktorarbeit wurde durch das Deutsche Verbundprojekt SOPRAN II (FKZ 03F0611A), das Bundesministerium für Bildung und Forschung (BMBF) und das EU-Projektes SHIVA (FP7-ENV-2007-1-226224) ermöglicht.

Eidesstattliche Erklärung

Hiermit erkläre ich, dass ich die vorliegende Dissertation, abgesehen von der Beratung durch meine Betreuer, unter Einhaltung der Regeln guter wissenschaftlicher Praxis der Deutschen Forschungsgemeinschaft selbstständig und ohne Zuhilfenahme unerlaubter Hilfsmittel erarbeitet und verfasst habe. Alle benutzten Quellen und Hilfsmittel wurden vollständig angegeben. Diese Arbeit hat weder ganz, noch zum Teil an anderer Stelle im Rahmen eines Prüfungsverfahrens vorgelegen. Sie ist nicht veröffentlicht und auch nicht zur Veröffentlichung eingereicht.

Kiel, September 2015

_____

(Steffen Fuhlbrügge)